Investigating the role of programmed necrosis in oncolytic adenovirus-induced death

Melanie Weigert

B.Sc.

Thesis submitted in fulfilment of the requirement for the Degree of Doctor of Philosophy

College of Medical, Veterinary and Life Sciences

University of Glasgow

March 2017

Abstract

Oncolytic viruses are a group of viruses that preferentially replicate in cancer cells and are a promising cancer treatment. However, how these oncolytic adenoviruses kill cancer cells is not fully understood. It was long thought that DNA viruses utilize apoptosis to induce cell death but there is now evidence that adenovirus and vaccinia cytotoxicity displays features of necrosis-like programmed cell death.

In order to investigate the role of necrosis in cell death as a result of oncolytic adenovirus infection, a panel of ovarian cancer cells with varying sensitivities to the oncolytic adenoviral mutant *dl*922-947 was used. Cells infected with *dl*922-947 displayed key features of necrotic death. Using necrosis inhibitors necrostatin-1, necrosulfonamide, GSK2791840B, GSK2399872B and GSK2393843A, as well as RNAi-mediated knockdown of RIPK1, RIPK3 or MLKL, I showed that cells undergo RIPK3-dependent necrosis and that blockage of the downstream effector mixed lineage kinase domain-like (MLKL) attenuated cell death.

While Tumour necrosis factor-α (TNF-α)-induced programmed necrosis(Laster, Wood and Gooding 1988) relies on the (RHIM)-dependent interaction of RIPK1 and RIPK3 (Li et al. 2012, Wu et al. 2014), RIPK1 seems to be redundant for adenovirus-induced death. Further, the addition of TNF-α blocking antibody to virus-infected cells showed no effect on either cell death.

Using a RIPK3 overexpression model, I showed that the amount adenovirus-induced cell death correlated with the amount of RIPK3 expression and that RIPK3 expression did not affect virus production, infectivity or the expression of viral proteins.

Further, *in vivo* experiments using human xenografts showed that expression of RIPK3 significantly improved anti-tumour activity following intra-tumoural injection of *dl*922-947.

Contents

Acknowledgment

I would like to thank my supervisor Prof. Iain McNeish for taking me on as his PhD student. I will never forget the day I had my interview with him. I was guided through a rabbit hole into his dark and scary office in the basement of the Cancer Research UK Beatson Institute. Luckily his office at the Wolfson Wohl Cancer Research Institute looks way nicer now! Thank you for your guidance and patience when I was knocking on your door literally every five minutes.

I would also like to thank Team McNeish. They all made working in the lab fun and enjoyable, especially on days with cake. I want to give special mention to Suzanne and Darren who always listened to my complaints and frustrations, which come with a PhD but also for listening and advising me on matters of personal nature. I certainly won't be missing Darren talking to himself non-stop and confusing and distracting me like hell! I will be missing doing my little non-work related side experiments with Suzanne though. I just say ECL in the dark room and liquid nitrogen! I also want to thank Malcolm for helping me with my Flow Analysis...It is just witchcraft/ dark magic to me! And also many thanks to Alex, my necrosis twin, for helping my out with my CoIP every now and then...Looks like the student has overcome his master and I don't like it!

I especially want to thank my friends outside of my PhD, the people from Glasgow University Judo Club for always looking after me and making sure I am not working too hard, even though this would mean that they would drag me along to competitions which ended in me hurting myself. I will miss our training sessions, where I could get rid of my work frustrations caused by failing experiments.

I also would like to thank Mr Shisha (Carlo-Schmid-Oberschule, Berlin, Germany), my former chemistry teacher and the person who inspired me in pursuing a carrier in science instead of becoming an architect. He always supported me as the one of the very few girls in his chemistry class and never failed to awaken my curiosity. I never left one single class of his without being overly excited for what the next class might bring. Unfortunately he died way too early. He was an inspiration and even now he is still dearly missed by his former student.

Last but not least I would like to thank my family, my mother Sabine and my brother Sebastian for their support during my PhD. It was a pretty hard time being far away from home with the distance making it difficult to “just” come around. Nevertheless I enjoyed coming home seeing them even if it was just once a year for Christmas and usually ended up being so stressful. I hope they can forgive me the way too many times I forgot to Skype them.

Declaration

I declare that the data and work presented in this thesis were done by Melanie Weigert (the author) at the Wolfson Wohl Cancer Research Centre, Institute of Cancer Sciences, University of Glasgow. All external sources have been properly acknowledged, referenced and required licences obtained

Abbreviations

3-MA	3-methyladenine
Ad	Adenovirus
AIF	apoptosis-inducing factor
AKT/PKB	Protein kinase B
AO	Acridine orange
Apaf-1	Apoptotic protease activating factor
APS	Ammonium persulphate
ARID1A	AT-rich interaction domain 1A
ATG	Autophagy-related
ATP	Adenosine triphosphate
BAK	BCL-2 antagonist/killer
BAX	BCL-2 associated X protein
BCL-2	B-cell lymphoma 2
BH3	Bcl-2 homology domain 3
BRAF	B-rapidly accelerated fibrosarcoma
BRCA	Breast cancer gene
BSA	Bovine serum albumin
BSU	Biological Services Unit
$CaCl_2$	Calcium chloride
CAR	Coxsackie-adenovirus receptor
Caspases	Cysteine-aspartic proteases
CDK12	Cyclin-Dependent Kinase 12
CH	Switzerland
CIAP	Cellular inhibitor of apoptosis protein
CK7	Cytokeratin 7
CMV	Cytomegalovirus
CO_2	Carbon dioxide
CQ	Chloroquine
CRISPR	Clustered regularly-interspaced short palindromic repeats
CsCl	Caesium chloride
CTLA-4	Cytotoxic T lymphocyte-associated protein 4
CTNNB1	Catenin Beta 1
DAI	DNA-dependent activator of interferon regulatory factors

DAMP	Damage-associated molecular pattern
DAPI	4',6-diamidino-2-phenylindole
DISC	Death-induced signalling complex
DMEM	Dulbecco's modified Eagle medium
DMSO	Dimethyl sulphoxide
DNA	Deoxyribonucleic acid
dsRNA	Double-stranded RNA
DTT	Dithiothreitol
EC_{50}	Efficient concentration 50%
ECL	Enhanced chemiluminescence
E.coli	Escherichia coli
EGF	Epidermal growth factor
EGFR	Epidermal growth factor receptor
EOC	Epithelial ovarian cancer
ERA	Epithelial related antigen
Est.	Estimated
FADD	Fas-Associated protein with Death Domain
FBS	Foetal bovine serum
FDA	Food and Drug Administration
FLIP	FLICE-like inhibitory protein
FOXM1	Forkhead box M1
FSC	forward scatter
GER	Germany
GFP	Green fluorescent protein
GM-CSF	Granulocyte macrophage colony-stimulating factor
GSK	GlaxoSmithKline
H&E	Haematoxylin and eosin
H_2O	Water
HCC	Hepatocellular carcinoma
hCMV	Human cytomegalovirus
HER2	Human epidermal growth factor receptor 2
hr	Hour
HRP	Horseradish peroxidase
HSV1	Herpes simplex virus 1
hTERT	human telomerase reverse transcriptase

IAP	Inhibitor of apoptosis protein
ICD	Immunogenic cell death
ICP	Infected cell protein
IFN	Interferon
IL	Interleukin
Kb	Kilobase
KCl	Potassium chloride
kDa	Kilodalton
KRAS	Kirsten rat sarcoma viral oncogene homolog
LB	Lennox L Broth
LC3	Light chain 3
LMP	Lysosomal membrane permeabilisation
LPS	Lipopolysaccharide
MAPK	Mitogen-activated protein kinase
mCMV	Murine cytomegalovirus
MDC	Monodansylcadaverine
MDM2	Mouse double minute 2
$MgCl_2$	Magnesium chloride
Min	Minute
MLKL	Mixed-lineage kinase like
MOMP	Mitochondrial outer membrane permeabilisation
mRNA	Messenger RNA
MSC	Mesenchymal stem cell
mTOR	Mechanistic target of rapamycin
MTS	(3(4,5-Dimethylthiazol-2-yl)-5-(3-carboxymethoxyphenyl)-2-(4-sulfophenyl)-2H-tetrazolin
MTT	(3(4,5-Dimethylthiazol-2-yl)-2,5-diphenyltetrazolium bromide)
Na_2HPO_4	Disodium hydrogen phosphate
NaCl	Sodium chloride
NBF	Neutral-buffered formalin
NDV	Newcastle disease virus
Nec-1	Necrostatin-1
NF1	Neurofibromin 1
NF-κB	Nuclear factor-kappaB
NIMP	Anti-Neutrophil antibody

NIS	Thyroidal sodium iodide symporter gene
NK	Natural killer
NRAS	Neuroblastoma RAS viral oncogene homolog
NT	Non-targeting
NTC	Non-template control
OD	Optical density
OTC	Ornithine transcarbamylase
PAMP	Pathogen-associated molecular pattern
PARP	Poly (ADP-ribose) polymerase
PBS	Phosphate buffered saline
PBST	Phosphate buffered saline tween
PCD	Programmed cell death
PCR	Polymerase chain reaction
PD-1	Programmed cell death protein 1
PD-L1	Programmed cell death protein ligand 1
PI3K	Phosphatidylinositol 3'-kinase
PI3KCA	Phosphatidylinositol 3'-kinase catalytic alpha polypeptide
pfu	Plaque forming unit
PKR	RNA-dependent protein kinase
PPP2R1α	Protein phosphatase 2 regulatory subunit alpha
pRB	Retinoblastoma protein
PTEN	Phosphatase and tensin homologue
qRT-PCR	Quantitative real time polymerase chain reaction
RGD	Arg-Gly-Asp
RID	Receptor internalization and degradation
RIPK1	Receptor interacting protein kinase 1
RIPK3	Receptor interacting protein kinase 3
RNA	Ribonucleic acid
ROS	Reactive oxygen species
SDS	Sodium dodecyl sulphate
s	Second
SEM	Standard error of mean
siRNA	Small interfering RNA
SMAC	Second mitochondrial-derived activator of caspases
SSC	Side scatter

STDEV	Standard deviation
TAA	Tumour-associated antigens
TSA	Tumour-specific antigens
TBS	Tris-buffered saline
TBST	Tris-buffered saline tween-20
TBT	Tris-buffered Tween
TBTB	Thiazolyl Blue Tetrazolium Bromide
$TCID_{50}$	Tissue culture inhibitory dose 50%
TCR	T cell receptor
TEMED	Tetramethylethylenediamine
TERT	Telomerase reverse transcriptase
TK	Thymidine kinase
TLR	Toll-like receptor
TNFR	Tumour necrosis factor receptor
TNF-α	Tumour necrosis factor α
TP53	Tumour protein p53
TRADD	Tumour necrosis factor receptor type 1-associated death domain
TRAF	TNF receptor associated factor
TRAIL	TNF-related apoptosis-inducing ligand
TRIF	TIR-domain-containing adapter-inducing interferon-β
TZM	Temozolomide
TSZ	Tnf-α, smac mimetic and zVAD-fmk
TWEAK	TNF-like weak inducer of apoptosis
UK	United Kingdom
UMFIX	Universal Molecular FIXative
USA	United States of America
V	Volt
VEGF	Vascular endothelial growth factor
vIRA	Viral inhibitor of RIP activation
VSV	Vesicular stomatitis virus
VV	Vaccinia virus
WT	Wild-type
XIAP	X-linked inhibitor of apoptosis proteins
Z.VAD.fmk	N-Benzloxycarbonyl-Val-Ala-Asp(O-Me) fluoromethyl ketone

Chapter 1

Introduction

1 Introduction

Maintaining the balance between cell death and cell division is of great importance in multicellular organisms (Fuchs and Steller 2015). Cancer is characterized by an imbalance in overall cell number, where cell division exceeds cell death due to mutations that can drive uncontrolled cell-cycle progression (Beltrami et al. 2004). Normally events like these would be expected to trigger a variety of tumour suppressive mechanisms that would drive the cell into apoptosis or cellular senescence, yet still cancer cells do not die, due to acquired mechanisms that promote tumour growth. In 2000, Hanahan and Weinberg published a paper describing those traits (Hanahan and Weinberg 2000) calling them the "Hallmarks of Cancer". In 2011 the same authors wrote a newer version including several new hallmarks (Hanahan and Weinberg 2011). Figure 1-1 shows defects in signalling pathways that counteract tumour growth and are abnormally regulated in tumours.

Figure 1-1: Hallmarks of cancer
Figure shows pathways that can be abnormally regulated in cancer. Figure adapted from: Cell 2011 144, 646-674DOI: (10.1016/j.cell.2011.02.013)

1.1 Ovarian Cancer

1.1.1 Epidemiology of ovarian cancer

Ovarian cancer is the general term for non-uterine cancers arising from the pelvic and peritoneal area. It is the 15th most common cancer in the UK and 6th most common cancer in females with 7300 new cases diagnosed in the UK in 2013 (Weblinks 1-4). Ovarian cancer is typically found in post-menopausal women. Figure 1-2A shows the average number of ovarian cancer cases at the age of diagnosis indicating that women at the ages of 65-69 have the highest incidence for the disease.

Early detection of the disease has proved to be difficult since it often presents with non-specific symptoms, such as persistent abdominal pain and/ or bloating, back pain and loss of appetite (CRUK, 2016) and the non-availability of efficient and effective early screening methods (Jacobs et al. 2016, Buys et al. 2011). Therefore, the majority of ovarian cancers fall into the advanced stage of the disease (Figure 1-2B), which has only a 52.8% chance of one-year relative survival for women diagnosed with stage IV and only a 3% chance of five-year relative survival (Figure 1-2D).

Overall survival rates have improved since the introduction of platinum-based chemotherapy in the 1980s and the introduction of paclitaxel in the 1990s, but survival rates have stagnated for the past 20 years (Coleman et al. 2011) as shown in figure 1-2C. Especially survival rates for women diagnosed with late stages of the disease have barely improved since they will often develop relapsed disease leading to chemoresistance and death.

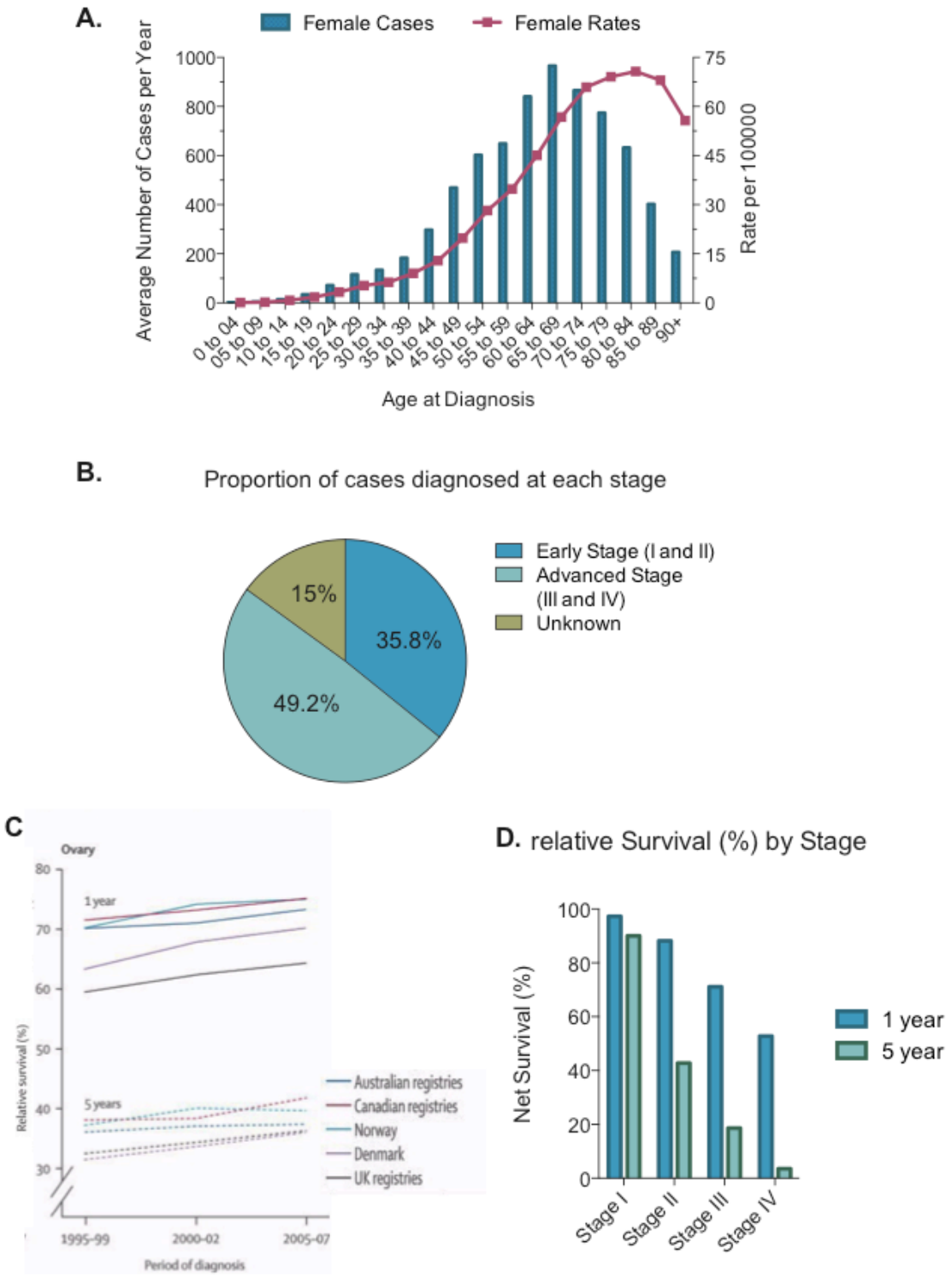

Figure 1-2: Ovarian cancer statistics

A) Average number of ovarian cancer cases and rate per 100,000 at age of diagnosis.

B) Proportion of cases diagnosed at each stage in England in 2014. Data derived from Cancer Research UK.

C) 2016 Ovarian cancer survival trends over time. Graph shows one and five age-standardised net-survival over a time frame from 1995 until 2007 for women aged 15-99 years in Australia, Canada, Norway, Denmark and UK.

D) One- and five-year relative survival by stage in women aged 15-99 years in England in 2012.

Graph A, C and D adapted from Cancer Research UK, (Weblinks 1-4) Graph C taken from M P Coleman *et al.* 2011.

1.1.2 Origins of ovarian cancer

As mentioned before, ovarian cancer is the general term for cancers arising from the pelvic and peritoneal area that share the same anatomical location; the ovaries. Ovarian cancer can be categorized in two main groups; epithelial derived tumours and non-epithelial derived tumours (Chen et al. 2003), with non-epithelial derived tumours being further divided into sex cord-stromal and germ cell tumours. Epithelial tumours are the most common type of ovarian cancer and can be further divided into the following subtypes: High-grade serous, low-grade serous, endometrioid, clear cell and mucinous cancers. Interestingly, some of these subtypes may be derived from non-ovarian tissues (Vaughan et al. 2011). For example, most mucinous invasive ovarian cancers may represent metastases to the ovaries, which have been derived from another solid cancer originating in the stomach, colon or appendix (Gastrointestinal area), while clear cell and endometrioid ovarian cancers are associated with embedding of cells of the endometrium into other organs like the ovaries, fallopian tubes, the lining of the abdomen, intestines or bladder, a condition known as endometriosis. Many high-grade serous ovarian cancers originate from secretory cells in the fimbriae of the fallopian tube, while low-grade serous ovarian cancers may originate from the cortical inclusion cysts derived from invaginated ovarian epithelial cells. Figure 1-3 shows where ovarian cancer can originate from within the pelvic and peritoneal area.

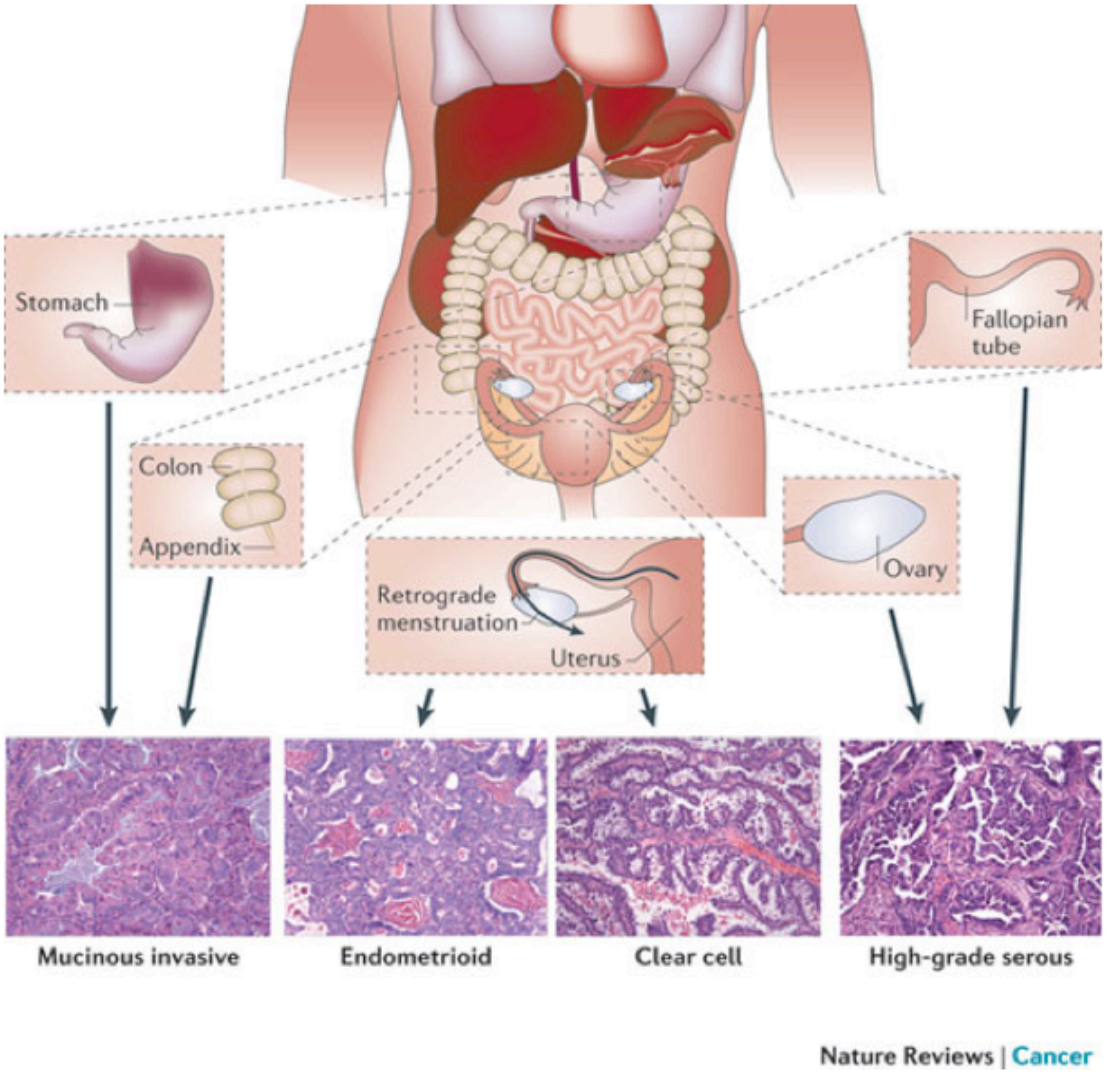

Figure 1-3: Origins of ovarian cancer from within the pelvic and peritoneal area
Mucinous invasive ovarian cancers are often metastasis arising in the gastrointestinal tract but localise in the ovaries. Endometrioid and clear cell ovarian cancer are cancers associated and originating from endometriosis, while many high-grade serous ovarian cancers originate from secretory cells from the fallopian tube. Nature Reviews Cancer 11, 719-725 (October 2011).

1.1.3 Mutations associated with ovarian cancer

As described earlier, epithelial ovarian cancers can be categorised into four subgroups with each of the subgroups being associated with the occurrence of certain mutations. High-grade serous ovarian cancer is characterised by near universal *TP53* abnormalities, genomic instability and abnormalities in the DNA copy number. They also contain low prevalence somatic mutations in *NF1, BRCA1/2, RB1* and *CDK12* (Cancer Genome Atlas Research 2011). Low-grade serous ovarian cancers most commonly contain mutations in *BRAF* or *KRAS* leading to the activation of the mitogen-activated protein kinase (MAPK) signalling pathway (Singer et al. 2003). About 30% of endometrioid and clear cell

ovarian cancers carry mutations in *PI3KCA* and *AKT* leading to the activation of the PI3K pathway (Banerjee and Kaye 2013). They also have frequent mutations in *ARID1A*. Mucinous ovarian cancers contain nearly universal mutations in *KRAS* and show in about 18% of all cases amplification or overexpression of HER2 (Banerjee 2013, Anglesio et al. 2013). Table 1 shows mutations associated with each subtype.

Table 1: Mutations associated with each epithelial ovarian cancer subtype.
Table adapted from G C Jayson *et al.* 2014.

	High-grade serous	Low-grade serous	Endometrioid	Clear cell	Mucinous
Mutations	TP53	BRAF	ARID1A	ARID1A	KRAS
	BRCA1/2	KRAS	PI3KCA	PI3KCA	HER2 ampl.
	NF1	NRAS	PTEN	PTEN	
	CDK12	ERBB2	PPP2R1α	CTNNB1	
	Defective homologous recombination		mismatch repair deficiency	PP2R1A	
	RB1				
	Alterations in PI3K/Ras/Notch/ FoxM1 pathway				

1.1.4 Treatment of ovarian cancer

First line treatment for ovarian cancer consists of primary debulking surgery. However, in cases where surgery is not feasible due to patient health or dissemination of the tumour, neoadjuvant platinum- and taxane-based chemotherapy is given. In neoadjuvant chemotherapy, the patient is treated with chemotherapy prior to debulking surgery. Whether a patient is treated with debulking surgery or neoadjuvant chemotherapy first can also depend upon the hospital site and the approach of the gynaecological oncology surgeon. When patients receive neoadjuvant chemotherapy, they undergo interval debulking, where the debulking surgery is performed after 3-4 cycles of chemotherapy. Platinum-based chemotherapy, has been the standard treatment for ovarian

cancer for the last 40 years (Jayson et al. 2014). For the treatment of ovarian cancer, platinum-based chemotherapeutics like carboplatin and cisplatin are usually given in combination with a taxane (Usually paclitaxel but docetaxel is equally effective (Vasey et al. 2004)).

In recent years, new treatment strategies have evolved since many women treated with platinum-based chemotherapy become resistant over time. One of those treatments involves the use of poly (ADP-ribose) polymerase (PARP) inhibitors for patients with mutations in *BRCA1* or *BRCA2*. BRCA1 and BRCA2 are involved in the repair of DNA double strand breaks making cancers carrying these mutations rely on the non-homologous end joining pathway to repair DNA damage. Clinical trials using the PARP inhibitors olaparib, niraparib and rucaparib in patients carrying these mutations showed impressive anti-tumour responses (Fong et al. 2009, Kaye et al. 2012).

Another treatment involves targeting the growth and spread of tumour blood vessels, a term called angiogenesis. Vascular endothelial growth factor (VEGF) is a signal protein that stimulates the production of blood vessels. It has been shown that VEGF is secreted by malignant ovarian epithelial cells (Olson et al. 1994, Premalata et al. 2016). Bevacizumab, a monoclonal anti-VEGF antibody, has shown in first line trials that its addition to chemotherapy followed by single agent maintenance treatment improves progression-free and overall survival in patients (Burger et al. 2011, Perren et al. 2011).

In recent years research has shown an increasing interest in the role of immunity in cancer progression, since it has been demonstrated that immune cells can recognise and kill tumour cells through the expression of tumour-associated antigens (TAA) and tumour-specific antigens (TSA) (Koebel et al. 2007). The expression of immune checkpoint proteins on effector T-cells can contribute towards immune evasion of cancer cells. Especially the immune checkpoint proteins cytotoxic T lymphocyte-associated protein 4 (CTLA-4) and programmed cell death protein 1 (PD-1) have drawn great attention, since their ligation can inhibit T-cell priming and activation or the lytic activity of effector T-cells. Ipilimumab a CTLA-4 targeting antibody, showed in a phase I/II trial a 11% response rate for ovarian cancer (1 out of 9 patients; NCT01611558). In a Phase-

1b study treatment with with pembrolizumab (PD-1 antibody) resulted in 1 complete response, 2 partial responses and 6 patients with stable disease from a cohort of 26 patients with PD-L1 positive advanced ovarian cancer (Varga A 2015).

Despite these advances in the treatment of ovarian cancer, less than 50% of all patients survive their disease for more than five years making it important to search for new therapies and treatment options.

1.2 Oncolytic Virotherapy

Oncolytic viruses are viruses that replicate selectively in tumours cells. These viruses specifically exploit the mechanisms that aid tumour growth, therefore making them selective for cancerous cells, while not affecting healthy tissues. In addition to their ability to infect and lyse tumour cells, virus-induced cell lysis is often associated with the induction of inflammation and release of damage-associated molecular patterns (DAMPS) as well as pathogen-associated patterns (PAMPS) leading to a type of cell death known as immunogenic cell death (ICD). This in turn can stimulate an adaptive immune response enabling the immune system to recognize the tumour, potentially leading to anti-tumour immunity. Oncolytic viruses can be classed into three broad categories consisting of 1) native viruses, which preferentially replicate in tumour cells, 2) genetically-modified viruses, which have can have deletions within the viral genome or tropism modifications and 3) genetic modified viruses that express therapeutic transgenes.

Many pre-clinical studies have successfully demonstrated the efficacy and high selectivity of oncolytic viruses *in vitro* and *vivo*, with numerous making it into phase I/II clinical trials although only fewer into phase II or III trials.

Accumulating evidence suggests that the host immune response is a critical factor for assessing the efficacy of oncolytic viruses (Taipale et al. 2016, Cerullo et al. 2012). Natural resistance from pre-existing immunity can lead to the production of neutralizing antibodies and can therefore lead to the elimination of the virus rather than the development of an adaptive immune response towards the tumour. Even the route of virus administration can pose challenges

in treatment. For systemic treatment, agents must have a high tumour tropism to ensure that no healthy cells are being targeted and clinical studies investigating virus-tumour tropism (Green et al. 2012) have been already been undertaken.

1.2.1 Naturally oncolytic viruses

Native or naturally occurring oncolytic viruses are replication-competent viruses that selectively infect and kill tumour cells without requiring any genomic alteration. Observations in the early 1900s showed that patients with leukaemia who contracted influenza, underwent periods of remission, which produced beneficial effects for the patients (Dock 1904, Pelner, Fowler and Nauts 1958). In 1950 Pack *et al.* described the use of a virus for the treatment of cancer. He observed that a patient with malignant melanoma was cleared of her tumour after receiving the rabies vaccine following a dog bite. Following his observation, he performed a small controlled study in 12 patients with melanoma using the Harris rabies vaccine. Two of his 12 patients showed tumour reduction following treatment (Pack 1950).

1.2.1.1 Reovirus

Reoviruses are non-enveloped double-stranded RNA viruses that naturally occur in the human respiratory and gastrointestinal tract. They infect a variety of cells but preferentially replicate in Ras-transformed cells (Strong et al. 1998, Norman et al. 2004, Shmulevitz, Marcato and Lee 2005). In non-Ras activated cells, viral replication is inhibited through the autophosphorylation of protein kinase R (PKR). PKR binds to viral dsRNA leading to the phosphorylation of eIF2α and the inhibition of protein synthesis (Stark et al. 1998, de Haro, Mendez and Santoyo 1996). In Ras-transformed cells PKR autophosphorylation is inhibited allowing the translation of viral proteins. The most extensively studied oncolytic reovirus is Reolysin. Multiple clinical trials in prostate cancer (Gollamudi et al. 2010), malignant glioma (Kicielinski et al. 2014), multiple myeloma (Sborov et al. 2014), metastatic melanoma (Galanis et al. 2012) and solid tumours (Gollamudi et al. 2010, Kolb et al. 2015, Morris et al. 2013) have demonstrated the safety and anti-tumour activity of Reolysin. In 2015 the US FDA granted Reolysin an orphan drug status for the treatment of malignant glioma, ovarian cancer, fallopian tube cancer and pancreatic cancer (FDA, 2015).

1.2.1.2 Paramyxoviridae

Paramyxoviridae form a family of viruses that uses humans and birds as their natural hosts. Two naturally occurring oncolytic viruses that belong to this group are the measles virus and the Newcastle disease virus (NDV). PV701 is a naturally occurring attenuated strain of NDV. It is a negative strand RNA virus that preferentially replicates in tumour cells that have defects in interferon signalling. Defects in interferon signalling are believed to give tumours growth and survival advantages, disabling interferon's antiviral function. Phase one clinical trials using PV701 have shown that it is safe to use and patients usually showed mild flu-like symptoms, which diminished with repeated administration. S. A. Laurie *et al*. observed tumour regression in one patient, and disease stabilization in four patients, who had previously progressed following standard anti-cancer therapy (Laurie et al. 2006).

Measles virus is an enveloped single-stranded, negative sense RNA virus that infects the respiratory system in humans. Oncolytic measles viruses (MV) are based on the attenuated live Edmonston vaccine strain, which preferentially enters tumour cells that overexpress the CD46 (Dorig et al. 1993, Anderson et al. 2004) receptor. MV-NIS is a measles virus that has been engineered to express human thyroidal sodium iodide symporter (NIS) gene. A clinical phase I trial evaluated the intravenous treatment of MV-NIS in patients with recurrent or refractory multiple myeloma (Clinical identifier: NCT00450814) and has led to further phase II trials of MV-NIS for the treatment of multiple myeloma (NCT02192775) and patients with ovarian, fallopian or peritoneal cancers (NCT02364713).

1.2.2 Genetically modified oncolytic viruses

Besides naturally occurring oncolytic viruses, viruses can also be genetically modified to selectively replicate within tumour cells while not being able to replicate in healthy tissues.

1.2.2.1 Herpes simplex virus 1

Herpes simplex virus 1 (HSV1) is a large enveloped double-stranded, linear DNA virus known to produce cold sores in humans. In 2015, Talimogene laherparepvec (T-VEC, Imlygic) was the first oncolytic virus approved by the US FDA for the treatment of melanoma (Andtbacka et al. 2015, Greig 2016). Talimogene laherparepvec (T-VEC) has deletions in the genes coding for infected cell protein 34.5 (ICP) and ICP47. ICP34.5 is a neurovirulence factor with a critical role in viral replication, in particular suppression of the PKR/eIF2α response following infection. Due to its ICP34.5 deletion, T-VEC can only replicate in cells with defects in the PKR pathway. ICP47 is involved in inhibiting $CD8^+$ T recognition of infected cells. Further, the deletion of ICP47 increases the expression of the US11 gene, which counteracts host-mediated shutoff of protein translation (Katze 1995, Attrill et al. 2002, Goldsmith et al. 1998). The insertion of granulocyte macrophage colony-stimulating factor (GM-CSF) leads to the recruitment and activation of antigen-presenting cells leading to a tumour-specific T-cell response (Toda, Martuza and Rabkin 2000, Dranoff et al. 1993, Mach et al. 2000, Liu et al. 2003).

1.2.2.2 Vaccinia virus

Vaccinia virus is an enveloped, linear, double-stranded DNA virus that replicates in the cytoplasm of infected cells. JX-594, also known as Pexa-Vec is a replication-competent oncolytic and immunotherapeutic vaccinia virus derived from the Wyeth vaccine strain. It has a deletion in the thymidine kinase (TK)-coding gene and has been modified to express GM-CSF. Pexa-Vecs cancer selectivity is driven by multiple mechanisms. It selectively replicates in cells that have activations in the epidermal growth factor receptor (EGFR)/Ras signalling pathway, high levels of TK and are resistant to type-I interferons (Parato et al. 2012). At the moment Pexa-Vec's effectiveness in combination with sorafenib is being assessed in a phase III study (PHOCUS trial) (NCT02562755) in patients diagnosed with advanced, unresectable hepatocellular carcinoma (HCC). In 2013 the US FDA and EU EMA granted Pexa-Vec orphan drug status for the treatment of HCC.

In vivo studies as well as clinical trials have shown that most oncolytic viruses are safe to use when careful safety procedures are in place. These studies have shown that most common treatment associated toxicity consisted of ‘flu-like’ symptoms. Table 2 shows further oncolytic viruses that have been evaluated in clinical trials.

Table 2: Other oncolytic viruses used in clinical trials.

Virus group	Name	Phase of development; targeted tumours	Clinical Identifier/ Outcome
HSV1	G207	Orphan drug since 2002; glioma	Only Phase I studies published
	HSV1716	Ongoing; Phase I/II; malignant pleural mesothelioma	NTC01721018
	TBI-1401 (HF10)	Recruting; Phase II; for unresectable melanoma	NTC02272855
	PV-10	Recruiting; Phase III;recurrent cutaneous melanoma	NTC02288897
Cox-sackievirus	CAVATAK/ CVA21	Phase II completed; melanoma	NCT01636882 No results
Seneca Valley virus	NTX-010	Orphan drug since 2008; neuroendocrine tumours	Only Phase I studies published
	SVV-001	Phase I; relapsed neuroblastoma, rhabdomysosarcoma	NTC01048892 No study results
Maraba virus	MG1MA3	Recruiting; Phase I; MAGE-A3 protein-expressing cancers	NTC02285816
Vaccinia virus	GL-ONC1	Recruting; Phase I; ovarian cancer, peritoneal carinomatosis, fallopian tube cancer	NCT02759588
	PROSTVAC+ /- GM-CSF	Ongoing phase III; treatment of prostate cancer	NTC01322490
Reo virus	Wild type	Ongoing phase II; ovarian epithelial, fallopian tube and primary peritoneal cancers	NTC01199263
Measles virus	MV-NIS	Phase II; treatment of ovarian, fallopian and peritoneal cancers	NCT02364713 No study results

Despite their general safety, in 1999 the first death of a patient who participated in a clinical trial for gene therapy was reported. Jesse Gelsinger had a metabolic disorder, ornithine transcarbamoylase (OTC) deficiency, and joined a clinical trial run by the University of Pennsylvania in 1999, where he was given an infusion of an attenuated adenovirus virus, which encoded the corrective OTC gene (Raper et al. 2003). Four days after injection, he died due to a severe inflammatory immune reaction to the adenoviral vector used to deliver the gene. The principal investigators in this study broke several rules of conduct, which increased the likelihood of his death. Jesse as well as his parents had never been informed about the fact that several patients experienced serious side effects. Further, three monkeys died during pre-clinical studies due to severe liver inflammation and a clotting disorder. Further, he should not have been included in the study due to abnormal liver function tests (Sibbald 2001). Following this incident, the US FDA introduced two new programmes in 2000 to enhance patient protection.

Besides their use as a single agent, oncolytic viruses can also be used in combination with chemotherapy and/or radiotherapy, and clinical studies investigating the efficacy of these combination therapies have shown a greater antitumour effect compared to single therapy (Xia et al. 2004, Nemunaitis et al. 2000).

1.3 Adenoviruses

1.3.1 History

Adenoviruses were first discovered in 1953 when Rowe *et al*. attempted to establish tissue culture cell lines from tonsils and adenoidal tissue and observed a transmissible agent that induced spontaneous degeneration in tissue culture (Rowe et al. 1953). Today there are 57 different adenovirus serotypes, which can be classified based on their neutralization with specific antisera (Horwitz 1996).

Table 3: Adenovirus subgroups, serotypes and their respective cellular attachment receptors, if those have been identified.
[A]CAR, [B]CD46, [C]SA, [D]CD80/86, [E]Heparan sulphate and [F]Desmoglein 2

Human Adenovirus subgroup	Serotype
A	12[A], 18, 31[A]
B, type 1	3[B,D,F], 7[F], 16[B], 21[B], 50[B], 55
B, type 2	11[B,F], 14[B,14], 34, 35[B]
C	1, 2[A,E], 5[A,E], 6, 57
D	8[C]-10, 13, 15[A], 17, 19p[A], 19a[C], 20, 22-30, 32, 33, 36, 37[B,C]-39, 42-49,51, 53, 54, 56
E	4[A]
F	40, 41[A]
G	52

1.3.2 Adenovirus structure

Adenoviruses are non-enveloped, icosahedral particles of approximately 70-100nm diameter. The capsid that surrounds the 36kbp linear dsDNA core consists of 240 hexon and 12 penton capsomers at the vertices with a projecting fiber, containing a knob domain, at each penton base. The linear dsDNA is associated with two major core proteins (polypeptide V and VII) and μ as well as a 55kDa terminal protein that is attached at the 5' end of the linear dsDNA. Figure 1-4 shows the simplified structure of an adenovirus virion (Doerfler 1996).

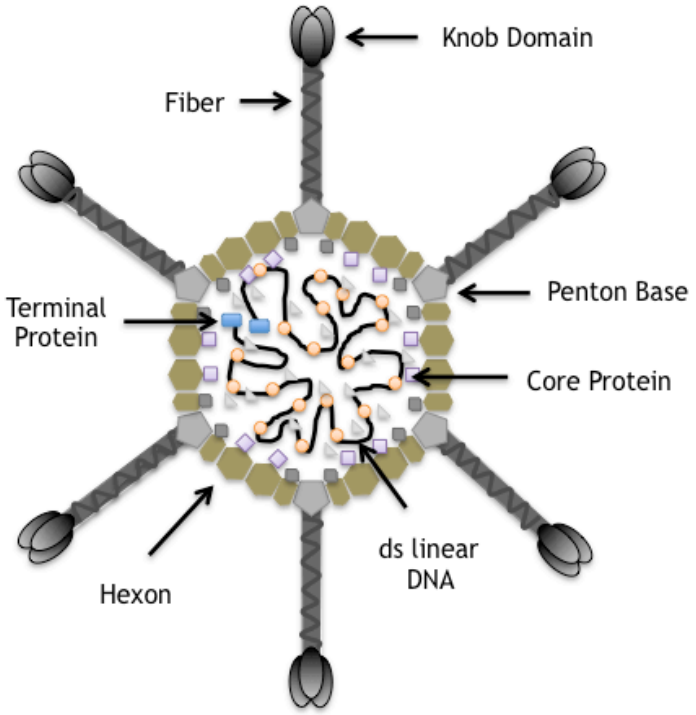

Figure 1-4: Simplified structure of an adenovirus virion

1.3.3 Adenovirus genome

The adenovirus genome is about 35-36kb long and shown in figure 1-5. The transcription of viral genes, as well as virion assembly, takes place in the nucleus. All genes are transcribed by RNA pol II, which is provided by the host cell. Genes that are being transcribed by RNA pol II give rise to multiple mRNAs through alternative splicing.

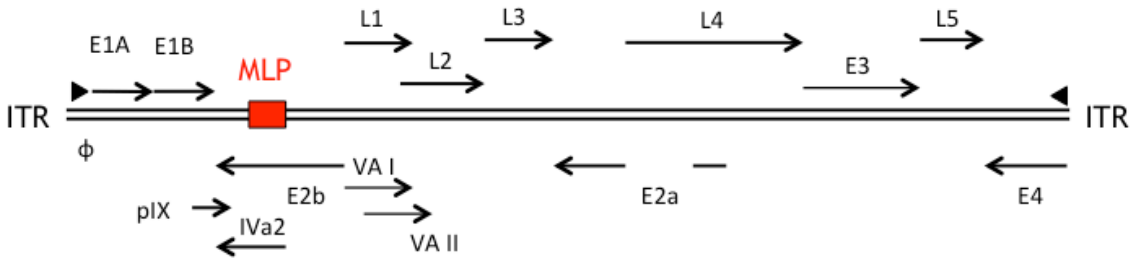

Figure 1-5: Simplified transcription map of the adenovirus genome
E: early transcription unit. L: late transcription unit. MLP: major late promoter. ITR: inverted terminal repeat. φ: packaging signal. pIX: protein IX. VA I and II: adenovirus VA RNA-derived miRNAs. Iva2: transcriptional activator of major late promoter.

The first genes transcribed during adenovirus replication are, in order, E1A, E1B, E2, E3 and E4, these genes are being referred to as early transcription units. Proteins of E1A are involved in activating the transcription of viral genes and inducing the host cell to enter S phase, while proteins of E1B are mainly involved in the suppression of apoptosis. Proteins of E3 are involved in supressing and modulating antiviral host responses. E2A and E2B are involved in the replication of viral DNA and whilst E4 proteins regulate transcription of viral DNA and mediate the nuclear export of mRNA as well as apoptosis. The inverted terminal repeat functions as a DNA replication origin and can be found at each end of the viral genome. After the initiation of viral replication the three delayed early viral promoters IX, IVa2 and E2 late become active (Ying, Tollefson and Wold 2010). There are also five families of late mRNA L1 to l5, which are alternative splice products of the single major late transcription unit and are involved in the production and assembly of the virion capsid. The packaging signal φ is located between the left terminal repeat and the region coding for E1A and is involved in the packaging of the genome into virion capsids (Shenk 2001).

1.3.3.1 *dl*922-947 genome

The oncolytic virus *dl*922-947 is an adenovirus type 5 deletion mutant. It carries a 24 bp deletion in E1A conserved region 2 (CR2) region (Figure 1-6) and a 745bp deletion in E3B from Ad5 bp 30005-30750 which was then substituted with 642bp of heterologous DNA. This alteration leads to deletion of E3 14.7K and RID α/ß proteins of adenovirus (Bett, Krougliak and Graham 1995). As described earlier, E1A is the first protein to be expressed during adenovirus infection. The CR2 domain of E1A binds to the retinoblastoma protein (pRb), which leads to the release of E2F-1 from the pRb-E2F complex in quiescent cells. Free E2F will then stimulate cell entry into S-phase for viral replication and transactivate the adenovirus E2 promoter. Therefore *dl*922-947 can only replicate in cells that have abnormalities in the pRb pathway, which is the case for over 90% of human cancers (Sherr and McCormick 2002, Flak et al. 2010), leading to its high selectivity for cells with high levels of free E2F.

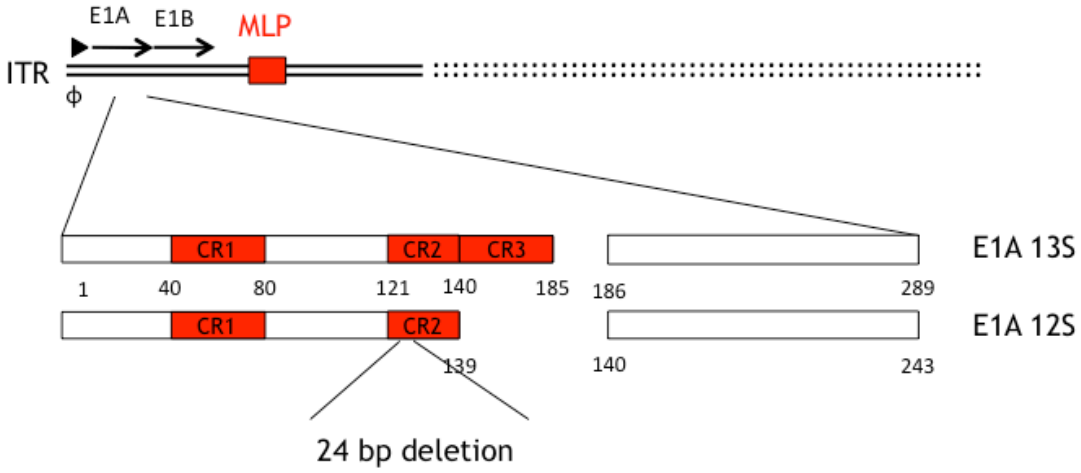

Figure 1-6: *dl*922-947 genome showing the position of its 24bp deletion
Numbers indicate aminoacid position. CR: conserved region. E: early transcription unit. MLP: major late promoter. ITR: inverted terminal repeat. φ: packaging signal.

1.3.4 Adenovirus type 5 adsorption and cell entry

During attachment, the adenoviral fiber binds to receptors on the cell surface. Different adenovirus serotypes will use different cellular receptors for initial attachment. Table 3 shows an overview of which serotypes use which kind of cellular receptors for attachment. For adenovirus type 5, infection occurs through binding of the adenoviral fiber to the coxsackie-adenovirus receptor (CAR) (Bergelson et al. 1997) followed by the interaction of the penton base with $\alpha_v\beta_3$, $\alpha_v\beta_5$ and to a lower extent $\alpha_v\beta_1$ integrins (Davison et al. 2001, Wickham et al. 1993), which leads to the detachment of the viral fibers and stimulates integerin-mediated endocytosis of the fibreless virion into clathrin-coated vesicles. Inside the endosome the virus undergoes a pH-dependent process called uncoating, which involves the partial disassembly of the capsid within the endosome to mediate permeabilization of the endosomal membrane and facilitates the endosomal escape of partially uncoated virions into the cytosol. Microtubules will then transport the virus particles to the nucleus, where it will associate with nuclear pore complexes (NPC) leading to the release of viral DNA into the nucleus. After hexon and penton capsomers have been produced in the cytoplasm, they are imported into the nucleus for virion assembly. Infectious virion assembly is completed once the precursor proteins of VI, VII, VIII, μ and the terminal proteins are cleaved by a viral protease, which is included in the virus particle. Infectious virions are then being released from the cell and virus progeny can spread to other cells.

1.4 Adenoviruses in oncolytic virotherapy

Oncolytic adenoviruses have already been used in models of pre-clinical research, where they have showed promising activity in metastatic breast cancer models (Heise et al. 2000, Bazan-Peregrino et al. 2008, Bazan-Peregrino et al. 2013), prostate (Satoh et al. 2007), glioma (Kaliberov et al. 2016, Qiao et al. 2015), bladder (Wang et al. 2006), pancreatic (Cherubini et al. 2011, Bhattacharyya et al. 2011) and ovarian cancer (Lockley et al. 2006). The huge diversity of DNA and RNA viruses as well as viruses with certain tropisms, offers a huge therapeutic window to choose from; and thanks to the development of new techniques we are getting more successful at selecting potent anticancer viruses.

1.4.1 Adenovirus deletion mutants

One of the best-described oncolytic adenoviruses is the E1B 55-kDa deleted adenovirus ONYX-015 (*dl*1520), which was originally thought to replicate selectively in cells that are p53-deficient. However, it wasn't until 2004 that the mechanism for its selectivity was fully unravelled, when O'Shea *et al*. showed that the late functions of E1B-55K, specifically its involvement in the preferential export of late viral RNAs, was the main determent or its selectivity. Late viral export is defective in ONYX-015 and therefore restricts its replication in primary cells, while tumour cells that allow ONYX-015 replication provide E1B-55Ks RNA export function (O'Shea et al. 2004).

In 2000 Khuri *et al*. performed a trial of *dl*1520 in recurrent head and neck cancer (Khuri et al. 2000), where it was used in combination treatment with the chemotherapeutic drug cisplatin and 5-fluorouracil. They showed that combination treatment was well tolerated by patients and showed disease stabilization in some patients. They also observed tumour-selective viral replication and the induction of necrosis in injected tumours. In the following year Ganly *et al*. performed a phase I study on *dl*1520 (Ganly et al. 2001) in recurrent head and neck cancer, where they showed that intratumoural administration with *dl*1520 was well tolerated and associated with biological activity. This was followed up by a phase II trial performed by Nemunaitis *et al*. in 2001 (Nemunaitis et al. 2001) and a phase III randomized clinical trial by Xia *et al*. in 2004 (Xia et al. 2004). The virus used in Xia *et al*. study, H101, is a

modification of *dl*1520 and the world's first approved oncolytic therapy in combination with chemotherapy for squamous cell cancer of head and neck or esophagus. Further studies and trials with *dl*1520 were conducted in colorectal cancer (Reid et al. 2001) and refractory tumours (Reid et al. 2002), where chemotherapy-associated anti-tumoural activity and evidence for chemo sensitization were observed.

1.4.2 Adenoviruses with transgenes and other modifications

Another well-described oncolytic adenovirus is called delta-24-RGD. Delta-24-RGD is very similar to *dl*922-947, containing the same E1A-CR2 deletion, but which additionally has an RGD-4C peptide motif inserted into the adenoviral fiber. This motif allows the virus to anchor directly to integrins by passing primary CAR attachment. Various pre-clinical studies and *in vivo* studies (Jiang et al. 2014, Dembinski et al. 2010) have shown that Ad-Δ-24-RGD shows antitumour activity in the treatment of glioma (Fueyo et al. 2003, Avci et al. 2015, Alonso et al. 2008), medulloblastoma (Stolarek et al. 2004), cervical cancer(Bauerschmitz et al. 2004) and brain tumour stem cells (Jiang et al. 2007). ICOVIR-5 (Cascallo et al. 2007), a modified Ad-Δ-24-RGD, has shown potent anti-glioma effects *in vivo* (Alonso et al. 2007) in combination with RAD001 or temozolomide (TZM). In 2010 García-Castro *et al*. performed an exploratory study with ICOVIR-5 for the treatment of metastatic neuroblastoma (Garcia-Castro et al. 2010, Ramirez, Garcia-Castro and Alemany 2010). They used autologous mesenchymal stem cells (MSC) to systemically deliver ICOVIR-5. They showed that the treatment was well tolerated and that one patient was in complete remission 3 years after therapy.

1.4.3 Directed evolution adenoviruses

One of the most recent approaches in producing highly selective and potent anticancer viruses involved the directed evolution of adenoviruses. A pool of different adenovirus serotypes was grown and passaged under conditions that invited recombination between the different serotypes. The viral pools were then placed under directed selection. The pool with the highest potency (low IC_{50} (Viral particles/cell)) as measured by 3-(4,5-dimethylthiazol-2-yl0-5-(3-carboxymethoxyphenyl)-2-(4-sulfophenyl)-2H-tetrazolium (MTS) assay and higher

relative potency compared to Ad5 was used. To generate highly potent viral agents, individual plaques from the pool with the highest potency were purified, and the isolated viruses were screened by MTS assay for their lytic potential. The result of this method, enadenotucirev (EnAd; also known as ColoAd1), is an Ad3/Ad11p chimeric virus with high selectivity for tumour cells and a higher potency than other clinical oncolytic adenoviruses, like ONYX-015 *in vitro, vivo* and *ex vivo* (Kuhn et al. 2008).

This virus has shown to be 2-3 logs more potent and selective than ONYX-015 (*dl*1520) (Kuhn et al. 2008, Bauzon et al. 2009) and is undergoing several early phase clinical trials including one phase 1/2 clinical trial for the treatment of ovarian cancer (OCTAVE). This trial recruits women with platinum-resistant disease, ie those whose cancer has recurred within six months of their most recent platinum-based chemotherapy. Besides the clinical use of EnAd, new and improved oncolytic adenoviruses are needed to increase the therapeutic output for patients. One way of improving oncolytic adenoviruses is by better understanding the mechanisms of viral infection, replication, spread and killing as well as the immune responses they elicit *in vitro* and *vivo*.

The oncolytic adenoviruses described here are just very few. Table 4 shows further oncolytic adenoviruses that have or are being evaluated in clinical research.

Table 4: On-going and completed clinical trials using oncolytic adenoviruses

Virus name	Proposed tumour targeting mechanism	Phase of development and targeted tumours	References/ Clinical Identifier
CG0070	pRB pathway-defective cells	Phase II/III	(Burke et al. 2012)
EnAd	Unknown	Phase I/II ongoing; solid tumours of epithelial origin, metastatic colorectal and/or bladder cancer	NTC02028442
*dl*1520/ ONYX-015	Cells that provide E1B-55Ks function in late RNA export	Phase II conducted; advanced sarcoma, metastatic colorectal cancer, hepatobiliary tumours	(Galanis et al. 2005, Hamid et al. 2003, Makower et al. 2003)
*dl*922-947	pRB pathway abnormalities	Pre-clinical studies	(Lockley et al. 2006)
H101	p53-deficient cells	Approved therapy for squamous cell cancer of head and neck or esophagus	(Xia et al. 2004)
ICOVIR-5	pRB pathway abnormalities	Phase I/II completed; metastatic neuroblastoma	(Garcia-Castro et al. 2010)
ICOVIR-7	pRB pathway abnormalities	Phase I conducted; advanced and refractory solid tumours	(Nokisalmi et al. 2010)
LOAd703		Phase I/IIa ongoing; pancreatic cancer	NCT02705196
ONCOS-102	pRB pathway abnormalities	Phase II; unresectable malignant pleural mesothelioma	NTC02879669

1.5 Cell Death Mechanism

As described earlier one hallmark of cancer is its ability to evade cell death mechanism leading to an imbalance in overall cell number due to mutations or alterations in proteins that are involved in cell death initiation and/or execution. Currently we can distinguish between three regulated cell death pathways: apoptosis, autophagy and necroptosis (Fuchs and Steller 2015).

1.5.1 Type I cell death: Apoptosis

Apoptosis is the best-defined cell death pathway and is well conserved between higher multicellular organisms. This pathway has evolved to keep the number of cells tightly regulated by controlling the rate of cell division as well as by controlling the rate of cell death.

Apoptosis is morphologically characterized by cell shrinkage, chromatin condensation and fragmentation of the cell (Kroemer et al. 2009) and is regulated by a variety of stimuli coming from within a cell (Intrinsic cell death pathway) like the production of reactive oxygen species (ROS) or from its environment (Extrinsic cell death pathway) e.g. TNF receptor ligation (Steller 2008). The intrinsic cell death pathway is mainly dependent on the activation of caspases, which are aspartate-specific cysteine proteases that play an important role in the induction, transduction and amplification of apoptotic signals(Fan et al. 2005). The extrinsic pathway is stimulated through the binding of an extracellular ligand with its cell surface receptor. One example is the tumour necrosis factor (TNF) superfamily, which interacts with a corresponding superfamily of receptors. Those receptor-ligand interactions are involved in different biological events as e.g. proliferation, through the activation of the NF-κB pathway, differentiation of immature myeloid cells (Sade-Feldman et al. 2013), inflammation and apoptosis signalling (Igaki et al. 2002). Defects in TNF signalling are associated with autoimmune disorders and cancer. Deregulation of TNF can lead to immune-mediated inflammatory diseases like Crohn's disease and rheumatoid arthritis, which can be treated with TNF-blocking antibodies. The extrinsic and intrinsic apoptosis death pathways are further described in detail in figure 1-7, below.

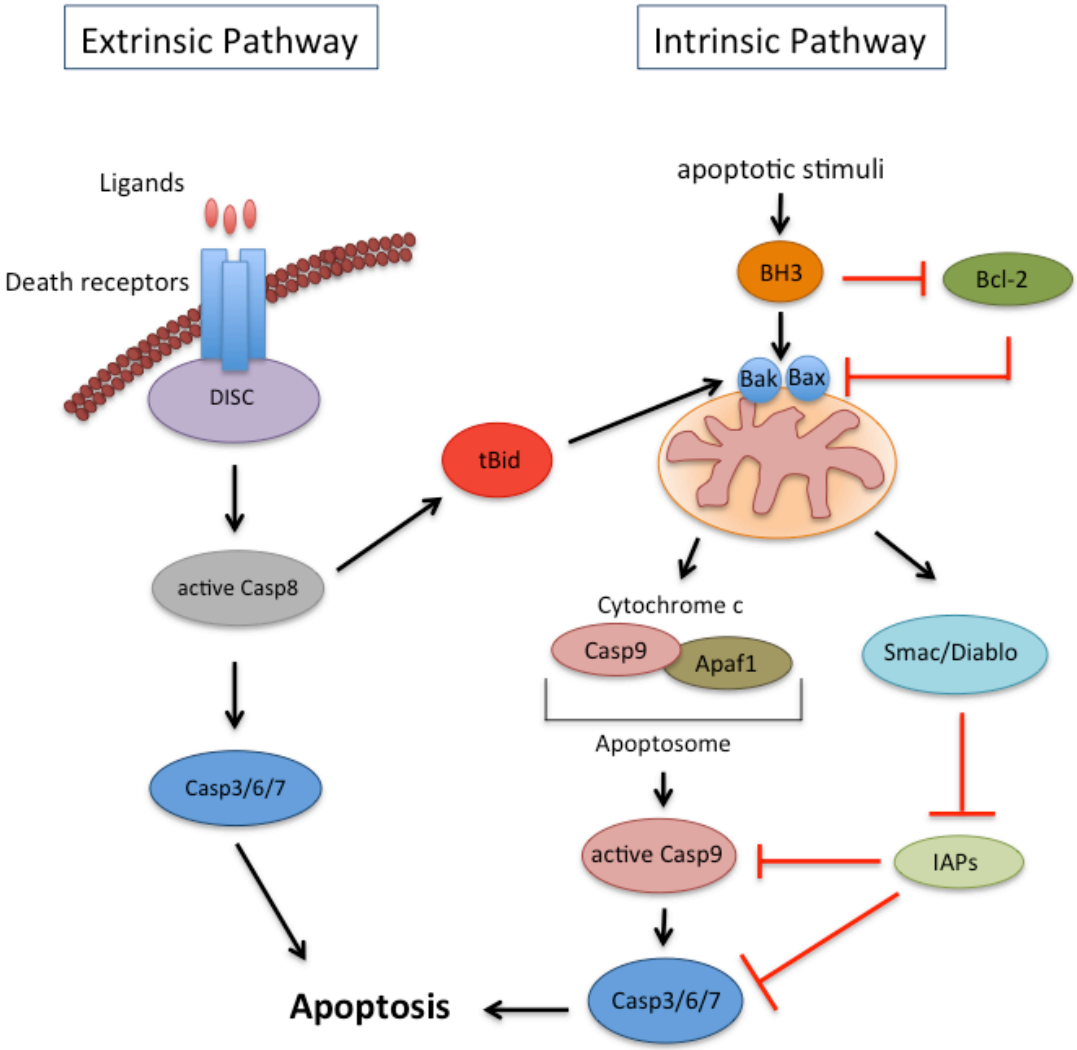

Figure 1-7: Simplified apoptotic signalling in mammals
Apoptosis can be induced through the extrinsic or intrinsic pathways. Extrinsic apoptosis signalling is induced by the interaction of death ligands (FasL, TNF-α, TRAIL etc.) with their corresponding transmembrane receptors. This ligation leads to the formation of a Death-inducing signalling complex (DISC), which will lead to the activation of the initiator caspase-8 and the activation of the executioner Caspases 3, 6 and 7 resulting in apoptosis. Low levels of caspase-8 can also lead to the activation of Bak and Bax through cleavage of Bid to the truncated protein tBid. Intrinsic apoptosis signalling on the other hand is initiated by a variety of stimuli coming from within the cell, like DNA damage or chemotherapy. These stimuli lead to the activation of pro-apoptotic BH3 proteins. BH3 proteins will promote a conformational shift in Bak and Bax leading to their association with the mitochondrial membrane. This leads to the release of Cytochrome c during a process called mitochondrial outer membrane permeabilisation (MOMP). This leads to the formation of the apoptosome followed by activation of Caspase9 and Caspase 3, 6 and 7, which execute apoptosis. Alternatively, the pro-apoptotic mitochondrial proteins Smac/Diablo can be released into the cytosol during apoptotic stimuli, where they interact with inhibitors of apoptosis proteins (IAPs) leading to the activation of Caspases and therefore apoptosis.

1.5.1.1 Inhibition of apoptosis by adenovirus type 5

As described above, maintaining the balance between cell death and cell division is a tightly regulated process that is of great importance in multicellular organisms during development and homeostasis. In addition, besides its role in these processes, apoptosis plays a functional role as an antiviral defence mechanism by limiting the replication of virus-infected cells. Therefore, viruses have to overcome host-induced cell death after infection to ensure the maturation of virions.

One of the anti-apoptotic proteins expressed by adenoviruses is E1B-19K. E1B-19K is a BCL-2 homologue that blocks TNF-α-mediated death signalling (Perez and White 2000). It can associate with Bax (Sundararajan and White 2001) and Bak (Subramanian et al. 2015) to prevent MOMP and the release of cytochrome c into the cytoplasm and therefore prevent apoptosis. E1B-55K is another anti-apoptotic protein encoded by adenovirus. E1B-55K can block apoptosis by binding directly to the N-terminal activation domain of p53, by blocking interactions between p53 and cellular co-activators of transcription and by blocking its interaction with MDM2. Besides this function, E1B-55K can also associate with E4orf6 and other cellular proteins to form an ubiquitin ligase complex, which can bind p53 leading to p53 polyubiquitination and resulting in proteosomal degradation of p53 (Coffin 1996, Schwartz et al. 2008). E4orf6 is another viral protein that is able to interact directly with, and inhibit, p53. However, besides inhibiting p53, E4orf6 is also able to bind to p73, which is able to activate transcription through p53 binding sites. Therefore E4orf6 is able to block the function of both p53 and p73 (Coffin 1996). Another viral protein involved in inhibiting apoptosis is the receptor internalization and degradation (RID) complex, which consists of the E3 proteins 10.4K and 14.5K. They are able to form a complex in the plasma membrane and have been shown to down-regulate surface levels of tumour necrosis factor receptor 1 (TNFR1) (Chin and Horwitz 2006, Chin and Horwitz 2005, Fessler, Chin and Horwitz 2004) and to inhibit NF-κB activation (Fessler et al. 2004). Besides RID being able to down-regulate TNFR1, it can also down-regulate FAS (Chin and Horwitz 2005, Zanardi et al. 2003, Shisler et al. 1997, Elsing and Burgert 1998, Tollefson et al. 1998) surface expression, TNF-related apoptosis-inducing ligand receptor 1 (Tollefson et al. 2001, Lichtenstein et al. 2002) and 2 (Benedict et al. 2001, Lichtenstein et

al. 2004) (TRAIL1 and 2) and mediates internalization of epidermal growth factor (EGFR) (Zanardi et al. 2003, Tollefson et al. 1991, Carlin et al. 1989). Finally, the adenovirus E3-14.7K protein is also able to inhibit TNF-induced apoptosis, by blocking ligand-induced TNFR1 internalisation by inhibiting the endocytotic machinery (Schneider-Brachert et al. 2006).

A summary of proteins expressed by adenoviruses that interfere with the apoptotic machinery is shown in table 5.

Table 5: Inhibition of apoptosis by adenovirus
Table describes viral proteins involved in inhibiting host-induced apoptotic cell death, their host target proteins and their mode of action.

Viral Protein	Target	Mode of action	References
E1B-19K	BAX, BAK	Anti-apoptotic MCL-1 viral mimic	(Subramanian et al. 2015, Tarakanova and Wold 2010, Lomonosova, Subramanian and Chinnadurai 2005, Lomonosova, Subramanian and Chinnadurai 2002, Cuconati et al. 2002, Sundararajan et al. 2001, Tollefson et al. 2001, Sundararajan and White 2001, Perez and White 1998, Han, Sabbatini and White 1996b, Debbas and White 1993)
E1B-55K	p53	Binds p53 and directs p53 poly-ubiquitination	(Schreiner et al. 2010, BenJilani et al. 2002, Maheswaran et al. 1998, Debbas and White 1993)
E1B-55K & E4orf6	p53	Proteosomal degradation	(Coffin 1996, Schwartz et al. 2008)
RIDα/β (E3A 10.4K/14. 5K)	TNFR1, FAS, TRAIL-R1/2, EGFR	Down-regulation of cell surface receptors	(Chin and Horwitz 2006, Chin and Horwitz 2005, Fessler et al. 2004, Zanardi et al. 2003, Shisler et al. 1997, Elsing and Burgert 1998, Tollefson et al. 1998, Benedict et al. 2001, Tollefson et al. 2001, Lichtenstein et al. 2002, Tollefson et al. 1991, Carlin et al. 1989, Lichtenstein et al. 2004)
E3-14.7K	TNFR1	Inhibits internalization of TNFR1	(Ranheim et al. 1993, Schneider-Brachert et al. 2006)
E4orf6	p53, p73	Antagonizes p53 and p73 function	(Coffin 1996, Luo et al. 2007)

1.5.1.2 *dl*922-947 and apoptosis

It has been shown in previous work that ovarian cancer cells infected with oncolytic adenoviral mutants (E.g. *dl*922-947 and *dl*CR2) undergo cell death that is not characterized by the features of classical apoptosis (Baird et al. 2008). In their investigation, the host lab showed that infecting IGROV1 and OVCAR4 cells with *dl*922-947 showed no detectable activation of caspase-3 after 72 hrs of infection in comparison to cells treated with the apoptosis inducer cisplatin. Addition of the pan-caspase inhibitor Z.VAD.fmk to *dl*922-947-infected cells showed no effect on virus-induced cytotoxicity. Western blotting of infected cells showed minor cleavage of both caspase-3 and poly-ADP ribose polymerase (PARP) cleavage during infection. Similarly, there was only trivial phospatidylserine (PS) exposure, and only at late time points, while 75% of cisplatin treated cells were Annexin V-positive after 72 hrs.

Next they investigated the role of mitochondria in *dl*922-947 induced cell death, since mitochondria play a pivotal role in the intrinsic apoptotic pathway. They showed that overexpression of the anti-apoptotic protein BCL-2 had no effect on viral cytotoxicity. They also showed that during *dl*922-947 infection no increase in cytochrome c release was observed. Even the addition of cyclosporine A, which prevents the mitochondrial permeability transition pore from opening and thus releasing cytochrome c into the cytoplasm, showed no effect *dl*922-947 induced death. Besides the published data on *dl*922-947 Abou El Hassan *et al*. showed, using the E1A CR2-deleted viruses, Ad5-Δ24, with E3 region deleted, and the infectivity-enhanced Ad5-Δ24RGD in which E3 was intact, that the p53-Bax apoptotic pathway was not involved in virus cytotoxicity and that inhibiting caspases by overexpressing the X-linked inhibitor of apoptosis or by treating cell with Z.VAD.fmk did not inhibit adenovirus-induced cell death, leading to their conclusion that adenoviruses trigger a non-apoptotic cell death (Abou El Hassan et al. 2004). The results presented in both studies show that cells that infected with E1A CR2-deleted adenoviruses do not undergo classical apoptosis as previously thought.

1.5.2 Type II cell death: Autophagy

Autophagy (Macroautophagy) is a catabolic process of self-degradation of cellular components mediated by the lysosomal machinery. It plays an important role in response to starvation and stress, as well as in development, cell death, aging, immunity and cancer. During starvation autophagy can promote cell survival by the production of amino acids and mitochondrial substrates. Besides its association with survival, it has been suggested that autophagy may also function in cell death since autophagic death is activated in cells lacking Bax and Bak or cells that overexpress Bcl-2 or BCL-x_L upon cytotoxic treatment (Shimizu et al. 2004). We also know that autophagy is a type programmed cell death (PCD) that is required during the development of diverse animal groups, like amphibians and insects (Baehrecke 2003). Programmed autophagic cell death occurs when larval tissues are replaced with adult tissues, for example, salivary glands, showing its important role in physiological cell death. Therefore, defects in autophagy may play critical roles in cancer, by eliminating defective organelles (E.g. mitochodonria) which otherwise can lead to genomic instability, the production of ROS and inflammation which ultimately results in an increase in tumorigenesis (Degenhardt et al. 2006). The process of autophagy is divided into distinct steps: induction, cargo recognition and selection, vesicle formation, autophagosome-vacuole fusion and breakdown of the cargo and the release of the products into the cytosol. The autophagy pathway in mammals is further described in detail in figure 1-8.

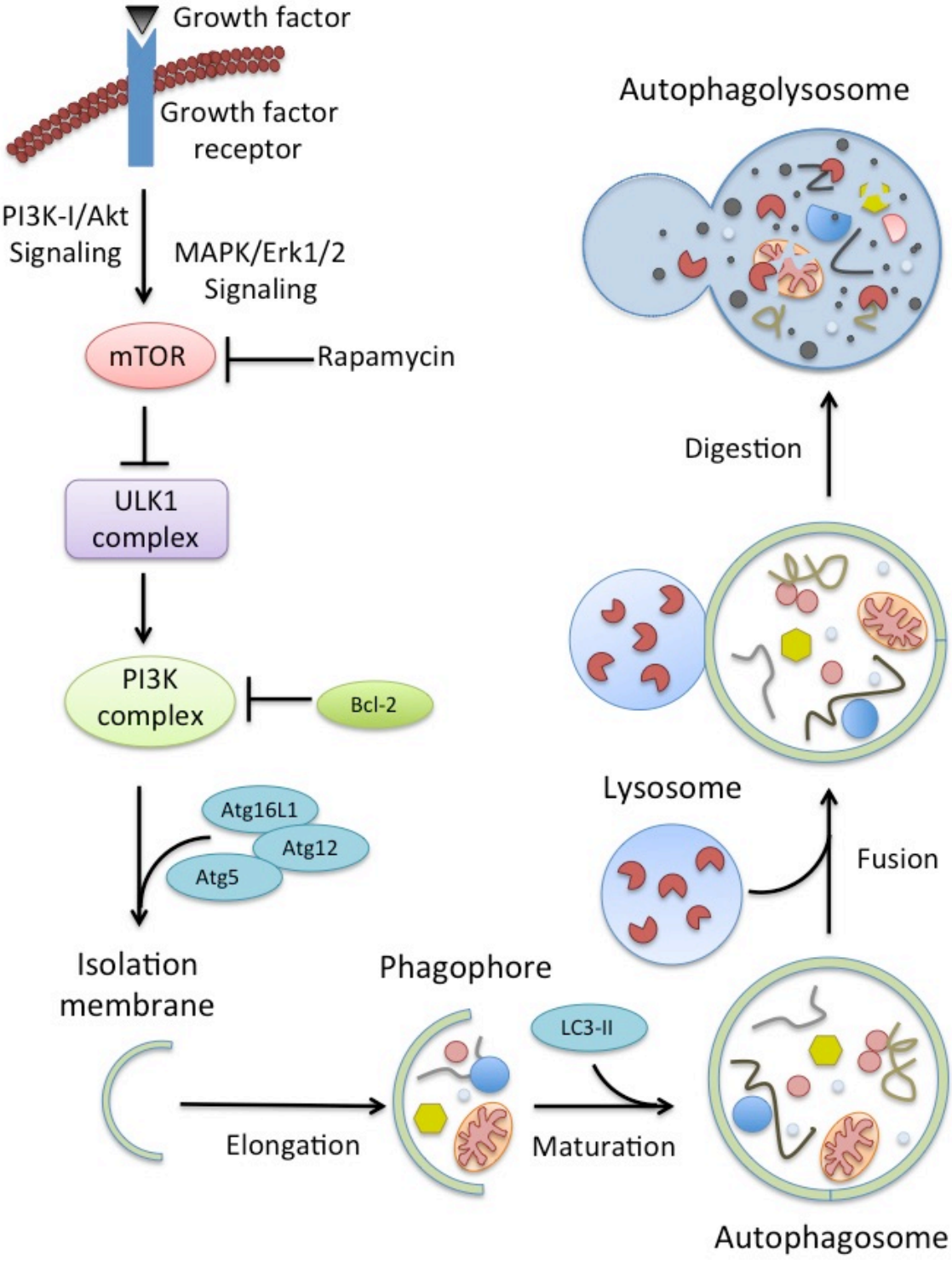

Figure 1-8: Autophagy in mammals
When growth factors are available, autophagy is inhibited by mammalian target of rapamycin (mTOR), but upon growth factor withdrawal, pathogen infection or amino acid starvation, mTOR is inhibited leading to the formation of the ULK complex (consisting of ULK1/2, autophagy-related gene (ATG)13, ATG101 and FIP200) and ATG9L (ATG9L1/2) and the recruitment of the phosphatidylinositide 3-kinases (PI3K) complex consisting of ATG14L, VPS34, beclin-1 and VSP15. The ATG16L1 complex consisting of ATG16L1, ATG5 and ATG12 will then localize to the isolation membrane, which will dissociate again upon autophagosome formation. Upon autophagy induction, cytosolic LC3-I is cleaved to LC3-II and conjugated to phoshatidylethanolamine (PE) at the phagophore. During fusion of the autophagosome with the lysosome the content will be digested by lysosomal proteases.

1.5.2.1 Autophagy and Adenovirus

In 2006 Ito *et al*. suggested that conditionally replicating adenovirus induces autophagic cell death in malignant glioma cells (Ito et al. 2006). They used the conditionally replicating virus hTERT-Ad (in which the adenoviral E1A promoter is replaced with a 255-bp hTERT promoter fragment (Wirth et al. 2003)) and showed by using electron microscopy that U87-MG cells infected with hTERT-Ad exhibited autophagic and empty vacuoles, which are autophagic features. They further observed an increase in acidic vesicular organelles and as well as an increase in the ratio of LC3-II compared to LC3-I, indicating that hTERT-Ad induces autophagy in malignant cells. Addition of 3-Methyladenine (3-MA), a type III Phosphatidylinositol 3-kinases (PI3K) inhibitor that blocks autophagosome formation, showed an increase in cell viability in U373-MG cells infected with hTERT-Ad and suppressed the formation of acidic vesicles. Experiments using HeLa and PC3 cells showed the same results, suggesting that autophagy is a common feature of cells infected with hTERT-Ad and that cells infected with hTERT-Ad undergo autophagic cell death.

1.5.2.2 *dl*922-947 and Autophagy

As mentioned above, recent research by the host lab (SK Baird *et al*. 2008) showed that ovarian cancer cells infected with *dl*922-947 undergo a novel mode of programmed cell death in ovarian cancer. Lysosomes play an important role during autophagy. After fusion of the lysosome with the autophagosome its cargo will be digested by the proteases inside the lysosome. Sarah Baird examined the involvement of autophagy in *dl*922-947 induced cell death by examining cells that were stained with monodansylcadaverine (MDC) under a transmission electron microscope (TEM). MDC is an autofluorescent dye that accumulates in autophagic vacuoles through ion trapping and lipid interactions. She showed that the number of autophagosomes increased during *dl*922-947 and the formation of punctate LC3 staining in IGROV1 cells co-infected with *dl*922-947 and Ad GFP-LC3. Addition of 3-MA, during *dl*922-947 infection, lead to an augmentation in cell death. The same results were observed when chloroquine (CQ), a lysosomotropic agent that prevents endosomal acidification and therefore inhibits lysosomal enzymes, was used. These results confirmed that autophagy occurs during viral infection in ovarian cancer.

In accordance with our lab findings, in 2012 G Botta *et al*. published an article under the title "Inhibition of autophagy enhances the effects of E1A-defective oncolytic adenovirus *dl*922-947 against glioma cells *in vitro* and *in vivo*" (Botta et al. 2012). When Botta *et al*. infected U87MG and U373MG glioma cells with *dl*922-947 and performed AO staining they observed a MOI-dependent increase in fluorescence. Further, western blotting showed an increase in LC3-I to LC3-II conversion in cells infected with *dl*922-947. Next they infected U373 GFP-LC3 cells with *dl*922-947, which resulted in a localized punctate pattern indicating that LC3-II is recruited to the autophagosome. Following this they examined the levels of p62/SQSTM1, an autophagy specific substrate, which shows a decrease in p62 protein levels upon autophagy. Cells infected with *dl*922-947 showed decreased protein levels of p62 showing that autophagy occurs during *dl*922-947-infection. When cells were then infected with *dl*922-947 and then either treated with 3-MA or CQ, an increase in virus-induced cytotoxicity was observed, which was further observed in cell clones expressing Atg5 shRNA. Using a mouse xenograft model where tumours were infected with *dl*922-947 and treated with CQ or not, they observed a significant reduction in tumour volume of mice treated with *dl*922-947 and CQ. Of note here is that Botta *et al*. observed that inhibition of autophagy with CQ lead to caspase-3 activation, which is an indicator of apoptosis-mediated cell death. These results lead to their conclusion that CQ treatment enhances the oncolytic effects of *dl*922-947 in glioma cells in vitro and in vivo.

1.5.3 Type III cell death: Programmed necrosis

Necrosis is a form of caspase-independent cell death that has, until recently, been regarded as a purely accidental and uncontrolled form of death, which is associated with the death of damaged and diseased tissues.

Necrotic cell morphologically is characterized by an increasingly translucent cytoplasm, oncosis (An increase in cell volume, also referred to as swelling), the swelling of organelles, a lack of nuclear disintegration including dilatation of the nuclear membrane and the loss of membrane integrity leading to cytoplasmic leakage (Vanlangenakker, Vanden Berghe and Vandenabeele 2012).

1.5.3.1 Programmed necrosis induced by TNF-α/TNFR1 ligation

In 1988, Scott M. Laster discovered that TNF-α can induce both apoptotic and necrotic forms of cell death depending on the cell type, thereby questioning the purely unregulated nature of necrosis (Laster, Wood and Gooding 1988). Ever since then, accumulating evidence has led to the conclusion that necrosis can indeed be regulated (Scaffidi, Misteli and Bianchi 2002, Zong et al. 2004, Zong and Thompson 2006). A new form of regulated necrosis was introduced, termed programmed necrosis (Necroptosis) (Vandenabeele et al. 2010b). There are several pathways of programmed, regulated necrosis, of which the best known is induced by the ligation of TNF-α and Tumour necrosis factor receptor 1 (TNFR1), which is described in detail in figure 1-9.

The mechanisms of how MLKL induces membrane rupture (Wang et al. 2014a) in the final stages of necrosis have been researched by several groups. Wang *et al*. and Dondelinger *et al*. have shown evidence that MLKL is able to puncture the membrane to form pores. When MLKL becomes phosphorylated it undergoes conformational changes (Murphy et al. 2013), leading to the formation of oligomers and translocation to the plasma membrane (Hildebrand et al. 2014), where its N-terminal domain will directly bind to negatively charged phosphatidylinositol phosphates (PIPs) (Dondelinger et al. 2014, Wang et al. 2014a, Hildebrand et al. 2014, Quarato et al. 2016) and cardiolipin (CL) (Wang et al. 2014a) leading to the formation of pores. Another model suggests that MLKL may regulate ion channels at the plasma membrane during programmed necrosis to mediate osmolysis (Chen et al. 2014, Cai et al. 2014, Xia et al. 2016).

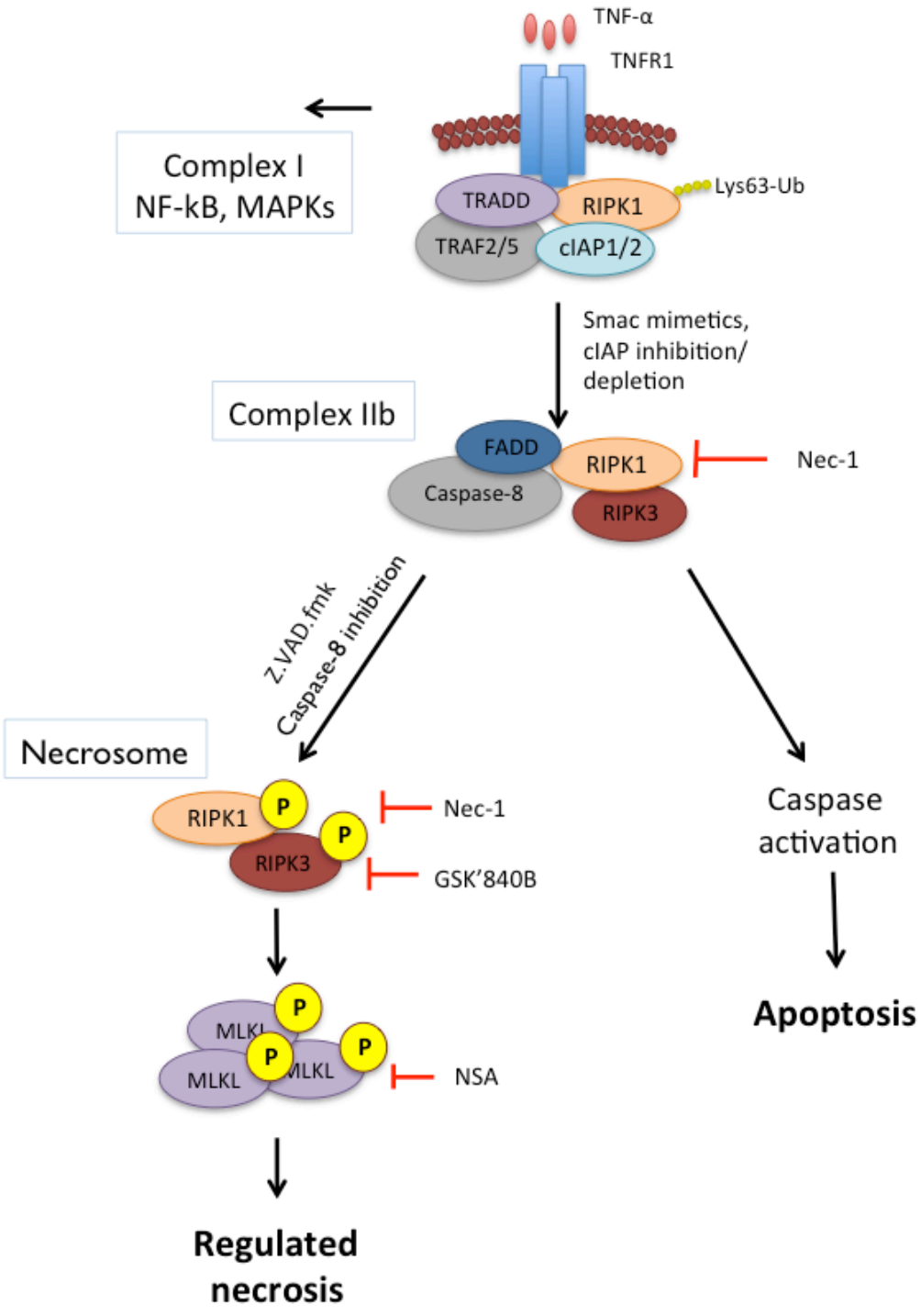

Figure 1-9: TNF-induced programmed necrosis
Tumour necrosis factor receptor 1 (TNFR1) undergoes conformational changes upon (TNF-α) binding, which leads to the assembly of the pro-survival TNFR complex I. This complex consists of the TNF receptor associated death domain (TRADD), receptor-interacting protein1 (RIPK1), cellular inhibitors of apoptosis 1 and 2 (cIAP1/cIAP2), TNF receptor –associated factor 2 (TRAF2) and TRAF5. CIAP1/2 catalyses Lys63-linked polyubiquitylation of RIPK1 at Lys377, which in turn leads to the recruitment of serveral proteins, which initiate nuclear factor-κB (NF-κB) activation, leading to the transcription of cytoprotective genes and to cell survival (Vandenabeele et al. 2010b). When cIAPs are inhibited (by smac mimetics) or depleted, another complex called complex IIb, which consists of RIPK1/3, FAS-associated protein with a death domain (FADD) and caspase8 (Vanlangenakker et al. 2012) forms. This complex can either lead to the activation of Caspases resulting in apoptosis or when caspase 8 is deleted or its activity blocked, programmed necrosis can be induced. The necrosome requires the kinase activity of the proteins RIPK1 and RIPK3, which will interact at their RHIM domains leading to the formation of microfilament-like

structures. Mixed lineage kinase (MLKL) (Sun et al. 2012) then binds to RIPK3 through its C-terminal kinase-like domain, which is phosphorylated at Thr 231/Ser232 by RIPK3 leading to its activation and translocation to the cell membrane, where it is involved in the formation of pores.

1.5.3.2 Programmed necrosis induced by genotoxic stress: The ripoptosome

In 2011, two groups Tenev *et al.* and Feoktistova *et al.* published the discovery of a novel death-inducing complex, called the ripoptosome (Figure 1-10) that forms upon gentoxic stress and/or IAP-depletion (Tenev et al. 2011, Feoktistova et al. 2011). They showed that this complex was able to stimulate caspase-8 mediated apoptosis or caspase-independent necrosis depending on the cellular context. Interestingly, this complex is able to form independently of death ligands (TNF-α) and the mitochondrial pathway. Further, they showed that RIPK1 kinase activity is required for the assembly of the ripotosome as well as RIP-mediated induction of apoptosis and necroptosis.

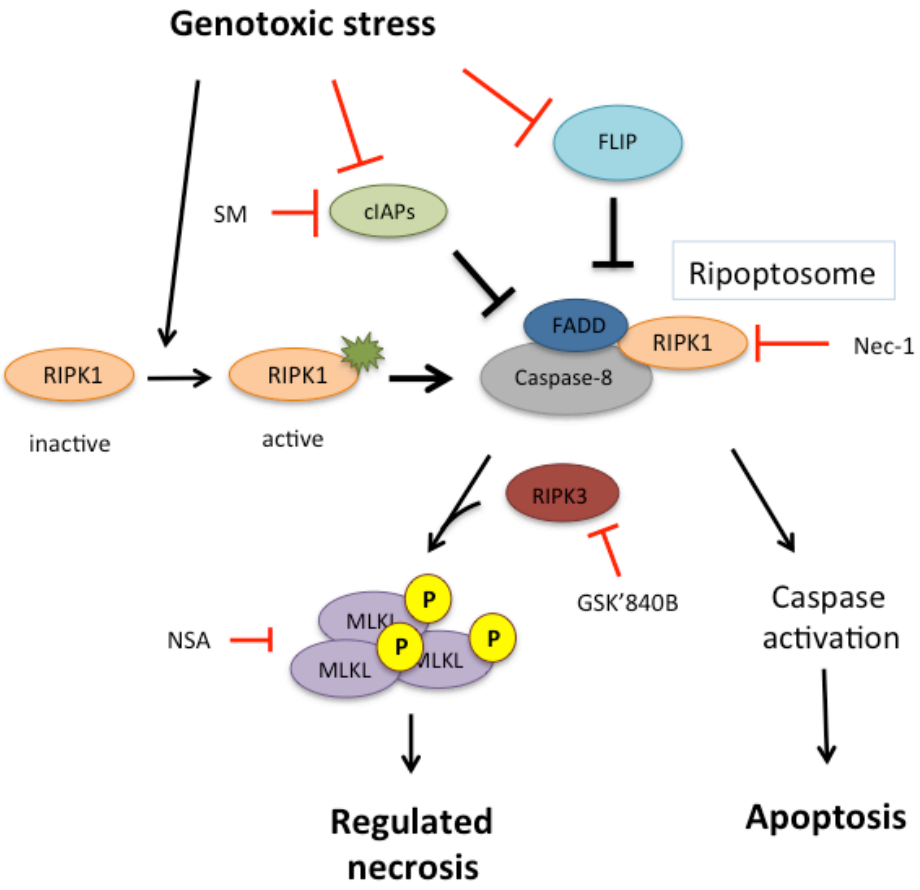

Figure 1-10: Formation of the ripoptosome
Under baseline conditions RIPK1 is in a closed (Inactive) conformation but upon genotoxic stress or cIAP depletion, RIPK1 changes into an active conformation, which allows its association with FADD and Caspase-8 to form the ripoptosome. FLIP and cIAP negatively regulate the formation of this complex. Depending on the cellular context, if caspase-8 is available, this complex leads to the induction of apoptosis or if caspase-8 is blocked or depleted leading to regulated necrosis, through the interaction of rIPK1 and RIPK3 and phosphorylation of MLKL.

1.5.3.3 Programmed necrosis induced by Toll-like receptors

Toll-like receptors are well known for their involvement in mediating inflammation and innate immunity by detecting various microbial patterns (Medzhitov 2009), but it wasn't until recently that an intricate connection between cell death and inflammation was discovered. To limit infection, the host needs to eliminate cells that are carrying infections, while at the same time it needs to warn the neighbouring cells and immune system to avoid further spread. Therefore it is not surprising that Toll-like receptors (TLRs) can despite mediating inflammation also mediate cell death (Silke, Rickard and Gerlic 2015, Han, Zhong and Zhang 2011a, Blander 2014) as depicted in figure 1-11.

Caspase-8, which is well known for inducing apoptosis by TNF-α/TNFR1 ligation is also central for TLR3 and TLR4 induced apoptosis. Interestingly, deletion/deficiency of caspase-8 or mutant caspase-8 expression has shown to lead to systemic inflammation (Wallach et al. 2014, Kang et al. 2013, Kovalenko et al. 2009) and necroptosis (Gunther et al. 2011), showing that caspase-8 is an important suppressor of inflammation *in vivo,* as well as the intricate involvement of caspase-8 in cell death and inflammatory signalling pathways.

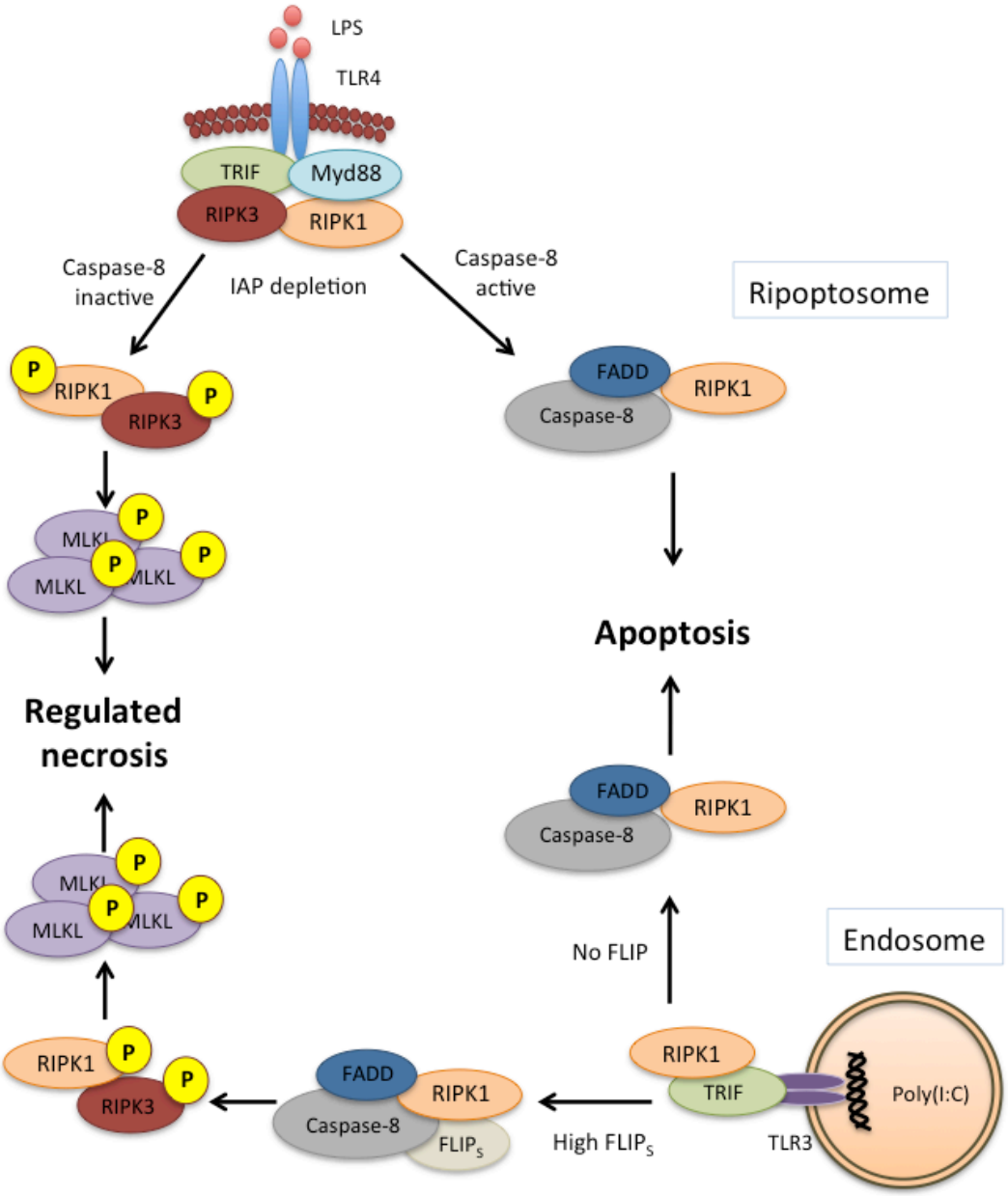

Figure 1-11: Necroptosis induced by TLR ligation
Upon recognition of lipopolysaccharide (LPS) by TLR4 and IAP depletion, a complex consisting of TRIF, Myd88, RIPK1 and RIPK3 forms (Kaiser et al. 2013a). If caspase-8 is active a complex called the ripoptosome forms leading to apoptosis. If caspase-8 is inactive, the necrosome consisting of RIPK1 and RIPK3 forms leading to the activation of MLKL and the induction of regulated necrosis(Lawlor et al. 2015, Silke et al. 2015, Dondelinger et al. 2016). Binding of TLR3 with poly(I:C) the TIR domain-containing adaptor protein inducing IFNβ (TRIF), the ripoptosome is recruited. The presence of FLICE-like inhibitory protein (FLIP) isoforms in the ripoptosome results in different outcomes. The absence of FLIP leads to induction of apoptosis, while high levels of $FLIP_S$ in the ripoptosome leads to recruitment of RIPK3 and RIPK3/RIPK1 interaction leading to the activation of MLKL and necrosis (Blander 2014, Dondelinger et al. 2016).

1.5.3.4 Other necrosis triggers

Besides the above-discussed necrotic pathways, there are further triggers of necrotic cell death. Over the years many different necrotic triggers have been identified; those include but are not limited to FASL (Holler et al. 2000b), TNF-related apoptosis-inducing ligand (TRAIL) (Holler et al. 2000a), TNF-related weak inducer of apoptosis (TWEAK) (Wilson and Browning 2002), stimulation of T cell receptor (TCR)(Ch'en et al. 2008), pathogen-associated molecular patterns (PAMPS) (Kalai et al. 2002), interferons (IFN) (Thapa et al. 2013), retinoic acid inducible gene I (RIG-I)-like receptors (Zou et al. 2013) and anticancer drugs like shikonin (Han et al. 2007, Huang et al. 2013) .

1.5.3.5 Viruses and necrosis

Since many viruses, including adenovirus, encode suppressors of cell death (e.g. viral caspase 8 inhibitors), being able to execute both apoptotic and necrotic cell death is of benefit for the host's defence. It has been shown now that necrosis can be induced by infection with several different viruses like vaccinia virus (VV) (Cho et al. 2009), murine cytomegalovirus (MCMV) (Upton, Kaiser and Mocarski 2010) and herpes simplex virus type-1 (HSV-1) (Holler et al. 2000b). Some of these even encode inhibitors that prevent the cell from undergoing regulated necrosis.

1.5.3.5.1 Vaccinia virus

Lynsey M Whilding, from the host lab, published data in 2013 showing that vaccinia virus (VV) induces programmed necrosis in ovarian cancer (Whilding et al. 2013). Using TEM she showed that cells infected with VV showed necrotic morphology. She also showed that treatment of cells with the RIPK1 inhibitor necrostatin-1 (Nec-1) upon VV infection significantly increases cell viability (Whilding et al. 2013); furthermore TNF-resistant cells can become sensitized to TNF-induced cell death upon infection with VV. Further, they showed that VV infection lead to the formation of a pro-necrotic complex consisting of RIPK1, RIPK3 and caspase-8 (Cho et al. 2009, Chan et al. 2003, Whilding et al. 2013).

1.5.3.5.2 Murine cytomegalovirus

Cells infected with murine cytomegalovirus (MCMV) show the opposite effects of VV infected cells, as they are resistant to TNF-induced necroptosis due to the MCMV M45 protein-encoded inhibitor of RIP activation (vIRA) (Upton, Kaiser and Mocarski 2012). MCMV vIRA has a RIP homotypic interaction motif (RHIM), which targets RIPK3 and disrupts RIPK3-RIPK1 interactions. The same lab has also shown that DNA-dependent activator of interferon (DAI) can form a RHIM-dependent complex with RIPK3 to mediate virus-induced programmed necrosis, suggesting the existence of another pathway than classical TNF/TNFR necrosis (Upton, Kaiser and Mocarski 2012).

1.5.3.5.3 Herpes simplex virus-1

Another virus that encodes a protein that interacts with the necrotic machinery is Herpes simplex virus-1 (HSV-1). HSV-1 encodes a protein called infected cell protein 6 (ICP6). HSV-1 is a virus that has evolved to successfully infect and replicate within mouse and human cells and therefore deploys two different approaches to block the induction of programmed necrosis. In murine cells ICP6 binds to RIPK1 and RIPK3 through RHIM interactions, leading to the phosphorylation of RIPK3 followed by MLKL phosphorylation and the induction of necroptosis. In this scenario the induction of programmed necrosis limits virus propagation (Wang et al. 2014b, Huang et al. 2015). In human cells on the other hand ICP6 suppresses necroptosis by inhibiting the RHIM-dependent interaction of RIPK1 and RIPK3 (Guo et al. 2015).

1.5.3.5.4 *dl*922-947 and Adenovirus

As stated above, in 2008 Sarah Baird in the host lab showed that ovarian cancer cells infected with oncolytic adenoviral mutants (e.g. *dl*922-947 and *dl*CR2) undergo cell death that is not characterized by the features of classical apoptosis (Baird et al. 2008). Further investigations showed that cell death induced by oncolytic adenoviruses does not rely upon mitochondria, autophagy as well as on cathepsins and lysosomal membrane permeability, leading to the conclusion that a novel mode of programmed cell death must be involved. Using phase-contrast and transmission electron microscopy, they further examined cell morphology, showing that virus-infected cells showed a rounded morphology,

which became more apparent over time with few cells showing membrane blebbing, a marker of apoptotic cell death. They further observed chromatin condensation and dilation of membranous organelles like mitochondria, Golgi apparatus and the endoplasmatic reticulum, which are associated with apoptosis. Examination of cellular ATP levels showed an increase following infection rather than a decrease, which is associated with necrosis. In another study by Abou El Hassan *et al*, it was shown that oncolytic adenoviruses kill non-small-cell lung cancer cells via a necrosis-like programmed cell death (Abou El Hassan et al. 2004). In this study, the authors showed that the p53-Bax apoptotic pathway was not involved and that inhibiting caspases by overexpressing the X-linked inhibitor of apoptosis or by treating cell with Z.VAD.fmk did not inhibit adenovirus-induced cell death, leading to their conclusion that adenoviruses trigger a necrosis-like cell death.

1.5.4 Other forms of cell death

Besides the above well-described three major programmed cell death pathways, further cell death mechanisms have been discovered in the recent years.

1.5.4.1 Lysosomal membrane permeabilization

Lysosomes contain many different hydrolases (E.g. phosphatases, proteases and lipases), which take part in the digestion of endocytosed and autophagocytosed material. The cathepsins are the most well studied hydrolases and are categorised by their active site amino acids: cysteine, aspartate and serine. In response to stress lysosomal contents can be released to the cytoplasm by lysosomal-membrane permeabilization (LMP) (Kroemer and Jaattela 2005, Werneburg et al. 2002). While the massive release of lysosomal hydrolases will lead to necrosis, minor LMP can lead to caspase-dependent apoptosis or alternative caspase-independent cell death. Changes within this pathway, by deregulation or mutations of its components contribute to tumour development and invasion (Chi et al. 2010).

1.5.4.1.1 *dl*922-947 and lysosomal membrane permeabilisation

Sarah Baird showed in 2008 that when IGROV1 or OVCAR4 cells were infected with *dl*922-947 and additionally treated with E64, an irreversible cysteine protease inhibitor, minimal effects were observed on virus mediated cell death. The same was observed when the aspartic acid protease inhibitor pepstatin A was used. The cysteine protease inhibitor E64 is known to inhibit several cysteine proteases like cathepsin B and L as well as calpain, while the aspartic acid protease inhibitor pepstatin A inhibits cathepsin D. Since inhibiting the main lysosomal proteases Cathepsin B and D showed no effect on cell survival, lysosomal cell death was excluded in the involvement of *dl*922-947 mediated cell death. Further experiments with acridine orange showed that virus infection caused lysosomes to stabilize instead of undergoing lysosomal membrane permeabilization (Baird et al. 2008).

1.6 Aim of the project

Oncolytic viruses have shown promise as a cancer therapy in several human cancers in pre-clinical as well as clinical research, but little is known about how they induce cell death in human cancers. The aim of this project was to investigate how oncolytic adenoviruses, specifically *dl*922-947, induce cell death in human ovarian cancer. This goal was further divided into two specific research aims:

1.) To investigate programmed necrosis pathways involved in *dl*922-947-induced cell death in ovarian cancer.

2.) To investigate whether anti-tumour efficacy can be increased, by augmenting programmed necrosis in *dl*922-947-infected cells and tumours.

The overall goal of this research was aimed at identifying the mechanisms of adenovirus-induced cell death in ovarian cancer, with a special emphasis on programmed necrotic cell death mechanisms.

The long-term aim of this study is to identify targets that can increase oncolytic adenovirus efficacy in lysing tumour cells.

Chapter 2

Materials and Methods

2 Materials and Methods

2.1 Cell lines and culture

Human cell lines were cultured in Dulbecco's Modified Eagle Medium (DMEM) (Gibco by Life Technologies, UK) with 10% heat-inactivated foetal bovine serum (FBS) (Gibco by Life technologies, UK), 2mM L-Glutamine (Gibco by Life Technologies, UK), 100 units/mL penicillin and 100µg/mL streptomycin (Gibco by Life Technologies, UK) while human primary cells were cultured in Roswell Park Memorial Institute medium (RPMI) supplemented with 25% autologous ascitic fluid, 2mM L-Glutamine (Gibco by Life Technologies, UK), 100 units/mL penicillin and 100µg/mL streptomycin (Gibco by Life Technologies, UK). All cell lines were maintained in a 37ºC humidified incubator with 5% CO_2 (Galaxy 170R, Eppendorf) and were routinely passaged with 0.05% trypsin-EDTA (Gibco by Life Technologies, UK) every time they reached 80% confluency. All cell lines were verified by Short Tandem Repeat profiling (STR) at the Cancer Research UK Beatson Institute using the Promega GenePrint 10 system (Promega, UK), which is a STR multiplex assay that amplifies 9 tetranucleotide repeat loci and the Amelogenin gender determining marker. Cell lines were tested for mycoplasma every second week. Cell lines were cultured for 10 passages and removed afterwards, while new aliquots were resurrected from liquid nitrogen. For long time storage, cells were trypsinized and pelleted by centrifugation in a Sigma 3-16KL centrifuge (Sigma, GER) and the resulting cell pellet was resuspended in FBS containing 10% dimethyl sulphoxide (DMSO) (Fisher Scientific, UK). Cells were transferred into a Freezing Container (Nalgene, UK) and left for overnight storage at -80 degrees before transferring into liquid nitrogen.

The human cervical cancer cell line HeLa were obtained from CRUK Cell Services from Clare Hall. JH293 and 293 cells were kindly provided by Dr Yaohe Wang (Barts Cancer Institute, London, UK). The human ovarian cancer cell line IGROV1 and OVCAR4 were obtained from the National Cancer Institute (NCI, Frederick, MA, USA), and TOV21G cells were obtained from Fran Balkwill (Barts Cancer Institute, London, UK). The embryonic kidney cell lines 293T and Phoenix-AMPHO cells as well as the human colorectal cancer cell line HT-29 were kindly provided by Dr. Stephen Tait (University of Glasgow, UK).

Human primary cells were obtained from patients with ovarian cancer, who were drained of ascites for diagnostic cytology and/or symptom relief. 200 mL of ascites were transferred into a 250mL Corning centrifuge tube (Corning Incorporated, USA) and spun at 2500 revolutions per minute (rpm) for 15 minutes at room temperature (RT). The supernatant (autologous fluid) was removed, aliquoted into 50mL falcon tubes (Corning Incorporated, USA) and stored -80ºC for later use. The cell pellet was incubated for 10 minutes in 5mL red blood cell lysis buffer (Sigma-Aldrich, USA) and then transferred to a 50mL tube, topped up with 30mL Phosphate-buffered saline (PBS) (Sigma-Aldrich, USA) and spun at 2000 rpm for 10 minutes. The supernatant was removed and the pellet gently resuspended in RPMI medium with 25% autologous fluid in a T75 flask (Corning, UK).

2.2 Adenovirus preparation

2.2.1 Generating seed stock

293 cells were plated on a 150mm plate (Corning, UK). When cells reached 80-90% confluency cells were infected with 100-200µL of concentrated virus stock. When cytopathic effect (Cpe) was evident, cells were pipetted up and down until all were detached. The cells and medium were collected and snap-frozen in liquid nitrogen. Afterwards cells were freeze/thawed in liquid nitrogen/37ºC waterbath three times. The seed stock was stored at -70ºC immediately.

2.2.2 Bulk preparation

293 cells were plated onto 20 x 150mm plates. When cells reached 80% confluency, the seed stock was defrosted at 37ºC and spun at 2000 rpm for 15 minutes to pellet cell debris. Medium was carefully removed and 200mL of serum-free DMEM were added. 1mL of virus seed stock and 10mL growth medium were added to each 150mm plate. After 48-72 hours, when full cpe was evident, cells and medium were harvested, transferred to 6 x 250mL Sorvall centrifuge bottles (Corning, UK), and spun at 2000rpm for 15 minutes. Medium was aspirated, each pellet resuspended in 4.3mL 0.1M Tris pH 8.0 and the total transferred to a 50mL Falcon tube (Corning, UK). The tube was snap-frozen in liquid nitrogen and freeze/thawed three times and stored at -70ºC.

2.2.3 Caesium Chloride (CsCl) purification

Virus stock was defrosted at 37ºC, spun at 4500rpm for 15 minutes and supernatant transferred to a fresh tube. A CsCl gradient was achieved by adding 11.4mL 1.25g/mL (Buoyant density) CsCl to a 30mL Ultraclear Beckman tube (Beckman Coulter, UK) followed by the addition of 7.6ml 1.4g/mL CsCl underneath the 1.25g/mL layer without disturbing the interface. The viral supernatant was added on top of the CsCl double layer and spun at 25,000rpm for 2 hours at 15ºC in an Optima XPN-90 Ultracentrifuge (Beckman Coulter, USA) using a SW32 Ti rotor. After centrifugation three distinctive layers were visible in the tube. The top layer contains cell debris, the second layer contains empty virions and the lowest layer contains the properly packaged virions.

The layer containing the packaged virions was removed by puncturing the tube with a 5mL syringe (Beckton, Dickinson and Company, UK) using a 21-gauge needle (Beckton, Dickinson and Company, UK). The layer was aspirated off while avoiding contamination from the other layers. The virus was divided between 2 x 5mL Beckman tubes (Beckman Coulter, UK) followed by the addition of 1.35g/mL CsCl. The virus was spun at 40,000rpm overnight at 15ºC using a SW55 Ti rotor. After centrifugation a single band of virus should be visible. Using a syringe and needle the virus was aspirated and transferred to a new falcon tube.

2.2.4 Dialysis

2 mL TSG buffer (TSG buffer solution A: 150mM NaCl, 1mM Na_2HPO_4, 5mM KCl, 30mM Tris base and 90mL distilled water at pH 7.4. TSG buffer solution B: 200mM $MgCl_2$, 180mM $CaCl_2$ and 10mL distilled water. 90mL of solution A was added to 450µL of solution B and 38.5 mL glycerol making TSG buffer) was added to the virus and inserted into a Slide-A-Lyzer dialysis cassette (Thermo Scientific, UK) using Slide-A-Lyzer 20mL syringe and 18 gauge needle accessories (Thermo Scientific, UK). The virus was dialyzed in the cold room for 24 hours in 2 litres of dialysis buffer (10mM Tris pH 7.4, 1mM $MgCl_2$, 150mM NaCl and 10% glycerol) with gentle stirring. After overnight dialysis, the virus was removed from the dialysis cassette, aliquoted and stored at -70ºC.

2.2.5 Measuring particle count

To measure the particle count, 100µL virus stock were added to 100µL 2x adenoviral lysis buffer (1% SDS, 0.04M Tris-Cl) and heated for 10 minutes at 55°C. 300µL distilled water were added and the optical density (OD) at 260nm was read on a BioPhotometer D30 (Eppendorf, UK).

The particle count per mL is calculated the following (Mittereder, March and Trapnell 1996):

$$\frac{\mathrm{OD}_{260} \text{ x dilution factor}}{9.09 \text{ x} 10^{-13}}$$

2.2.6 $TCID_{50}$

Production of infectious virus progeny was determined by tissue culture infectious dose $(TCID)_{50}$ assay. Tumour cells were plated in triplicate onto a 6 well plate at a density of $1x10^5$ per well. The following day, they were infected with *dl*922-947 at 10 pfu/cell in 1mL serum-free medium. After 2 hours cells were re-fed with normal growth medium. To measure intracellular virus production, cells were harvested at desired time points (24-72h post-infection) by aspirating the medium, washing cells twice in cold 0.1M Tris pH 8.0 and scraping into 0.5mL 0.1M Tris pH 8.0. The Tris, containing the cells, was transferred into a sterile Eppendorf tube and placed on ice. Following this samples were freeze/thawed (Liquid nitrogen/37°C) three times. At this point samples were centrifuged at 13,000 rpm for 5 minutes and the supernatants were either frozen at -80°C or kept on ice for use straight away.

JH293 cells were plated in a 96 well plate at a density of $1x10^4$ cells/per well in 180µL of normal growth medium the day before the assay, with at least 4 plates per condition.

The virus sample was defrosted on ice and serial dilutions were prepared ranging from 10^{-1}-10^{-6} depending on the cell line and conditions used. The first row of each 96 well plate was used as a negative control. Starting from the second row 20µL of the diluted virus stock was added per well. Using a multichannel pipette 20µL were removed from the second row and added to the third row while

pipetting up and down to ensure mixing. This was repeated throughout the whole plate so that the samples were diluted 1:10 between the rows. Plates were incubated at 37ºC for 10 to 11 days at which point the number of wells displaying cytopathic effect at each dilution was counted.

The following calculation was used to determine the $TCID_{50}$ value:

$TCID_{50}$ = A-D (S-0.5)

A= Log of the highest dilution showing CPE in more than 50% of the wells
D= Log of the dilution factor
S= ratio of the number of wells per row with CPE : number without CPE

This yields $TCID_{50}$ for 20µL virus, and is divided by 0.02 to give $TCID_{50}$/mL. This is then converted to pfu/mL based upon Poisson distribution using the following:

$P(o)= e^{(-m)}$

P(o)= proportion of negative wells in a 96 well plate
m= mean number of infectious units per volume (PFU/mL)

For any titre expressed as a $TCID_{50}$: P(o)= 0.5,
And therefore $e^{(-m)}= 0.5$
m= -ln0.5≈ 0.7

Because $TCID_{50}$ overestimated viral titre by 0.7 log compared to plaque assay, $TCID_{50}$ is converted to pfu/mL using the following formula:

$Pfu/mL = 10^{n-0.7}$
Where n = log$TCID_{50}$/mL

This titration technique is only valid if the lowest dilution gives ≥50% CPE, the highest dilution gives ≤50% CPE and the negative control shows no CPE in any well.

2.3 Cell Survival Assays

2.3.1 MTT assay

Cell death was measured using MTT (Sigma, UK) assay (Mosmann 1983). MTT is a colorimetric assay, which measures the metabolic activity of cells. It is a tetrazole of yellow colour, which is reduced to non-water-soluble formazan by NAD(P)H-dependent cellular oxidoreductase enzymes in viable cells. Since formazan is non-water-soluble it must be dissolved in acidified isopropanol or other solvents before further analysis. In the experiments described below dimethyl sulfoxide (DMSO) (Fisher chemical, UK) was used as solvent.

For MTT assay cells were plated on a 24 well plate at a density of $1x10^4$ cells/well. Cells were either infected with virus or treated with drugs or/and inhibitors. Cell proliferation was measured by adding MTT stock solution (5mg/mL) to each well equal to one tenth of the culture volume. Cells were incubated for 3 hours with MTT before the medium was removed and DMSO added to dissolve the formazan crystals. The plates were read on an Infinite M200 Pro (Tecanplate, CH) reader at 560nm.

2.3.2 Sulphorhodamine B assay

Cells were plated in a 24 well plate at a density of $1x10^4$ cells per well. After desired treatment and incubation, cells were washed once in 1mL PBS and 250µL of 10% trichloroacetic acid (TCA) were added to each well and incubated for 30min at 4ºC. Afterwards the TCA was removed, the plate washed 3 times with 1mL of distilled water and left to dry at room temperature. After plates were dried, 250µL of sulphorhodamine B (0.4%) were added to each well and incubated for 30 min. The sulphorhodamine B was discarded afterwards and the plates washed with 1% acetic acid until running clear. After the plates were dried, 500µL of 10mM Tris pH 9 were added to each well, incubated for 5 min at room temperature and the absorbance measured at 565nm.

2.3.3 Response to TSZ treatment

Cells were tested for their ability to undergo programmed necrosis by treatment with a combination of TNF-α, Smac-mimetic and zVAD-fmk (TSZ). Cells were plated at a density of $1x10^4$ cells per well in a 24 plate in 700µL growth medium per well. The next day cells were treated with 20ng/mL recombinant human TNF-α (PeproTech, UK), 1µM LCL-161 (Smac-mimetic (Chemie Tek, USA)) and 25µM zVAD-fmk (Tocris Bioscience, USA). Cell survival was assessed 24, 48 and 72 hours post treatment as described previously.

2.3.4 Dose response to adenovirus strains

An MTT assay was performed to measure the sensitivity of different cells lines to Adenovirus Ad5WT, Ad5 *dl*922-947, Ad5, *dl*309, Ad11 and Ad35 infection. $1x10^4$ cells were plated per well in a 24 well plate as above. After 24 hours cells were infected in triplicate with 10-fold serial dilution of virus in 500µL serum-free medium. After 2 hours 500µL of growth medium was added to each well. 120 hours post-infection cell survival was analysed as described in 2.4.1. Using GraphPad Prism version 6.0d for Macintosh (GraphPad Software, San Diego, USA) a sigmoidal curve was generated and the half maximal effective concentration (EC_{50}) calculated. The EC_{50} value describes the dose that is required to kill 50% of cells.

2.3.5 Cytotoxicity of Inhibitors

The cytotoxicity of all drugs was assessed prior to treatment to select appropriate concentrations for combination assays. Cytotoxicity of zVAD-fmk, necrostatin-1 (Enzo Life Sciences, CH) and necrosulfonamide (Calbiochem, USA) was assessed by MTT assay. $1x10^4$ cells were plated per well in a 24 well plate as above. The next day cells were treated in triplicate with 10µM, 15µM, 20µM and 25µM zVAD-fmk or 10µM, 30µM, 50µM and 100µM for necrostatin-1 or with 1µM, 3µM, 5µM and 10µM for necrosulfonamide. Cell survival was assessed either 72 or 120 hours post treatment as described in 2.4.1.

For assessing cytotoxicity of RIPK3 inhibitors from GSK concentrations of 0.5µM, 1µM, 3µM and 5µM were tested for GSK2791840B, GSK2399872B and GSK2393843A. Cell survival was assessed as described before.

To assess the cytotoxicity of RIPK1 inhibitors from GSK concentrations of 1nM, 10nM, 100nM and 1μM were used for GSK2791728A, GSK3002963A, GSK2791729A and GSK3002962A. Cell survival was assessed as described before.

2.3.6 Testing the stability of inhibitors

Since treatment of cells with inhibitors occurs over a time period of 72 to 120 hours, experiments to ensure inhibitor stability and performance were performed. Necrostatin-1, necrosulfonamide and the GSK inhibitors were incubated at desired concentration in appropriate growth medium in tissue culture medium for 24, 48, 72, 96 and 120 hours in a tissue culture incubator. TOV21G cells were plated at a density of $1x10^4$ cells per well in a 24 well plate. The next day cells were treated with TSZ and incubated inhibitors as described in 2.4.2 for 24 hours. Cell survival was assessed as described before.

2.3.7 Combination assays of virus, siRNA, drugs and inhibitors

When inhibitors were used in combination with virus, cells were plated and infected with appropriate virus as described in 2.4.3. Two hours after infection the appropriate amount of inhibitor was added to each well. Cell survival was assessed 120 hours post-transfection as described in 2.4.3.

To assess the effect of human TNF-α blocking antibody (R&D Systems, UK) on adenovirus cytotoxicity, 20μg/mL human TNF-α antibody were added 2 hours post-infection. Cell survival was measured 120 hours post-infection as described in 2.4.3.

When siRNA was used in combination with *dl*922-947, cells were transfected with siRNA as described in 2.5.2 and infected with *dl*922-947 in triplicate 24 hours post-transfection. Multiplicity of infection (MOI) was based upon EC_{50} from previous virus dose responses for the relevant cell line. Cell survival was assessed 120 hours post-infection as described previously.

2.4 Protein expression levels

2.4.1 Whole protein lysate preparation

For whole protein lysate preparation, cells were trypsinised and combined with their respective media to inactivate the trypsin. Cells were then pelleted by centrifugation and washed in PBS before they were centrifuged again. After the supernatant was aspirated, cells were lysed on ice for 15 minutes in radioimmunoprecipitation assay (RIPA) buffer (50mM Tris-HCL, pH 7.4, 1% NP-40, 0.5% Sodium-deoxycholate, 0.1% SDS, 150mM NaCl and 2mM EDTA) containing one protease inhibitor cocktail tablet (Roche, GER) per 20mL of RIPA buffer. Samples were then centrifuged at 15,000 rpm for 20 minutes and the supernatant was transferred to clean 1.5mL Eppendorf tubes. The protein concentration was determined using Bio-Rad Protein Assay Dye reagent concentrate (Bio-Rad, UK). BSA (Sigma, UK) standards were prepared by diluting a 1mg/mL BSA stock solution with RIPA buffer. 10µL of BSA standard or sample were added per well in a 96 well plate in triplicates before 200µL of the Bio-Rad Protein Assay Dye working solution (1:5 dilution of the Bio-Rad Protein Assay Dye reagent concentrate in water) were added to each well. The dye was incubated for 10 minutes at room temperature before reading at 595nm. A linear standard curve was created using Microsoft Excel Mac 2011 (Microsoft, USA) by plotting absorbance against concentration for each BSA standard. The resulting formula for this standard curve was used to calculate the protein concentration for each unknown sample.

Samples were prepared in water and 5x Laemmli buffer (300mM Tris-HCL pH 6.8, 10% SDS, 50% Glycerol, 20% ß-mercaptoethanol and 250mg bromphenol blue) to a final protein concentration of 1µg/µL. Samples were denatured at 95ºC for 5 minutes and used immediately or stored at -20ºC.

2.4.2 SDS Gel electrophoresis

Samples were run on a 5% stacking gel (3.7125mL distilled water, 850µL 30% Acrylamide, 312.5µL 2M Tris-HCl pH 6.8, 50µL 10% SDS, 50µL 10% AMPS and 5µL TEMED and 8% resolving gel (5.25mL distilled water, 2.675 mL 30% Acrylamide, 1.875mL 2M Tris-HCl pH 8.8, 100µL 10% SDS, 100µL 10% AMPS and 6µL TEMED). The gels were prepared on a gel cast system (Bio-Rad, UK). The resolving gel mix

was added to the gel cast system and allowed to settle before the stacking gel mix was added, and a comb was inserted. The whole gel was allowed to set a room temperature before it was transferred for storage into a container with distilled water at 4ºC or it was used straight away.

The gel was placed in a Mini-PROTEAN tetra system (Bio-Rad, UK) with 1x Tris-Glycine SDS PAGE running buffer (25mM Tris, 192mM glycine, 0.1% SDS, pH 8.3) and 20µg of protein were loaded per well with the addition of one well containing 7µL of Novex Sharp pre-stained protein standards (Invitrogen, UK).

The separated proteins were then transferred onto a nitrocellulose blotting membrane (GE Healthcare, UK) using the Mini-PROTEAN tetra system by briefly soaking the membrane, gel and blotting paper (Bio-Rad, UK) in transfer buffer (25mM Tris, 192mM glycine, 20% methanol). The stack was assembled as described with one sponge on the bottom followed by one blotting paper, the membrane, the gel, another blotting paper and the sponge. The proteins were then transferred for 1 hour at 100V.

After transfer membranes were stained with Ponceau S solution (AppliChem, GER) to check for successful transfer of proteins onto the membrane. The Ponceau S solution was then washed off with Tris-buffered saline buffer (TBS) (20mM Tris-HCl pH7.4, 500mM NaCl) until clean. The membrane was then blocked in 5% (w/v) non-fat milk (Marvel, IRE) in TBST (TBS with 0.2% Tween-20) for 1 hour at room temperature. Membranes were briefly washed with TBST before incubation with primary antibody overnight at 4ºC or for 1 hour at room temperature with gentle rocking motion. Antibodies and conditions are listed in table 6 and 7. The membranes were washed 3 times for 5 minutes in TBST, followed by incubation in Horseradish Peroxidase (HRP) conjugated secondary antibody in 2% BSA-TBST at room temperature for 1 hour. Afterwards the membranes were washed in TBST a further 3 times for 5 minutes each.

Proteins were detected using either enhanced chemiluminescence (ECL) Western Blotting analysis system or its Prime version (GE Healthcare, UK) and visualized using the Bio-Rad ChemieDoc MP Imaging System (Bio-Rad, UK).

For the detection of other proteins on the same membrane, membranes were stripped for 45 minutes at 50°C in 50-degree warm harsh stripping buffer (20mL 10% SDS, 12.5mL 0.5M Tris-HCl pH 6.8, 67.5mL Distilled water, 0.8 mL ß-mercaptoethanol). The membrane was then washed extensively in running tap water and was re-blocked in 5% milk in TBST for 1 hour before incubation with the next primary antibody.

Table 6: Antibodies used for protein detection by western blotting.

Primary Antibodies	Catalogue number	Condition	Supplier
Adenovirus-2/5 E1A	sc-430	1:1000 in 5% BSA TBST	Santa Cruz Biotechnology, USA
Anti-Adenovirus	ab36851	1:500 in 3% BSA TBST	Abcam, UK
Caspase 8	554002	1:1000 in 5% BSA TBST	BD Pharmingen, UK
Caspase 8	4790	1:300 in 5% BSA TBST	Cell Signaling, USA
FADD	610399	1:1000 in 5% BSA TBST	BD Pharmingen, UK
GAPDH	ab9485	1:1000 in 3% BSA TBST	Abcam, UK
MLKL	MABC604	1:1000 in 3% BSA TBST	Millipore, UK
MLKL	ab184718	1:1000 in 3% BSA TBST	Abcam, UK
Phospho-MLKL	91689	1:1000 in 5% BSA TBST	Cell Signaling, USA
RIPK1	3493	1:1000 in 5% BSA TBST	Cell Signaling, USA
RIPK3	NBP2-24588	1:1000 in 3% BSA TBST	Novous Biologicals, UK
B-Actin	ab6276	1:1000 in 3% BSA TBST	Abcam, UK

Table 7: Secondary Antibodies used for Western Blotting.

Secondary Antibodies	Catalogue number	Condition	Supplier
Goat Anti-Mouse heavy chain	ab97240	1:1000 in 2% BSA TBST	Abcam, UK
Rabbit Anti-Mouse	P026002-2	1:1000 in 2% BSA TBST	Dako, USA
Goat Anti-Rabbit	P044801-2	1:2000 in 2% BSA TBST	Dako, USA
Rabbit Anti-Goat	P044901-2	1:1000 in 2% BSA TBST	Dako, USA
Rabbit Anti-Rat	P0450	1:1000 in 2% BSA TBST	Dako, USA
Rat Anti-Mouse kappa light chain	ab99632	1:2000 in 3% BSA TBST	Abcam, UK

2.4.3 Co-Immunoprecipitation (Co-IP)

Co-immunoprecipitation was performed to detect the formation of either the RIPK1/RIPK3/FADD/Caspase 8-containing ripoptosome or the RIPK1/RIPK3/MLKL-containing necrosome. $5x10^6$ TOV21G cells were plated in a T150 flask (Corning, UK). The next day cells were infected with *dl*922-947 at 10 plaque-forming units per cell (pfu/cell) in serum-free medium. After 2 hours the medium was replaced with normal growth medium. As a positive control cells were either treated with 100μM etoposide (Fresenius Kabi, UK), 25μM Z.VAD.fmk and 20ng/mL TNF-α for 24 hours or with TSZ (1μM SM, 25μM Z.VAD.fmk and 20ng/mL TNF-α) for 6 hours. Untreated cells were used as a negative control. Cells were trypsinised and pelleted by centrifugation at 1200 rpm for 3 minutes in their respective medium. The supernatant was then removed and cells were washed once in ice cold PBS followed by centrifugation at 1200 rpm for 3 minutes. The supernatant was removed and the pellet was resuspended on ice in 1mL of NP40 buffer (10mM Tris pH 8.0, 150 mM NaCl, 1% Nonidet P-40) with protease and phosphatase inhibitor cocktail 2 (Sigma-Aldrich, UK). The lysate was incubated for 15 minutes on a rolling wheel at 4ºC and then centrifuged for 20 minutes at 14,000 rpm at 4ºC. The supernatant was transferred to a fresh Eppendorf tube and its protein concentration was determined by Bradford assay. Samples at a concentration of 1μg/μL in Laemmli buffer were prepared and denatured at 95ºC

for 5 minutes for use as protein input controls while the rest of the sample was used for co-IP.

For co-IP 1mg of each protein sample was prepared in a total volume of 500µL. The antibodies shown in table 8 were used for the co-immunoprecipitation of death-inducing complexes.

Table 8: Antibodies used for co-immunoprecipitation.

Antibody	Concentration	Supplier	Catalogue number
Caspase-8	1:50	Enzo	ADI-AAM-118-E
RIPK3	1:50	SantaCruz	Sc-374639

For detection of the ripoptosome, an anti-Caspase 8 antibody (Enzo, UK) was added to the lysates while for detection of the necrosome an anti-RIPK3 antibody (SantaCruz, USA) was added to the lysates. The lysate/antibody mix was then incubated overnight at 4ºC on a rolling wheel. The next day 15µL of Dynabeads Pan Mouse IgG magnet beads (Invitrogen, UK) per sample were washed once in lysis buffer before they were added to the lysate/antibody mix. The lysate/antibody/bead mix was then incubated for 2 hours at 4ºC on a rolling wheel. After the incubation step the lysates were washed 3 times in ice-cold NP40 buffer. To pull down the desired complex 16µL of water and 4µL of 5x Laemmli buffer were added to the beads, vortexed and denatured at 95ºC for 5 minutes. The magnetic beads were removed and the samples run on a SDS-PAGE gel.

The SDS gel electrophoresis was performed as described previously. To detect human FADD an HRP-conjugated goat anti-mouse IgG1 heavy chain (Abcam, UK) specific antibody was used.

2.5 Transfection

2.5.1 Transfection of plasmids into cells

Two wells were plated for each plasmid/guide at a density of 40000 cells/well in a six well plate (Costar, USA). The next day 10µL of Lipofectamine 2000 (Invitrogen, UK) were carefully added to 240µL Opti-MEM (Gibco by Life Technologies, UK) in an Eppendorf tube and mixed by inverting the tube three times. In a new tube 4µg of the desired plasmid were carefully added to 250µL Opti-MEM and mixed by inverting the tube three times. The tubes were spun briefly and incubated at RT for 5 minutes. After 5 minutes the contents of both tubes were combined and gently mixed by inverting the tube three times. The mix was briefly spun down and incubated for 20 minutes at RT. After 20 minutes the whole content (500µL) was added to the intended well by pipetting drops over the well. To assure even mixing the plate was gently swirled in the figure of an eight. The next day the medium was removed from each well and replaced with fresh medium. The following day the media was removed from each well and replaced with new media containing 2.5µg/mL puromycin (Sigma-Aldrich, UK). After all control wells have died replace media with new media without puromycin and let cells grow until they reach 80% confluency.

2.5.2 Transfection of small interfering ribonucleic acid (siRNA)

Cells were seeded into a six well plate at a density of $5x10^5$ cells per well in antibiotic free medium. The following day 2µL Dharmafect 1 (Thermo Scientific, UK) and 198µL serum-free Opti-MEM per sample were added, mixed and incubated for 5 minutes. Different concentrations of target small interfering ribonucleic acid (siRNA) (100nM, 60nM, 30nM and 10nM) were prepared by diluting the siRNA in a total volume of 200µL serum-free Opti-MEM. The siRNA was mixed and incubated for 5 minutes at room temperature. The same conditions were used for the non-targeting control siRNA. Afterwards the Dharmafect mix was added to the siRNA mix and mixed by gently pipetting up and down and left to incubate for 30 minutes at room temperature. The mix was added in droplets to each well. To ensure even mixing the plate was gently swirled in the figure of an eight.

Cells were incubated with siRNA for 24 hours before the medium was replaced with normal growth medium. Depending on the experimental conditions cells were harvested 24 - 120 hours post-transfection and prepared for whole protein lysis to confirm knockdown of target proteins by western blotting.

2.5.3 Retroviral Transduction

The pBabe-Bcl-2 plasmid was obtained from KM Ryan, Institute of Cancer Sciences University of Glasgow and Cancer Research UK Beatson Institute, Glasgow, UK.

The Lzrs-RIPK3 plasmid was obtained from S Tait, Institute of Cancer Sciences University of Glasgow and Cancer Research UK Beatson Institute, Glasgow, UK and described in (Rodriguez et al. 2016)

Phoenix Ampho cells were plated at a density of $2x10^6$ cells per 10cm plate (Corning, UK). The next day a transfection mix was prepared by adding 400µL Opti-MEM to 5µg retroviral plasmid and 400µL of Opti-MEM to 10µL Lipofectamine 2000. Each mix was incubated for 5 minutes at room temperature before they were combined, briefly centrifuged and incubated for another 20 minutes at room temperature. 6.2mL antibiotic-free DMEM were added to the 810µL transfection mix and added to the cells. After 6 hours of incubation, cells were gently washed twice with PBS and normal medium was added to the cells. After 48 hours the viral supernatant was collected, filtered, polybrene added at a 1:1000 dilution and added to the desired target cells. New medium was added to Phoenix Ampho cells to maintain virus production. The next day viral supernatant was collected as described before and target cells were infected for a second time. The next day the transduced cells were washed twice with PBS and fresh growth medium was added. Cells were left to recover before selection medium containing antibiotics was added.

2.6 Flow Cytometry

2.6.1 Measuring viral cell entry

Flow cytometry was used to measure infectability of cells. Cells were plated in triplicate on 6 well plates at a density of $5x10^5$ cells per plate. After 24 hours

cells were infected with Ad-GFP, an E1-deleted Ad5 vector that expresses the green fluorescent protein driven by a CMV-promoter, at MOI 5 and 50 for each condition. Cell were trypsinised 24 hours after infection, washed three times in PBS and resuspended in a total volume of 500µL PBS. Samples were analysed in a BD FACS Calibur cytometer (BD Biosciences, USA) using FlowJo software 8.8.4. Infectivity was determined by comparing the percentages of GFP-positive events after a total of 10,000 events were recorded.

2.7 Microscopy

2.7.1 Transmission Electron Microscopy (TEM)

TOV21G and OVCAR4 cells were plated separately on Thermanox coverslips (Agar Scientific Ltd., UK) at a density of $5x10^5$ cells/well in a 6 well plate in 2mL of growth medium. The next day cells were infected in triplicate with *dl*922-947 in serum-free medium (MOI 1 pfu/cell for TOV21G, MOI 3 for OVCAR4). After 2 hours the medium was replaced with normal growth medium. As a positive control cells were treated with 1mM SM, 25µM Z.VAD.fmk and 20ng/mL TNF-α for 6 hours (TOV21G) or 24 hours (OVCAR4). In both cases untreated cells were used as a negative control. Cells were then washed in PBS and fixed in 1.5% glutaraldehyde/0.1M sodium cacodylate buffer for 1 hour at 4ºC. Afterwards the cells were washed three times for 5 minutes each in 2% sucrose/0.1M sodium cacodylate buffer rinse.

Further processing was carried out by Margaret Mullin, Electron Microscopy Facility, University of Glasgow. Samples were post-fixed in 1% osmium tetraoxide/0.1M sodium cacodylate buffer for three times 10 minutes and washed for 30 minutes in distilled water. Samples were then block stained with 0.5% aqueous uranyl acetate for 1 hour in the dark and washed again twice for 1 minute each with distilled water. The samples were then dehydrated through a graded ethanol series of 30%, 50%, 70% and 90% ethanol for 10 minutes for each concentration followed by absolute ethanol for four times for 5 minutes each. Afterwards the samples were transferred into dried absolute ethanol four times five minutes each and moved into propylene oxide for three times 5 minutes each. The samples were then put into 1:1 propylene oxide: araldite/epoxy 812 resin overnight. The next day samples were changed to fresh resin, embedded in

flat bed moulds and polymerized for 48 hours at 60ºC. The coverslip was removed by inverting into liquid nitrogen and the coverslip was “popped-off” leaving the cells embedded in the resin.

60-70nm ultrathin sections were produced using a LEICA Ultracut UCT (Leica Microsystems, UK) and Diatome diamond knife (Diatome, USA) at an angle of 6 degrees. Sample sections were picked up on 100mesh formvar coated copper grids and then contrast stained with 2% methanolic uranyl acetate for 5 minutes followed by Reynolds Lead Citrate for 5 minutes.

Samples were viewed on a FEI Tecnai T20 (Zeiss, UK) at an accelerating voltage of 200kV and images were captured using the GATAM Digital Imaging system.

2.8 Gene Editing Techniques

2.8.1 Clustered regularly-interspaced short palindromic repeats (CRISPR)

CRISPR/Cas9 technology was used to induce gene deletions in human Mixed-lineage kinase like (MLKL) in TOV21G cells.

2.8.1.1 Designing guides

The desired gene target sequences were analysed for potential guides using https://chopchop.rc.fas.harvard.edu and http://crispr.mit.edu/. Guides were chosen depending on a high score, which represented the inverse likelihood of off-target binding. Another selection criterion for guide selection was that guides should target important functional structures within the protein needed for the induction or execution of programmed necrosis.

For MLKL the following guide for MLKL was used:
Guide 5: AACACAGACTTCCATGAGTTTGG located at MLKL’s catalytic sites and

Oligos were ordered from Invitrogen (Invitrogen, UK).

2.8.1.2 Annealing of oligos and restriction digest

Oligos were resupended at 100μM in nuclease-free water (Ambion, USA) and 1μL of each oligo was added to 1μL of 10x annealing buffer (100mM Tris, pH 7.5, 500mM NaCl, 10mM EDTA) and 7μL nuclease-free water. The annealing mix was placed in a mini dry bath (Flowgen Bioscience, UK) for 3 minutes at 95ºC and then left for another 20 minutes with the mini dry bath being switched off and was then left to cool to room temperature (RT). A sample of the annealed oligos was diluted 1 in 250 with nuclease-free water.

The plasmid pX335 was digested with Bbsl (New England Biolabs, UK). 20 units of Bbsl were added to 1μg of DNA, 5μL of 10x NEB buffer (50mM NaCl, 10mM Tris-HCL, 10mM $MgCl_2$, 100μg/mL Bovine serum albumin (BSA), pH 7.9 at 25ºC and topped up with nuclease free water to a total reaction volume of 50μL. The reaction mix was then incubated at 37ºC for 1 hour on a Grant JBN/5 water bath (Grant Instruments, UK).

The digest was run on a 0.7% agarose (Melford biolaboratories Ltd, UK) gel with 0.002% ethidium bromide solution (Sigma, UK). 0.7% w/v agarose was dissolved in Tris-acetate-EDTA (TAE) buffer (40mM Tris pH 7.6, 20mM acetic acid, 1mM EDTA) and casted in a Bio-Rad Sub-Cell GT chamber (Bio-Rad, UK) with combs and allowed to set at room temperature. Once the agarose gel was set, the chamber was filled with TAE buffer. 10μL of 6x Orange DNA loading dye (Thermo Scientific, UK) was added to the whole digest and added to one well of the gel alongside with 5μL O'GeneRuler 1kb DNA ladder (Thermo Scientific, UK). The gel was run at 20V overnight at room temperature.

2.8.1.3 DNA Extraction

To extract linearised plasmid DNA a QIAquick Gel Extraction Kit (Qiagen, UK) was used. The gel was excised on a high performance transilluminator (Ultra Violet Products, USA) and the desired DNA fragment was removed using a disposable scalpel (Swann-Morton, UK). The removed slice of gel was transferred to a clean Eppendorf tube and weighed on a Secura 224-1CEU scale (Satorius, UK). 3 volumes of buffer QG were added to 1 volume gel. The buffer and gel were incubated at 50ºC for 10 minutes with vortexing on a Grant-bio PV-1 Vortex Mixer (Grant, UK) or until the gel slice was completely dissolved resulting in a

yellow colour of the mix. One volume of isopropanol (Sigma-Aldrich, UK) was added to the sample and mixed well. Afterwards the sample was placed in a QIAquick spin column with the provided collection tube and centrifuged on an Eppendorf Centrifuge 5424 (Eppendorf, UK) at full speed for 1 minute. The flow-through was discarded and 500µL of buffer QG were added to the column and centrifuged at full speed for 1 minute. The flow-through was discarded again and 750µL of buffer PE were added and left to incubate for 5 minutes. Then the mix was spun at full speed for 1 minute twice to remove residual wash buffer while the flow-through was discarded each time. To elute the DNA 50µL of buffer EB were added to the centre of the membrane, incubated for 3 minutes and centrifuged for 1 minute at full speed. The DNA concentration was measured on a Nanodrop 2000 Spectrophotometer (Thermo Scientific, UK).

2.8.1.4 Ligation and transformation into competent E.coli

To ligate the oligos with the vector a ligation mix was prepared using the Roche rapid Ligation Kit. 50ng of pX335 vector were added to 1µL of diluted annealed oligos and toped up with nuclease-free water to a total volume of 9µL. Then 10µL of the 2x reaction buffer and 1µL of T4 DNA Ligase were added and left for incubation at room temperature for 5 minutes.

25µL of One Shot TOP10 chemically competent E. coli cells (Invitrogen, UK) were transformed with 2µL of the ligation mix. The cells were first left on ice for 5 minutes, were then heat shocked at 42ºC in a water bath for 30 seconds and were then immediately transferred back on ice for another 2 minutes. 1mL of warm super optimal broth with catabolite repression medium (S.O.C.) (2% w/v Tryptone, 0.5% w/v yeast extract, 10mM NaCl, 2.5mM KCl, 10mM $MgCl_2$, 10mM $MgSO_4$, 20mM glucose) (Invitrogen, UK) was added and incubated for 1 hour at 37ºC. The cell suspension was then spun down, resuspended in 100µL water and plated out on 100 µg/mL ampicillin (Calbiochem, USA) containing Lennox L broth (LB) (1% w/v SELECT peptone 140, 0.5% w/v SELECT yeast extract, 0.5% w/v NaCl, 1.5% w/v Agar (Sigma, UK)) (Invitrogen, UK) plates. The plates were incubated overnight at 37ºC in a Genlab mini/75 incubator (Genlab Limited, USA).

2.8.1.5 Plasmid Miniprep and sequencing

After overnight incubation, three different single colonies were picked from each plate, transferred to 7mL LB containing 100µg/mL ampicillin in culture tubes (VWR, USA) and incubated overnight at 37ºC in an Innova 44 incubatorshaker series (New Brunswick Scientific, UK). The next day 2mL of cell culture were put aside for later expansion and the left 5mL were spun down at 2000 rpm for 15 minutes on an Allegra x-12R centrifuge (Beckman Coulter, USA). The supernatant was removed and the resulting pellet was used for sequencing.

All plasmids were sequenced by the molecular technology and reagent service at the Cancer Research UK Beatson Institute on an Applied Biosystems 3130xl sequencer (Applied Biosystems, UK) using the BigDye v3.1 Cycle Sequencing Kit (Applied Biosystems, UK).

2.8.1.6 Plasmid isolation

After sequencing results were obtained one colony was chosen and expanded by adding the 2mL of the remaining cell culture to 250mL of LB containing 100µg/mL ampicillin. The starter culture was incubated overnight at 37ºC. The next day cells were pelleted at 2000 rpm for 15 minutes on a Beckman Coulter J6-MI centrifuge (Beckman Coulter, USA) and the resulting cell pellet was used for plasmid isolation.

Plasmids were isolated and purified by the molecular technology and reagent service at the Cancer Research UK Beatson Institute using a Qiagen 8000 Biorobot (Qiagen, UK).

2.8.1.7 Transfection with CRISPR/Cas9 guides

Guides were transfected as described in 2.5.1.

2.8.1.8 Dilution Cloning and screening for deletion clones

Once cells reached 80% confluency, they were trypsinized and resuspended in medium and counted on a Cellometer Auto 1000 (Nexcelon Bioscience, UK). To make dilution clones 200,000 cells were resuspended in 5mL of medium followed by two 10x dilutions of 500µL cell suspension in 4.5mL medium. After the last

dilution 1mL of this dilution was added to 39mL of media to give an average of 10 cells per mL. 200µL of the cell suspension were pipetted into each well of a 96 well plate (Costar, USA) to give an average of 2 cells per well. Five days after plating the wells were inspected for visible colonies and single cell colonies were recorded. After another 4 days plates were checked again as colonies become more obvious over time.

After single cell colonies reached 80% confluency, cells were trypsinized and resuspended in 150µL medium. Single cell clones were plated on a 96 well plate by adding 50µL of the cell suspension to 150µL new medium, resulting in three 96 well plates with one replicate of each single cell clone. Once cells reached 60% confluency, one plate was frozen down for later use, one plate was used for picking control clones and one plate was used for the screen. Deletion clones were screened by treating the cells with 20ng/mL recombinant human Tumour Necrosis Factor-α (TNF-α) (PeproTech, USA), 1µM LCL-161/smac-mimetic (SM) (Chemie Tek, USA) and 25µM carbobenzoxy-valyl-alanyl-[O-methyl]-fluoromethylketone (Z.VAD.fmk) (ApexBio, USA). The next day surviving clones were recorded as potential knock out or deletion clones while dead clones were recorded as potential control clones. Clones were checked again 72 hours later to see if there was a time difference in response to the treatment.

2.8.1.9 DNA Extraction and PCR

DNA was extracted from cultured cells using the QIAamp DNA FFPE Tissue Kit (Qiagen, UK). $5x10^6$ cells were trypsinized, washed in PBS, centrifuged and resuspended in 200µL PBS and 10µL proteinase K was added. 200µL buffer AL was added, mixed and 96% ethanol were added and mixed thoroughly by vortexing. The mixture was transferred to a DNeasy spin column with 2mL collection tube and centrifuged at 6000xg for 1 minute. The flow-through was discarded and the column placed in a new collection tube. 500µL buffer AW1 were added, centrifuged at 6000xg for 1 minute and the flow-through was discarded with the collection tube. The spin column was placed in a new 2mL collection tube, 500µL buffer AW2 were added, centrifuged at 20,000xg for 3 minutes and the flow-through was discarded with the collection tube. The spin column was then transferred to a new 1.5mL eppendorf tube. DNA was eluted by adding 200µL nuclease-free water onto the membrane of the spin column, incubating it at

room temperature for 1 minute followed by centrifugation for 1 minute at 6000xg.

PCR mastermix was prepared by adding 1µL 10mM dNTP with 1.5µL 50mM $MgCl_2$, 2.5µL 10µM forward primer, 2.5µL 10µL reverse primer, 5µL 10x PCR buffer, 0.3µL Taq polymerase per reaction. 20ng template DNA was added to nuclease-free water to a total volume of 37.2µL per sample. The PCR mastermix was added to the sample (50µL total volume), gently mixed, centrifuged and incubated in a thermal cycler using the following conditions shown in table 9.

The following primer pair was used for clones targeted with guide 5:
Forward: TAGCAACAATCCCTGCCCTTTAC
Reverse: TCAAACTCCTCCAAGGACCACC

Primers were ordered from Invitrogen (Invitrogen, UK).

Table 9: PCR program settings

	Polymerase Activation/ DNA Denaturation	PCR Reaction		
Cycle	1	35 cycle		
Temperature (°C)	94	94	55	72
Time	3 mins	45 sec	30 sec	90 sec

An agarose gel was prepared and samples run as described previously.

2.8.1.10 Transformation of PCR product into competent E.coli

The TOPO TA Cloning Kit (Invitrogen, UK) was used for transformation of PCR amplified products into E.coli. 2µL of fresh PCR product was added to 1µL salt solution, 2µL water and 1µL TOPO vector. The reaction mix was incubated for 30 minutes at room temperature and transformed into competent E.coli as described previously, miniprepped and sequenced using M13 forward and reverse primers.

2.9 PCR based assays

2.9.1 qRT-PCR

2.9.1.1 RNA Extraction from Cells

The Qiagen RNeasy kit (Qiagen, UK) was used for RNA extractions from human cells. Cells were plated at a density of $5x10^6$ cells per 10cm dish (Corning, UK). The next day cells were harvested as a pellet, 350µL RLT buffer were added, vortexed followed by the addition of 350µL 70% ethanol. Following thorough mixing, the sample was transferred to an RNeasy Mini spin column with 2mL collection tube and centrifuged for 15 seconds at 8,000xg. The flow-through was discarded.

For the on-column DNase digestion 350µL buffer RW1 were added and centrifuged for 15 seconds at 8,000xg. The flow-through was discarded and a DNase incubation mix prepared. For every sample 10µL DNase 1 stock were added to 70µL buffer RDD. The mix was gently mixed by inverting and briefly centrifuged. 80µL DNase mix were added onto the membrane of each column and incubated for 15 minutes at RT. Afterwards 350µL of buffer RW1 were added to the column, centrifuged for 15 seconds at 8,000xg and the flow-through discarded. Then 700µL of buffer RW1 were added to the column, centrifuged for 15 seconds at 8,000xg and the flow-through was discarded. Samples were then washed twice with 500µL of RPE buffer by centrifugation for 15 seconds at 8,000xg and 2 minutes at 8,000xg. The flow-through was discarded after each wash in RPE. The column was placed in a new 1.5mL collection tube and 30-50µL RNase-free water were added and centrifuged for 1 minute at 8,000xg to elute the RNA. The eluted RNA was then aliquoted and stored at -80ºC for later use or used straight away. Samples were analysed on a Nanodrop 2000 spectrophotometer.

2.9.1.2 Reverse Transcription (RT)

The ABI High Capacity cDNA Transcription Kit (ABI, UK) was used for reverse transcribing total RNA. 0.5 -1µg RNA were transcribed per sample. The desired amount of RNA was prepared in a total volume of 10µL in nuclease-free water. A 2x RT mastermix was prepared by adding 2µL 10x RT buffer, 0.8µL 25x dNTP mix, 2µL 10x Random Primers, 1µL Reverse Transcriptase and 4.2µL nuclease-

free water per sample. 10µL of 2x RT mastermix were added to 10µL RNA sample in a fresh PCR tube and mixed gently before briefly centrifuging. Tubes were place on ice until they were ready to load onto the thermal cycler. Samples were run on a Veriti 96 well thermal cycler (Thermo Fisher, UK) using the conditions shown in table 10.

Table 10: Thermal cycler conditions for RT.

	Step 1	Step 2	Step 3	Step 4
Temperature (ºC)	25	37	85	4
Time (min)	10	120	4	∞

cDNA samples were removed from the thermal cycler and kept on ice while the universal probe mix (Bio-Rad, UK) was thawed at room temperature.

2.9.1.3 qRT-PCR for simplex experiment

Mastermix was prepared by adding 10µL 2x iTaq Universal Probe supermix to 1µL 20x Primer/Probe assay and 7µL nuclease-free water per sample. The mastermix was gently mixed, briefly centrifuged and kept on ice until ready to use. 2µL of DNA template were added to the bottom of a PCR plate well followed by the addition of 18µL of appropriate mastermix. The plate was sealed and run on a CFX96 Real time System (Bio-Rad, UK) using the conditions shown in table 11.

Table 11: Cycling conditions for BioRad iTaq Universal Probes conditions.

	Polymerase Activation/ DNA Denaturation	PCR Reaction	
Cycle	1	40 cycle	
Temperature (ºC)	95	95	60
Time	2-5 mins	2-5 sec	30 sec

Files were analysed in BioRad CFX Manager.

2.10 In vivo experiments

All animal experiments were performed in the Cancer Research UK Beatson Institute Biological Services Unit (registered facility 60/2607) under appropriate Home Office personal (40/04001) and project licence (60/4181) authority. All experiments adhered to NCRI Guidelines on the use of animals in medical research (Workman et al. 2010). Animals were allocated treatment randomly by cage. All injections and tumour measurements, as well as all decisions about animal welfare were taken by BSU staff to prevent bias. Tumour volume was calculated using equation:

$$\frac{x}{2} \times y \times y$$

Where *x*= longest diameter and *y*= perpendicular width

2.10.1 Intratumoural spread of *dl*922-947

Female CD1 nu/nu mice were injected subcutaneously with $5x10^6$ HeLa Lzrs, HeLa RIPK3 D2 or HeLa RIPK3 E4 cells in 100µL PBS. After tumours reached 100-200mm^3 in volume, mice were randomly separated into two groups of 4 per cell line. One group received a single intratumoural dose of $1x10^{10}$ particles of *dl*922-947 while the other group received a single intratumoural dose of PBS. 48 hours after injection mice were killed and tumours excised. Tumours were cut into two parts; one part was snap frozen on dry ice, whilst the other was fixed in 10% NBF over night before they were handed over to the histology service at the Cancer Research UK Beatson Institute, where they were processed and stained for adenoviral proteins by immunohistochemistry.

2.10.2 Intratumoural efficacy of *dl*922-947

Female CD1 nu/nu mice were injected subcutaneously with $5x10^6$ HeLa Lzrs, HeLa RIPK3 D2 or HeLa RIPK3 E4 cells in 100µL of PBS. Mice were randomly separated into two groups of 4 per cell line. Each group received a total of two-intratumoural doses of $1x10^{10}$ particles of *dl*922-947 or a dose of PBS. The first dose was administered after tumours 100-200mm^3 in volume followed by a second dose 9 days after the first injection. Mice were monitored for signs of ill health and tumour volumes were measured three times a week. Mice were killed

when tumours reached the maximum allowed size of 1.4cm^3 or when there were signs of ulceration in accordance with the UK Home Office regulations.

2.11 Immunohistochemistry

2.11.1 Tissue Preservation and Processing

Harvested tissues were fixed overnight in 10% Neutral Buffered Formaldehyde (NBF) (CellPath, UK). The overnight processing of the samples was performed by the histology service at the Cancer Research UK Beatson Institute. The following steps were performed at 40ºC in a Thermo Excelsior Tissue Processor (Thermo Scientific, UK) unless stated otherwise. The cassetted tissues were transferred to 70% ethanol for 35 minutes, followed by 40 minutes in 90% ethanol, 45 minutes in 95% ethanol, 50 minutes in 100% ethanol, another 50 minutes in 100% ethanol and a further 55 minutes in 100% ethanol. Tissues were then transferred through xylene for 45, 50 and 60 minutes and then immersed into wax at 61ºC for 70, 80 and 100 minutes. The tissues were then sectioned at 4µm and stained with Haematoxlin and Eosin (H&E) to display morphological structure.

2.11.2 Immunostaining on paraffin sections: Anti-Adenovirus-2/5 E1A

Anti-Adenovirus-2/5 E1A (Santa-Cruz Biotechnology, USA) or IgG control staining was performed on HeLa Lzrs, HeLa RIPK3 D2 and HeLa RIPK3 E4 tumours, which had been injected either with PBS or with or 1x10^{10} particles of *dl*922-947 for 48 hours. Staining was performed on 4µm sections by the histology service at the Cancer Research UK Beatson Institute.

Sections were de-waxed for 5 minutes in xylene, followed by rehydration through 2x 1 minute immersions in 100% ethanol, 1 minute in 70% ethanol followed by a 5 minute wash in water. Sections were placed for 25 minutes in PT Module (Dako, UK) containing pH6 sodium citrate retrieval buffer (Thermo Scientific, UK) at 98ºC and washed in Tris-buffered Tween (TBT).

All staining was performed on a Dako Autostainer Link48. Peroxidase block (Dako, UK) was initially dispensed on the sections were for 5 minutes to quench endogenous peroxidases before washing sections with TBT. Sections were incubated with anti-adenovirus-2/5 E1A at a 1:200 dilution for 35 minutes and

washed twice in TBT, followed by a 30-minute incubation with Rabbit EnVision (Dako, USA) and another 2 washes in TBT. Next sections were incubated for 10 minutes in 3,3'-Diaminobenzidine tetrahydrochloride to visualize antibody-antigen complex before washing for 1 minute in deionized water to terminate chromogenic reaction. The sections were then stained with Haematoxylin Z (Cellpath, UK) for 7 minutes and washed for 1 minute in deionized water. Sections were next dipped twice into 1% acid alcohol, washed for 30 seconds in water and transferred for 1 minute into Scotts Tap Water Substitute to blue the nuclei. Samples were then dehydrated through graded alcohol, cleared with xylene and mounted with DPX mountant for microscopy (CellPath, UK).

2.11.3 Immunostaining on paraffin sections: Anti-Adenovirus

The immunohistochemical protocol used for the anti-Adenovirus (Abcam, UK) or IgG control staining was the same as described in section 2.8.1.2 with the following exceptions: after the endogenous peroxidase was blocked, sections were washed twice in TBT. 2.5% Normal horse serum (Vector, UK) was applied to the section for 20 minutes before two washes with TBT. The anti-Adenovirus antibody was applied at a 1:1000 dilution for 35 minutes and two washes in TBT. Afterwards sections were incubated for 30 minutes in ImmPRESS anti-goat reagent (Vector, UK) followed by the steps described in section 2.8.1.2.

2.11.4 Immunostaining on paraffin sections: F4/80

The immunohistochemical protocol used for the Anti-F4/80 (Abcam, UK) or IgG control staining was the same as described in section 2.8.1.2 with the following exceptions: After sections were placed in 70% ethanol, they were washed under running tap water for 5 minutes, washed for 5 minutes in TBT and treated with Proteinase K solution (Dako, UK) for 10 minutes. Sections were then washed once in TBT, blocked for endogenous peroxidase for 5 minutes, washed twice in TBT and blocked for 30 minutes in ImmPRESS normal goat blocking serum. Afterwards section were washed twice in TBT, incubated for 35 minutes in F4/80 (Abcam, UK) at a 1:400 dilution, washed twice in TBT and incubated for 30 minutes in ImmPRESS anti-Rat reagent (Vector, UK) followed by the steps described in section 2.8.1.2.

2.11.5 Immunostaining on paraffin sections: NIMP

The immunohistochemical protocol used for the Anti-F4/80 (Abcam, UK) or IgG control staining was the same as described in section 2.8.1.2 with the following exceptions: After sections were placed in 70% ethanol, they were washed under running tap water for 5 minutes, washed for 5 minutes in TBT and treated with Proteinase K solution (Dako, UK) for 10 minutes. Sections were then washed once in TBT, blocked for endogenous peroxidase for 5 minutes, washed twice in TBT and blocked for 30 minutes in ImmPRESS normal goat blocking serum. Afterwards section were washed twice in TBT, incubated for 35 minutes in NIMP-R14 (Abcam, UK) at a 1:50 dilution, washed twice in TBT and incubated for 30 minutes in ImmPRESS anti-Rat reagent (Vector, UK). Next sections were incubated for 10 minutes in 3,3'-Diaminobenzidine tetrahydrochloride to visualize antibody-antigen complex before washing for 1 minute in deionized water to terminate chromogenic reaction and followed by the steps described in section 2.8.1.2.

2.11.6 Cytospin

Cytospin analysis was performed by Elaine Leung and Darren P. Ennis, Institute of Cancer Sciences, University of Glasgow. Slides with filter cards and sample chambers were put into slide holders and attached to the cytocentrifuge rotor. Next a stock solution containing $2x10^5$ cells/mL PBS was prepared. 0.1mL ($2x10^4$ cells/slide) was added to the cell suspension chamber and centrifuged at 1000rpm for five minutes. Slides were then removed and incubated in UMFIX for 3 minutes, followed by two washes, each five minutes in PBS.

2.11.7 Immunostaining on cytospin slides: CK7

Slides were stained by Jane MacMillan at the Histology service unit at the Queen Elizabeth University Hospital, Glasgow, UK, according to standard protocol for CK7 (NCL-L-CK7, Leica, UK).

2.11.8 Immunostaining on cytospin slides: ERA

Slides were stained by Jane MacMillan at the Histology service unit at the Queen Elizabeth University Hospital, Glasgow, UK, according to standard protocol for ERA (ERA M3525, DAKO, UK).

2.11.9 Histoscoring

Histoscoring was performed by Clare Orange, Institute of Cancer Sciences, University of Glasgow. Slides were digitised using the Hamamatsu NanoZoomer slide scanner, at 20x objective lens with 0.75 numerical aperture (NA). Images were then stored on our dedicated servers and loaded to Leica Microsystems Slidepath Digital Image Hub v4.0 (DIH).

Images were analysed using the Image Analysis module of the DIH. Algorithms are available for nuclear, cytoplasmic and membranous staining using the Measure Stained Cells algorithm embedded in the software. The algorithms are applied on a threshold and segmentation basis and parameters can be adjusted within these algorithms to suit the size, shape and proximity of cells of interest.

Cells are classed as positive or negative and then further graded as strong, moderate or weak depending on the intensity thresholds set. Results are returned as a weighted Histoscore along with number and percentage of negatively and positively stained cells.

Areas of necrosis within tumours (defined as regions lacking nuclei) was measured using the area measuring tool on Slidepath Digital Image HUB and presented as percentage total tumour area per section.

2.12 Statistics

Microsoft Excel 2011 for Macintosh (Microsoft Corporation, USA) was used to normalise cell survival in treated cells as, presented as percentage of untreated cell (100%) and to calculate mean and standard deviation.

GraphPad Prism version 6.0d for Macintosh (GraphPad Software, San Diego, USA) was used to generate sigmoid dose response curves and to calculate the EC_{50}, which describes the dose that is required to kill 50% of cells.

All statistical analyses were performed using GraphPad Prism (version 6.0d). Cell survival and IC50 values were compared using unpaired t-test or One Way ANOVA

with multiple comparisons and $p<0.05$ (*) was considered statistically significant throughout. The level of statistical significance is shown using asterisk (*$p<0.05$, **$p<0.01$, ***$p<0.001$ and ****$p<0.0001$).

Chapter 3

Adenoviruses and their potential in ovarian cancer treatment

3 Adenoviruses and their potential in ovarian cancer treatment

3.1 Introduction

As discussed in the chapters above, adenoviruses contain features that make them suitable for oncolytic virotherapy, especially viruses of the serotype 5 that have been tested in many models of pre-clinical research (Davison et al. 2001, Heise et al. 2000, Satoh et al. 2007, Cherubini et al. 2011, Bhattacharyya et al. 2011), where they have showed promising activity. In this chapter, I aim to assess the potential of *dl*922-947 for the treatment of ovarian cancer and to compare the cytotoxicity induced by Ad5WT, Ad11, Ad35 and *dl*922-947. I further aim to assess the potential of *dl*922-947 for the treatment of ovarian cancer, cytotoxicity, infectivity and the expression of viral proteins during infection *in vitro* was assessed in IGROV1, OVCAR4 and TOV21G and its efficacy in lysing human primary ascites cells.

3.2 Cytotoxicity of adenovirus *in vitro*

To test the oncolytic efficacy of several adenovirus serotypes, human ovarian cancer cell lines were infected with wild-type Ad5 (Ad5WT), Ad11, Ad35 as well as the E1A CR2-deleted Ad5 vector *dl*922-947 to examine their sensitivity to oncolytic adenovirus and to evaluate their potential as a therapeutic agent.

A panel of human ovarian cancer cells was infected with increasing MOI of indicated adenovirus serotypes and cell survival was measured 120 hours post-infection by MTT assay (Figure 3-1). Adenovirus serotype 35 (Ad35) showed the same sensitivity in IGROV1 (EC_{50}: 1.6 pfu/cell), OVCAR4 (EC_{50}: 3.3 pfu/cell), and TOV21G (EC_{50}: 1.8 pfu/cell), with no significant difference between EC_{50}. Adenovirus serotype 11 (Ad11) also showed no difference in sensitivity between cell lines: IGROV1 (EC_{50}: 41.8), OVCAR4 (EC_{50}: 38.9) and TOV21G (EC_{50}: 40.1). TOV21G (EC_{50}: 1.2) was most sensitive to Adenovirus 5 wild type (Ad5WT) while IGROV1 (EC_{50}: 40.8), was the least. Sensitivity of OVCAR4 (EC_{50}: 14.6) was in the middle of IGROV1 and TOV21G, when infected with Ad5WT. The amount of cell death induced by *dl*922-947 was either comparable or significantly higher than Ad5WT for each cell line. TOV21G (EC_{50}: 0.1) was most sensitive to *dl*922-947,

followed by OVCAR4 (EC_{50}: 4.4) and with IGROV1 (EC_{50}: 5.6) being least sensitive. These results are consistent with previous publications from the host lab (Lockley et al. 2006).

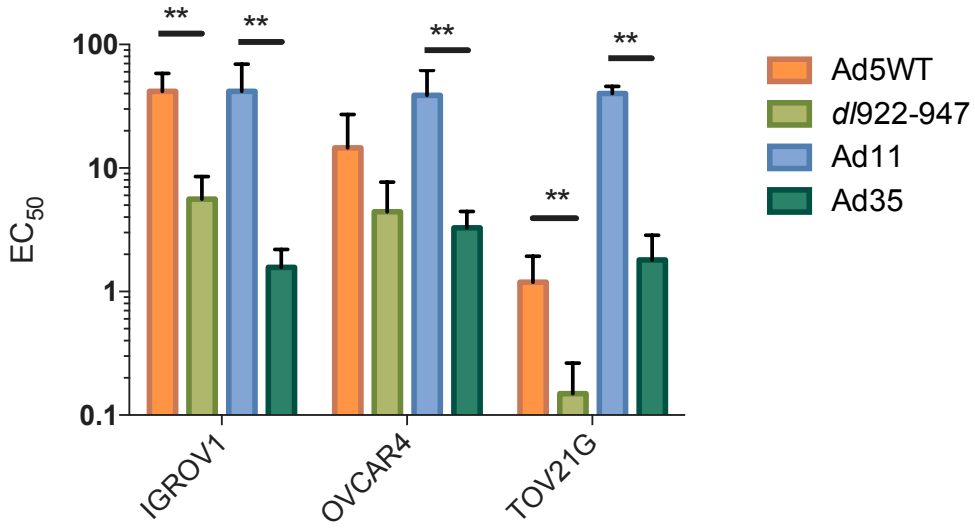

Figure 3-1: Cytotoxicity of Ad5WT, *dl*922-947, Ad11 and Ad35 in the human ovarian cancer cell lines IGROV1, OVCAR4 and TOV21G

Cells were infected in triplicate with a serial dilution of indicated viruses and cell survival was assessed 120 hours post-infection by MTT assay. Cell survival was normalized to uninfected cells and the EC50 values calculated from sigmoidal dose response curves using GraphPad Prism. Shown are EC50 values. Points represent mean EC50 +/- STDEV from at least three experiments with each experiment performed in triplicate.

P values are calculated using One way ANOVA with multiple comparisons ** shows $p<0.01$.

3.3 Infectability with adenovirus type 5 vectors

As shown in table 3 adenoviruses of the serotype 5 use CAR as their primary cellular attachment receptor, but the expression of CAR itself varies between cell lines and as shown previously, can even be up-regulated in paclitaxel resistant cells (Ingemarsdotter et al. 2015). Therefore, I wanted to investigate if differences in infectivity in cell lines can be a cause for the differences in cytotoxicity described above.

A way to measure infectivity is by infecting different cell lines with Ad-GFP, which is an E1-deleted non-replicating type 5-adenovirus. Ad-GFP contains a CMV early promoter, which drives the expression of the green fluorescent protein (GFP). 24 hours after cells have been infected at a known MOI, infectivity can be determined as the percentage of GFP-positive cells and be compared between different cell lines using flow cytometry. IGROV1, OVCAR4 and TOV21G were infected with Ad-GFP at MOI 5. 24 hours post-infection, cells were analysed and infectivity was determined after 10,000 total events were recorded.

Figure 3-2 shows infectability of IGROV1, OVCAR4 and TOV21G with Ad-GFP. After 24 hours post-infection at MOI 5 76.7% of IGROV1 cells were GFP-positive, 57.7% of OVCAR4 cells were positive and 92.3% of TOV21G cells were positive. According to this data TOV21G is the most infectable cell line followed by IGROV1 and with OVCAR4 being the least infectable cell line. For easier reading table 12 shows GFP percentage for each cell line and condition.

Table 12: Percentage of GFP positive cells for each condition.

Cell line	GFP positivity (%)	
	***dl*922-947 MOI 5**	**Ad-GFP MOI 5**
IGROV1	0.011	76.7
OVCAR4	0.057	57.7
TOV21G	0.022	92.3

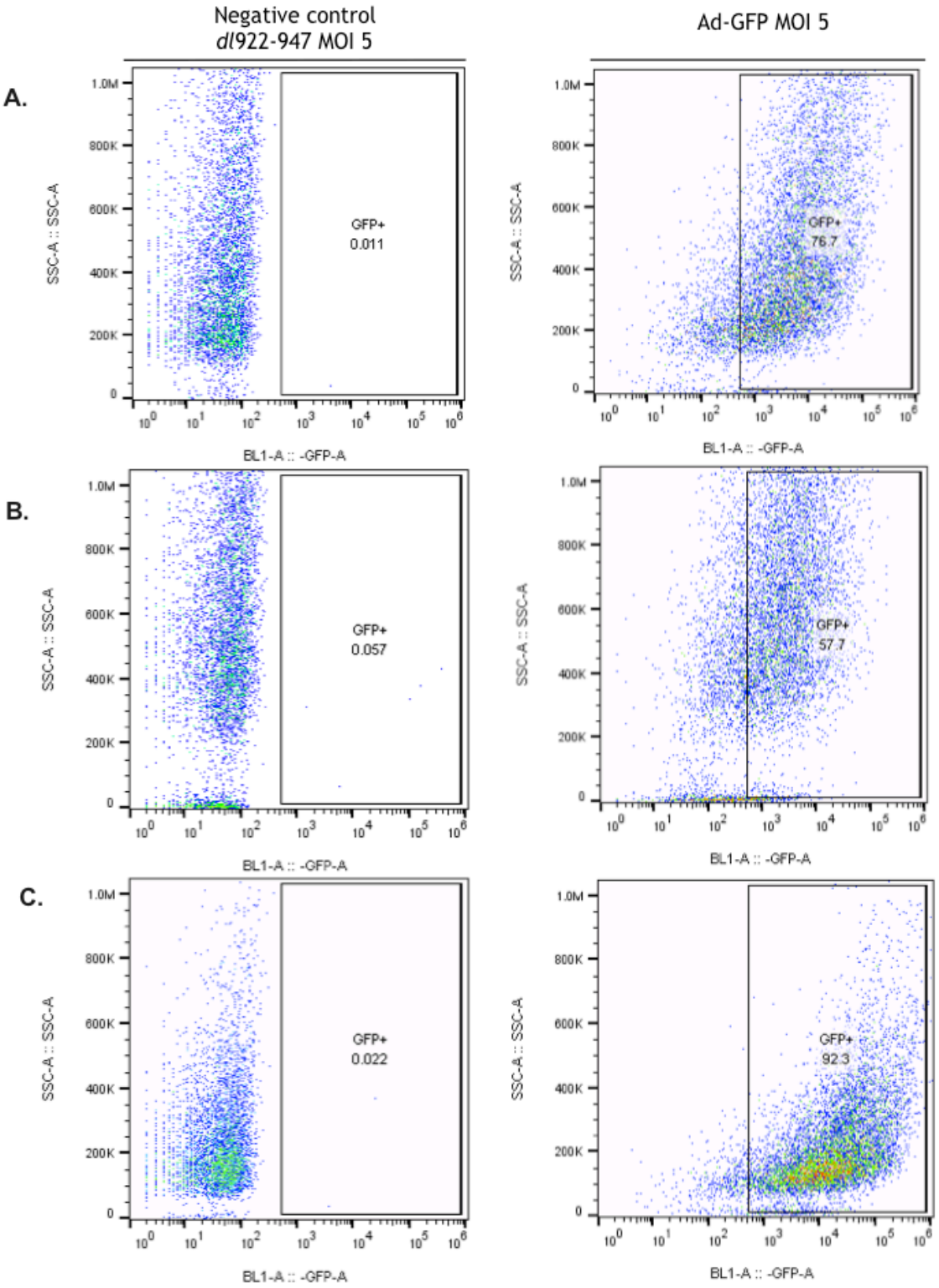

Figure 3-2: Infectability of IGROV1, OVCAR4 and TOV21G with Ad-GFP *in vitro*
A) IGROV1,
B) OVCAR4 and
C) TOV21G were either infected with *dl*922-947 or Ad-GFP at MOI 5 for 24 hours in duplicate. After 24 hours, cells were prepared for flow cytometry analysis. Cells were analysed for GFP expression after 10,000 events were recorded. Shown are representative graphs from one experiment performed in duplicate.

3.4 Expression of viral proteins during *dl*922-947 infection

Besides infectivity, the expression of viral proteins can differ from cell line to cell line, meaning that some cell lines might have the machinery to allow faster transcription and/or translation of viral proteins. This can lead to the production of more infectious virus particles resulting in more cytotoxicity.

To analyse the expression of viral proteins in different cell lines; IGROV1, OVCAR4 and TOV21G cells were infected with either *dl*922-947 or Ad5WT at MOI 10. Samples were taken 0, 24 and 48 hours post-infection for western blot analysis.

Figure 3-3 shows the expression of early and late viral proteins during *dl*922-947 and Ad5WT infection. The first viral protein to be expressed during adenovirus infection is E1A. As shown below E1A protein expression can be seen in all shown cell lines infected with *dl*922-947 at 24 hours post-infection as well as the expression of viral core and capsid proteins. TOV21G cells infected with *dl*922-947 show more expression of E1A at 24 hours in comparison to IGROV1 and OVCAR4, while E1A expression starts to decrease in TOV21G at 48 hours, an increase in E1A expression from 24 to 48 hours post-infection is observed in IGROV1 and OVCAR4. The expression of viral core and capsid proteins can be observed in all cell lines at 24 hours post-infection with an increase in protein level at 48 hours. Interestingly, E1A expression is higher at 24 hours post-infection in *dl*922-947 infected cells compared to Ad5WT with OVCAR4 showing very low amounts of E1A at 24 hours post Ad5WT infection. Also the expression of viral core and capsid proteins is delayed in Ad5WT infected cells compared to *dl*922-947 infected cells. While cells infected with *dl*922-947 start showing expression of core and capsid proteins at 24 hours post-infection, cells infected with Ad5WT only show the expression of these proteins at 48 hours.

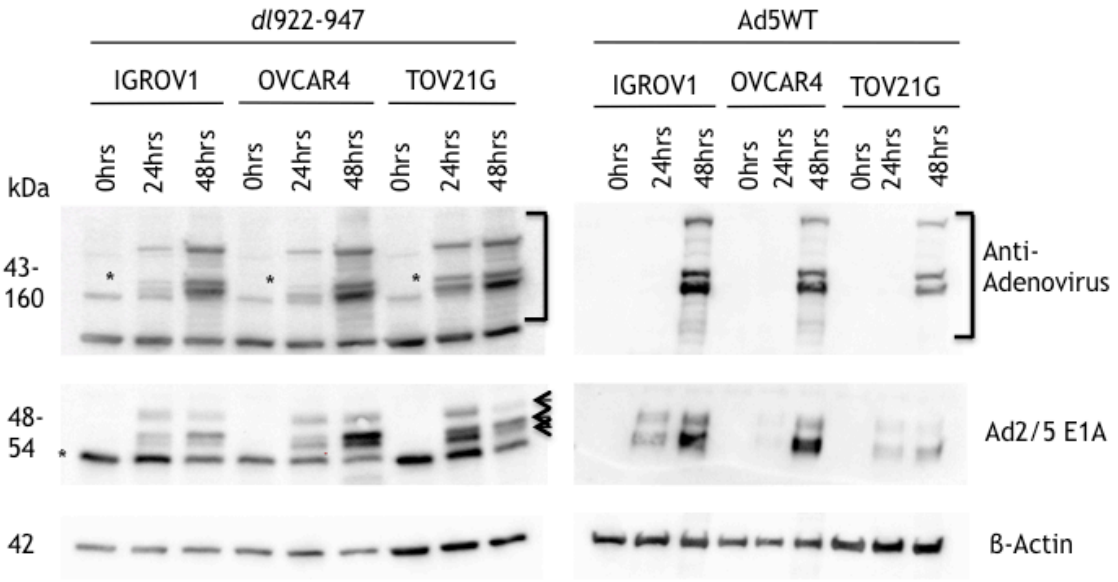

Figure 3-3: Western blot of viral proteins in IGROV1, OVCAR4 and TOV21G
IGROV1, OVCAR4 and TOV21G were infected with Ad5WT at MOI 10 or mock-infected. Samples were taken at indicated time points and prepared for Western blot analysis. Samples were blotted for β-actin (42 kDa), Ad2/5 E1A (48-54 kDa) and Anti-Adenovirus (Hexon at 108kDa and penton base at 63 kDa). One representative western blot out of 2 experiments is shown.
Asteriks indicate non-specific bands. Arrows indicate Ad2/5 E1A bands.

3.5 Replication of *dl*922-947

To further assess differences in *dl*922-947 sensitivity in different cell lines, I aimed to study its replication kinetics for those. Replication was assessed using $TC_{ID}50$ in the human ovarian cancer cell lines IGROV1, OVCAR4 and TOV21G over a time period of 48 hours, infected at MOI 10.

Figure 3-4A shows the replication of *dl*922-947 in a panel of ovarian cancer cell lines. Viral titres increase in IGROV1 and OVCAR4 from 24 to 48 hour post-infection, while they decrease in TOV21G due to virus-induced cell death (Figure 3-4B). Further, OVCAR4 and TOV21G show similar titres at 24 hour post-infection, while IGROV1 shows decreased replication at the same time point, but reaches similar titres as OVCAR4 at 48 hour post-infection.

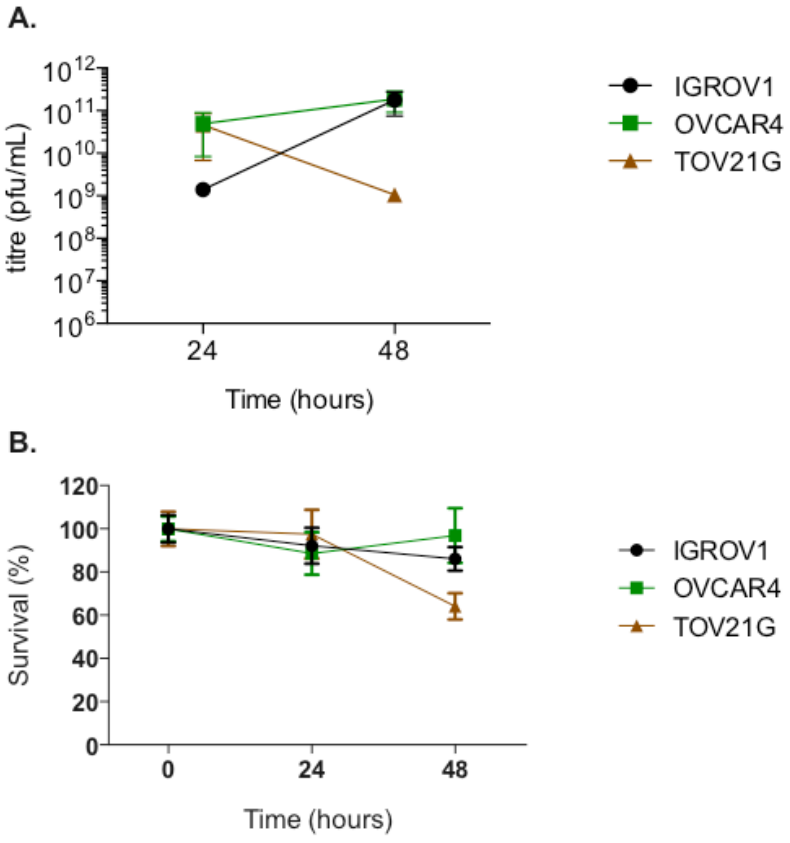

Figure 3-4: Replication of *dl*922-947 in ovarian cancer cell lines
A) Cells were infected with *dl*922-947 at MOI 10 over a time course of 48 hours. Viral titres were determined by $TC_{ID}50$ assay. Points represent mean +/- STDEV from one experiment performed in triplicate.
B) Cells were infected with *dl*922-947 at MOI 10 and cell survival was assessed at 0, 24 and 48 hours post-infection by MTT assay and normalized to uninfected cells. Shown is survival as percentage. Points represent mean +/- STDEV from one experiment performed in quadruplicate wells.

3.6 Isolation of human primary ascites cells

After *dl*922-947 ability to infect and lyse established tissue culture cell lines was analysed, I sought to further determine its efficiency in human primary ascites cells. Human primary ascites cells were isolated, cultured and then prepared for cytospin. Cells were stained for the epithelial cell markers, cytokeratin 7 (CK7) and epithelial related antigen (ERA).

Figure 3-5 shows that human primary ascites cells are positive for CK7 and ERA, showing their epithelial origin. Interestingly, upon closer examination it was observed that a mix of different cell types had been isolated.

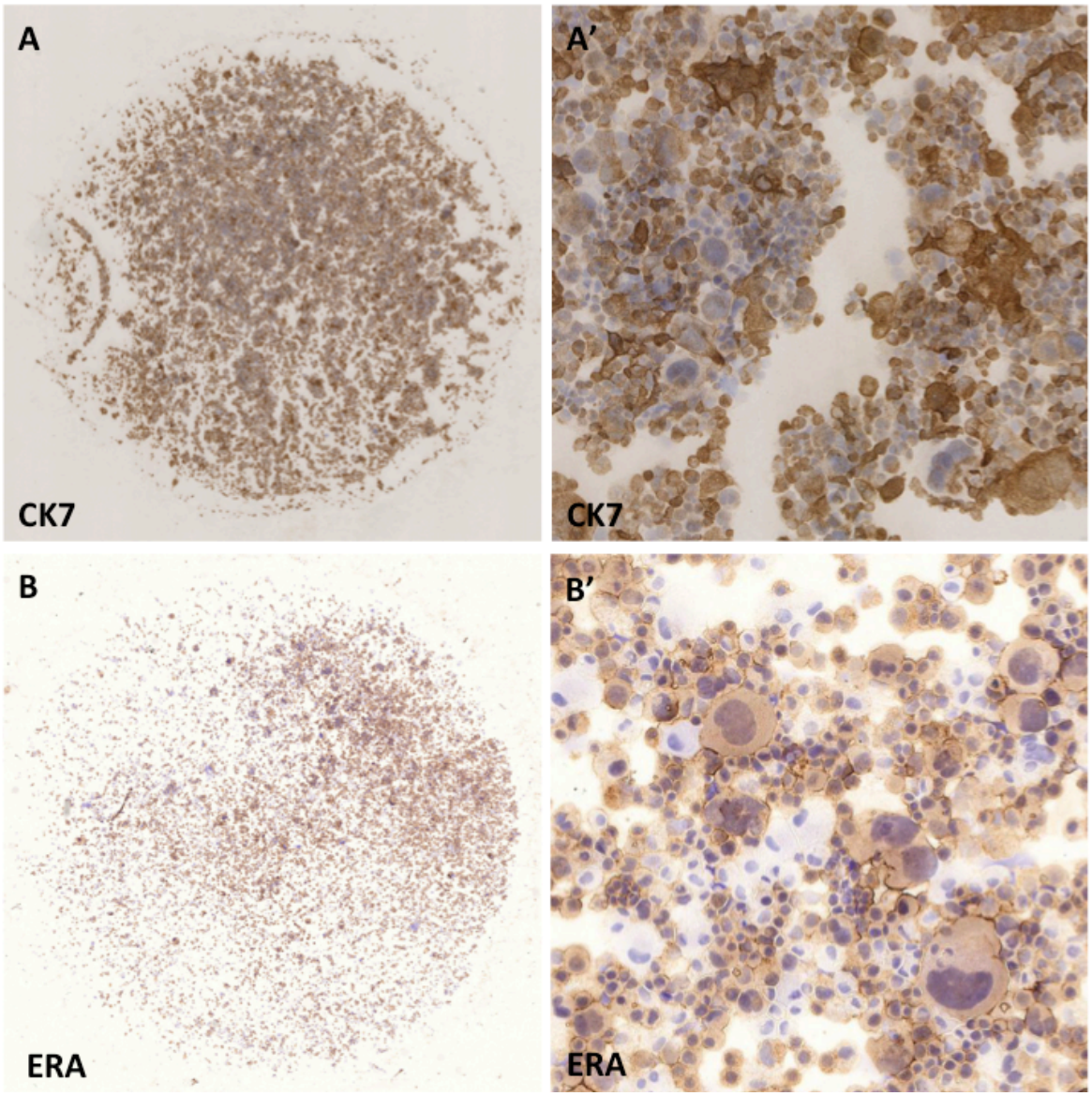

Figure 3-5: CK7 and ERA immunohistochemistry of human primary ascites cells
Human ascites cells were collected and processed for cytospin as described in chapter 2. Samples were stained for cytokeratin 7 (CK7) and epithelial related antigen (ERA).
A) CK7 staining of ascites cells with A') being a magnified picture of A).
B) ERA staining and B') magnified picture of B).

3.7 Cytotoxicity of *dl*922-947 in human primary ascites

Next, I wanted to further investigate *dl*922-947's efficacy in lysing human primary ascites cells.

As shown in figure 3-6, *dl*922-947 showed great variance in lysing human primary ascites between different patient samples. *dl*922-947 was most successful in lysing patient sample AB followed by the patient samples AS and ED. *dl*922-947 was the least efficient in lysing patient samples DW, JMcD, MH and MMcL.

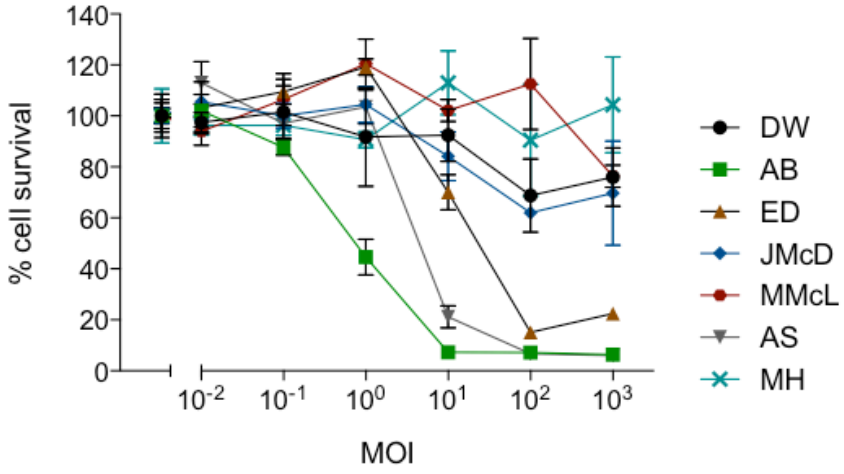

Figure 3-6: *dl*922-947s ability to lyse cells varies between different primary human ascites samples.
Primary human ascites cells were infected with *dl*922-947 at indicated MOI. Cell survival was assessed 120 hours post-infection by MTT assay and normalized to uninfected cells. Points represent mean +/- STDEV from one experiment performed in triplicate wells.

3.8 Discussion

Oncolytic adenoviruses have already been used in models of pre-clinical research, where they have shown promising activities in several cancer models, but only few made it into clinical trials. As described earlier a few oncolytic adenoviruses (ONYX-015, H101 and EnAd) have been evaluated in clinical trials, with one of them being approved in combination with chemotherapy for the treatment of squamous cell cancers of head and neck or oesophagus in China. New and improved oncolytic adenoviruses are needed to increase the therapeutic outcome for patients. There are many different aspects that can be researched in further detail, to help understand the mechanisms behind successful virotherapy. These include, but are not limited to, better understanding the mechanistics of viral infection and replication. The spread of viral particles and how viruses induce cell cytotoxicity as well as what immune responses virus elicit *in vitro* and *vivo* and how these can be modified to increase immunogenicity.

The use of Ad5 –based oncolytic adenoviruses in research has come across several difficulties in the recent years, with one of its major limitations being the down-regulation of its primary cell entry receptor in several human tumours due to Raf-MAPK pathway activity (Anders et al. 2003), while CD46 (Ad11 and Ad35 entry receptor) is commonly up-regulated in human cancers (Thorsteinsson et al. 1998, Hulin-Curtis et al. 2016). Comparison of the adenovirus subgroup B, type 2 adenoviruses Ad11 and Ad35 as well as of the subgroup C adenovirus Ad5 in the ovarian cancer cell lines IGROV1, OVCAR4 and TOV21G showed that sensitivity greatly varied between cell lines and adenoviruses. While Ad11 and Ad35 showed similar EC50 values between cell lines, Ad5WT and the E1A-CR2 deleted Ad5 mutant *dl*922-947 showed greater variation between the cell lines. Adenoviral efficacy partly depends on the expression of the primary cell entry receptors on the host cell, as in the case for Ad11 and Ad35, CD46 is their respective primary entry receptor, but even though they are using the same entry receptor, cytotoxicity was significantly different between those two adenoviruses in the same cell line, with Ad35 being significantly more cytotoxic in each cell line than Ad11. Research performed by (Wong et al. 2012) showed that the expression of CD46 did not correlate with Ad11-mediated cytotoxicity, showing that other mechanisms determine Ad-induced cytotoxicity, and explains

why a significant difference between Ad11 and Ad35-induced cytotoxicity was observed in the same cell line, which was also observed by (Shashkova, May and Barry 2009). They further showed that Ad11's potency was also not related to its infectivity but rather that the expression of early gene transcription mediates Ad11 cytotoxicity (Wong et al. 2012). Since Ad11 and Ad35 were used for the same cell lines, differences in intracellular events or mutation status can be excluded, leading to the conclusion that differences in the biology of Ad11 and Ad35 determined their efficacy to induce cytotoxicity. (Stone et al. 2003) published the complete DNA sequence and transcription map of Ad11; and analysis and genome sequence comparison showed that Ad35 and Ad11 show the highest genome homology (>98%) with major base pair mismatches found in the hexon and fiber genes region. Their overall conclusion was that: "… Ad11 was evolutionarily derived from a cross-serotype fiber substitution into the Ad35 genome, or that Ad35 was derived in the same manner from an Ad11 genome." This further shows that, though Ad11 and Ad35 show high genome homology, they differ in their biology. Evidence further suggests that Ad11 might utilize another unidentified receptor (Tuve et al. 2006), offering another explanation for differences in sensitivity between Ad35 and Ad11. Further, the consistently low amounts of cytotoxicity induced by Ad11 observed here, could hinder its use as an oncolytic adenovirus. Though Ad35 showed promising sensitivity in ovarian cancer cells, its ability to down-regulate CD46 and the slow complete restoration time of CD46 expression are known problems (Sakurai et al. 2007).

Though Ad5WT showed greater cytotoxicity in some ovarian cancer cells (OVCAR4 and TOV21G) than Ad11, Ad5WT showed a great variability between cell lines with an average EC50 of 41 pfu/cell for IGROV1, 14 pfu/cell for OVCAR4 and an average of 1 pfu/cell for TOV21G at 120 hours post-infection. Also the E1A-CR2 deleted Ad5 mutant *dl*922-947 showed greater variation between the cell lines with an average EC50 of 5 pfu/cell for IGROV1, 4 pfu/cell for OVCAR4 and 0.1 pfu/cell for TOV21G though it showed to induce significantly higher cytotoxicity than Ad5WT. This observation is in line with findings by the host lab that, *in vitro*, *dl*922-947 induced lysis with greater efficacy than Ad5WT (Lockley et al. 2006). This was further confirmed by western blot analysis, showing that adenoviral proteins are being expressed at earlier time points in *dl*922-947 infected cells than in Ad5WT infected cells. This observation is again

in line with Lockley, et al. 2006, where they showed that *dl*922-947's increase in efficacy was marked by earlier expression of viral proteins, as well as the earlier induction of S-phase.

Besides *dl*922-947s superior efficiency *in vitro* in comparison to Ad5WT, intratumoral and intravenous efficacy of *dl*922-947 was assessed *in vivo* by the lab of David Kirn (Heise et al. 2000), showing that tumour-bearing animals treated with *dl*922-947 showed superior survival and tumour regression in comparison to vehicle controls or *dl*1520 treated mice, making it a promising treatment of cancer from the pre-clinical point of view.

It was of great interest that, though cells were sensitive to *dl*922-947, experiments demonstrated that sensitivity could vary at least 50-folds between cell lines. To further analyse the differences in sensitivity, infectivity between the cell lines using Ad-GFP, an E1 deleted non-replicating type 5-adenovirus that contains a CMV early promoter that drives GFP expression, was compared. 24 hours post-infection with Ad-GFP at MOI 5, 92% TOV21G cells were GFP positive, while 76% of IGROV1 were positive and only 57% of OVCAR4 cells were GFP positive offering another explanation for the observed differences in cytotoxicity. The most likely explanation is that IGROV1, OVCAR4 and TOV21G express different amounts of CAR and integrins on the cell surface, which are used by *dl*922-947 to enter the host cell, resulting in differences in infectivity with Ad-GFP and also resulting in differences in viral load. In accordance with this explanation, Okegawa *et al*. reported significant differences in CAR expression in several human bladder cancer cell lines and that those correlated with their sensitivity to adenovirus infection (Okegawa et al. 2000) making different levels of CAR expression a possible answer.

In line with this, analysis of viral protein production showed that viral proteins are being produced at earlier time points in TOV21G, which was also the easiest to infect cell line. Strong E1A expression was observed at 24 hours post-infection followed by a decrease in E1A at 48 hours, which is associated with an increase in adenoviral core and capsid proteins. This shows that there is a higher availability of viral proteins which can lead to an earlier assembly of new

infectious viral particles, which will once the particles are assembled lead also to an earlier induction of cell death to help viral spread.

Further analysis of differences in replication kinetics of *dl*9222-947 showed that TOV21G and OVCAR4 produced a higher titre than IGROV1 24 hours post-infection. Interestingly TOV21G cells showed a reduction in viral titre at 48 hours post-infection, which was associated with a decrease in cell survival. The resulting cell death in TOV21G at 48 hours leads to the release of infectious particles allowing another round of viral infection and lysis. This observation gives a further explanation for why TOV21G is so sensitive to *dl*922-947-induced cytotoxicity and why differences in sensitivity between the cell lines are observed.

Overall, a higher infectivity rate, which results in a higher load of adenovirus particles, leads to the early and high expression of adenoviral proteins. This allows earlier viral assembly and induction of virus-induced death and explains partly why TOV21G showed greater sensitivity to Ad5WT and *dl*922-947-induced cytotoxicity than IGROV1 and OVCAR4. Besides these observations a study by Connell CM *et al.* has shown that virus-induced host cell DNA damage signalling and repair mechanisms are a further key determinant of oncolytic adenoviral efficacy (Connell et al. 2011) in human ovarian cancer and in addition, Tookman *et al.* showed in a recent paper that intact homologous recombination (HR) function promotes viral DNA replication and augments overall oncolytic adenoviral efficacy (Tookman et al. 2016). Therefore, showing the highly complex biology of how adenovirus efficacy is influenced by cellular intrinsic mechanisms.

Human primary ascites cells (MH) were analysed for their expression of the epithelial markers CK7 and ERA. Though cells were shown to be positive for the markers, confirming their epithelial origin, upon further inspection it was observed that the ascites that were cultured did not consist of a homogenous population but rather consisted of several cell types. Considering the origin of the ascites cells and that the cells are nucleated, it is likely that those cells could be lymphocytes, monocytes/macrophages or even neutrophils that are in circulation and have been isolated as well. To confirm the origin of these cells

further IHC on NIMP (Neutrophil marker), F4/80 (Macrophage marker) and PAX-5 (B-cell marker) etc. need to be performed until then their origin can only be speculated. Further, for successful *in vitro* use, these cells need to be further isolated to avoid background induced by different cell populations within the culture.

Besides CK7 and ERA IHC, Tagged-amplicon sequencing (TAm-sequencing) of MH using a high-grade serous ovarian cancer panel, performed by Anna Piskorz at the CRUK Cambridge Centre, showed that cells were *TP53* mutant (data not shown), which is in line with data showing that *TP53* mutations are near universal in HGSOC (Ahmed et al. 2010, TCGA 2011) and indicates that those cells are likely to be ovarian high grade serous carcinoma cells.

When isolated human primary ascites cells were infected with *dl*922-947 they showed great variability in cytotoxicity. One of the reasons why primary ascites showed differences in sensitivity is that they might express different levels of *dl*922-947s primary cell attachment receptor as described earlier. This might be the most likely case for cells that were completely resistant to *dl*922-947 like MH, DW, MMcL and JMcD. Primary ascites cells ED and AS showed to be somewhat sensitive to *dl*922-947 induced infection at higher MOI. This shows that the virus was able to infect the cell, but intrinsic mechanisms lead to a lower viral efficacy, while ascites cells AB showed the highest sensitivity. Mechanistically speaking those cells must have allowed for easy viral infection and replication, which is highly desirable for oncolytic virotherapy. Unfortunately, limited availability and difficulty in maintaining primary cells in culture beyond 3-4 passages did not allow us to follow up on further experiments to address as to why these patient samples showed different sensitivities. These data are also in line with my *in vitro* data and published research showing that *dl*922-947 efficacy varies greatly between different cell lines and tumours and that it greatly depends on CAR expression (Okegawa et al. 2000), but besides *dl*922-947's dependency on CAR and its down-regulation in many cancers (Anders et al. 2003) the host lab showed in 2015 that CAR expression is up-regulated in paclitaxel-resistant ovarian cancer cells and patient samples (Ingemarsdotter et al. 2015), making administration of Ad5 derived oncolytic adenoviruses a

possible future therapy for women with ovarian cancers resistant to conventional paclitaxel treatment.

To conclude this chapter, the host lab and I have been able to show that *dl*922-947 shows superior efficiency to Ad5WT and to the well-described oncolytic adenovirus ONYX-015 (*dl1520*) in lysing tumour cells *in vitro (Lockley et al. 2006)*. We showed, that changes in efficacy between different cell lines resulted from differences in infectivity, replication, the production of viral proteins and *dl*922-947's ability to induce S-phase in the host cells. Besides its efficacy *in vitro*, the host lab also showed that *dl*922-947 infection resulted in a dramatic *in vivo* survival advantage. Further, I have been able to show that *dl*922-947 was able to induce cell death in three out of seven patient derived human primary ascites cells. These results show that *dl*922-947 may have clinical potential for the treatment of ovarian cancer.

Chapter 4

Mechanisms of *dl*922-947-induced death

4 Mechanisms of *dl*922-947-induced cell death

4.1 Introduction

Programmed cell death is important for homeostasis, the development of organisms, during injury and as a response mechanism to infections. To limit infection, multicellular organisms have developed several defence mechanisms; these include innate and adoptive immune responses as well as the induction of interferons, which can lead to the activation of programmed cell death, therefore limiting the production and release of viral progeny.

As described previously, adenoviruses encode several inhibitors of apoptosis but how they induce cell death has not been studied in detail. It has been shown that several adenovirus proteins are implicated in the induction of apoptosis e.g. E1A (Debbas and White 1993, Lowe and Ruley 1993), E4 (Marcellus et al. 1996) and E3 (Tollefson et al. 1996) to facilitate cell lysis and the release of viral progeny, but both Abou Hassan *et al*. 2004 and Sarah Baird *et al*. 2008 showed that oncolytic adenoviral mutants may induce a novel mode of cell death.

In this chapter I aim to further characterize cell death induced by *dl*922-947 in ovarian cancer cell lines, with an emphasis on programmed necrosis

4.2 Apoptosis

4.2.1 Z.VAD.fmk does not inhibit *dl*922-947 induced cell death

To further examine the involvement of apoptosis in *dl*922-947-induced cell death, I made use of Z.VAD.fmk, which is a non-cytotoxic, cell permeable pan-caspase inhibitor that irreversibly binds to caspase proteases through their catalytic sites. It has been previously shown that Z.VAD.fmk is able to inhibit Caspase-1, 2, 3, 4, 5, 6, 7, 8 and 9 (Ekert, Silke and Vaux 1999, Garcia-Calvo et al. 1998) making it a broad spectrum inhibitor for the intrinsic as well as extrinsic apoptotic pathway.

To test whether Z.VAD.fmk was able to rescue *dl*922-947-induced cell death, IGROV1, OVCAR4 and TOV21G cells were infected with *dl*922-947 at varying MOI and treated with 25μM Z.VAD.fmk or DMSO.

As seen in figure 4-1A, no significant reduction in cytotoxicity was observed in IGROV1 and OVCAR4 when cells were infected with *dl*922-947 in the presence of 25μM Z.VAD.fmk. Comparisons of average EC_{50} values for vehicle (DMSO) versus Z.VAD.fmk treatment showed no significant difference, while for TOV21G there was a significant increase in *dl*922-947-induced cell death in the presence of Z.VAD.fmk. This observation is in accordance with the necrosis literature, showing that inhibition of caspases can lead to a more extensive non-apoptotic form of cell death (Figure 4-1A and D)(Vercammen et al. 1998).

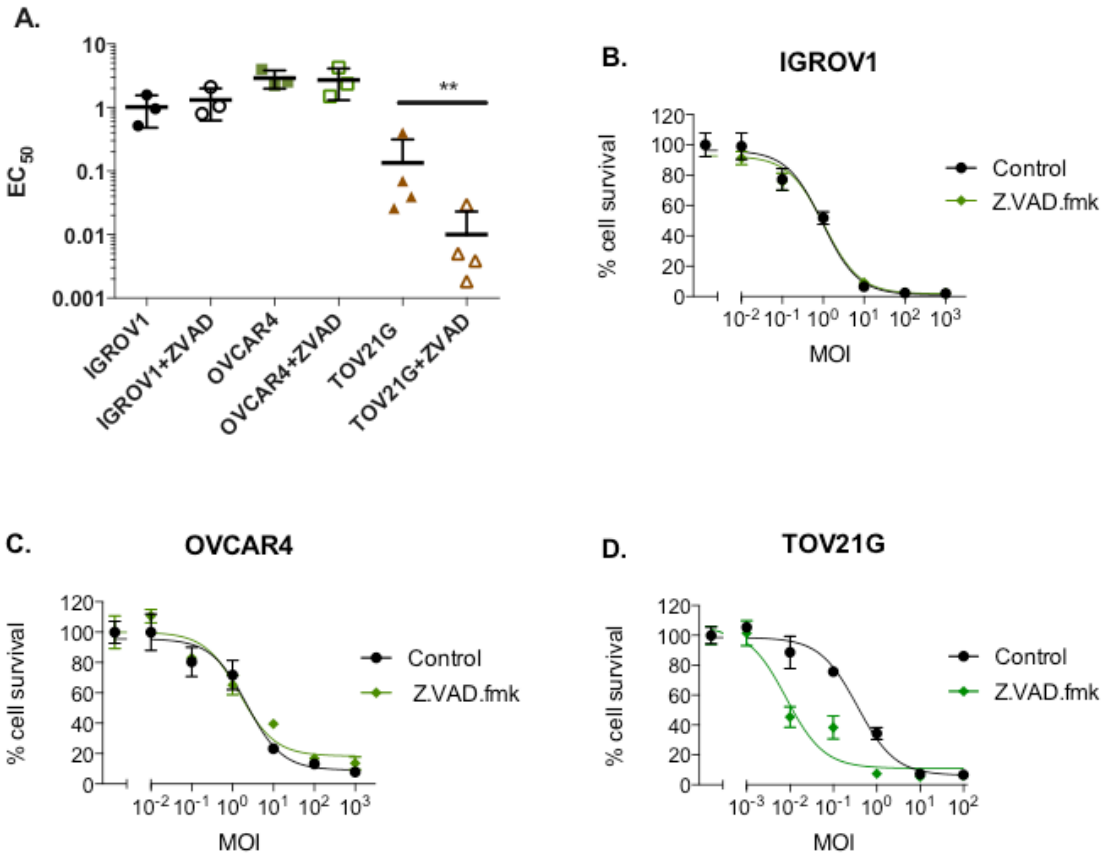

Figure 4-1: *dl*922-947 induced cell death is not rescued by the addition of the pan-caspase inhibitor Z.VAD.fmk

A) IGROV1, OVCAR4 and TOV21G were infected with *dl*922-947 and were either treated with 25uM Z.VAD.fmk or vehicle. Cell survival was assessed 120 hours post treatment by MTT assay. Points represent mean EC50 +/- STDEV from at least three experiments with each experiment performed in triplicate wells. Differences in EC50 values between treated and untreated cells are not significant unless indicated in the figure.

B-C) show representative dose response curves for each cell line.

P values are calculated using unpaired t-test, ** shows p<0.01.

4.2.2 BCL-2 overexpression does not inhibit *dl*922-947-induced cell death

B-cell lymphoma 2 (BCL-2) belongs to the BCL-2 family of proteins that regulate pro- and anti-apoptotic signalling. BCL-2, with the anti-apoptotic proteins BCL-x_L and BCL-w, is known for its regulatory function and inhibition of apoptosis, and is a well-known oncogene.

Next, I wanted to investigate if *dl*922-947-induced cell death was triggered through the activation of the apoptotic mitochondrial pathway (intrinsic pathway) as a result of cellular stress during virus infection. Therefore, I created a cell line that overexpressed the anti-apoptotic protein BCL-2, which blocks apoptosis by inhibiting the pro-apoptotic proteins Bax and Bak.

As seen in figure 4-2A, OVCAR4 cells do not express BCL-2, while cells transduced with a retrovirus encoding BCL-2 show expression of BCL-2 on the protein level. In figure 4-2B, staurosporine, a well-known inducer of apoptosis (Falcieri et al. 1993, Bertrand et al. 1994, Koh et al. 1995), was used to assess if BCL-2 overexpression would rescue cell death as described in the literature (Reynolds et al. 1996, Takeda et al. 1997). As seen in figure 4-2B, staurosporine induces apoptosis in OVCAR4 cells, which can be significantly rescued by BCL-2 overexpression, but has no effect on *dl*922-947-induced cell death, figure 4-2C.

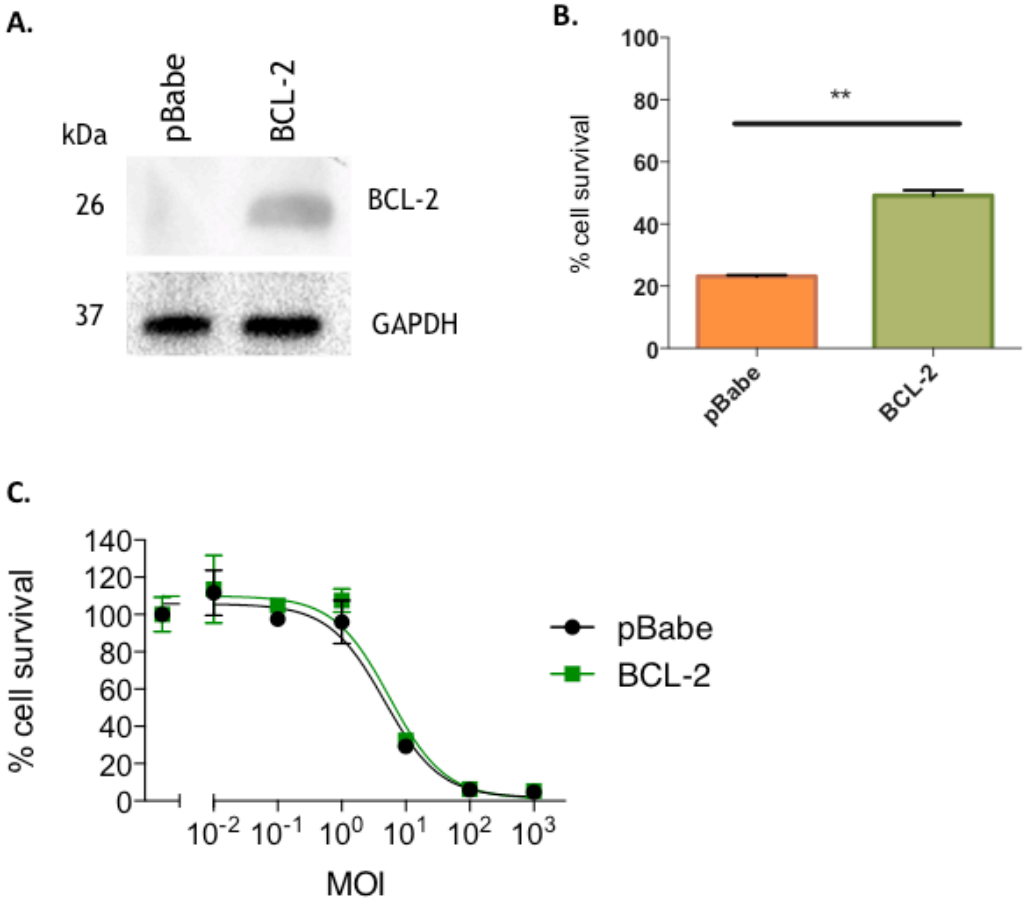

Figure 4-2: BCL-2 overexpression does not rescue *dl*922-947-induced cell death in OVCAR4
OVCAR4 cells were transduced with retroviruses containing an empty pBabe vector or pBabe containing the BCL-2-alpha protein sequence.
A) Immunoblot of OVCAR4 cells with and without BCL-2 overexpression. Samples were blotted for GAPDH (37 kDa) and BCL-2 (26 kDa). One representative western blot from two experiments is shown.
B) OVCAR4-pBabe and OVCAR4-BCL-2 were treated with 1μM staurosporine for 10 hours. Media was then removed and new medium was added and sulforhodamine B assay was performed 72 hours post treatment. Points represent mean +/- STDEV of one experiment performed in quadruplicate wells.
C) OVCAR4-pBabe and OVCAR4-BCL-2 were infected with *dl*922-947 at indicated MOI. Cell survival was assessed 120 hours post-infection by MTT assay and normalized to uninfected cells. Points represent mean +/- STDEV from one experiments performed in triplicate.
P values are calculated using unpaired t test, ** shows $p<0.01$.

4.3 Programmed necrosis

Historically necrosis was considered for a long time as an unregulated form of accidental cell death that is caused by sudden tissue damage. This view of necrosis has been rewritten in the past two decades with data showing that necrosis can be regulated (Laster, Wood and Gooding 1988). It has been shown that receptor interacting kinases are critical regulators of what has now been termed “Programmed Necrosis”.

4.3.1 Inducing programmed necrosis in ovarian cancer cell lines

It has previously been shown that Smac-mimetic (SM) can induce apoptosis in certain cancer cell lines and that the addition of a pan-caspase inhibitor, such as Z.VAD.fmk or Q-VD-OPH, can inhibit cell death (Bertrand and Vandenabeele 2011). For some cell lines, this treatment in combination with TNF-α can lead to exacerbated cell death. These cells show morphological features of necrosis, such as discontinuous cytoplasmic membranes and swollen mitochondria. In addition, death can be blocked with the receptor interacting protein kinase 1 (RIPK1) inhibitor necrostatin-1 (Nec-1) (Degterev et al. 2008) or the mixed-lineage kinase-like protein (MLKL) inhibitor necrosulfonamide (NSA) (Sun et al. 2012).

A panel of ovarian cancer cell lines was tested to assess their ability to undergo programmed necrosis by treating cells with different combinations of TNF-α (T), Smac-mimetic (S), Z.VAD.fmk (Z), Nec-1 and NSA for 24 hours.

As seen in Figure 4-3, no cell death was observed when IGROV1 cells were treated with TS, therefore no rescue could be observed when they were additionally treated with TSZ, TSZ+Nec-1 or NSA. Treatment of OVCAR4 with TS resulted in cell death, which could be rescued by Z.VAD.fmk. No further increase in cell survival was observed when cells were additionally treated with Nec-1 or NSA. Treatment of TOV21G with TS led to a great reduction in cell survival, which was further increased by the addition of Z.VAD.fmk. The addition of Nec-1 or NSA to TSZ treated TOV21G cells was able to significantly increase cell survival.

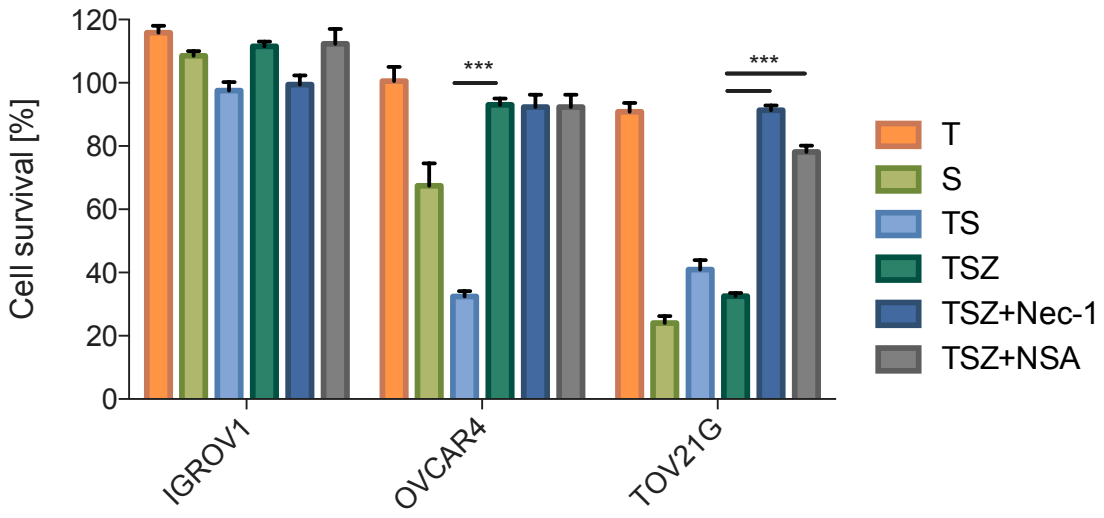

Figure 4-3: TOV21G undergoes programmed necrosis during TSZ treatment
IGROV1, OVCAR4 or TOV21G cells were treated with TS, TSZ, TSZ+Nec-1 or TSZ+NSA at the following concentrations: TNF-α: 20ng/mL, Smac mimetic: 1μM, Z.VAD.fmk: 25μM, necrostatin-1: 10μM and necrosulfnamide: 1μM. Cell survival was assessed 24 hours post-treatment by MTT assay. Data show % cell survival +/- STDEV of a single experiment, performed in triplicate wells. P values are calculated using One Way ANOVA with multiple comparisons, *** shows $p<0.001$.

4.3.2 RIPK3 expression determines cellular ability to undergo programmed necrosis

It has been shown that the execution of programmed necrosis induced by TSZ relies on the expression of the protein receptor interacting protein kinase 3 (RIPK3) and that RIPK3 expression in different cell lines correlates with the responsiveness to necrosis induction, making it the critical determinant of cellular necrosis in response to TNF-α (He et al. 2009). Other components involved in the necrotic machinery include the protein RIPK1, which directly interacts with RIPK3 through its RIP homotypic interaction motif (RHIM) domain forming the necrosome (Sun et al. 2002), and the downstream mediator MLKL (Sun et al. 2012, Zhao et al. 2012). Therefore, protein expression levels of RIPK1, RIPK3 and MLKL in IGROV1, OVCAR4 and TOV21G were analysed by Western blotting.

In keeping with results from figure 4-3, IGROV1 expressed no RIPK3 protein at 57kDa, which correlates with data shown for programmed necrosis induction using TSZ. In addition, IGROV1 expressed low amounts of RIPK1 protein at 78 kDa in comparison to OVCAR4 and TOV21G. OVCAR4 expresses low amounts of RIPK3, resulting in a very faint band at 57kDa, while TOV21G shows expression of both proteins, RIPK1 and RIPK3. As seen in figure 4-4 all three cell lines express MLKL to comparable levels.

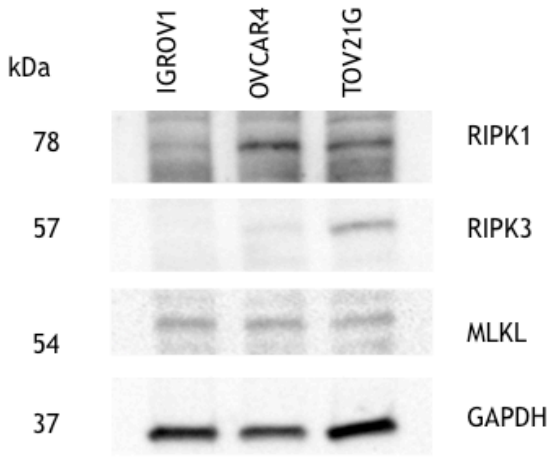

Figure 4-4: Protein expression of RIPK1, RIPK3 and MLKL in IGROV1, OVCAR4 and TOV21G
Cell lysates were prepared, run on SDS-PAGE, transferred to a nitrocellulose membrane and blotted for indicated proteins. Samples were blotted for RIPK1 (78 kDa), RIPK3 (57 kDa), MLKL (54 kDa) and GAPDH (37 kDa). One representative western blot from two experiments is shown.

4.3.3 Expression of necrotic core proteins in human primary ascites cells

Next, I wanted to assess if human primary ascites cells express the core proteins of the necrosome by western blot.

Figure 4-5, shows that most human primary ascites cells express RIPK1, RIPK3 and MLKL, though protein levels vary considerably between patient samples. Sample AC is the only one found that does neither express RIPK1 or RIPK3 on the protein level.

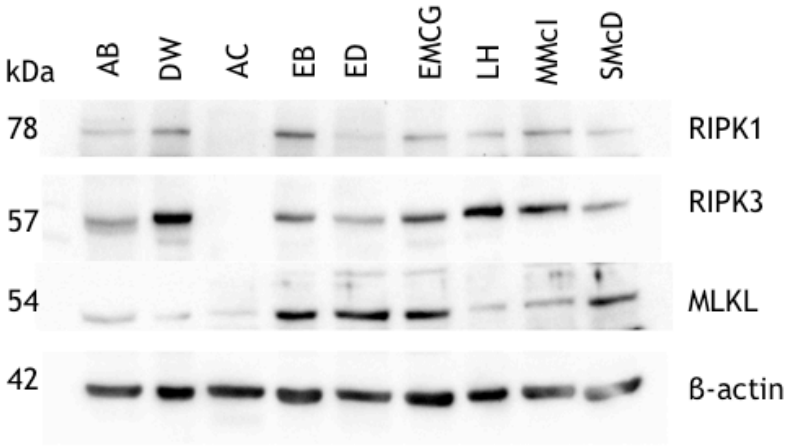

Figure 4-5: Human primary ascites cells express components of the necrosome
Human primary ascites cells were collected and prepared for western blot analysis. Samples were probed for RIPK1 (78 kDa), RIPK3 (57 kDa), MLKL (54 kDa) and β-actin (42 kDa).

4.3.4 Levels of RIPK1, RIPK3, Caspase 8 and MLKL during *dl*922-947 infection

It has been shown that during adenovirus infection, host protein translation is down-regulated to allow the translation of viral proteins, which are needed for the assembly of new infectious virions (Cuesta, Xi and Schneider 2004, Walsh 2010). In addition, many host proteins themselves are targeted for proteasomal degradation to promote viral gene expression, translation, assembly and spread. To determine if adenovirus infection alters the expression of core necrotic proteins, the ovarian cancer cell line IGROV1, OVCAR4 and TOV21G were infected with *dl*922-947 at MOI 10 for 0, 24 and 48 hours and changes in protein expression were analysed.

Figure 4-6 shows that there are no changes in the expression of the core necrotic proteins RIPK1, Caspase 8 and MLKL during *dl*922-947 infection. Interestingly, RIPK3 protein expression is down-regulated in TOV21G during infection.

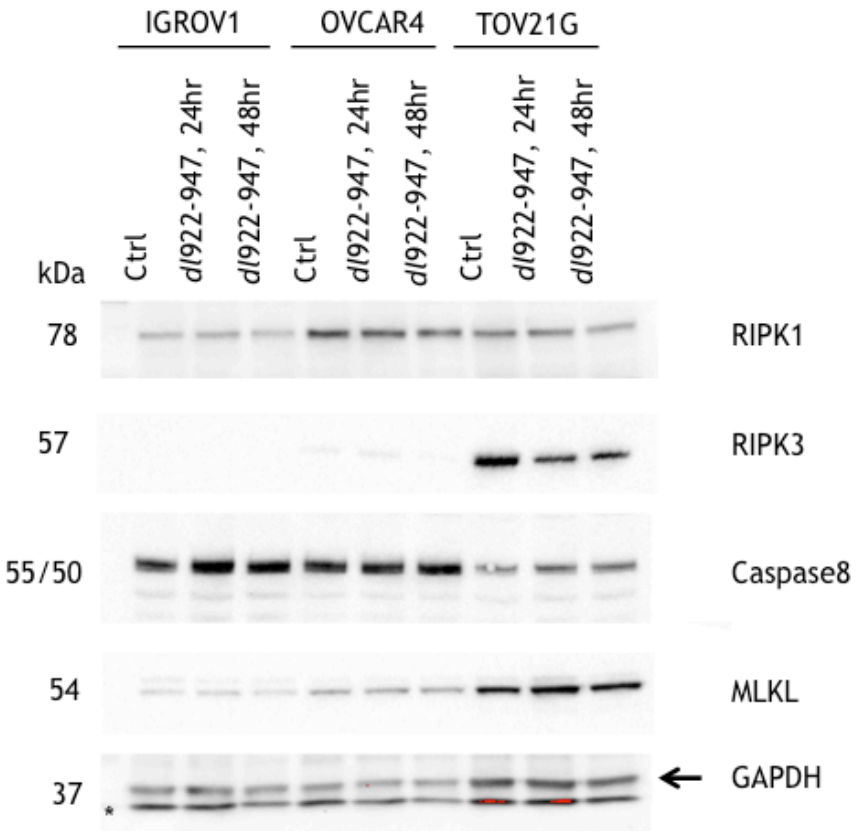

Figure 4-6: Expression of RIPK1, RIPK3, Caspase 8 and MLKL during *dl*922-947 infection
IGROV1, OVCAR and TOV21G were infected with *dl*922-947 at MOI 10 for 0, 24 and 48 hours and analysed according to western blotting protocol. Samples were blotted for RIPK1 (78 kDa), RIPK3 (57 kDa), MLKL (54 kDa), Caspase 8 (55/50 kDa) and GAPDH (37 kDa). One representative western blot from 2 experiments is shown. Asterisk indicates an unspecific band.

4.3.5 Ovarian cancer cells display necrotic features during *dl*922-947 infection

During programmed necrosis, cells undergo distinct morphological changes that are different from other modes of cell death such as apoptosis or autophagy. Morphological changes of necrotic cell death include the dilatation of the nuclear membrane and the condensation of the chromatin, swelling of the cell, mitochondria and other organelles as well as the loss of plasma membrane integrity resulting in the leakage of the cellular content.

Transmission Electron Microscopy (TEM) was performed on TOV21G and OVCAR4 cells to examine morphological changes during adenovirus infection. Cells were either mock infected, treated with TSZ for 6 hours (TOV21G) or infected with *dl*922-947 at MOI 1 (TOV21G) or MOI 3 for 72 hours (OVCAR4). Cells were prepared in accordance with the TEM preparation protocol and then imaged at the Electron Microscopy Facility at the University of Glasgow and further analysed.

Figure 4-7A shows the morphology of OVCAR4 cells during mock-infection. The cells are elongated and show normal nuclear and organelle morphology. Figure 4-7B shows an OVCAR4 cell during *dl*922-947 infection. Morphological changes in *dl*922-947-infected cells included a ‘swelling’ phenotype of the cell, where cells seem to lose their epithelial cell morphology and start to round up. Further, cells showed clear evidence of infection in the nucleus. A mix of mature and immature virions could be detected in the nucleus (Figure 4-7C).

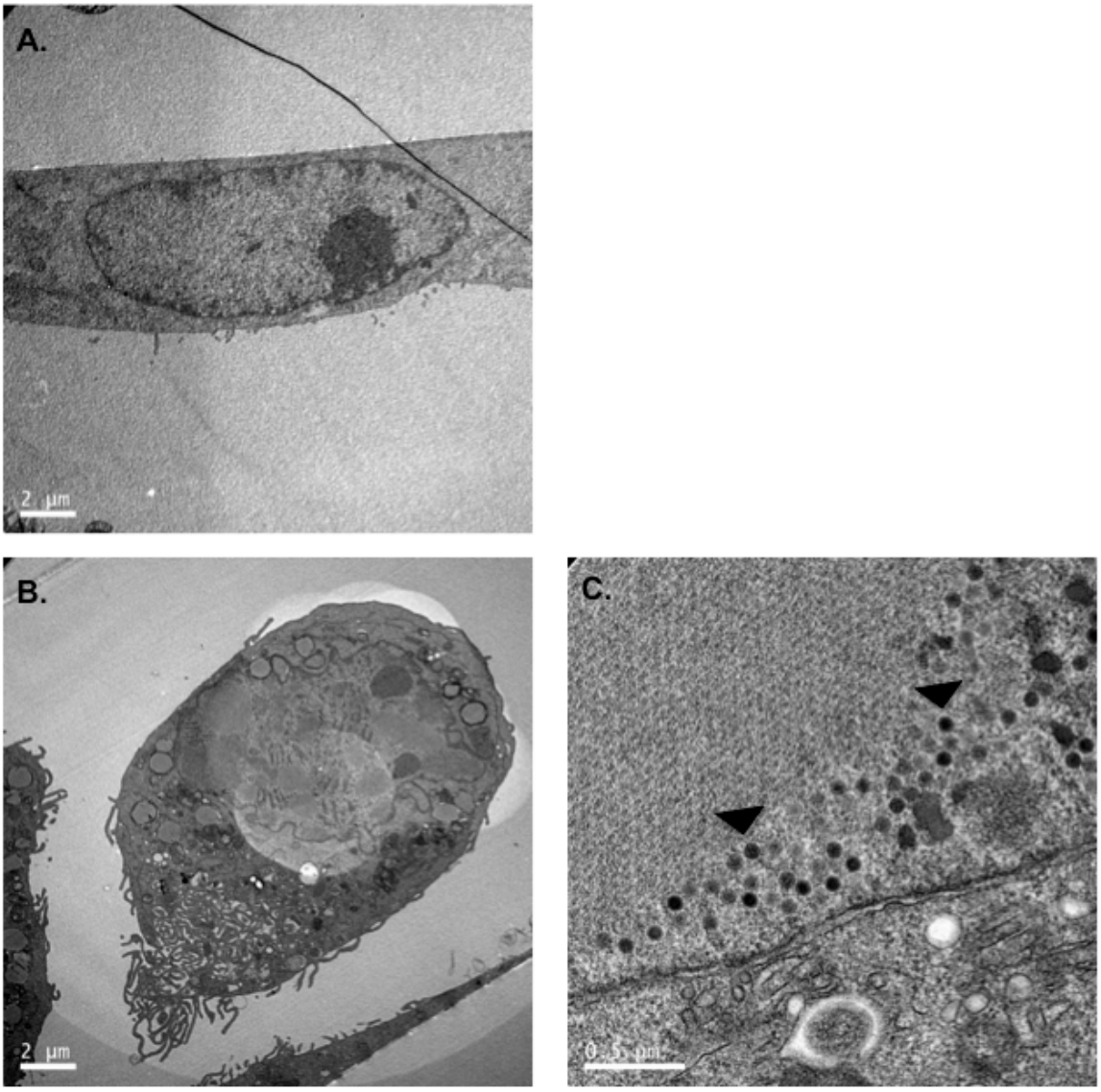

Figure 4-7: Transmission electron microscopy of *dl*922-947 virions in OVCAR4
A) OVCAR4 cells were either mock-infected and then further processed for transmission electron microscopy. Mock-infected cells show normal epithelial morphology.
B-C) OVCAR4 cells were infected with *dl*922-947 at MOI 3 for 48 hours. B) shows a cell during the early stages of *dl*922-947 infection with the lattice and virions located within the nucleus.
C) shows virions within the nucleus of an infected cell. Arrowheads indicate mature virions.

TOV21G cells that were treated with TSZ showed a necrotic morphology (Figure 4-8C-F) in comparison to mock treated cells (Figure 4-8A-B). Mock treated TOV21G cells showed epithelial morphology with healthy looking nuclei and mitochondria (Figure 4-8A-B), while TSZ treated cells showed enlarged and swollen nuclei (Figure 4-8C), signs of plasma membrane rupture, condensation of the chromatin into patches (Figure 4-8C, D and F), as well as an increasingly translucent cytoplasm, rupture of the nuclear membrane (Figure 4-8E) and dense mitochondria (Figure 4-8F).

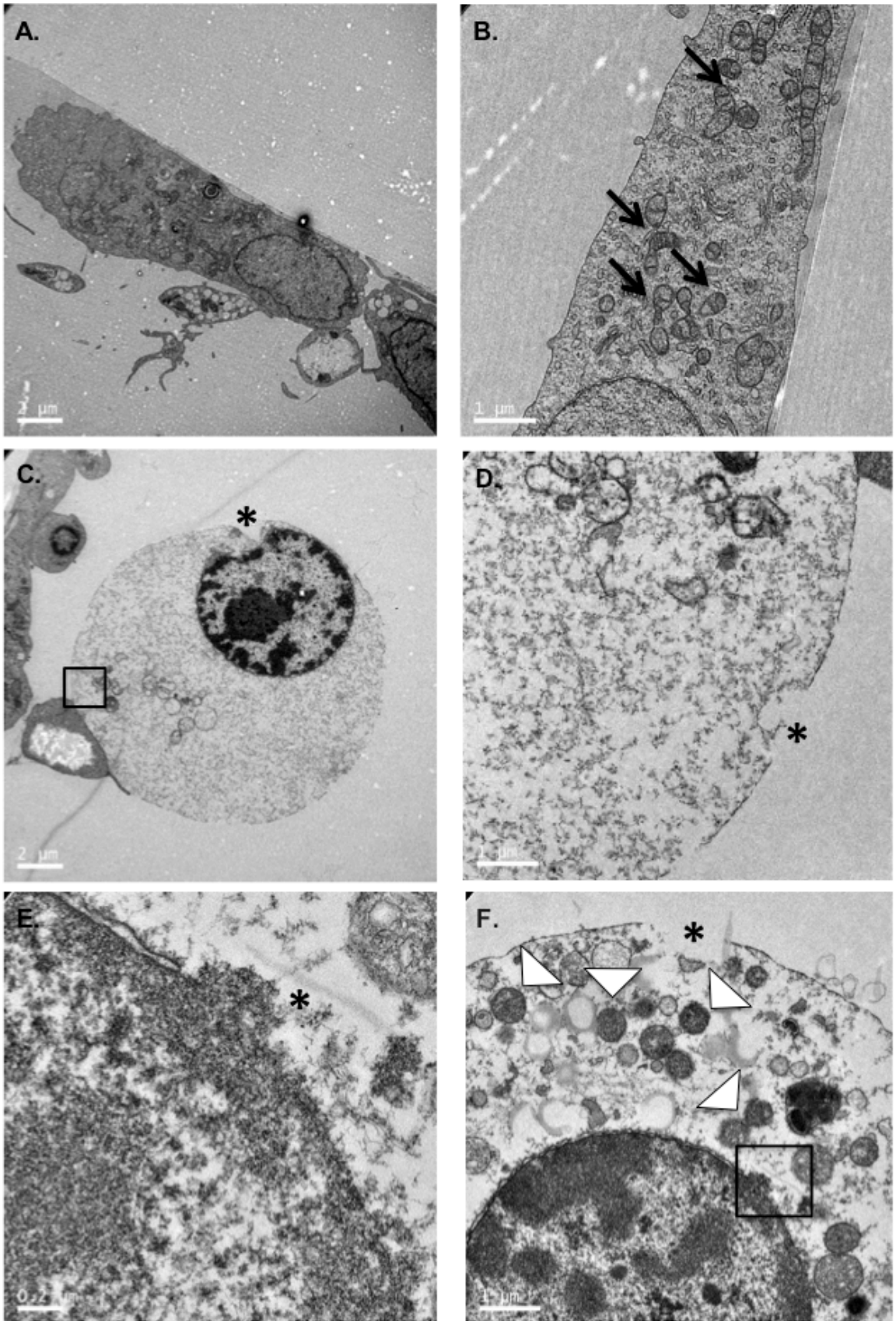

Figure 4-8: TOV21G cells treated with TSZ show necrotic morphology

A-B) TOV21G cells were mock-treated with DMSO and then further processed for transmission electron microscopy. A) shows normal epithelial morphology of a mock-treated cell and B) shows the morphology of normal mitochondria as indicated by arrows.

C-F) show TOV21G cells treated with with 20ng/mL TNF-α, 1μM smac-mimetic and 25μM Z.VAD.fmk (TSZ) for 6 hours. C-D) treatment with TSZ leads to the rounding up of the cell and the rupture of the plasma membrane. Asterisks indicate areas where the plasma membrane has

ruptured. Frames indicate magnified areas. E) is a magnified image of F) as indicated by frame and shows the rupture of the nuclear membrane. F) shows dense mitochondria (white closed arrowheads) in TSZ treated cells.

With similarity to TSZ treated cells, TOV21G infected with *dl*922-947 also show necrotic features during infection. Figure 4-9A shows TOV21G infected with *dl*922-947. Cells do not show signs of fragmentation. The cell has lost its epithelial morphology and parts of the cell are translucent due to loss of cytoplasmic integrity. Figure 4-9C shows the plasma membrane with ill-defined edges. According with infection vacuolisation can be observed (Figure 4-9B). Further, dense mitochondria were found in *dl*922-947-infected cells.

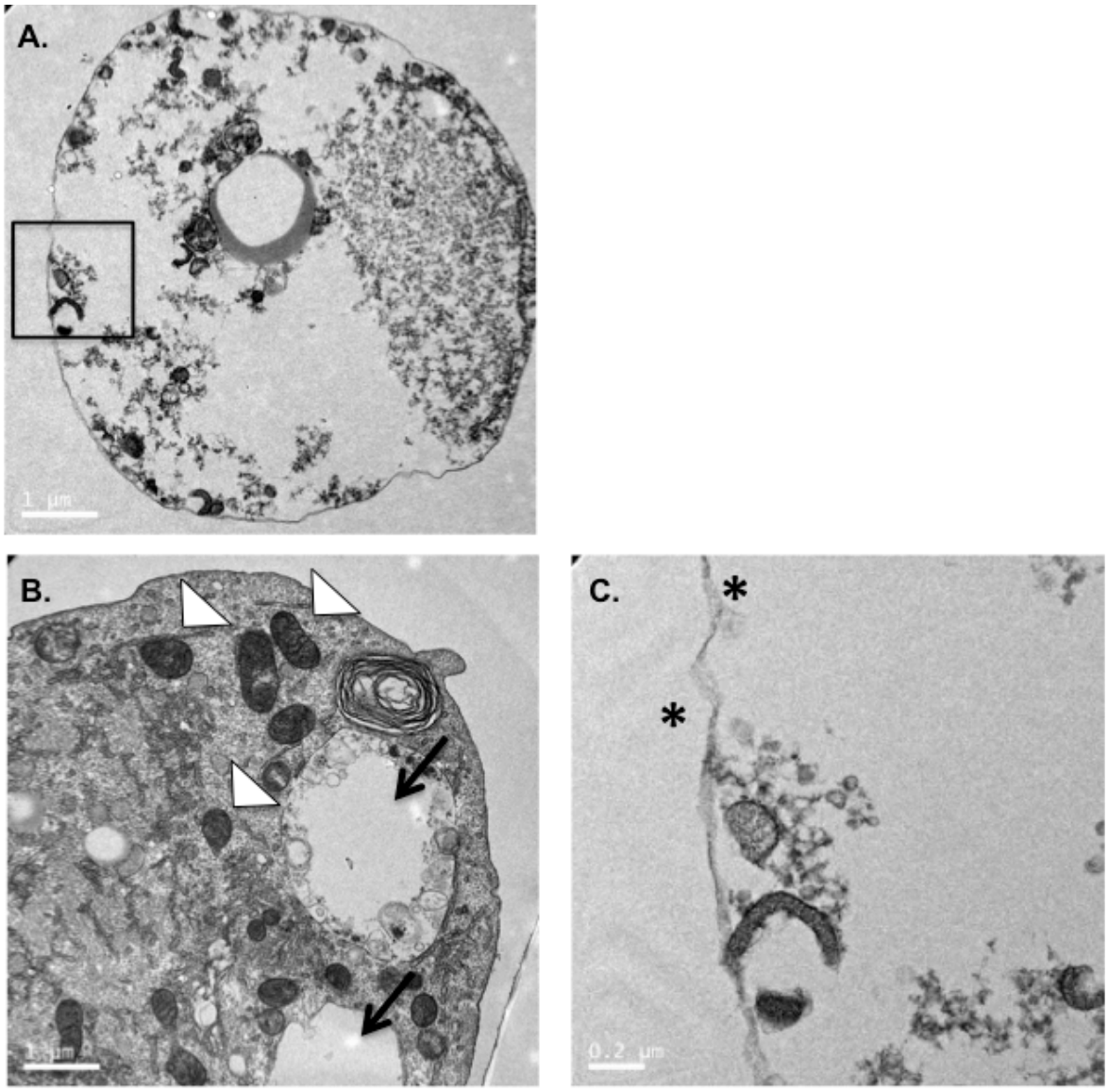

Figure 4-9: TOV21G infected with *dl*922-947 show necrotic morphology
A) TOV21G cells were infected with *dl*922-947 at MOI 1 for 48 hours and then further processed for transmission electron microscopy. Frames indicate magnified areas.
B) shows dense mitochondria (white arrow heads) and vacuolization (arrows).
C) is a magnified image of A, asterisks indicate areas where the plasma membrane starts to become translucent, before membrane rupture.

4.3.6 Investigating the role of TNF-α in *dl*922-947-induced cytotoxicity

There are several pathways of programmed, regulated necrosis, of which the best described pathway is induced by the ligation of TNF-α to the Tumour necrosis factor receptor 1 (TNFR1) (Han et al. 2011a). Besides the induction of programmed necrosis, the ligation of TNF-α with TNFR1 receptor can also lead to the activation of the NF-κB pathway or the induction of apoptosis depending on the cellular context. It is known that adenovirus infection induces acute inflammatory cytokine production including the upregulation of TNF-α (Salako et al. 2011). Therefore, adenovirus-induced programmed necrosis could be induced by autocrine TNF-α production and consequent TNF-α /TNFR1 interaction during infection.

To test if adenovirus-induced cell death depends on autocrine TNF- α production IGROV1, OVCAR4 and TOV21G cells were infected with *dl*922-947 at varying MOI and two hours post-infection, a human TNF-α blocking antibody was added at a concentration of 1µg/ml.

HeLa cells overexpressing the pro-necrotic protein RIPK3 (see chapter 5) are sensitized to cell death induction when treated with the cytokine TNF-α compared to their wild type counterpart. As shown in figure 4-10A, treating HeLa RIPK3 cells with 20ng/mL TNF-α resulted in a significant induction of cell death within two hours of treatment. This cell death could be completely and significantly rescued when cells were additionally treated with a human TNF-α blocking antibody. When cells were infected with *dl*922-947 and additionally treated with a TNF-α blocking antibody, no change in adenovirus-induced cytotoxicity was observed compared to vehicle treated cells infected at the same MOI (Figures 4-10B-D).

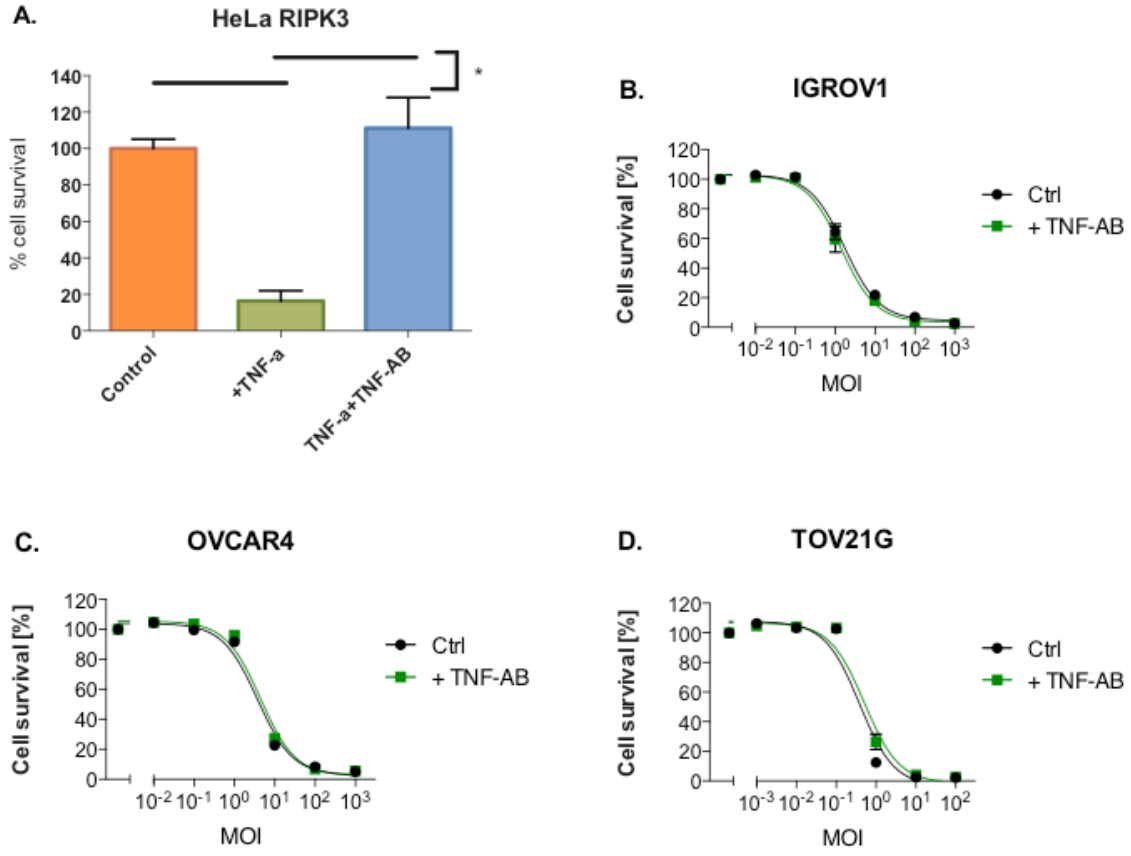

Figure 4-10: Blocking TNF-α using an anti-TNF-α antibody has no effect on *dl*922-947 induced cytotoxicity.

A) HeLa RIPK3 cells were treated with 20ng/mL TNF-α or with 20ng/mL TNF-α with the addition of 1µg/mL TNF-α blocking antibody. Cell survival was assessed 24 hours post treatment by MTT assay. Points represent mean +/- STDEV from one experiment performed in triplicate wells.
B-D) Show one representative dose response curve for each cell line from two experiments performed in triplicate wells.
P values are calculated using One Way ANOVA with multiple comparisons, * shows p≤0.05.

In experimental situations, programmed necrosis is induced by a combination of recombinant TNF-α, Smac-mimetic and Z.VAD.fmk. Interestingly the amount of TNF-α added to cells to induce programmed necrosis is higher than the amount of TNF-α that is generated by *dl*922-947 infected cells (Salako et al. 2011). Therefore, I wanted to investigate next if the further addition of TNF-α to *dl*922-947 infected cells would increase viral cytotoxicity by creating a more prominent necrotic phenotype.

As seen in figure 4-11A, the addition of 20ng/mL of TNF-α to *dl*922-947 infected IGROV1 cells had no effect on virus-induced cytotoxicity, but did lead to a significant increase in virus-induced cytotoxicity in OVCAR4 and TOV21G cells.

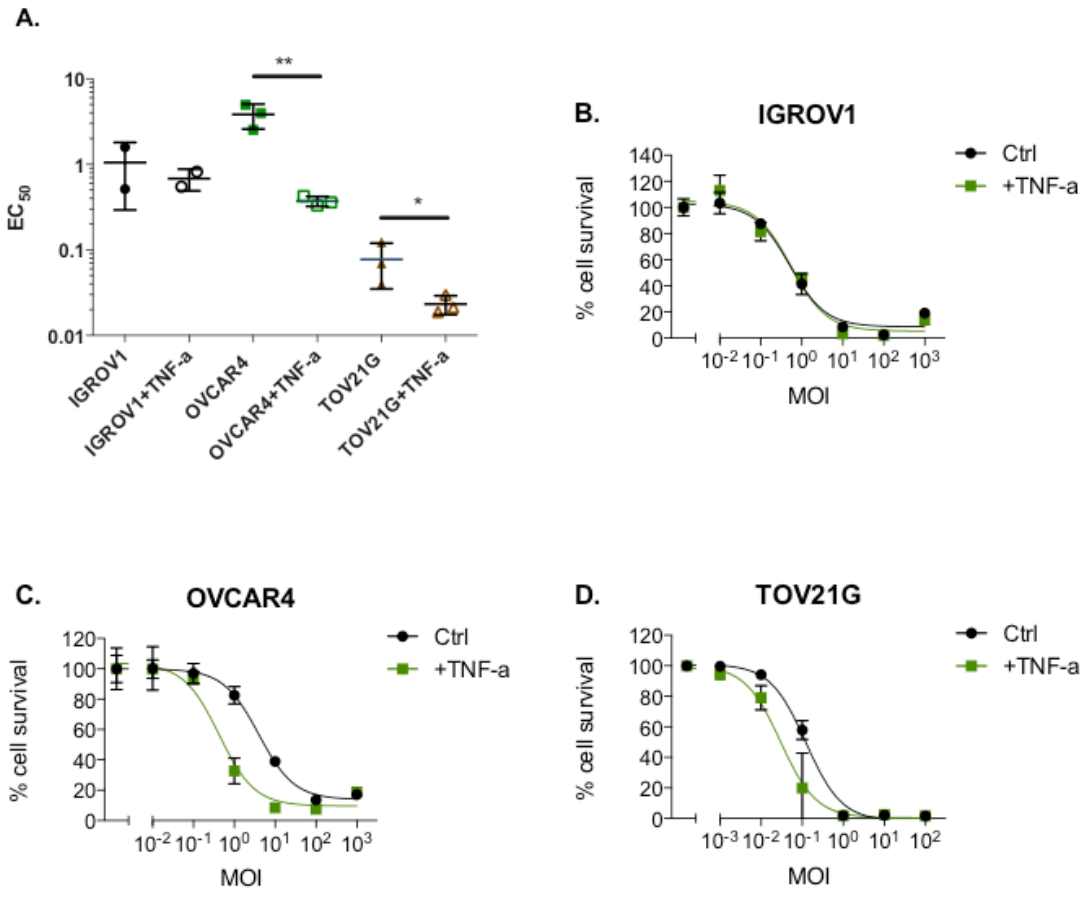

Figure 4-11: Addition of TNF-α to *dl*922-947 infected cells increases cytotoxicity in OVCAR4 and TOV21G

A) IGROV1, OVCAR4 and TOV21G were infected with *dl*922-947 with vehicle control or with *dl*922-947 with the addition of 20ng/mL TNF-α. Cytotoxicity was assessed 120 hours post treatment by MTT assay. Points represent mean EC50 +/- STDEV from at least two experiments with each performed in triplicate wells.

B-D) show representative dose response curves for each cell line.

P values are calculated using unpaired t test, *shows $p<0.05$ and **$p<0.01$.

Next, I investigated if the addition of TNF-α to *dl*922-947 infected OVCAR4 cells did indeed made cell death more necrotic. If cell death under these conditions was of an apoptotic nature, the addition of Z.VAD.fmk should be able to rescue cell death additionally induced by TNF-α. However, if it was of necrotic nature, Z.VAD.fmk should augment cell death or show no effect at all.

As shown in figure 4-12, Z.VAD.fmk was partly able to rescue cell death induced by TNF-α in *dl*922-947, but was not able to completely rescue cell death to vehicle-treated conditions.

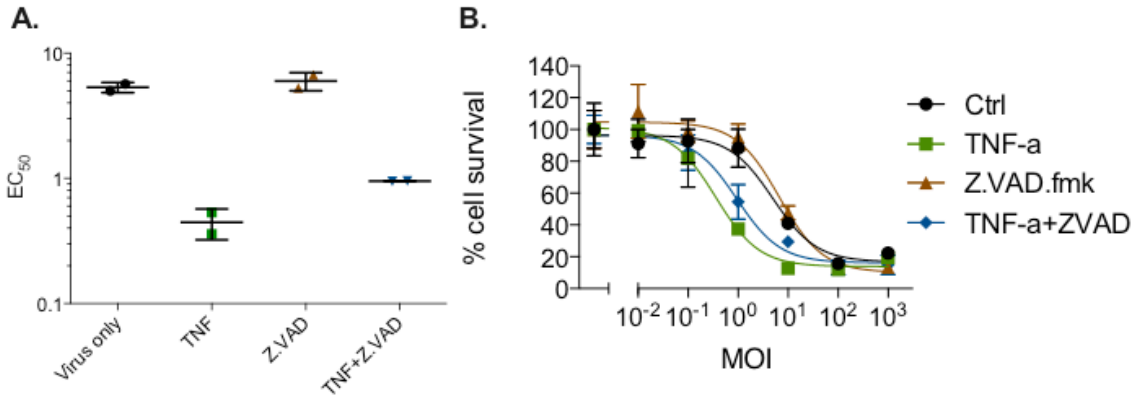

Figure 4-12: Z.VAD.fmk does not completely rescue cell death induced by the addition of TNF-α during *dl*922-947 infection

A) OVCAR4 cells were infected with *dl*922-947, *dl*922-947with 20ng/mL TNF-α, *dl*922-947 with 25μM Z.VAD.fmk or *dl*922-947 with 20ng/mL TNF-α and 25μM Z.VAD.fmk. Cytotoxicity was assessed 120 hours post treatment by MTT assay. Points represent mean +/- STDEV from 1 experiment performed in triplicate wells.

B) Figure shows one representative graph from two experiments performed in replicate wells.

4.3.7 Investigating the role of RIPK1 in *dl*922-947-induced cell death

4.3.7.1 Blocking RIPK1 with necrostatin-1

It has been shown that necrosis induced by VV (Whilding et al. 2013) depends on the formation of a pro-necrotic RIPK1-RIPK3 complex, due to sensitization of cells to TNF-induced cell death. Further, it has also been shown that treatment with necrostatin-1 (Nec-1) upon HSV-1 (Holler et al. 2000b) infection resulted in increased cell viability, showing that RIPK1 is important for the induction of cell death during VV and HSV-1 infection.

To determine the appropriate concentration of the RIPK1 inhibitor (Nec-1) for treatment, IGROV1, OVCAR4 and TOV21G were treated with increasing amounts of Nec-1 (10μM, 30μM, 50μM and 100μM) and incubated for 120 hours before cell survival was assessed using MTT assay.

As shown in figure 4-13A, Nec-1 does not induce any cytotoxicity in IGROV1 or OVCAR4 at concentrations as high as 100μM over a period of 5 days, while it induces dose-dependent non-specific cytotoxicity in TOV21G. As a compromise between induced cytotoxicity and concentrations used previously in the host lab (Whilding et al. 2013), 30μM Nec-1 was used in all the following experiments.

After the optimal concentration was determined, the stability of Nec-1 was assessed. Nec-1 was dissolved in tissue culture medium at desired concentration and incubated for 1, 2, 3, 4 and 5 days in a tissue culture incubator. After the indicated incubation period, TSZ was added to Nec-1 to investigate Nec-1's ability to block programmed necrosis.

As shown in figure 4-13B, Nec-1 is stable over the indicated period of time, when added to tissue culture medium. Even when incubated in tissue culture medium at 37ºC for 5 days prior to necrosis induction, Nec-1 is still able to rescue TSZ-induced death.

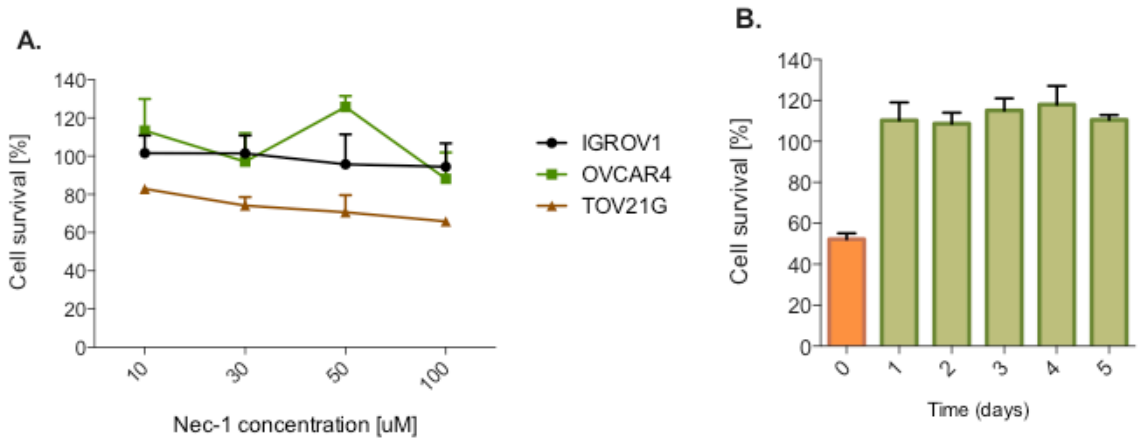

Figure 4-13: Necrostatin-1 induces unspecific cytotoxicity at high concentrations
A) IGROV1, OVCAR4 and TOV21G cells were treated with 10, 30, 50 or 100μM Nec-1. Cytotoxicity was assessed 120 hours post treatment by MTT assay. Points represent mean +/- STDEV from one experiment performed in triplicate well.
B) 30μM Nec-1 was incubated for 1, 2, 3, 4 and 5 days in DMEM at 37ºC in a tissue culture incubator before TSZ was added to induce programmed necrosis in TOV21G. Nec-1 stability was assessed 24 hours post treatment by MTT assay. Points represent mean +/- STDEV from one experiments performed in triplicate wells.

To investigate the importance of RIPK1 in oncolytic adenovirus-induced cell death IGROV1, OVCAR4 and TOV21G cells were infected with *dl*922-947 and treated with 30μM Nec-1 two hours after infection. 72 hours after infection, medium was aspirated and replaced with fresh medium containing 30μM Nec-1.

Figure 4-14C shows that there is no significant difference in EC_{50} values between cell lines infected with *dl*922-947 when treated with vehicle or 30μM of Nec-1. Figures 4-14D-F show typical dose response curves for cells either treated with vehicle or 30μM Nec-1 during *dl*922-947 infection.

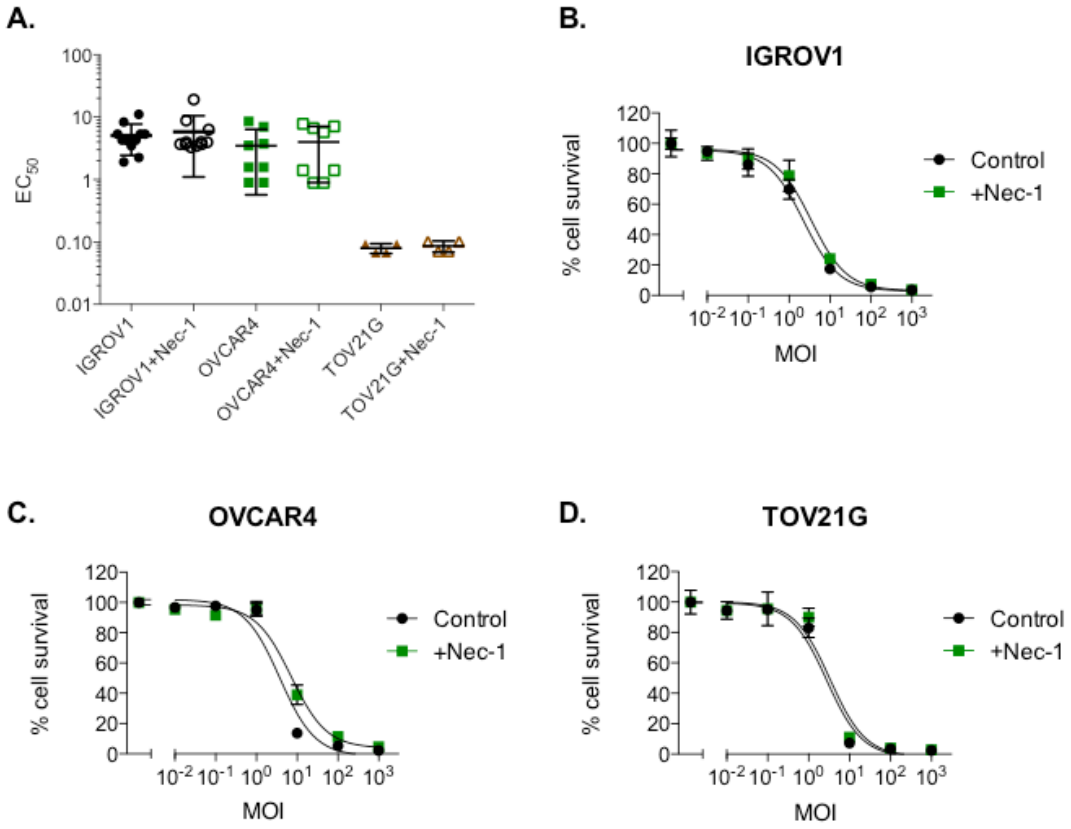

Figure 4-14: Necrostatin-1 treatment does not rescue *dl*922-947-induced cell death
A) IGROV1, OVCAR4 and TOV21G were infected with *dl*922-947 and treated with vehicle or 30μM Nec-1. Medium was replaced 72 hours post-infection and fresh medium containing 30μM Nec-1 was added. Cytotoxicity was assessed 120 hours post treatment by MTT assay. Points represent mean EC50 +/- STDEV from at least four experiments with each experiment performed in triplicate wells. Differences in EC50 values between treated and untreated cells are not significant unless indicated in the figure.
B-C) show representative dose response curves for each cell line.

4.3.7.2 Blocking RIPK1 with novel GSK inhibitors

It has been shown in recent studies that the RIPK1 inhibitor Nec-1 is chemically identical to an inhibitor of the immunomodulatory enzyme indoleamine 2,3-dioxygenase (IDO) called methyl-thiohydantoin-tryptophan (MTH-Trp), therefore making it an inhibitor both RIPK1 and IDO (Takahashi et al. 2012, Vandenabeele et al. 2013). Therefore, new analogues of Nec-1 are required to study the contribution of RIPK1 in cell death and survival. Besides the analogues Nec-1i (inactive) and Nec-1s (more stable variant) (Degterev, Maki and Yuan 2013) GlaxoSmithKline (GSK) has developed new RIPK1 inhibitors GSK2791728A (GSK'728A) and GSK3002963A (GSK'963A)) as well as their inactive controls (GSK2791729A (GSK'729A) and GSK3002962A (GSK'962A)) for future cell death studies. In 2015, GSK identified and described a new RIPK1 kinase inhibitor (GSK'963), which showed a 100-fold increase over Nec-1 in cell-based assays and increased selectivity for RIPK1 over other kinases. GSK'962A is the inactive enantiomer of GSK'963A and used to confirm off-target effects (Berger, Bertin and Gough 2015a, Berger et al. 2015b).

Next I wanted to test if using the more selective GSK'963A inhibitor and its respective inactive form GSK'962A had an effect on *dl*922-947-induced cell death.

As seen in figure 4-15A, GSK'728A and GSK'963A are able to significantly rescue TSZ-induced programmed necrosis induced in TOV21G. GSK'728A and GSK'963A are able to rescue cell death to comparable levels as the well described necrosis inhibitors Nec-1 and NSA. The inactive enantiomers GSK'729A and GSK'962A are not able to rescue TSZ-induced cell death and show comparable amounts of cell death to TSZ treatment alone. Figure 4-15B-D shows representative graphs of IGROV1, OVCAR4 and TOV21G infected with *dl*922-947 and treated with vehicle, 20nM GSK'962A or 20nM GSK'963A. As shown below, no difference in *dl*922-947-induced cytotoxicity was observed.

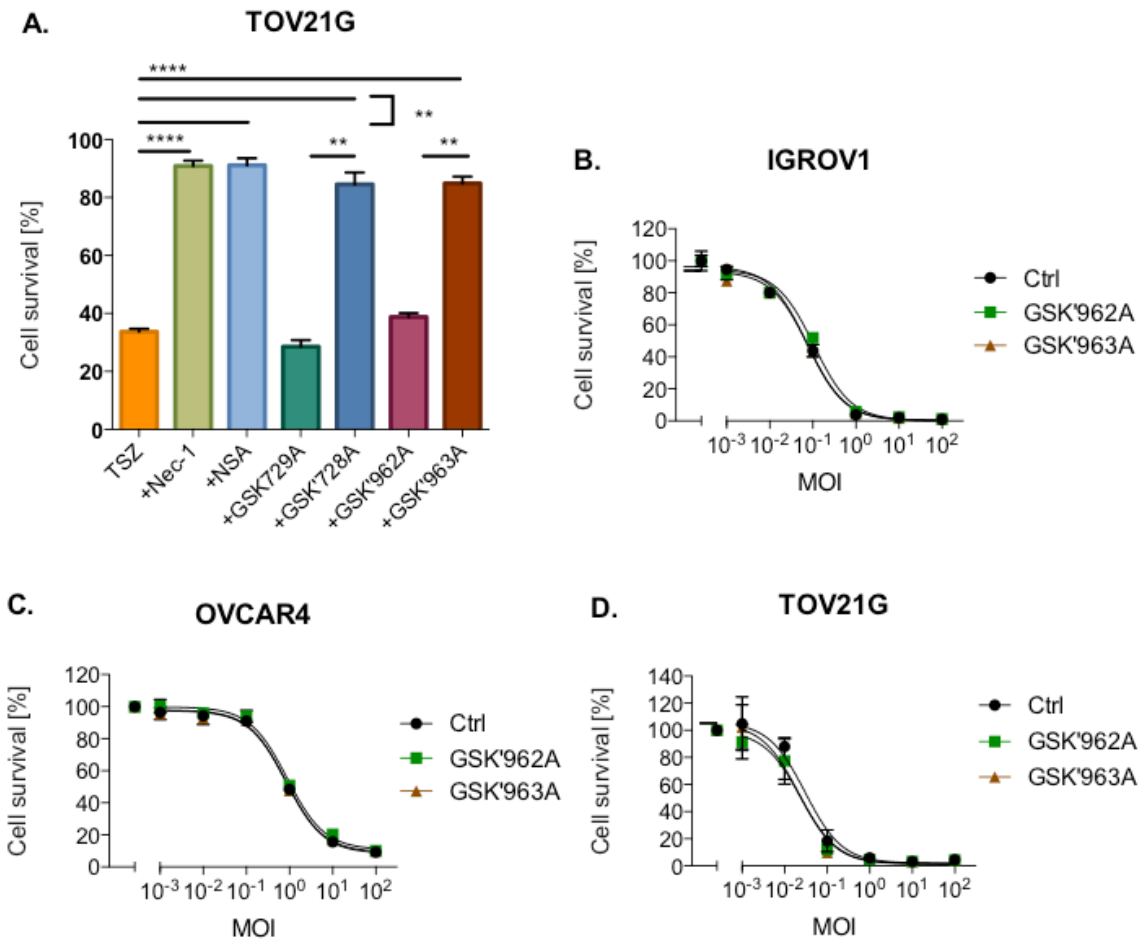

Figure 4-15: GSK RIPK1 inhibitors do not rescue *dl*922-947-induced cell death
A) TOV21G cells were treated with TSZ and either vehicle, 10μM Nec-1, 3μM NSA, 10nM GSK'729A, 100nM GSK'728A, 10nM GSK'962A or 10nM GSK'963A were added. Cell survival was assessed 24 hours post-treatment by MTT assay. Data shows mean +/- STDEV of a single experiment, performed in triplicate wells.
B-D) IGROV1, OVCAR4 and TOV21G cells were infected with *dl*922-947 with the addition of vehicle, 20nM GSK'962A or 20nM GSK'963A. Cell survival was assessed 120 hours post-infection by MTT assay and normalized to uninfected cells. Shown is one representative graph, where points represent mean +/- STDEV from one experiment performed in triplicate wells.
P values are calculated using One Way ANOVA with multiple comparisons, ** shows $p<0.01$ and ****$p<0.0001$.

4.3.7.3 Knock down of RIPK1 using siRNA

To exclude the possibility that RIPK1's presence alone might lead to the autophosphorylation of its interaction partner RIPK3 and other non-specific effects induced by using chemical inhibitors, RIPK1 was knocked down using siRNA to see if loss of RIPK1 would have any effect on adenovirus-induced death.

First I determined the lowest concentration of siRNA that would give a complete protein knock-down after 24 hours.

As shown in figure 4-16 there is no difference in RIPK1 expression between non-transfected and 100pmol scrambled siRNA transfected cells, while all used concentrations of RIPK1 siRNA gave a complete protein knock-down after 24 hours of transfection. To avoid any siRNA-mediated off-target effects, the lowest amount of RIPK1 siRNA (10pmol) was used for all following experiments using RIPK1 siRNA.

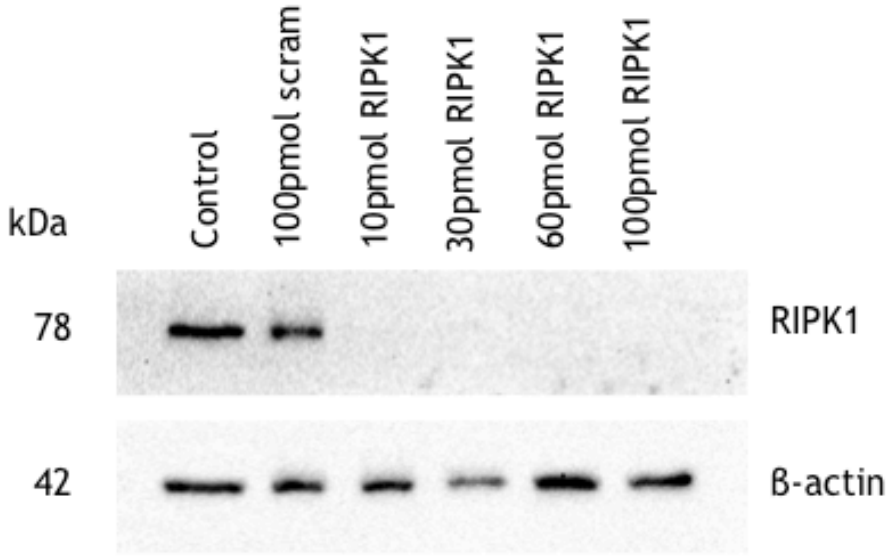

Figure 4-16: RIPK1 knock-down in TOV21G using siRNA
TOV21G cells were transfected with 100pmol scrambled or 10, 30, 60 or 100pmol of RIPK1 siRNA for 24 hours. After 24 hours samples were taken and prepared for western blot analysis. Samples were blotted for RIPK1 (78 kDa) and β-actin (42 kDa). One representative western blot from two experiments is shown.

Next, IGROV1 and TOV21G cells were transfected with 10pmol scrambled or 10pmol of RIPK1 siRNA. After 24 hours cells were then infected with *dl*922-947. The effect of siRNA-mediated knock down of RIPK1 in virus-infected cells was analysed 120 hours post infection.

Figure 4-17 shows the effect of siRNA-mediated knockdown on adenovirus-infected cells. As shown in figure 4-17E) siRNA-mediated knock down of RIPK1 significantly rescues TSZ-induced cell death in TOV21G while in figure 4-17A) siRNA-mediated knock down of RIPK1 does not rescue cell death in A) IGROV1 and C) TOV21G cells during *dl*922-947 infection. Western blot analysis was performed at time of MTT assay, showing that RIPK1 protein levels are down-regulated in IGROV1 B) and TOV21G D).

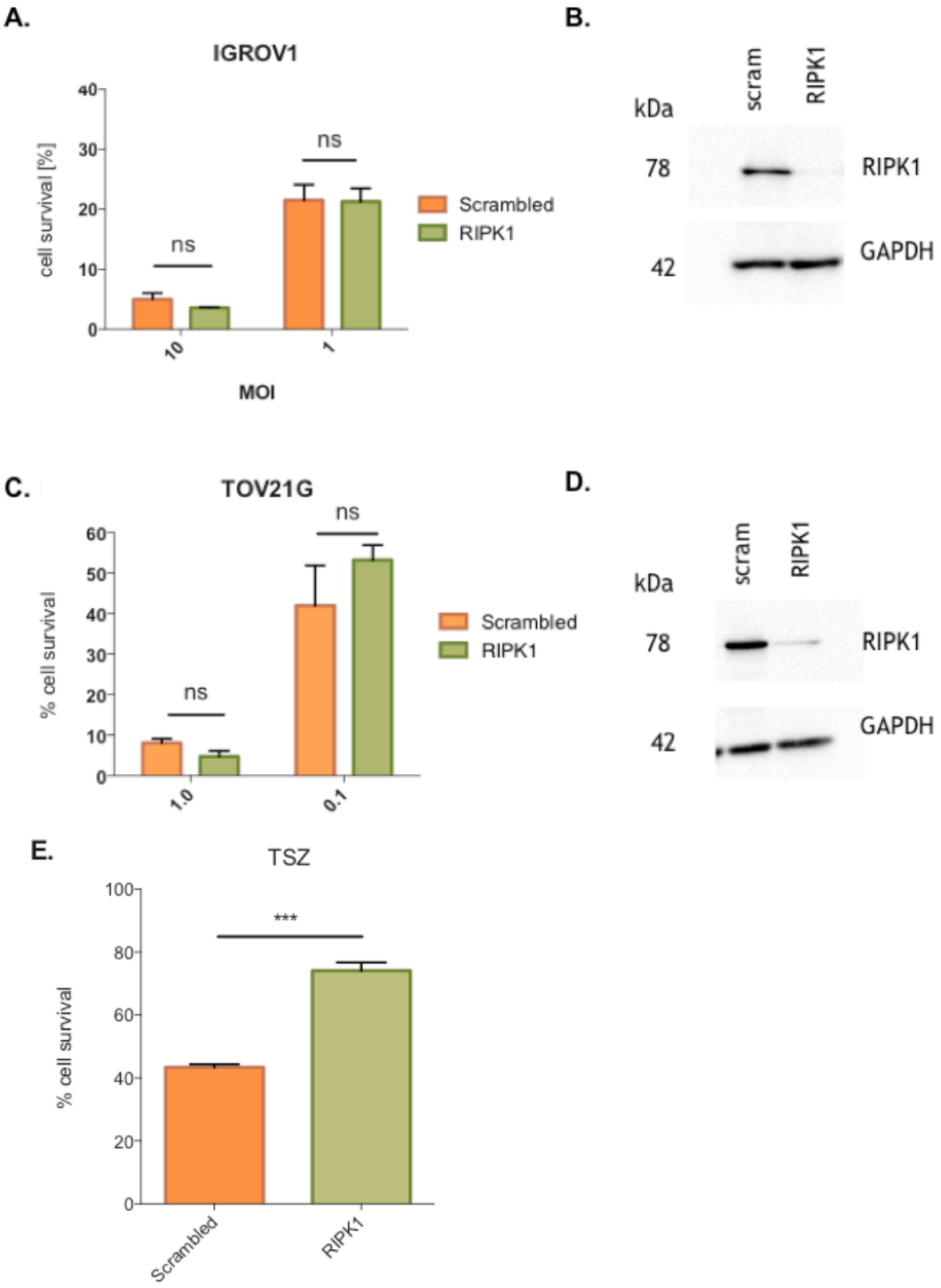

Figure 4-17: siRNA-mediated knock down of RIPK1 does not rescue *dl*922-947-induced cell death

A) IGROV1 and C) TOV21G cells were transfected with 10pmol scrambled or 10pmol RIPK1 siRNA. 24 hours post-transfection cells were infected with *dl*922-947 at indicated MOI. Cell survival was assessed 120 hours post-infection by MTT assay and normalized to uninfected cells treated with the same amount of siRNA. Points represent mean +/- STDEV from one experiment performed in triplicate wells.

B) IGROV1 and D) TOV21G samples were taken 120 hours post infection and blotted for RIPK1 (78 kDa) and GAPDH (37 kDa). One representative western blot from three experiments is shown.

E) TOV21G cells were transfected with 10pmol scrambled or 10pmol RIPK1 siRNA. 24 hours post-transfection cells were treated with 20ng/mL TNF-α, 1μM smac-mimetic and 25μM Z.VAD.fmk. Cell survival was assessed 48 hours post-treatment by MTT assay. Points represent mean +/- STDEV from one experiment performed in triplicate wells. P values are calculated using unpaired t-test, *** shows $p<0.001$.

4.3.8 Investigation of the role of RIPK3 in *dl*922-947-induced cell death

4.3.8.1 Inhibiting RIPK3 with novel GSK inhibitors

It has been shown that the execution of programmed necrosis relies on the expression of the protein RIPK3 and that its expression in different cell lines correlates with the responsiveness of these to necrosis induction, making it the determinant for cellular necrosis in response to TNF-α (He et al. 2009). So far the only known RIPK3 inhibitors have been described by Kaiser *et al.* (Kaiser, Upton and Mocarski 2013b) and were identified by screening small-molecule libraries in a collaboration with GSK. This screen revealed three compounds (GSK'840B, GSK'872B and GSK'843A) that bound RIPK3's kinase domain and therefore inhibited its kinase activity, while showing minimal cross-reactivity.

Using the new RIPK3 inhibitors provided by GSK, I wanted to investigate if they were able to rescue *dl*922-947-induced cell death by inhibiting the protein RIPK3.

As seen in figure 4-18A the RIPK3 inhibitor GSK'840B was able to rescue programmed necrosis induced by TSZ treatment to comparable levels as Nec-1 and NSA in TOV21G. The RIPK3 inhibitor GSK'872B was also able to rescue programmed necrosis, but to a lesser extent as GSK'840B. GSK'843A was not able to rescue programmed necrosis induced by TSZ in TOV21G. Figure 4-18B and C shows that treatment of OVCAR4 and TOV21G with 10μM GSK'840B or GSK'872B has no effect on *dl*922-947-induced cell death.

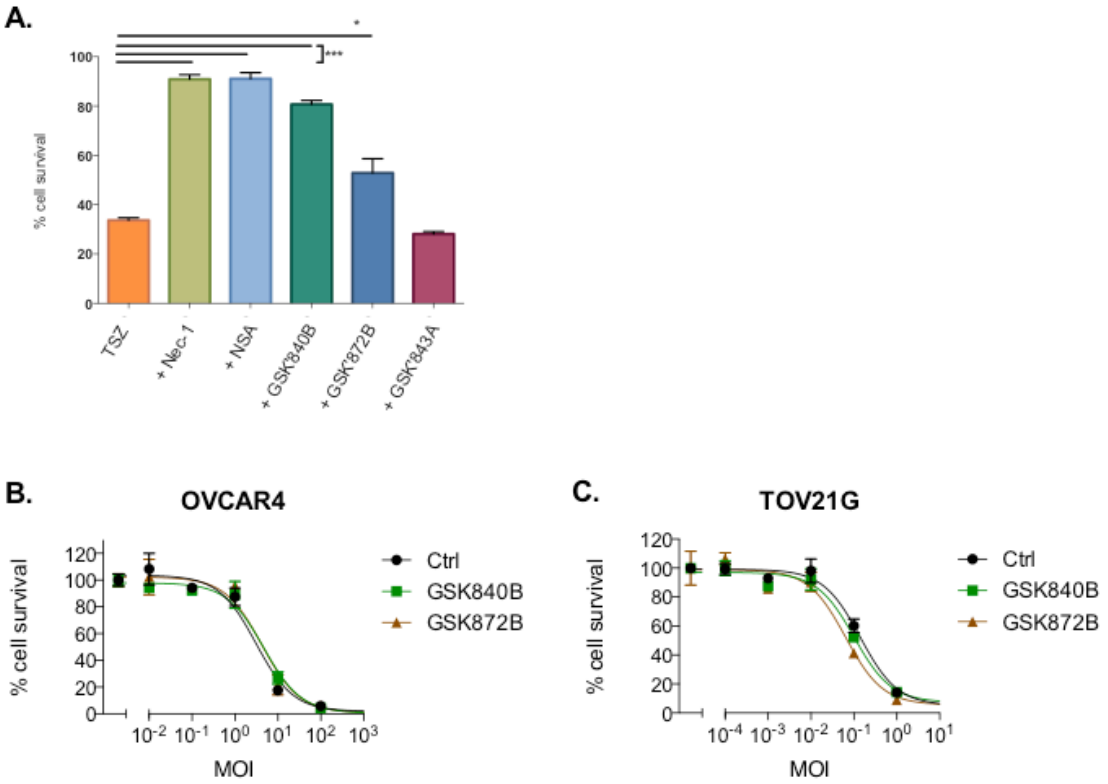

Figure 4-18: Inhibition of RIPK3 using inhibitors does not rescue *dl*922-947-induced cell death

A) TOV21G were treated with TSZ to induce programmed necrosis and 10μM GSK'840B, 10μM GSK'872B or 10μM GSK'843A. Points represent mean +/- STDEV from one experiment performed in triplicate wells.

B-C) OVCAR and TOV21G were infected with *dl*922-947 with the addition of vehicle, 10μM GSK'840B or 10μM GSK'872B. Cell survival was assessed 120 hours post-infection by MTT assay and normalized to uninfected cells treated with the same amount of vehicle or inhibitor. Shown is one representative graph from two experiments. Points represent mean +/- STDEV from one experiment performed in triplicate wells.

P values are calculated using One Way ANOVA with multiple comparisons, * shows $p<0.05$ and ***$p<0.001$.

4.3.8.2 Knock down of RIPK3 using siRNA

Next I wanted to test if siRNA-mediated knock down of RIPK3 was able to rescue *dl*922-947-induced cell death since pharmacological inhibitors can show off-target effects. First the lowest amount of RIPK3 siRNA was determined as described earlier.

As shown in figure 4-19 10pmol of RIPK3 siRNA are enough to achieve knock down of RIPK3 on the protein level. Further, figure 4-19 shows some very faint bands at 57kDa in all used concentrations.

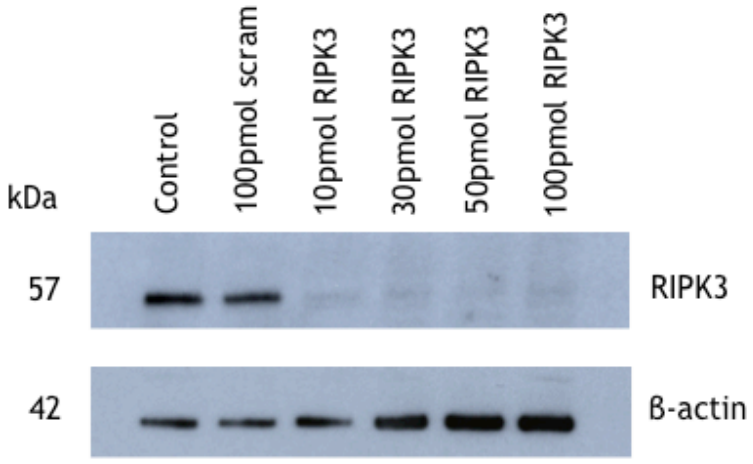

Figure 4-19: siRNA-mediated knock down of RIPK3 in TOV21G.
TOV21 cells were transfected with 100pmol scrambled or 10, 30, 60 or 100pmol of RIPK3 siRNA for 24 hours. After 24 hours samples were taken and prepared for western blot analysis. Samples were blotted for RIPK3 (57 kDa) and β-actin (42 kDa). One representative western blot from two experiments is shown.

TOV21G cells were then transfected with 10pmol scrambled or 10pmol of RIPK3 siRNA. After 24 hours, cells were infected with *dl*922-947 and the effect of siRNA-mediated RIPK3 knock down on virus-infected cells was analysed 120 hours post infection.

Figure 4-20B shows the effect of RIPK3 siRNA-mediated knock down on *dl*922-947 infected cells. Figure 4-20C shows that siRNA-mediated knock down of RIPK3 significantly rescues the induction of programmed necrosis in TSZ treated TOV21G cells, while as shown at figure 4-20A knock down of RIPK3 was partially able to rescue cell death induced by *dl*922-947. As shown in the figure there is a

considerable difference in the amount of rescue between cells that are infected at a MOI of 1 in comparison to cells infected at a MOI of 0.1. Western blot analysis at the time of MTT confirmed that RIPK3 was down regulated on the protein level.

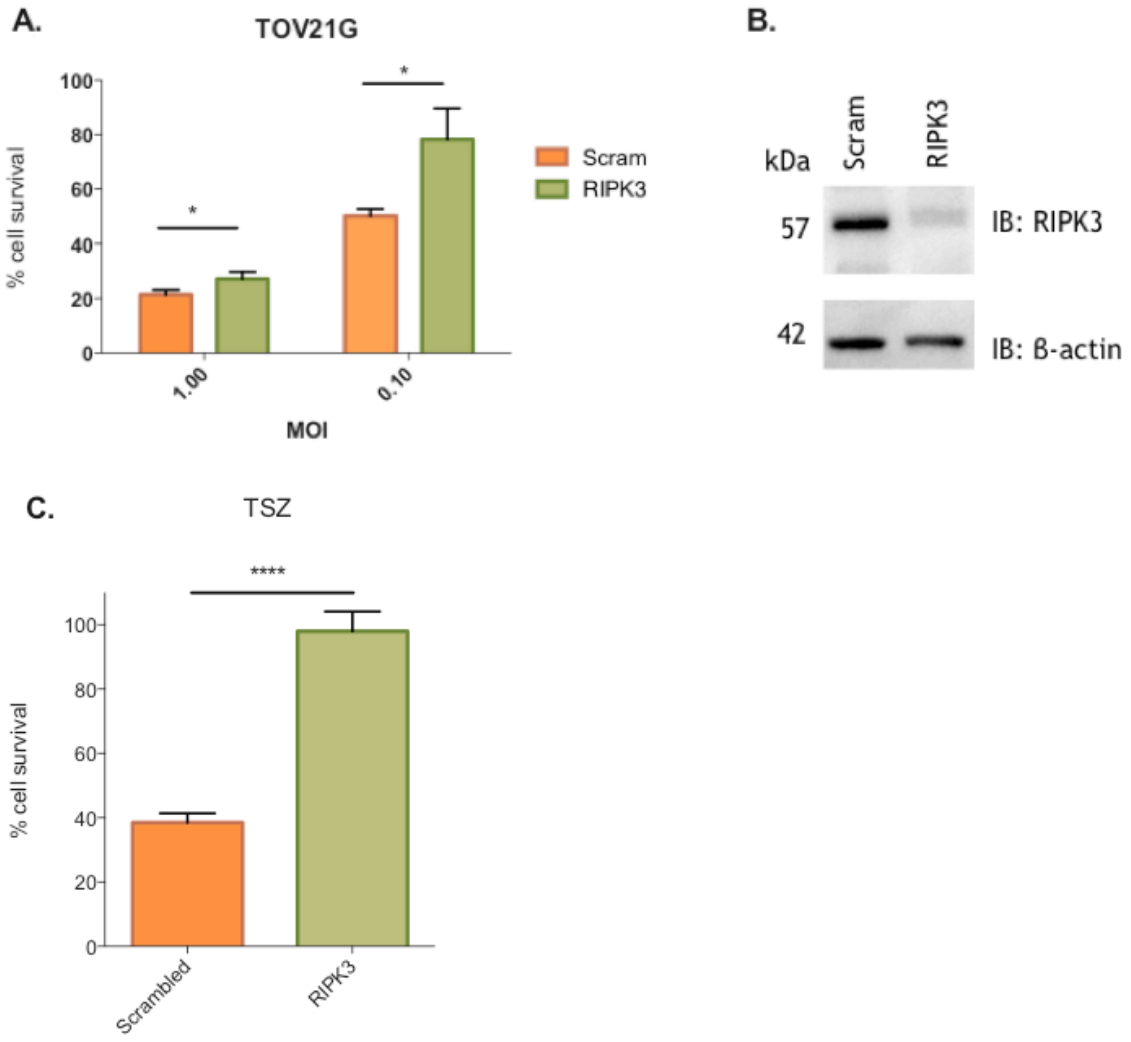

Figure 4-20: siRNA-mediated knock down of RIPK3 partially rescues *dl*922-947-induced cell death in TOV21G

A) TOV21G cells were transfected with 10pmol scrambled or 10pmol RIPK3 siRNA. 24 hours post-transfection cells were infected with *dl*922-947 at indicated MOI. Cell survival was assessed 120 hours post-infection by MTT assay and normalized to uninfected cells treated with the same amount of siRNA. Points represent mean +/- STDEV from one experiment performed in triplicate wells.

B) TOV21G samples were taken 120 hours post infection and blotted for RIPK3 (57 kDa) and β-actin (37 kDa). One representative western blot from three experiments is shown.

P values are calculated using unpaired t-test, * shows $p<0.05$.

C) TOV21G cells were transfected with 10pmol scrambled or 10pmol RIPK3 siRNA. 24 hours post-transfection cells were treated with 20ng/mL TNF-α, 1μM smac-mimetic and 25μM Z.VAD.fmk. Cell survival was assessed 48 hours post-treatment by MTT assay. Points represent mean +/- STDEV from one experiment performed in triplicate wells. P values are calculated using unpaired t-test, **** shows $p<0.0001$.

4.3.8.3 Investigating the role of MLKL in *dl*922-947-induced cell death

4.3.8.3.1 Inhibition of MLKL using necrosulfonamide

The protein Mixed lineage kinase domain-like protein (MLKL) has been identified as a RIPK3 substrate in a chemical compound screen (Sun et al. 2012). Sun *et al.* showed that MLKL binds to RIPK3 through its C-terminal kinase-like domain, which is phosphorylated at Thr231/Ser232 by RIPK3 and that NSA is able to block necrosis downstream of RIPK3 by covalently modifying MLKL.

First, I wanted to investigate further if MLKL is also a downstream component of adenovirus-induced cell death. I determined NSA-induced non-specific cytotoxicity by treating the cells with increasing concentration of NSA over a timeframe of 120 hours before cell survival was assessed. As shown in figure 4-21A NSA does induce non-specific cytotoxicity in OVCAR4 and TOV21G in a dose-dependent manner over an incubation period of 120 hours; therefore, 3µM of NSA was used in further experiments.

After the optimal concentration of NSA was determined, its stability was assessed as described earlier. As shown in figure 4-21B NSA is stable over a period of 120 hours and is able rescue TSZ-induced cell death.

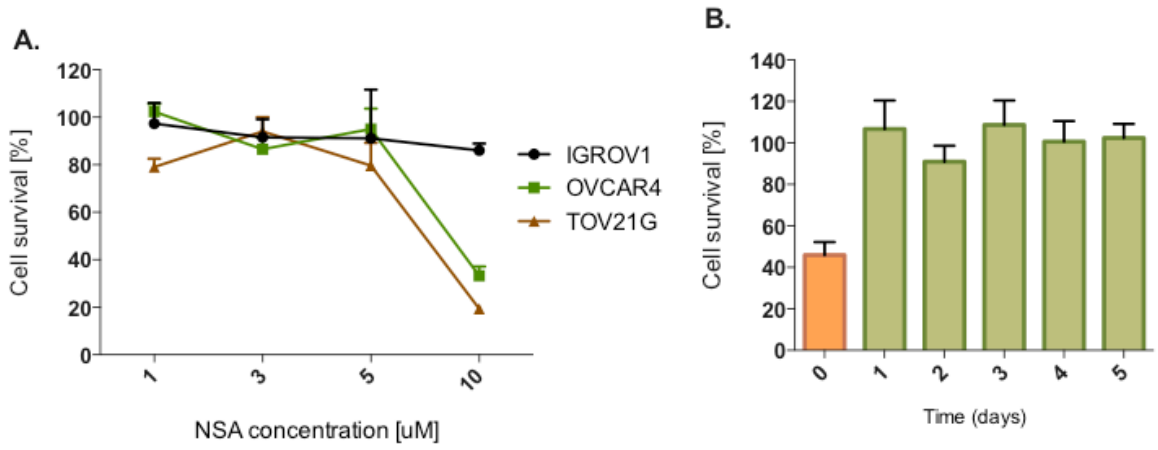

Figure 4-21: Necrosulfonamide induces non-specific cytotoxicity at high concentrations. A) IGROV1, OVCAR4 and TOV21G cells were treated with 1, 3, 5 or 10µM NSA. Cytotoxicity was assessed 120 hours post treatment by MTT assay. Points represent mean +/- STDEV from one experiment performed in triplicate wells. Shown is one representative graph from two experiments. B) DMEM containing a final concentration of 3µM NSA was incubated over a period of five days at 37ºC in a tissue culture incubator before TSZ was added to induce programmed necrosis in TOV21G. NSA stability was assessed 24 hours post TSZ treatment by MTT assay. Points represent mean +/- STDEV from one experiment performed in triplicate wells. One representative graph from two experiments is shown.

Next, cells were infected with *dl*922-947 and treated with either 3μM NSA or vehicle. After 72 hours the medium was changed and new medium containing 3μM NSA or vehicle was added.

Figure 4-22 shows that NSA was able to significantly reduce *dl*922-947-induced cytotoxicity in all three cell lines tested.

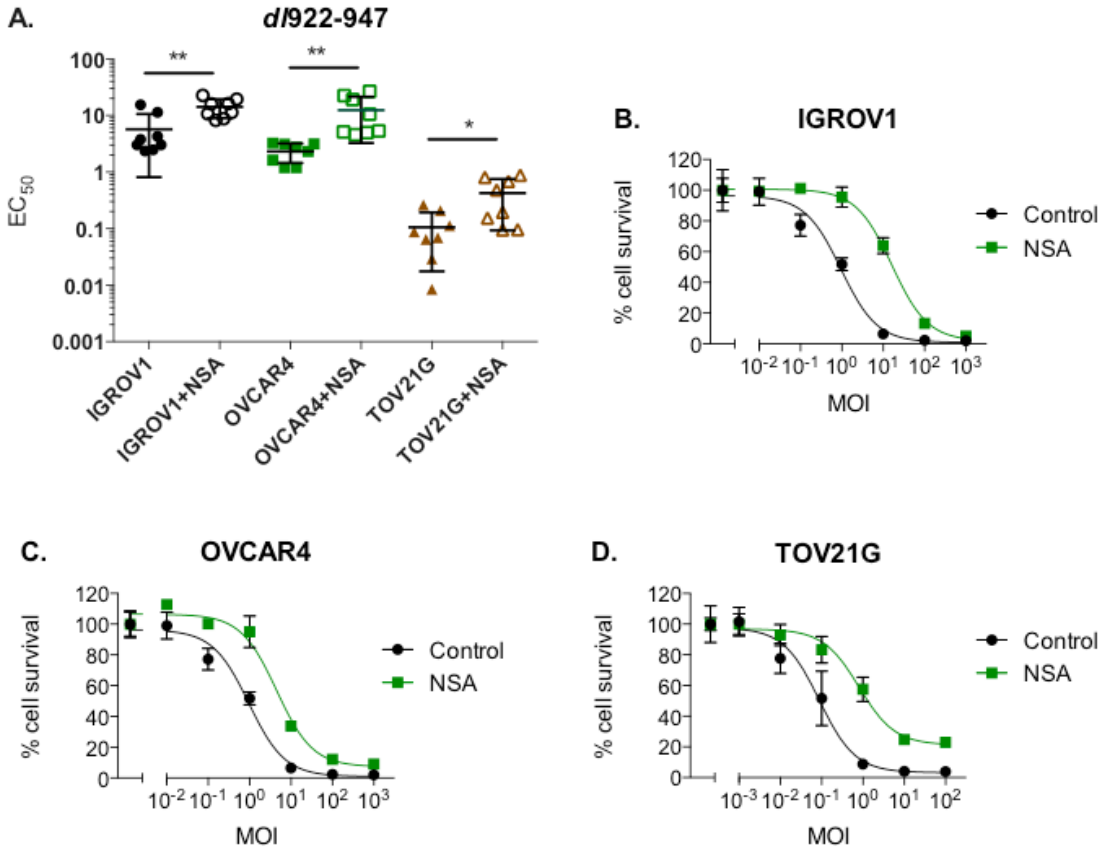

Figure 4-22: Necrosulfonamide reduces *dl*922-947-induced cytotoxicity
A) IGROV1, OVCAR4 and TOV21G were infected with *dl*922-947 and treated with vehicle or 3μM NSA. Medium was replaced 72 hours post-infection and medium containing 3μM NSA was added. Cytotoxicity was assessed 120 hours post treatment by MTT assay. Points represent mean EC50 +/- STDEV from at least four experiments with each experiment performed in triplicate wells.
B-D) shows one representative graph for each cell line.
P values are calculated using unpaired t-test, * shows $p<0.05$ and ** $p<0.01$.

To show that the increase of cell viability during *dl*922-947 infection was due to blockage of MLKL by NSA and not by NSA affecting other cellular events during viral infection, I performed western blotting of the early viral protein E1A during *dl*922-947 infection and NSA treatment.

Figure 4-23 shows that there is no difference in E1A expression between cells that have been treated with 3μM NSA or vehicle during *dl*922-947 infection.

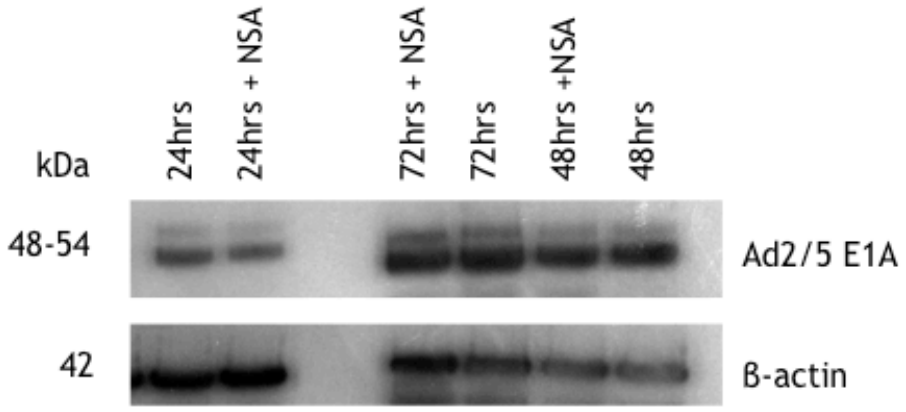

Figure 4-23: Necrosulfonamide treatment does not alter the expression of viral proteins
TOV21G cells were infected with *dl*922-947 and either treated with vehicle or 3μM NSA. Protein samples were taken at indicated time points and analysed for differences in viral E1A protein expression (48-54 kDa) and differences in β-actin (42 kDa). Figure shows one representative western blot from two experiments.

Next I wanted to assess if NSA might affect viral replication, leading to a lower viral titre that could lead to a decrease in viral cytotoxicity. Therefor a $TC_{ID}50$ assay was performed on OVCAR4 and TOV21G. Cells were infected with *dl*922-947 at MOI 10 and either treated with vehicle or 3μM NSA. 48 hours post-infection samples were taken and prepared for $TC_{ID}50$ assay as described before.

Figure 4-24 shows $TC_{ID}50$ assay performed on OVCAR4 and TOV21G treated with vehicle or 3μM NSA and infected with *dl*922-947 at MOI 10 for 48 hours. As shown in the figure, there are no differences in the production of infectious viral particles between cells treated with NSA or vehicle at 48 hours post-infection.

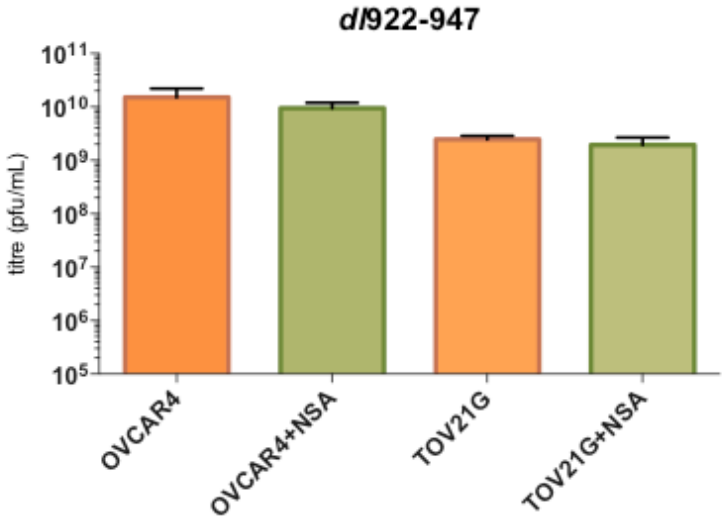

Figure 4-24: Necrosulfonamide treatment does not alter the production of infectious viral particles.
$TC_{ID}50$ assay was performed on OVCAR4 and TOV21G infected with *dl*922-947 at MOI 10 for 48 hours, treated with vehicle or 3μM NSA. Viral titres were determined by $TC_{ID}50$ assay. Points represent mean +/- STDEV from one experiment performed in quadruplicate.

4.3.8.3.2 Knock down of MLKL using siRNA

It has been shown in previous experiments that NSA induces non-specific cytotoxicity, which is cell- as well as dose-dependent. Therefore, siRNA mediated MLKL knock down was used to validate data obtained with NSA.

First, a siRNA dose response on TOV21G was done, to determine the lowest concentration of MLKL siRNA needed to achieve a complete protein knock down. As shown in figure 4-25, transfection of MLKL siRNA resulted in a considerable decrease in MLKL on the protein level but complete knock-down was not achieved. Since there was no considerable difference between the knock-down achieved by 10pmol or 100pmol of MLKL siRNA, a concentration of 10pmol was used for all following experiments.

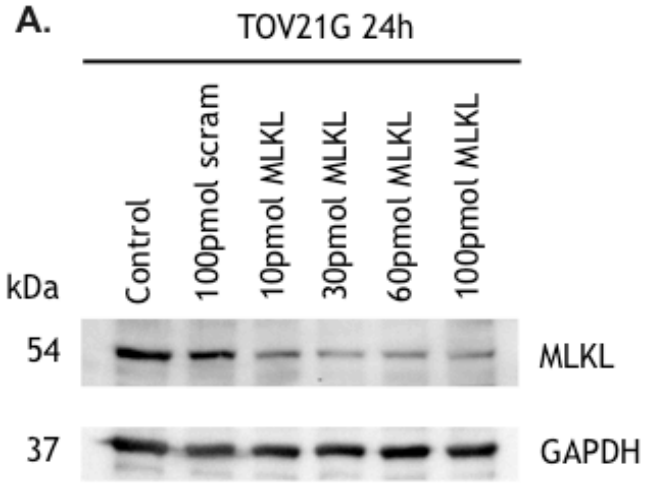

Figure 4-25: SiRNA is not able to completely knock-down MLKL
A) TOV21G was transfected with 100pmol scrambled or 10, 30, 60 and 100pmol RIPK3 siRNA. After 24 hours, cells were lysed and prepared for western blotting of MLKL (54 kDa) and GAPDH (37 kDa). Figure shows representative western blots from two experiments.

In the next experiment I wanted to evaluate if siRNA mediated knock down of MLKL was able to rescue *dl*922-947-induced cell death. Figure 4-26C shows that siRNA-mediated knock down of MLKL is able to significantly rescue cell death induced by TSZ treatment in TOV21G, while as shown in figure 4-26B MLKL is knocked down at protein level, but there is no consistent difference in *dl*922-947-induced cytotoxicity figure 4-26A.

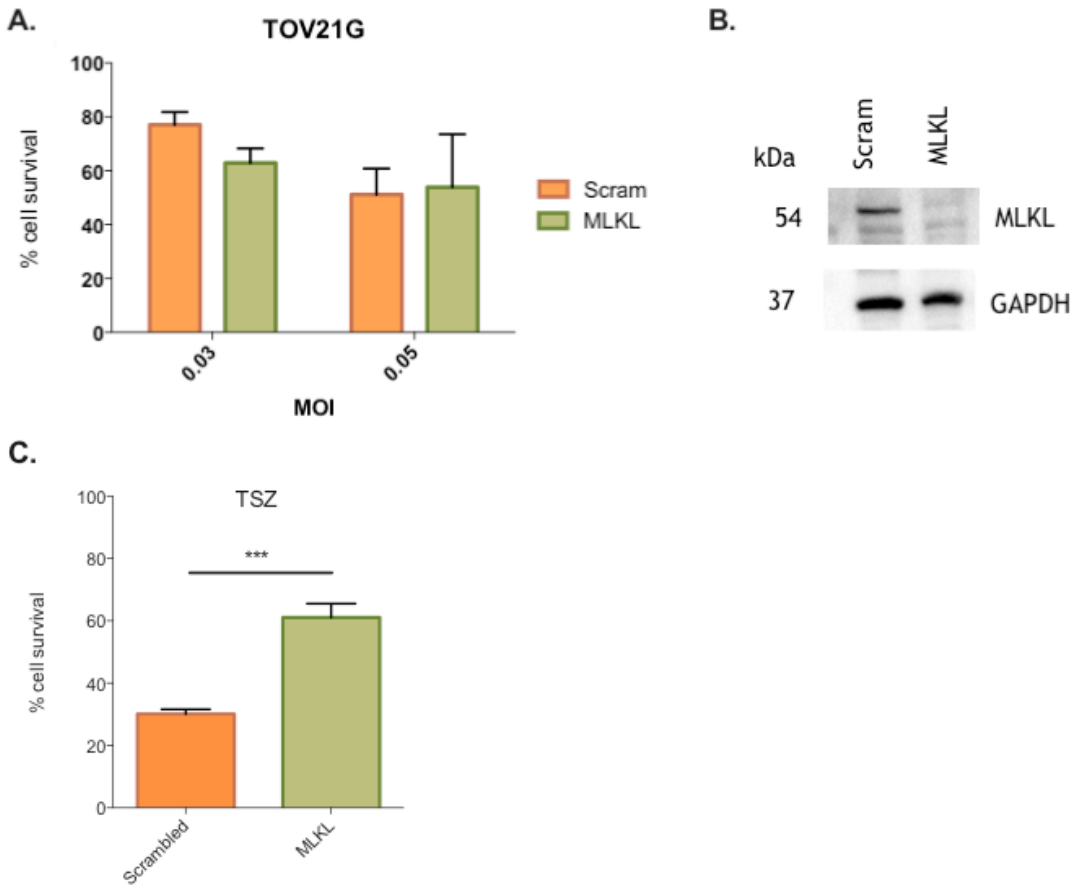

Figure 4-26: siRNA mediated knock down of MLKL does not rescue *dl*922-947-induced cell death

A) TOV21G cells was transfected with 10pmol scrambled or 10pmol RIPK3 siRNA for 48 hours. After 48 hours, cells were infected with *dl*922-947 at indicated MOI. Cell survival was assessed 120 hours post-infection by MTT assay and normalized to uninfected cells treated with the same amount of siRNA. Points represent mean +/- STDEV from one experiment performed in triplicate wells.

B) TOV21G samples were taken 120 hours post infection for western blotting to assess if MLKL was down regulated at time of MTT assay. Shown is one representative figure from two experiments.

C) TOV21G cells were transfected with 10pmol scrambled or 10pmol MLKL siRNA. 24 hours post-transfection cells were treated with 20ng/mL TNF-α, 1μM smac-mimetic and 25μM Z.VAD.fmk. Cell survival was assessed 48 hours post-treatment by MTT assay. Points represent mean +/- STDEV from one experiment performed in triplicate wells. P values are calculated using unpaired t-test, *** shows $p<0.001$.

4.3.8.4 Knockout of MLKL using CRISPR/Cas9

To further assess the potential importance of MLKL in virus-induced cell death, I aimed to create cells with stable knockout of MLKL, since siRNA mediated knock-down of MLKL is time limited and therefore would make further *in vivo* experiments more complicated.

Using the CRISPR/Cas9 system, I started by designing guides targeting specific regions of the gene encoding MLKL using the online designing tools provided http://crispr.mit.edu and http://chopchop.rc.fas.harvard.edu. Guides were chosen based on the amount of potential off-target effects and depending on if they were identified by both online programmes. The guides were then ligated into the pX335 vector and sequenced. TOV21G cells were then transfected with the resulting plasmid and selected with puromycin. Following dilution cloning, single cell clones were pre-selected by TSZ treatment.

Several clones from guide 5.1 were selected, their DNA extracted, PCR amplified using the primers listed in chapter 2 and run on an agarose gel.

Figure 4-27 shows PCR results for the region targeted by guide 5.1 with the parental PCR product running at approximately 836bp. Clones D3 and F5 are running at about the basepair length as parental, while clones D6, F9 and E8 show a double, indicating that something has happened to the original sequence.

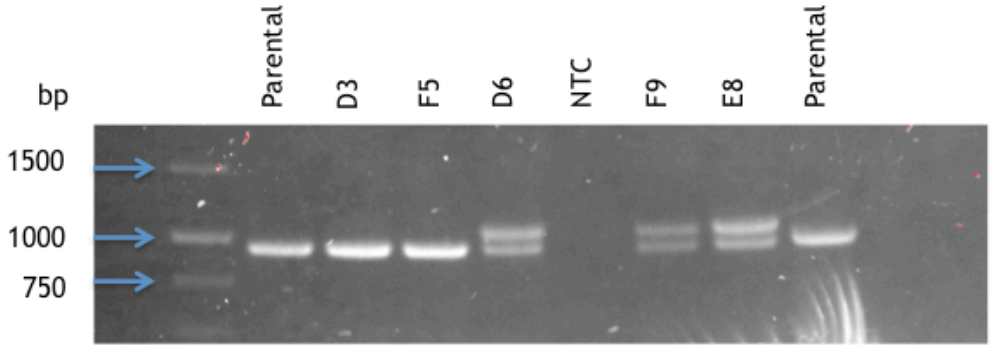

Figure 4-27: Identification of clones with edited MLKL
DNA was extracted from parental cells, clone D3, F5, D6, F9 and E8, PCR amplified with primers indicated in chapter 2 and run on an agarose gel.

Clones that showed a visibly shorter PCR product or double bands on the agarose gel and that were resistant to TSZ treatment were considered to have a modification in the sequence of MLKL, until sequencing was completed.

Following this, western blotting was performed to assess if clones showed differences in MLKL protein expression.

Figure 4-28 shows MLKL expression in parental and CRISPR/Cas9 transfected cells containing MLKL guide 5.1. Clone F5 shows similar MLKL protein expression as parental cells and clone D3 showing only slight down regulation of MLKL. The clones F9, E8 and D6 show the greatest down regulation of MLKL protein.

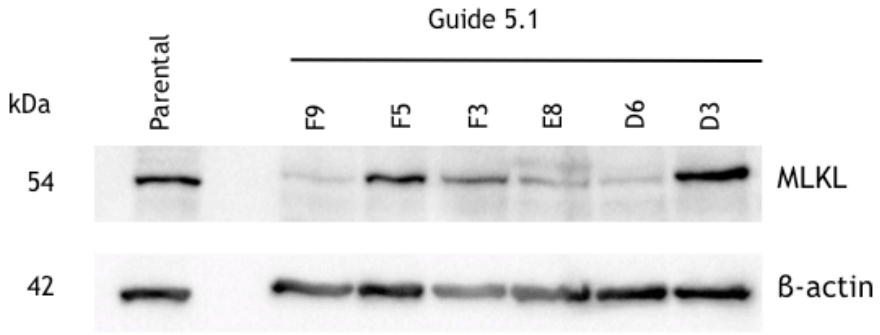

Figure 4-28: MLKL is downregulated in CRISPR/Cas9 transfected TOV21G containing MLKL guide 5.1
Parental cells and single cell clones of CRISPR/Cas9 transfected cells containing guides for MLKL were prepared for western blotting and samples were analysed for MLKL (54 kDa) and β-actin (42 kDa) expression.

Next I wanted to further assess how these clones react to TSZ treatment and if additional Nec-1 treatment would be needed to achieve complete rescue to TSZ-induced cell death.

As shown in figure 4-29, clones reacted in accordance with data shown in figure 4-28, meaning that clones showing MLKL expression on the western blot (Clone D3 and F5) were able to undergo TSZ-induced programmed necrosis. When clones D3 and F5 were treated with TS, the cells started to die and a further increase in cell death was observed when Z.VAD.fmk was added. Cell death induced by TSZ in these clones was rescued by the addition of Nec-1. Clones D6 and F9, which showed down regulation of MLKL, died in response to TS treatment, but cell death was in part rescued when cells were additionally treated with Z.VAD.fmk. This increase in cell viability could even be further

increased through the addition of Nec-1. Interestingly, the amount of cell death induced by TS treatment in clone D6 was considerably greater than in F9.

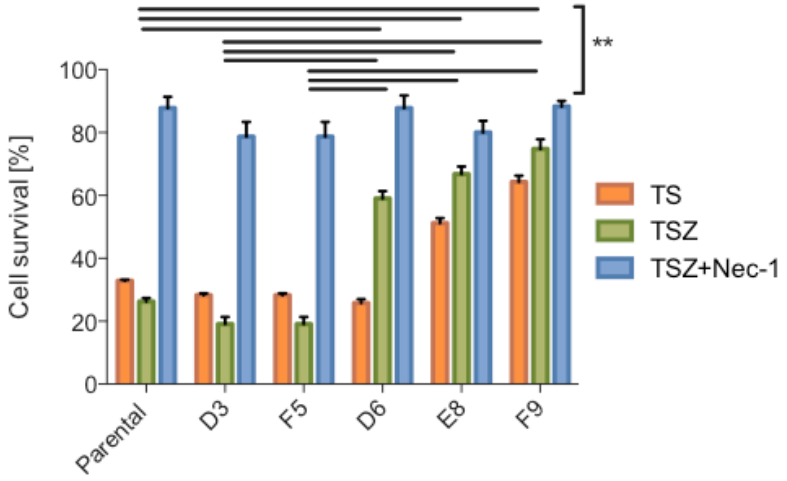

Figure 4-29: TSZ treatment in CRISPR/Cas9 transfected cells containing MLKL guide 5.1
Parental and single cell and single cell clones were treated with different combinations of 20ng/mL TNF-α (T), 1μM Smac-mimetic (S), 25μM Z.VAD.fmk (Z) or 10μM Nec-1. Cell survival was assessed 24 hours post-treatment by MTT assay and normalized to vehicle treated cells. Points represent mean +/- STDEV from one experiment performed in triplicate wells. Shown is one representative figure from two experiments.
P values are calculated using One ANOVA with multiple comparisons, ** shows $p<0.01$.

To further investigate the importance of MLKL in *dl*922-947-induced cell death, a panel of guide 5.1 clones was selected for *dl*922-947 infection. Figure 4-30 shows that down-regulation of MLKL has no effect on *dl*922-947 induced cytotoxicity. Clones D3 and F5, which behave like they have WT MLKL show similar amounts of cell death compared to parental TOV21G. Interestingly, clone F5 (mean cell survival: 61.5%), which is supposed to have WT MLKL shows lower amounts of cell death compared to parental cells (mean cell survival: 29.3%) and the other proposed clone containing WT MLKL, clone D3 mean cell survival: 34,8%) and the potentially MLKL edited clones D6 (mean cell survival: 37.6%), and F9 (mean cell survival: 24.8%). Another interesting observation is the changes in response to Z.VAD.fmk during *dl*922-947 infection. In keeping with results shown in Fig 4.1, *dl*922-947-induced cell death is augmented in Z.VAD.fmk treated parental TOV21G cells as well as in the potentially WT MLKL clones D3 and F5. However, in cells that are potentially edited for MLKL (clone D6 and F9), cell death is not augmented during additional Z.VAD.fmk treatment.

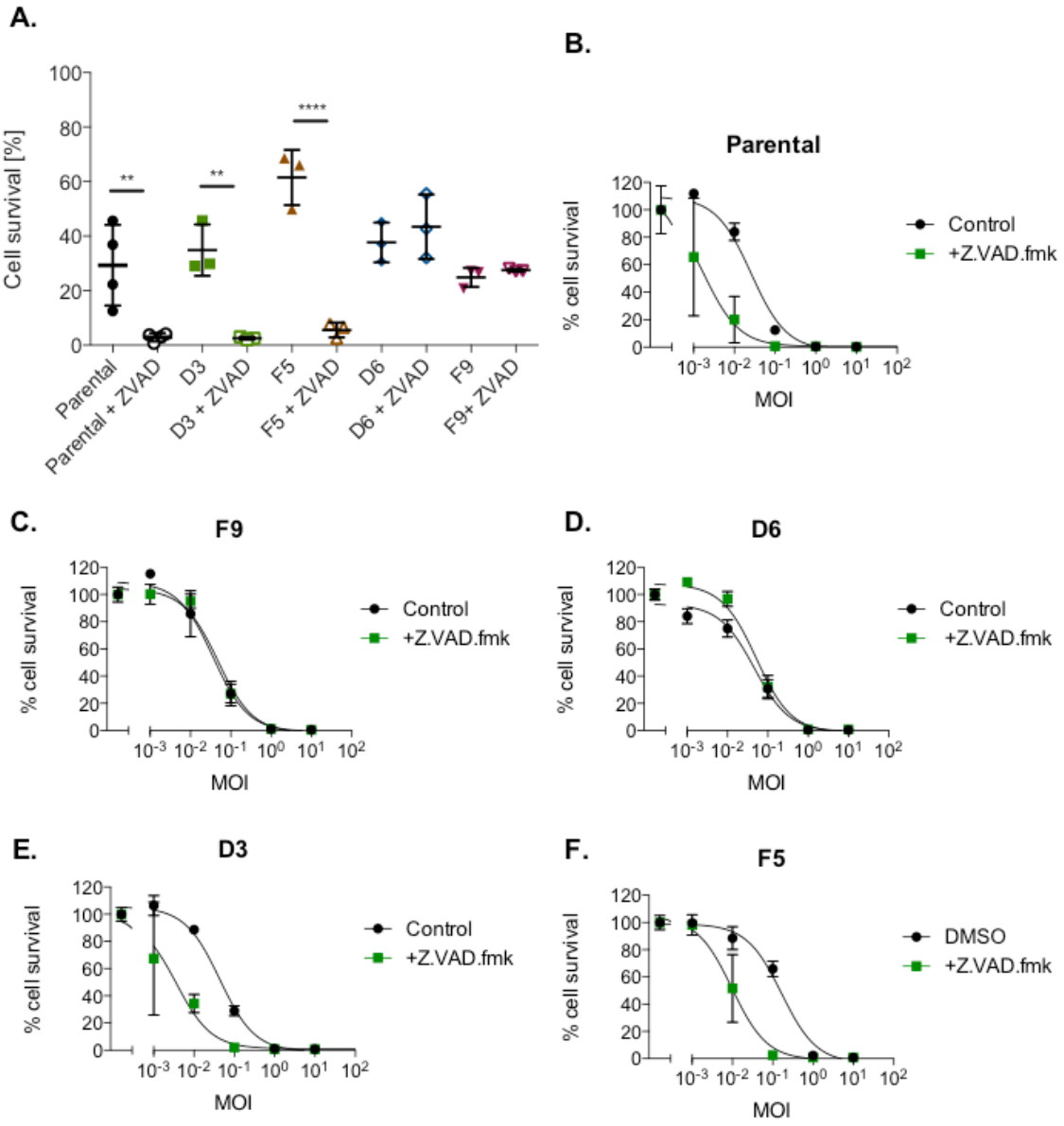

Figure 4-30: Down-regulation of MLKL rescues augmented cell death phenotype induced by Z.VAD.fmk during *dl*922-947 infection

A) Parental TOV21G and MLKL edited clones D3, F5, D6 and F9 were infected with *dl*922-947 at MOI 0.1 and either treated with vehicle or 25μM Z.VAD.fmk. Cytotoxicity was assessed 120 hours post treatment by MTT assay. Points represent mean +/- STDEV from at least three experiments with each experiment performed in triplicate wells.

B-F) Cells were infected with *dl*922-947 at indicated MOI and either treated with vehicle or 25μM Z.VAD.fmk. Cell survival was assessed 120 hours post-infection by MTT assay and normalized to uninfected cells. Shown is one representative graph, where points represent mean +/- STDEV from one experiment performed in triplicate wells.

P values are calculated using unpaired t-test, ** shows $p<0.01$ and ****$p<0.0001$.

4.3.8.4.1 MLKL phosphorylation during *dl*922-947 infection

Cai *et al*. showed in 2014 that plasma membrane translocation of MLKL is required for TNF-induced programmed necrosis. They also showed that MLKL forms trimers and is phosphorylated by RIPK3. They further showed that phosphorylation of MLKL is needed for its translocation to the plasma membrane (Cai et al. 2014). Later on in 2014 Chen *et al*. showed that MLKL can also form oligomers, which then translocate to lipid rafts of the plasma membrane (Chen et al. 2014). It was just a few months later in same year that Wang *et al*. showed that MLKL was phosphorylated at T357 and S358 by RIPK3 and binds to phosphatidylinositol lipids and cardiolipin. Besides discovering MLKL's phosphorylation sites, they also developed an antibody that specifically only recognised MLKL in its phosphorylated state (Wang et al. 2014a).

To further assess the involvement of MLKL in adenovirus-induced cell death, I wanted to investigate if MLKL is phosphorylated during *dl*922-947 infection. Therefore, TOV21G cells were either vehicle treated, treated with TSZ or with *dl*922-947 and changes in MLKL phosphorylation were analysed by western blot.

Figure 4-31 shows that MLKL is expressed during mock- and TSZ treatment as well as during *dl*922-947 infection, but phosphorylated MLKL is only observed during TSZ treatment.

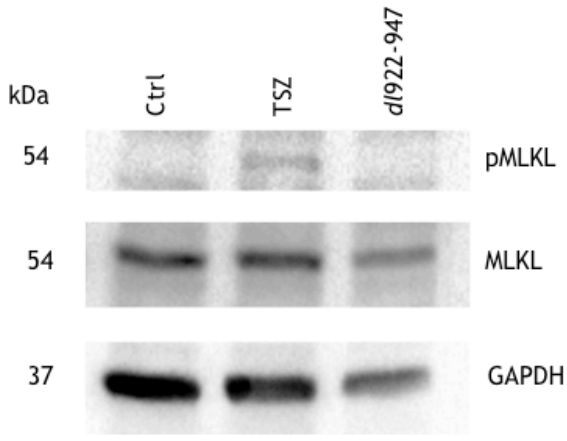

Figure 4-31: pMLKL levels during *dl*922-947 infection
TOV21G cells were mock-treated, treated with 20ng/mL TNF-α, 1μM Smac-mimetic and 25μM Z.VAD.fmk (TSZ) for 6 hours or infected with *dl*922-947 at MOI 10 for 48 hours. Samples were then prepared for western blot and analysed for pMLKL (54 kDa), MLKL (54 kDa) and GAPDH (37 kDa). Shown is one representative western blot from two experiments. pMLKL= phospho-MLKL.

4.4 Discussion

Adenoviruses were discovered first in 1953 (Rowe et al. 1953)and ever since then extensive research has been performed to better understand their nature. This research also includes insights into mechanisms adenoviruses employ to avoid immune cell detection and the induction of host-controlled cell death mechanisms to contain infection and further spread. For a long time, it was thought that adenoviruses induce apoptosis in host cells, but research from as early as 1992 (White et al. 1992)described that adenoviral genes encode proteins that can interfere with the intrinsic as well as extrinsic apoptotic machinery (Han et al. 1996a, Debbas and White 1993, Tollefson et al. 1991), which stands in conflict with the assumption that they induces apoptosis. Further, recent research performed by the host lab and others has shown that adenoviruses induce a novel mode of cell death that resembles necrosis (Baird et al. 2008).

Characterization of the ovarian cancer cells IGROV1, OVCAR4 and TOV21G showed that IGROV1 was resistant to apoptosis induced by TS, while OVCAR4 did undergo apoptosis during TS treatment, which could be rescue by Z.VAD.fmk and TOV21G was able to undergo apoptosis induced by TS as well programmed necrosis induced by TSZ. Further characterization of those cell lines showed that only few of them expressed the protein RIPK3, which determines if a cell can undergo programmed necrosis (Cho et al. 2009). Interestingly though, recent research has shown that RIPK3 is repressed through methylation near its transcriptional start site (Koo et al. 2015). The authors showed that normal cells express RIPK3 and suggest that upon tumour development RIPK3 deficiency is positively selected since it contributes to chemosensitivity through the induction of programmed necrosis. This would also explain why RIPK3 expression has been rarely observed in ovarian cancer cell lines. OVCAR4 cells expressed low amounts of RIPK3, but were not able to undergo programmed necrosis. This might be due to the fact that RIPK3 expression was too low to activate the threshold needed to induce programmed necrosis with TSZ. Further, morphological characterization during TSZ treatment confirmed that TOV21G cells were able to undergo programmed necrosis in response to TSZ.

I then decided to perform two small experiments with *dl*922-947, which should give an indication on if *dl*922-947 induces apoptosis. Apoptosis is a tightly

regulated form of cell death, which depends on the activation of aspartate-specific cysteine proteases (Caspases). Caspases play important roles in the induction, transduction and amplification of apoptotic signals and can therefore be categorised into initiator caspases (Caspase 2, 8 and 9) and effector caspases (Caspase 3, 6 and 7) (Tait and Green 2010). Research has discovered several proteins encoded by the adenoviral genome that can interfere with the apoptotic machinery, like E3A 10.4K/14.5K (Also known as RIDα/ß) that are able to down-regulate the cell death surface receptors like TNFR1, FAS, TRAILR1/2, which can stimulate caspase 8 activation and though there are known viral proteins that inhibit caspases directly as competitive, irreversible (e.g. baculovirus protein p35 (Clem, Fechheimer and Miller 1991) and Cowpox virus protein CrmA (Gagliardini et al. 1994)) none has been described for adenoviruses yet.

When *dl*922-947 infected cells were treated with Z.VAD.fmk either no rescue in cell death or, in the case of TOV21G, attenuation was observed. This observation was very interesting, since the host lab had published results showing that adenovirus infection can lead to the minor activation of procaspase 3 (Baird et al. 2008). This leads to the conclusion that firstly, though adenoviruses can block and interfere with intrinsic and extrinsic apoptosis signalling, the activation of procaspase 3 is still possible through not yet identified mechanisms, and secondly although there is minor procaspase 3 activation, it does either not contribute towards virus-induced cell death since blocking caspases with Z.VAD.fmk showed no effect on death or that there is not enough procaspase 3 activation to pass the threshold to lead to the induction of apoptosis. In the context of TOV21G and adenovirus infection this gets even more interesting. TOV21G can undergo programmed necrosis as shown before, whilst during adenovirus infection and Z.VAD.fmk treatment, caspases are being inhibited, which leads to attenuated cell death, which has been described extensively as a phenomenon that has been observed in and is associated with programmed necrosis (Vercammen et al. 1998). This is another indicator that adenoviruses cannot directly block caspases or at least, that they are not efficient in blocking them. Another method of studying the involvement of apoptosis is by using overexpression models of anti-apoptotic proteins like BCL-2. Alterations in anti-apoptotic proteins like BCL-2 can contribute to the pathogenesis and progression

of human cancers since BCL-2 overexpression can block the intrinsic apoptosis signalling by blocking the activation of BAX and BAK, but again overexpression of anti-apoptotic BCL-2 was not able to rescue *dl*922-947 –induced cell death, indicating that apoptosis is not induced. Further, it has been shown that adenoviruses encode proteins that can interfere with the induction of MOMP; for example E1B-19K functions as an anti-apoptotic MCL-1 viral mimetic that targets BAX and BAK, therefore inhibiting MOMP.

Overall, these findings, in accordance with findings previously published (Baird et al. 2008, Abou El Hassan et al. 2004) and in accordance with findings showing that adenovirus contain a multitude of proteins that specifically inhibit apoptosis (Tollefson et al. 2001, Han et al. 1996a, Schreiner et al. 2010, Tollefson et al. 1998, Schneider-Brachert et al. 2006, Luo et al. 2007), lead to my conclusion that apoptosis is not involved in *dl*922-947-induced cell death.

Further morphological characterization of TOV21G during *dl*922-947 infection showed that cells morphologically showed a necrotic phenotype. This was very interesting since pharmacological and or antibody inhibition of TNF-α, RIPK1 and RIPK3 was not able to rescue *dl*922-947-induced death. Furthermore knock-down of MLKL was also not able to rescue cell death, making those major programmed necrosis components redundant. Interestingly, though pharmacological inhibition of RIPK3 was not able to attenuate cell death, siRNA-mediated knock-down was. Since siRNA-mediated knock-down showed that RIPK3 protein levels were down-regulated over the complete time course of infection, I decided to give more weight to these results. Further, experiments performed with shRNA for confirmation, failed due to unstable knock-down (Data not shown). These data show that *dl*922-947 does not induce classical programmed necrosis through TNF/TNFR ligation, but rather might use one of the many other programmed necrosis pathways that have been described (Han et al. 2011b, Kalai et al. 2002, Thapa et al. 2013). One of those has been described by the lab of Pascal Meier (Tenev et al. 2011), who showed the formation of a RIPK1-dependent death-inducing complex called the ripoptosome, which forms upon genotoxic stress. This complex was able to induce caspase-dependent apoptosis as well as regulated necrosis independently of death ligands. Therefore, *dl*922-947 could potentially induce necrosis through the induction of the ripoptosome. It has

been shown that *dl*922-947 induces genomic DNA damage through the induction of DNA double strand breaks leading to the accumulation of γH2AX and RAD51 foci (Connell et al. 2011), a hallmark of cellular genotoxic stress (Lisby et al. 2004, Shah and O'Shea 2015) while at the same time inhibiting the repair mechanisms employed by cells to maintain genomic integrity (Boyer, Rohleder and Ketner 1999, Brestovitsky et al. 2016). This accumulation of DNA damage leads to the induction of genotoxic stress, which can then result in RIPK1-dependent cell death either through apoptosis or necrosis. Since experiments with *dl*922-947 suggested that RIPK1 expression is redundant, I further concluded therefore that the ripoptosome is also not the mediator of cell death-induced by *dl*922-947 infection.

Interestingly, so far the only indication that TOV21G undergoes necrosis during *dl*922-947 infection has been observed by siRNA-mediated knock-down of RIPK3 and by observing morphological changes. Besides trying to inhibit cell death induced by *dl*922-947, I made observations that indicated that *dl*922-947-induced cell death could be increased. This would be is of high relevance since one of the long-term aims is to identify targets that can increase oncolytic adenovirus efficacy. As mentioned earlier, Z.VAD.fmk was able to attenuate cell death induced by *dl*922-947 in necrosis competent cells and interestingly, this attenuated form of cell death was rescued in cells that had CRISPR/Cas9-mediated down-regulation of MLKL. Therefore I conclude that in necrosis-competent cells during *dl*922-947 infection, necrosis is not efficiently induced; firstly because siRNA-mediated RIPK3 knock-down was not able to completely rescue cell death and secondly because *dl*922-947 does not encode a direct inhibitor of Caspase 8, but upon inhibition of caspase 8 (as shown by Z.VAD.fmk experiments), the cell was able to induce programmed necrosis, which resulted in increased death, which in turn could be rescued by knock-down of MLKL.

Besides trying to block apoptosis in necrosis-competent cells to increase *dl*922-947 efficacy, the addition of recombinant hTNF-α can also attenuate cell death in certain cell lines. When OVCAR4 cells were infected with *dl*922-947 and recombinant hTNF-α was added, cell death was attenuated. Interestingly, this increase in cell death could only be partly rescued by the addition of Z.VAD.fmk, which showed that it was not completely of an apoptotic nature. This suggests

that the addition of hTNF-α can result in the induction of different cell death modalities in OVCAR4, since the treatment of *dl*922-947-infected cells with Z.VAD.fmk did neither completely rescue nor increase cell death. As I have shown before, OVCAR4 cells do not undergo programmed necrosis in response to TSZ, though they express small amounts of RIPK3, but the addition of hTNF-α in the context of *dl*922-947 infection might be able to pass the threshold to induce necrosis, and apoptosis to certain levels. Interestingly research performed by (Hirvinen et al. 2015) showed that a chimeric oncolytic adenovirus expressing hTNF-α (Ad5/3-D24-hTNFα) showed an increase in cytotoxicity *in vitro* and *in vivo* in a syngeneic melanoma model in immunocompetent C57Bl/6 mice, compared to a chimeric oncolytic adenovirus that does not express hTNF-α (Ad5/3-D24). Further, they were able to show that Ad5/3-D24-hTNFα increased immunogenicity and anti-tumour responses and that tumours treated with Ad5/3-D24-hTNFα and radiotherapy underwent apoptotic and necrotic cell death. Also, research performed by Nogusa, et al. has shown that host cells can activate parallel pathways of necroptosis and apoptosis to protect against influenza A virus infection (Nogusa et al. 2016).

To conclude this chapter, I have been able to show that the adenovirus deletion mutant *dl*922-947 does not induce apoptosis in the ovarian cancer cell lines IGROV1, OVCAR4 and TOV21G and that upon *dl*922-947 infection cells undergo morphological changes that strongly resemble necrosis. Further analysis of proteins involved in the programmed necrosis pathway showed that cell death induced by *dl*922-947 was independent of TNF-α, RIPK1 and MLKL, therefore excluding the involvement of classical programmed necrosis induced by TNF/TNFR ligation and by the ripoptosome. Further analysis showed that the inhibition of caspases in necrosis competent cells might be of therapeutic value as well as arming oncolytic adenoviruses with TNF-α.

Chapter 5

Devising a RIPK3 overexpression model for *in vivo* studies

5 Devising a RIPK3 overexpression model for *in vivo* studies

5.1 Introduction

In the previous chapter, my results suggested that inhibition of RIPK3 using small molecule inhibitors had little effect upon the efficacy of *dl*922-947, but siRNA-mediated knockdown partially reversed *dl*922-947 cytotoxicity in TOV21G. Therefore, I wanted to further investigate whether over-expression RIPK3 influenced adenovirus induced cell death *in vitro* and *in vivo*.

5.2 RIPK3 overexpression increases *dl*922-947 induced cytotoxicity

HeLa WT cells do not express RIPK3 and therefore do not undergo programmed necrosis in response to TSZ. However, the laboratory of Dr. Stephen Tait has cloned the sequence of human RIPK3 into a retroviral vector allowing the expression of human RIPK3. HeLa wild type cells were transduced with the retroviral vector Lzrs encoding human RIPK3 and tested for their expression of RIPK3 and their ability to undergo programmed necrosis when treated with a necrotic stimulus (TSZ) and following *dl*922-947 infection.

As seen in figure 5-1A HeLa Lzrs cells containing the empty vector express no detectable RIPK3 by immunoblot. Following selection, HeLa cells transduced with the Lzrs-RIPK3 lenivirus were dilution cloned and four separate single cell clones were expanded and analysed by western blotting. The selected clones express slightly different amounts of RIPK3. Figure 5-1B shows that all RIPK3 expressing clones undergo cell death when treated with TS, which induces apoptosis. HeLa Lzrs cells also undergo minor apoptosis following TS treatment, which can be rescued by the addition of the pan-caspase inhibitor Z.VAD.fmk. A small amount of rescue (approx. 10%) can be observed in the clones B2, E4 and E10. The addition of the MLKL inhibitor NSA was able to almost completely rescue TSZ-induced cell death, except for the clones D2 and E10. Only 50% total cell survival was achieved in clone D2 and 85% in cloneE4 and E10 when cells were treated with TSZ and additional NSA. Figure 5-1C and D show that RIPK3 expression significantly increases adenovirus-induced cytotoxicity and that the increase in cytotoxicity was RIPK3–dependent, since addition of the RIPK3

inhibitor GSK'840B restored cell survival to similar levels of the empty vector control (Figure 5-1E).

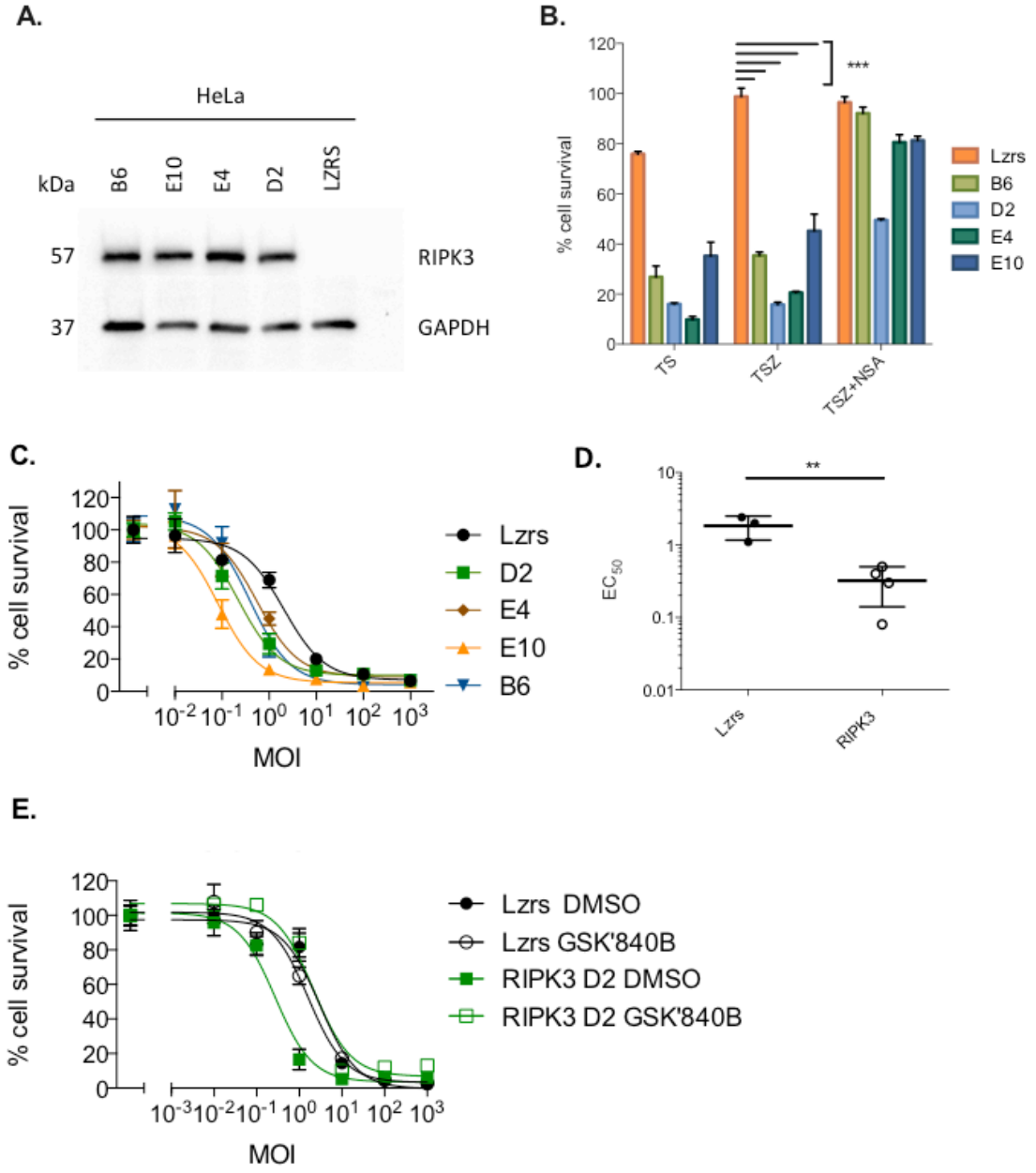

Figure 5-1: RIPK3 overexpression attenuates *dl*922-947-induced cell death

A) HeLa WT cells were either transduced with an empty Lzrs vector or one containing human RIPK3. Cells were selected, dilution cloning performed and protein samples taken to evaluate RIPK3 expression by western blot.

B) Cell were treated with different combinations of 20ng/mL TNF-α, 1μM Smac-mimetic, 25μM Z.VAD.fmk and 3μM NSA to induce cell death, programmed necrosis or to rescue programmed necrosis. Cell death was measured 24 hours after treatment using MTT assay. Points represent mean +/- STDEV from one experiment performed in triplicate wells. P values were calculated using One Way ANOVA with multiple comparisons, ***shows p<**0.001**

C) HeLa cells Lzrs or RIPK3 dilution clones were infected with *dl*922-947 in triplicate at indicated MOI. Cell survival was assessed 120 hours post-infection by MTT assay. Points represent mean +/- STDEV of one experiment performed in triplicate wells.

D) HeLa Lzrs and Hela RIPK3 expressing cells were infected with *dl*922-947 and their respective EC_{50} values for differences analysed. P values are calculated using unpaired t test, **shows p<0.01.

E) HeLa cells Lzrs or HeLa RIPK3 clone D2 were either treated with 10µM GSK'840B or vehicle and infected with *dl*922-947 in triplicate at indicated MOI. Cell survival was assessed 120 hours post-infection by MTT assay. Points represent mean +/- STDEV of one experiment performed in triplicate wells.

Next I wanted to investigate if the overexpression of RIPK3 would affect virus and viral protein production, since this can affect overall viral cytotoxicity. Therefore, I infected Hela Lzrs and the Hela RIPK3 clones D2 and E4 with *dl*922-947. Protein lysates were harvested at 0, 24 and 48 hours post-infection and analysed by western blot.

Picture 5-2 shows the expression of viral proteins in *dl*922-947 infected HeLa Lzrs and HeLa RIPK3 D2 and E4 cells. As expected no viral proteins were detected at 0 hours post infection. Expression of viral E1A can be observed at 24 hours post-infection. E1A expression is stronger in clone D2 and E4 at 24 hours post-infection in comparison to Lzrs but decreases more rapidly in both RIPK3-expresing clones by 48. The expression of viral core and capsid proteins is similar in Lzrs, HeLa RIPK3 D2 and E4.

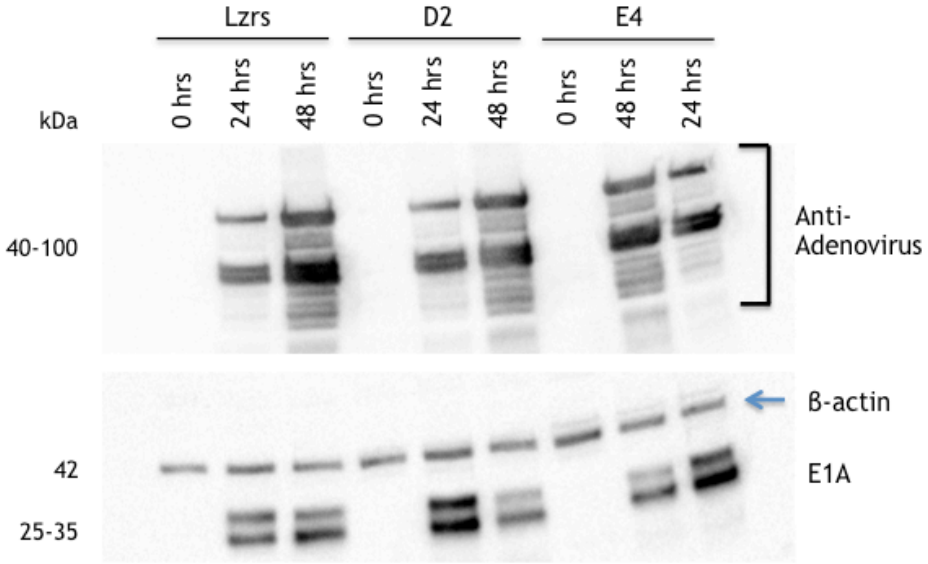

Figure 5-2: RIPK3 expression leads to changes in the expression of viral proteins
HeLa Lzrs (Lzrs), HeLa RIPK3 D2 (D2) and HeLa RIPK3 E4 (E4) were infected with *dl*922-947 at MOI 10 for 0, 24 and 48 hours. Sample were taken and further analysed for β-actin (42 kDa), E1A (25-35 kDa) and Anti-Adenovirus (40-100 kDa) by western blot. Shown is one representative western blot from two experiments. Lanes E4 48 hours and 24 hours have been labelled deliberately this way.

Next, I wanted to assess if RIPK3 expression could influence the production of infectious viral particles, since an increase in viral particle production could explain the increase in cytotoxicity. Figure 5-3 shows a $TC_{ID}50$ time plot of intracellular virus production between HeLa Lzrs and HeLa RIPK3 D2 and E4 cells over a period of 72 hours. The graph shows that virus production is slightly higher in clone E4 in comparison to Lzrs and clone D2 at 24 hours post-infection. Overall clone D2 produces a lower titre, while clone E4 and Lzrs produce similar amounts of virus at 48 and 72 hours post infection.

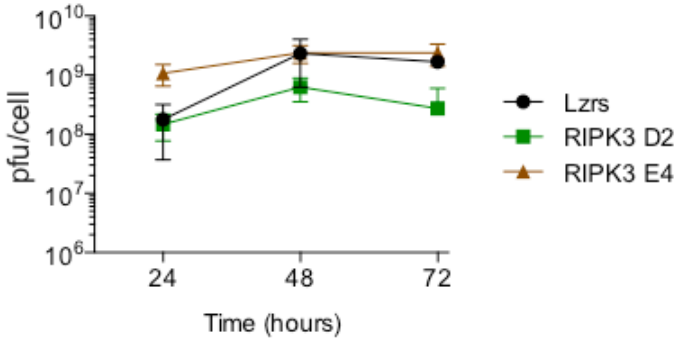

Figure 5-3: RIPK3 expression leads to changes in the production of infectious viral particles
HeLa Lzrs (Lzrs), HeLa RIPK3 D2 (RIPK3 D2) and HeLa RIPK3 E4 (RIPK3 E4) were infected with *dl*922-947 at MOI 10 over a time course of 72 hours. Viral titres were determined by $TC_{ID}50$ assay. Points represent mean +/- STDEV from one experiment performed in quadruplicate.

Next I analysed if the expression of RIPK3 leads to differences in viral infectivity leading to an increase in virus-induced death. Therefore, HeLa Lzrs and HeLa RIPK3 clone D2 and E4 were infected with the E1 deleted non-replicating type 5-adenovirus Ad-GFP, and infectivity determined 24 hours post-infection using flow cytometry.

Figure 5-4 shows differences in infectivity between HeLa Lzrs and the HeLa RIPK3 clones D2 and E4. GFP positivity was the same at MOI 5 , while at MOI 50 slight differences in infectivity could be observed at between Lzrs (97.3% GFP positive), HeLa RIPK3 D2 (97.2% GFP positive) and HeLa RIPK3 E4 (93.2% GFP positive). Table 13 summarises the percentage of GFP positive cells per condition as shown in figure 5-4.

Table 13: Percentage of GFP positive cells for each condition.

	GFP positivity (%)		
Cell line	**Mock**	***dl*922-947 MOI 5**	***dl*922-947 MOI 50**
HeLa Lzrs	0	68	97.3
HeLa RIPK3 D2	0	67.4	97.2
HeLa RIPK3 E4	0	67.3	93.2

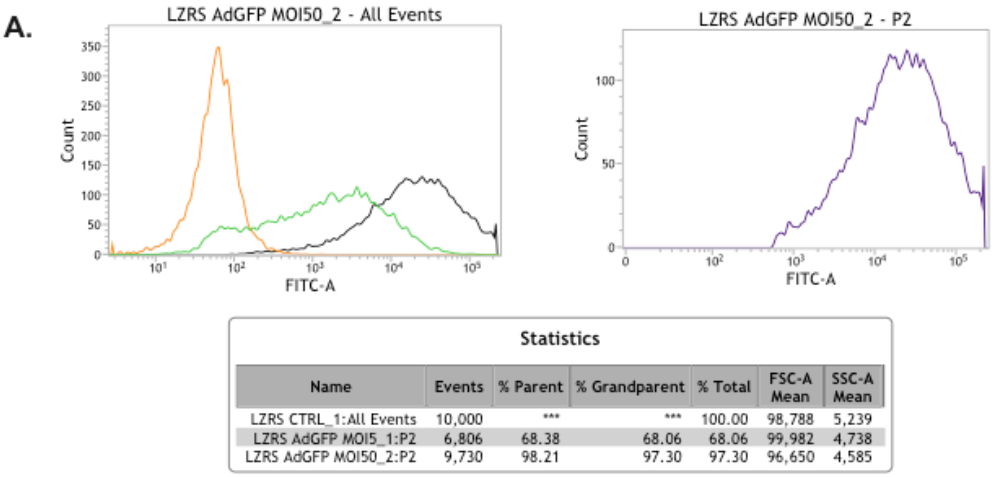

Statistics

Name	Events	% Parent	% Grandparent	% Total	FSC-A Mean	SSC-A Mean
LZRS CTRL_1:All Events	10,000	***	***	100.00	98,788	5,239
LZRS AdGFP MOI5_1:P2	6,806	68.38	68.06	68.06	99,982	4,738
LZRS AdGFP MOI50_2:P2	9,730	98.21	97.30	97.30	96,650	4,585

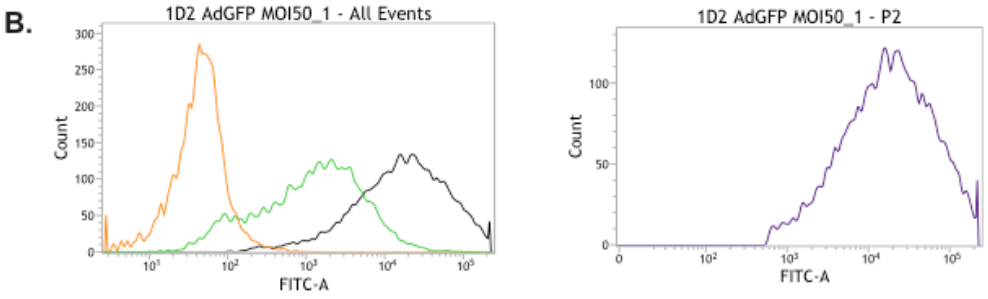

Statistics

Name	Events	% Parent	% Grandparent	% Total	FSC-A Mean	SSC-A Mean
1D2 CTRL_1:All Events	10,000	***	***	100.00	84,853	5,267
1D2 AdGFP MOI5_1:P2	6,740	70.17	67.40	67.40	88,330	4,821
1D2 AdGFP MOI50_1:P2	9,725	98.02	97.25	97.25	96,321	4,681

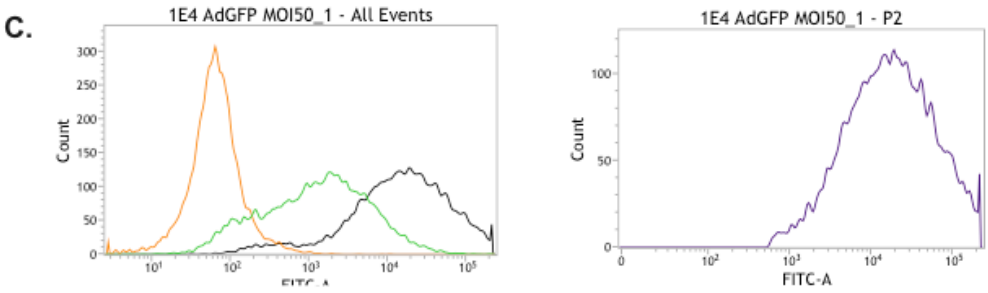

Statistics

Name	Events	% Parent	% Grandparent	% Total	FSC-A Mean	SSC-A Mean
1E4 CTRL_1:All Events	10,000	***	***	100.00	90,846	6,149
1E4 AdGFP MOI5_1:P2	6,730	70.23	67.30	67.30	92,627	5,273
1E4 AdGFP MOI50_1:P2	9,321	98.78	93.21	93.21	90,824	5,395

Figure 5-4: HeLa clones expressing RIPK3 show no difference in infectivity
A) HeLa Lzrs,
B) HeLa RIPK3 D2 and
C) HeLa RIPK3 E4 were either infected with *dl*922-947 or Ad-GFP at MOI 5 or MOI 50 for 24 hours in duplicate. After 24 hours, cells were prepared for flow cytometry analysis. Cells were analysed for GFP expression after 10,000 events were recorded. Shown are represented graphs from one experiment performed in duplicate. Orange lines indicated *dl*922-947, while green lines indicate Ad-GFP MOI 5 and purple lines indicate Ad-GFP MOI 50 infected samples.

5.3 Investigating the assembly of a RIPK3-containing death complex during *dl*922-947 infection

Since HeLa RIPK3 clones contain the normal and functional sequence of human RIPK3, I aimed to analyse the formation of the necrosome in HeLa RIPK3 expressing cells. The necrosome consists of the proteins RIPK1, RIPK3 and MLKL (Vandenabeele et al. 2010b, Vandenabeele et al. 2010a).

RIPK3 immunoprecipitation was performed in HeLa Lzrs and HeLa RIPK3 clone D2, to assess antibody specificity. As shown in figure 5-5 a RIPK3 pull-down was only detected in cells that express RIPK3. Further, a RIPK3 band was also detected in the supernatant, while no RIPK3 was seen in IgG-IP. As expected, no RIPK3 pull-down was seen in HeLa Lzrs cells. Interestingly, unspecific bands could be detected in non-IP samples.

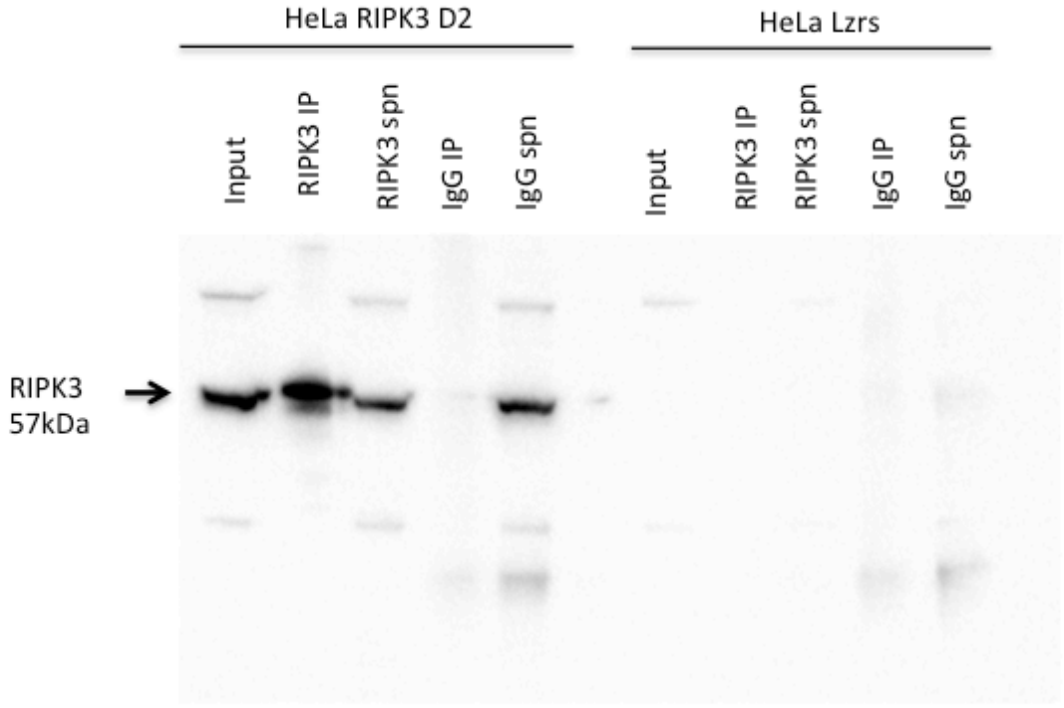

Figure 5-5: RIPK3 immunoprecipitation in HeLa RIPK3 clone D2 and HeLar Lzrs.
HeLa RIPK3 clone D2 and HeLa Lzrs samples were taken and prepared for immunoprecipitation with a RIPK3 or mouse IgG control antibody followed by western blot analysis. Samples were blotted IPK3 (57 kDa). One whole representative western blot from two experiments is shown. Arrow indicates RIPK3 band at 57kDa.

Co-immunoprecipitation of RIPK3 was performed on HeLa RIPK3 D2. Cells were either treated with TSZ for 1 or 2 hours (positive control) or infected with *dl*922-947 at MOI 10 for 24 and 48 hours. Afterwards, samples were prepared for co-immunoprecipitation of RIPK3 and analysed by western blot.

As shown in figure 5-6, RIPK3 can be successfully pulled down in RIPK3 expressing HeLa cells. MLKL was co-immunoprecipitated in cells treated with TSZ, which is in accordance with the known literature, and was also pulled-down in *dl*922-947 infected cells. However, no co-immunoprecipitation of RIPK1 was observed in either TSZ treated or *dl*922-947 infected cells. Interestingly, a strong band was detected in both *dl*922-947 infected samples at approximately 45kDa, which was not seen in any of the other samples.

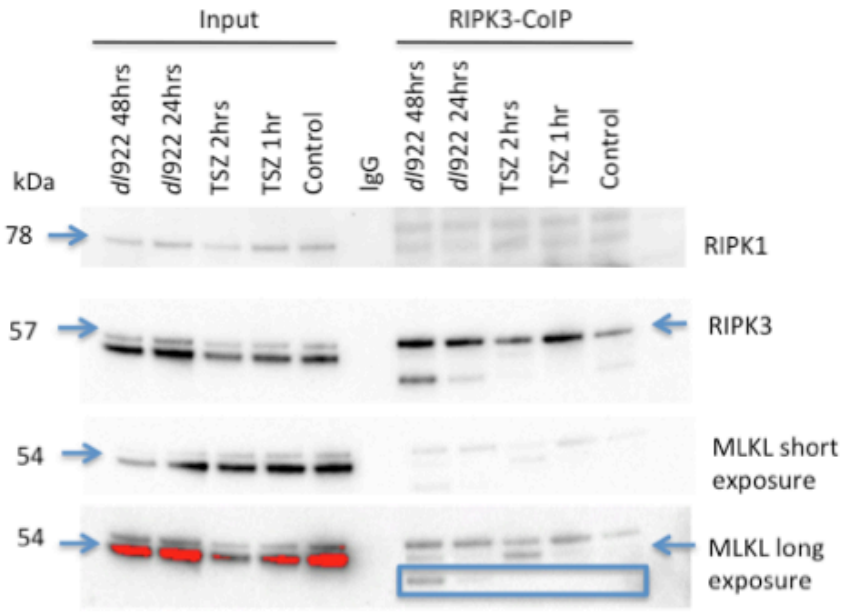

Figure 5-6: RIPK3 co-immunoprecipitation during *dl*922-947 infection in Hela RIPK3 clone D2
HeLa RIPK3 clone D2 cells were either treated with 20ng/mL TNF-α, 25μM Z.VAD.fmk and 1μM LCL-161 (smac mimetic) for 1 and 2 hours or infected with *dl*922-947 at MOI 10 for 24 and 48 hours. Samples were taken and prepared for co-immunoprecipitation with a RIPK3 antibody followed by western blot analysis. Samples were blotted for RIPK1 (78 kDa), RIPK3 (57 kDa) and MLKL (54 kDa). One representative western blot from two experiments is shown. Arrows indicate RIPK1, RIPK3 or MLKL in accordance with staining shown.

It has been shown that several viruses encode proteins that are able to interfere with the necrotic machinery (Wang et al. 2014b) by interactions with RHIM domain of RIPK3 leading to a block in the induction of programmed necrosis in the host cell. Therefore, I wanted to investigate if viral proteins were co-immunoprecipitated with RIPK3. I made use of an Anti-Adenovirus type 5

antibody that recognises several viral proteins including hexon and penton base as well as several adenovirus core proteins. Therefore, samples used in figure 5-6 were re-run, and analysed for viral proteins using an Anti-Adenovirus type 5 antibody.

Figure 5-7 shows that RIPK3 co-immunoprecipitation lead to the pull-down of three viral proteins. The three bands that were co-immunoprecipitated in *dl*922-947 treated cells were detected at an approximate molecular weight of 110 – 150 kDa and a double band at around 60 - 80 kDa. They could be detected at 24 as well as 48 hours post-infection. Further, pull-down of these viral proteins increased from 24 to 48 hours post-infection and was not due to changes in RIPK3 pull-down as shown in figure 5-6. Interestingly, the band observed at approximately 45kDa in figure 5-6 was observed when the anti-Adenovirus antibody was used, suggesting that it might not be a viral protein.

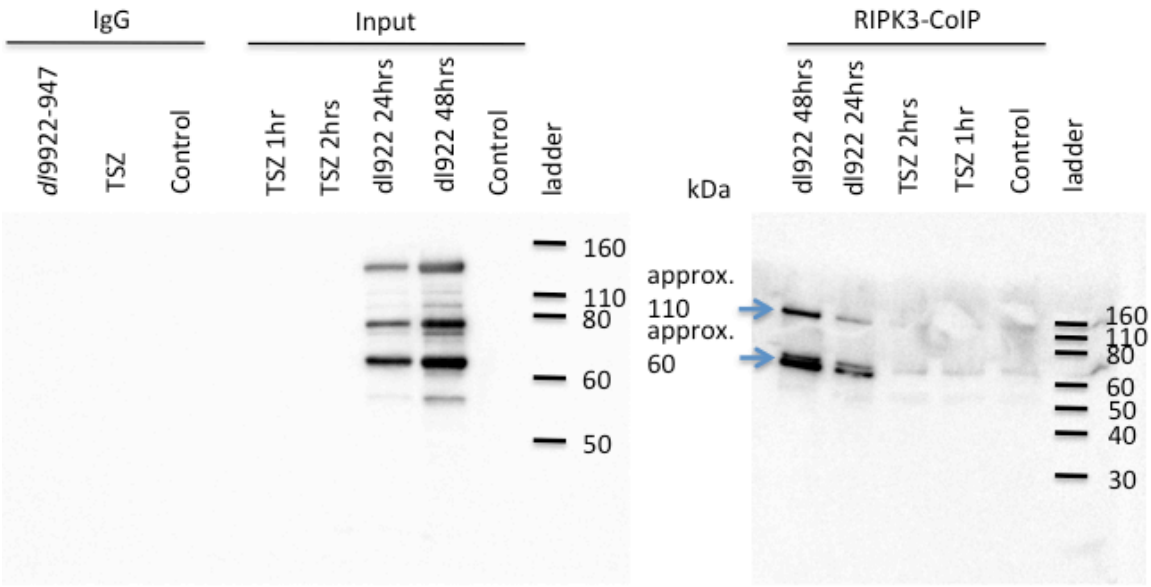

Figure 5-7: RIPK3 co-immunoprecipitation during *dl*922-947 infection in Hela RIPK3 clone D2 leads to the pull-down of adenoviral proteins

HeLa RIPK3 clone D2 cells were either treated with 20ng/mL TNF-α, 25μM Z.VAD.fmk and 1μM LCL-161 (smac mimetic) for 1 and 2 hours or infected with *dl*922-947 at MOI 10 for 24 and 48 hours. Samples were taken and prepared for co-immunoprecipitation with a RIPK3 antibody followed by western blot analysis. Samples were blotted anti-Adenovirus (14-110 kDa). One representative western blot is shown. Arrows indicate viral proteins that have been pulled down with RIPK3.

5.4 RIPK3 overexpression reduces xenograft tumour growth in CD1 nude mice

To determine if RIPK3 expression affects tumour growth in CD1 nude mice, mice were injected with HeLa Lzrs or HeLa RIPK3 expressing cells. Tumour growth was monitored by external measurement. After tumours reached between 50-100mm^3 in volume, mice were randomly separated into two groups with one group receiving 50µL of PBS and the other one receiving 1x10^{10} particles of *dl*922-947 intra-tumourally. Mice were culled 48 hours post virus/PBS injection.

Figure 5-8 shows tumour growth in mice over time frame of 19 days. As shown tumours start out at similar tumour volumes (HeLa Lzrs: 45mm^3, HeLa RIPK3 D2: 47mm^3 and HeLa RIPK3 E4: 41mm^3). Over time, two distinct growth patterns evolve with HeLa Lzrs tumours growing more rapidly over time in comparison to HeLa RIPK3 expressing tumours. At day of virus or PBS injection HeLa Lzrs tumours are significantly bigger in size than RIPK3 expressing tumours. At day of injection HeLa Lzrs tumours are 175mm^3 in volume, HeLa RIPK3 D2 are 96mm^3 and HeLa RIPK3 E4 tumours are 78mm^3 in volume.

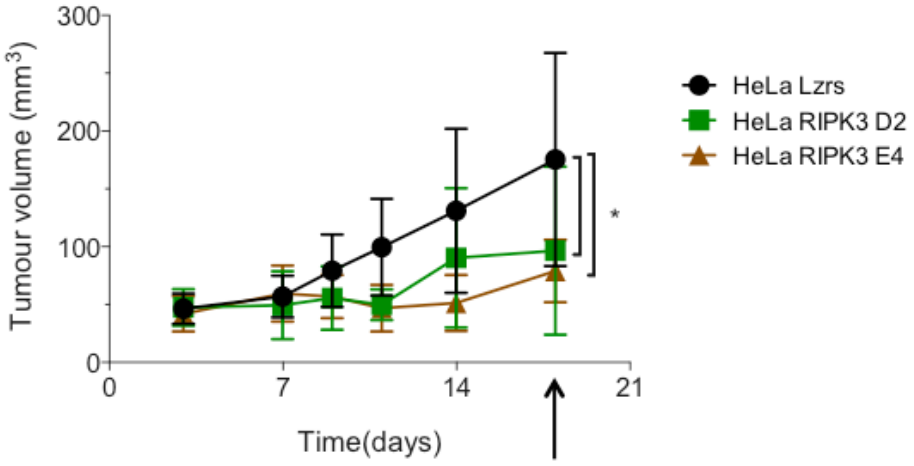

Figure 5-8: Tumour volume growth
CD1 nude mice were injected subcutaneously with 5x10^6 cells per mouse and tumours were grown until they reached between 50-200mm^3 in volume. Then mice were either injected intra-tumourally with 50µL PBS or 1x10^{10} particles of *dl*922-947. 48 hours after virus or PBS injection, mice were culled and tumours taken. Arrow indicates day of virus or PBS injection.
P values are calculated using unpaired one tailed t-test, * shows p<0.05.

5.5 HeLa RIPK3 cells retain RIPK3 expression after injection into CD1 nude mice

It has been shown recently, that in many cancers RIPK3 expression is repressed due to methylation-dependent mechanisms near its transcriptional start site, leading to greater resistance to death-induced by death receptor ligands and surprisingly to a greater resistance to chemotherapeutic agents (Koo et al. 2015). Further, it has been shown that the microenvironment can alter epigenetic and gene expression profiles (Hamm et al. 2010) and that tumours themselves can induce alterations in genomic DNA-methylation in the microenvironment to aid tumour growth (Xiao et al. 2016). Therefore, the transplantation of human cancer cells into mice could lead to a change in the methylation status of RIPK3 to create a more tumorigenic microenvironment.

To assess if tumours altered their RIPK3 expression after injection into CD1 nude mice, three random HeLa Lzrs and three random HeLa RIPK3 expressing subcutaneous tumours were taken for western blot analysis to confirm RIPK3 protein expression.

As shown in figure 5-9 HeLa RIPK3 cells injected into CD1 nude mice retain their RIPK3 expression *in vivo*.

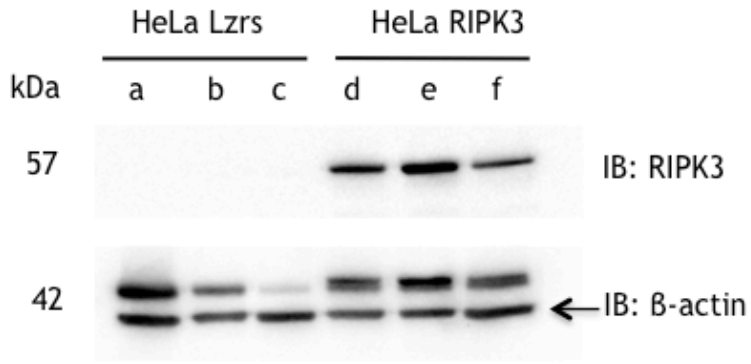

Figure 5-9: HeLa RIPK3 clones retain their RIPK3 expression after subcutaneous injection into mice

Tumours of three mice injected with HeLa Lzrs and three mice injected with HeLa RIPK3 cells were prepared for western blot. Western blot confirmed that tumours of mice injected with HeLa's that express RIPK3 retain their expression in an *in vivo* environment. Samples were blotted for β-actin (42 kDa) and RIPK3 (57 kDa).

5.6 RIPK3 expression in subcutaneous tumours does not affect adenovirus protein expression *in vivo*

Since tumours in mice were grown subcutaneously, direct injection of virus or PBS into the tumour site was chosen for delivery. Expression of viral proteins in subcutaneous tumours was analysed by immunohistochemistry to evaluate distribution of *dl*922-947, 48 hours post-infection.

As shown in figure 5-10 and figure 5-11 tumours injected with *dl*922-947 express E1A as well as adenoviral core and capsid proteins in comparison to PBS injected tumours, which don't. Further, histoscoring on tumours using a programmed algorithm showed that there was no significant difference between the expression of adenoviral E1A or adenoviral capsid and core proteins in HeLa Lzrs and HeLa RIPK3 tumours *in vivo*.

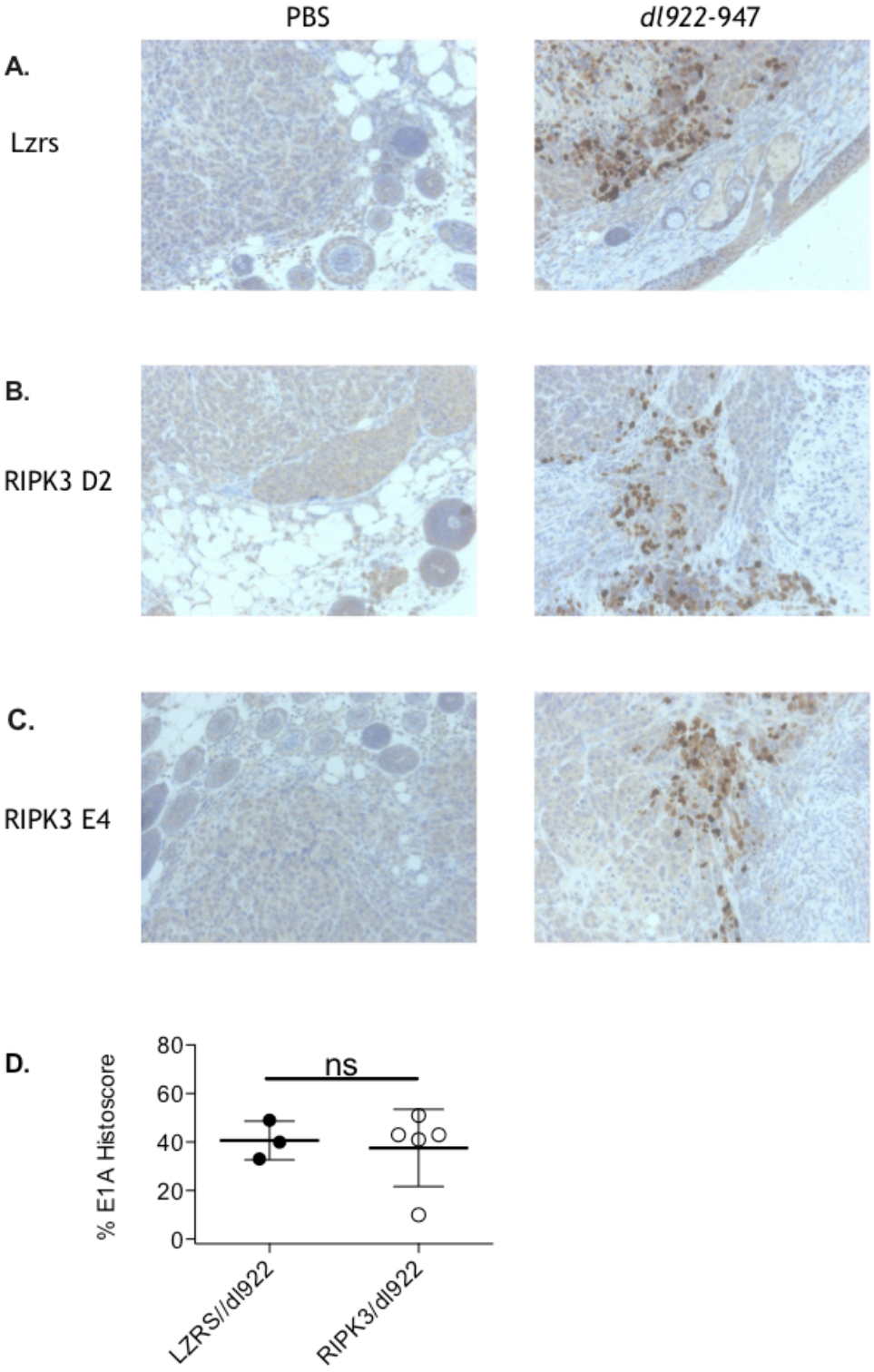

Figure 5-10: RIPK3 expression does not increase E1A protein expression *in vivo*.
A) HeLa Lzrs
B) HeLa RIPK3 D2 and
C) HeLa RIPK3 E4 expressing tumours were processed for E1A immunohistochemistry by the Histology service at the CRUK Beatson Institute. Pictures were taking using a light microscope. IgG controls were used as negative control to confirm specificity of the antibody.
D) E1A histoscores of *dl*922-947 injected tumours were analysed. No significant difference was observed between Lzrs and RIPK3 expressing cells.

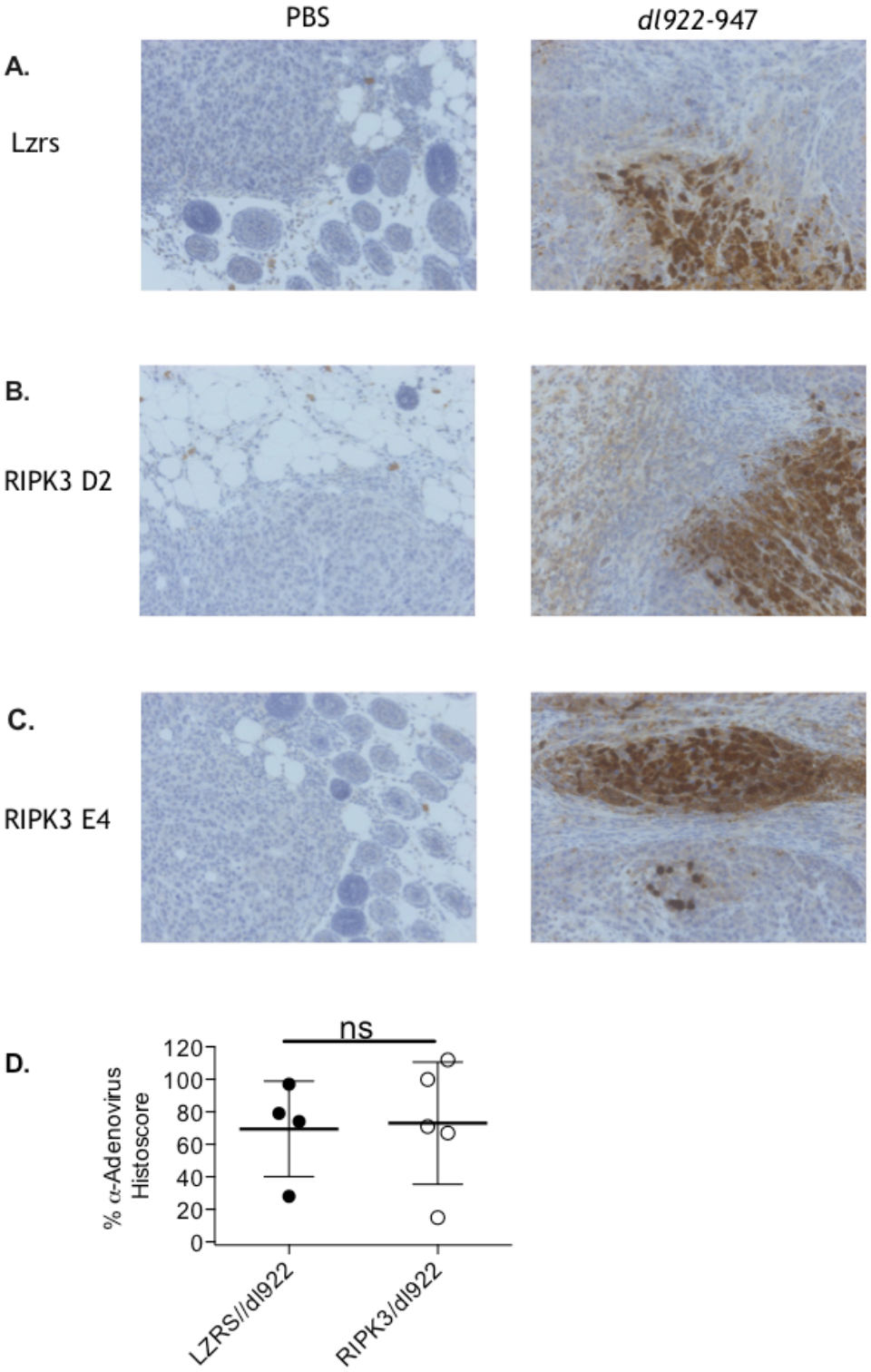

Figure 5-11: RIPK3 expression does not increase the expression of viral core and capsid proteins *in vivo*

A) HeLa Lzrs

B) HeLa RIPK3 D2 and

C) HeLa RIPK3 E4 expressing tumours were processed for α-Adenovirus immunohistochemistry by the Histology service at the CRUK Beatson Institute. IgG controls were used as negative control to confirm specificity of the antibody.

D) Anti-Adenovirus histoscores of *dl*922-947 injected tumours were analysed. No significant difference was observed between Lzrs and RIPK3 expressing cells.

5.7 RIPK3 expression increases adenovirus efficacy and necrosis *in vivo*

Next, I wanted to investigate further if the expression of RIPK3 would increase the amount of necrosis induced by *dl*922-947. Unlike apoptosis, there are no validated biochemical or IHC markers of necrosis for use *in vivo*. However, necrosis can be defined as regions within the tumour that lack nuclei. To measure the necrotic area, E1A positive slides were scanned and uploaded to slidepath. The desired files were opened and the draw-polygon tool was chosen. Using the draw polygon tool the necrotic area was outlined within the tumours and measured. The necrotic area was then normalized to the total tumour area and calculated at percentage of total tumour area.

Figure 5-12A shows an example of how the necrotic area within a tumour section was measured. As shown in figure 5-12B, expression of RIPK3 leads to a significant increase in necrosis in *dl*922-947 infected cells *in vivo* in comparison to HeLa Lzrs tumours infected with *dl*922-947.

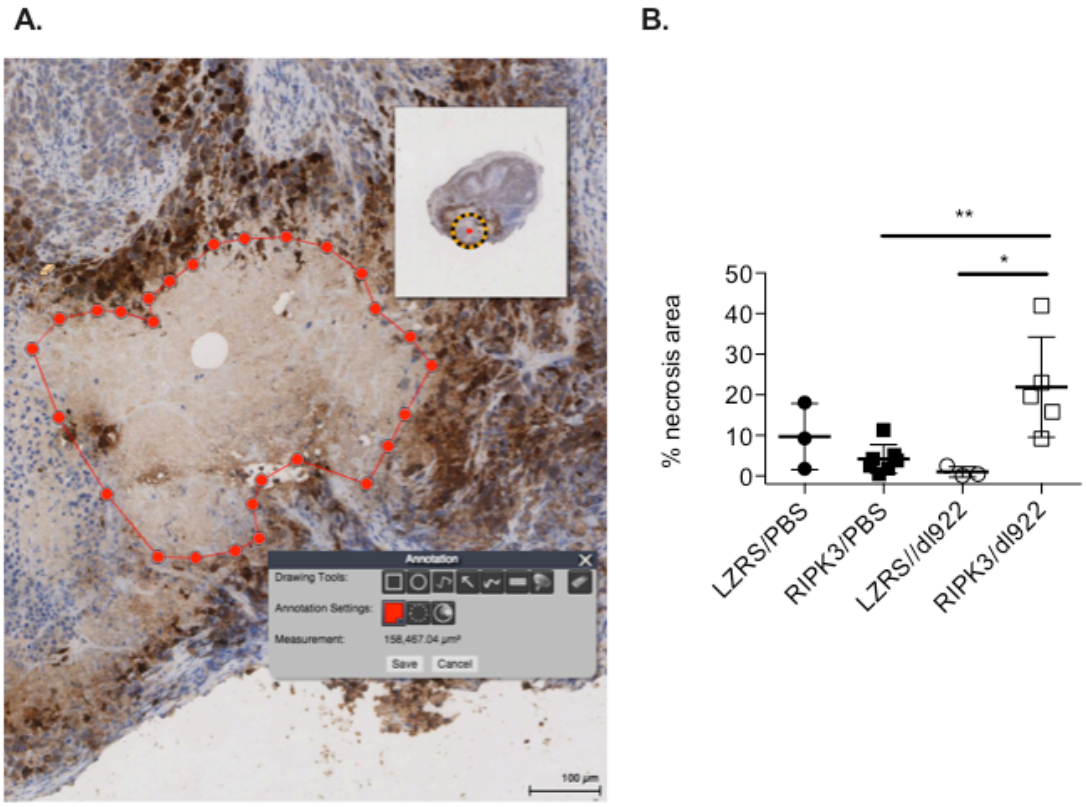

Figure 5-12: Tumours expressing RIPK3 show an increase in adenovirus-induced necrosis *in vivo*

A) shows an example of how necrotic area was measured using slidepath.

B) The necrosis area in HeLa Lzrs and HeLa RIPK3 tumours treated with PBS or *dl*922-947 was measured using slidepath. Necrosis area is shown as a percentage of whole tumour section. P values are calculated using unpaired t test, * shows $p<0.05$ and ** $p<0.01$.

Since RIPK3 expression in *dl*922-947 infected cells lead to an increase in cell death *in vitro*, I next assessed if RIPK3 overexpression in a human xenograft model would increase *dl*922-947 efficacy *in vivo*. CD1 nude mice were injected with HeLa Lzrs or HeLa RIPK3 expressing cells. Tumour growth was monitored by external measurement. After tumours reached between 50-100mm^3 in volume, mice were randomly separated into two groups with one group receiving two doses of 50µL of PBS and the other one receiving two doses of 1x10^9 particles of *dl*922-947 intra-tumourally. Mice were monitored and tumour volume measured.

Figure 5-13 shows *dl*922-947 efficacy *in vivo*. Figure 5-13A and B shows growth of HeLa Lzrs and HeLa RIPK3 tumours respectively. In the HeLa Lzrs mice, treatment with *dl*922-947 produced no significant reduction in tumour volume compared to PBS. By contrast, two intra-tumoural injections of *dl*922-947 produced a significant reduction in HeLa RIPK3 tumour volumes.

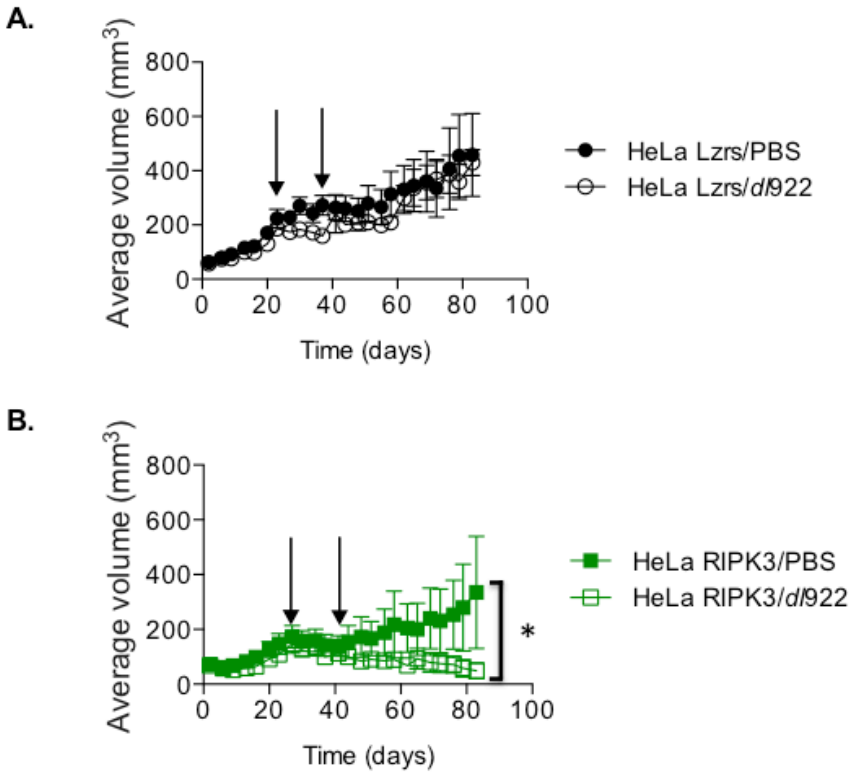

Figure 5-13: RIPK3 expressing increases *dl*922-947 efficacy in vivo
24 CD1 nude mice were randomly separated into two cohorts of 12 each and
A) either injected subcutaneously with 5x10^6 HeLa Lzrs cells per mouse. Tumours were grown until they reached between 50-200mm^3 in volume. 23 days post-injection mice were again randomly separated into cohorts of six and either twice-injected intra-tumourally with 50µL PBS or 1x10^{10} particles of *dl*922-947.
B) 12 CD1 nude mice were injected with 5x10^6 HeLa RIPK3 cells. Tumours were grown until they reached between 50-200mm^3 in volume. 28 days post-injection mice were again randomly separated into cohorts of six and either twice-injected intra-tumourally with 50µL PBS or 1x10^{10} particles of *dl*922-947. Tumour growth was monitored every second or third day. Mice were either

killed when tumours reached 1.4cm^3 in volume or if they showed signs of ill health. Arrows indicate days of PBS and *dl*922-947 injection.
P values are calculated using unpaired one tailed t-test, *shows $p<0.05$.

5.8 RIPK3 expression does not alter macrophage and neutrophil migration *in vivo*

Recent research has shown that the immune system plays an essential role in the efficacy of oncolytic virotherapy (Tong et al. 2012, Chiocca and Rabkin 2014), which lead to the development of viral strains that express factors like cytokines and chemokines that increase an anti-tumour response in clinical trials (Andtbacka et al. 2015, Cripe et al. 2015, Hemminki et al. 2015). Furthermore, research in reovirus has shown that a robust immune-dependent anti-tumour response was observed that was independent of viral replication and lysis (Prestwich et al. 2009).

CD1 nude mice have a dysfunctional and rudimentary thymus leading to a great reduction in T cells. This allows the engraftment of many different types of tissues and tumours. Although CD1 nude mice have a greatly reduced number of T cells, they still produce normal Antigen presenting cells (APC), NK cells and cells of myeloid lineage.

As shown above, RIPK3 expression leads to an increase in *dl*922-947 efficacy; to assess if the increase in efficacy was aided by an increase in immune cell infiltration, I aimed to investigate if RIPK3 expression and/or *dl*922-947 infection in tumours lead to changes in macrophage and neutrophil migration.

First I analysed if RIPK3 expression would influence the infiltration of macrophages into xenograft tumours. Figure 5-14 shows F4/80 immunohistochemistry performed on PBS and *dl*922-947 injected tumours. As shown in figures 5-14B and C, there was a non-significant trend towards reduced macrophage infiltration in *dl*922-947-treated tumours. However, expression of RIPK3 made no difference to this in macrophage infiltration.

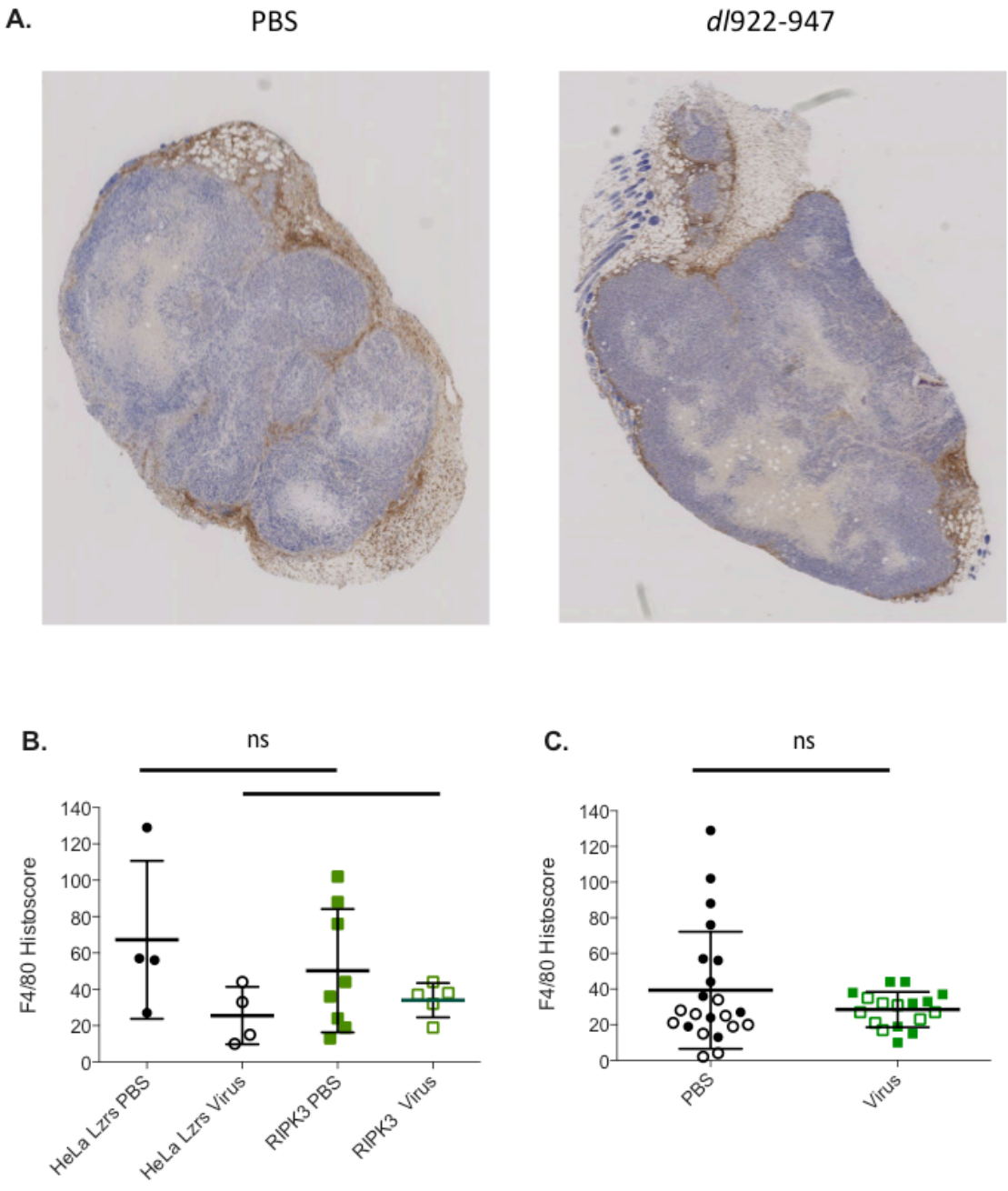

Figure 5-14: RIPK3 expression and/or *dl*922-947 infection does not alter macrophage migration

A) HeLa Lzrs and RIPK3 expressing tumours were processed for F4/80 immunohistochemistry and pictures were taking using a light microscope. IHC staining for a PBS or *dl*922-947 treated tumour is shown.

B) F4/80 histoscores of *dl*922-947 or PBS injected tumours.

C) Combined F4/80 histoscores from two independent experiments. Filled in symbols represent an experiment were CD1 nudemice were injected with HeLa Lzrs or HeLa RIPK3 expressing cells. Tumours were grown until they reached between 50-200mm^3 in volume. Then mice were either injected intra-tumourally with 50µL PBS or 1x10^{10} particles of *dl*922-947. 48 hours after virus or PBS injection, mice were culled and tumours taken. Empty symbols represent tumours that have been grown exactly the same but tumours were injected with 5x10^{10} particles of *dl*922-947.

Figure 5-15A shows that *dl*922-947 infection leads to an increase in neutrophil infiltration in a xenograft model. Immunohistochemical analysis of HeLa Lzrs and HeLa RIPK3 expressing tumours showed that RIPK3 expression did not lead to a significant increase in neutrophil migration (Figure 5-15B), but interestingly *dl*922-947 infection lead to a significant increase in neutrophil migration.

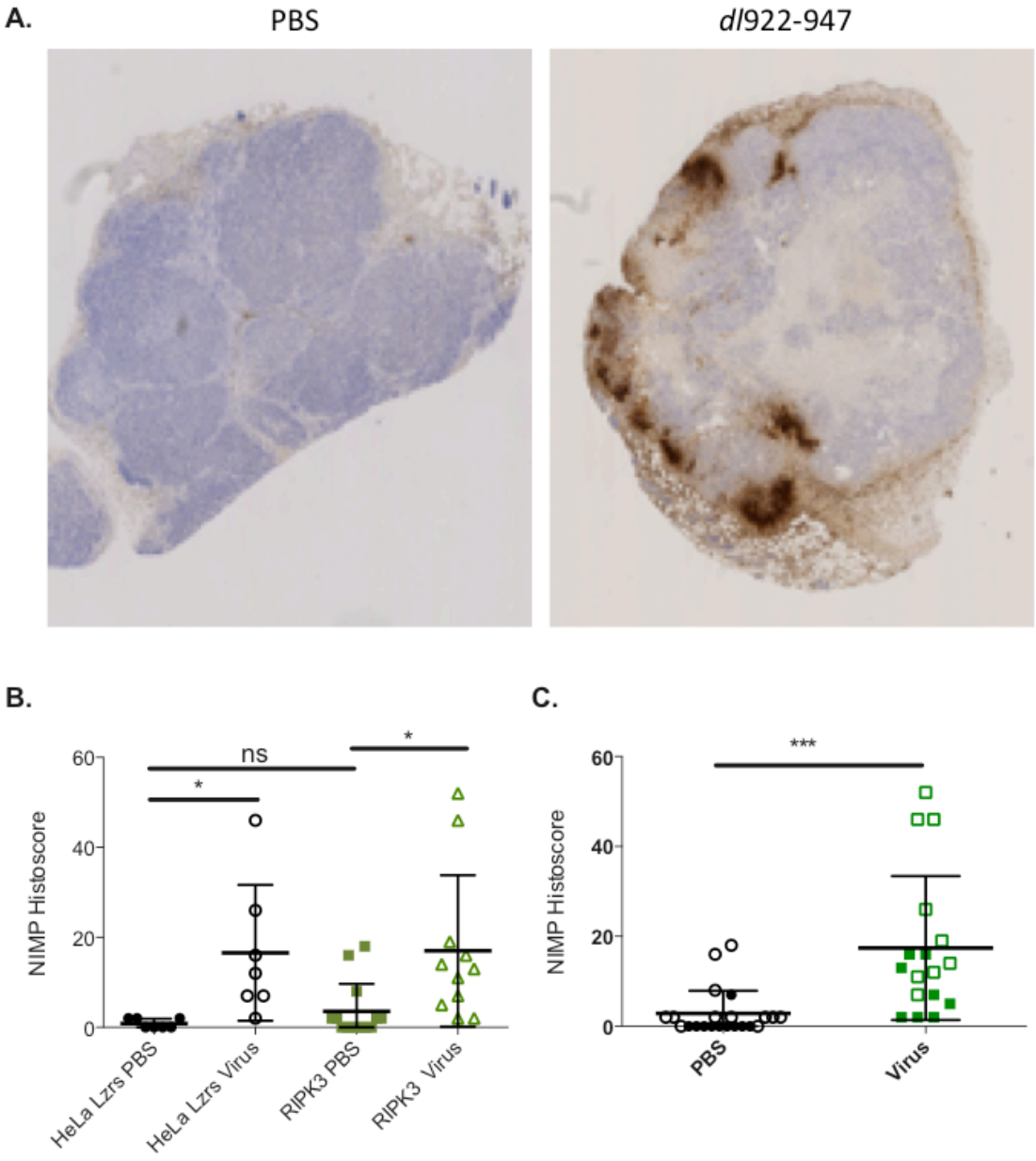

Figure 5-15: *dl*922-947 infection leads to an increase in neutrophil migration
A) HeLa Lzrs and RIPK3 expressing tumours were processed for NIMP immunohistochemistry and pictures were taking using a light microscope. Shown is IHC staining for a PBS or *dl*922-947 treated tumour.
B) NIMP histoscores of *dl*922-947 or PBS injected tumours.
C) Combined NIMP histoscores from two independent experiments. Filled in symbols represent an experiment were CD1 nude mice were injected with HeLa Lzrs or HeLa RIPK3 expressing cells. Tumours were grown until they reached between 50-200mm^3 in volume. Then mice were either injected intra-tumourally with 50µL PBS or 1x10^{10} particles of *dl*922-947. 48 hours after virus or PBS injection, mice were culled and tumours taken. Empty symbols represent tumours that have

been grown exactly the same but tumours were injected with $5x10^{10}$ particles of *dl*922-947. P values are calculated using unpaired t test, *shows $p<0.05$ and ***$p<0.001$.

5.9 Discussion

For a long time, necrosis was thought to be a form of unregulated cell death in response to accidental tissue injury. However, recent research has shown that programmed necrosis is a regulated type of cell death that is distinguishable from apoptosis and autophagy. In the centre of this pathway is the protein RIPK3, which induces programmed necrosis when apoptosis is blocked or inhibited, allowing cells to die from an alternative pathway in response to stress, injury or infection. Recent research in programmed necrosis in cancer cell lines has shown that RIPK3 is often silenced due to methylation dependent mechanisms, giving cancerous cells a potential survival advantage (Morgan and Kim 2015, Koo et al. 2015), and analysis of RIPK3 expression in ovarian cancer cell lines has shown the same. Using HeLa cells, I aimed to generate another cell line with stable overexpression of human RIPK3 to assess the therapeutic value of RIPK3 expression during adenovirus infection.

HeLa cells were retrovirally transduced and RIPK3 expressing cells selected by their zeocin resistance. Though a calculated MOI is used for transduction, often the MOI will vary from cell to cell within the same culture. This can lead to the integration of different copy numbers of the target gene into the host genome, therefore affecting the amount of protein expression and as shown by western blot, dilution cloning of HeLa RIPK3 expressing cells lead to the isolation of clones with slightly different levels of RIPK3 protein expression. Further characterization using TSZ showed that RIPK3 expressing cells were able to undergo programmed necrosis, while interestingly, clones varied in overall cell survival post TSZ treatment. This could be either due to the slight differences in RIPK3 expression or due to differences in the vector integration locus between the different RIPK3 clones. A different integration locus could potentially activate or inactivate other genes in the clones that are important for cell death induction and therefore lead to differences in cell death upon TSZ stimuli. During *dl*922-947 infection, RIPK3 expressing clones showed a higher sensitivity towards cell death compared to empty vector cells and this increase in cell death showed to be RIPK3-dependent, since the inhibition of RIPK3 using the RIPK3 specific inhibitor GSK'840B reversed the amount of cell death to similar levels of HeLa Lzrs cells.

Further analysis of RIPK3 expressing cells also showed that during *dl*922-947 infection a RIPK3/MLKL-containing complex is formed 48 hours post-infection. Interestingly no association of RIPK1 was observed in this complex, which further shows that RIPK1 is redundant in *dl*922-947-induced death and necrosis can be RIPK1-independent as shown by others (Tomasella, Blangy and Brancolini 2014, He et al. 2011). The formation of RIPK3 containing complexes that induce programmed necrosis has been extensively described (He et al. 2011, Upton, Kaiser and Mocarski 2012). Especially in viral induced necrosis, it has been shown that RIPK3 can associate with viral gene products like HSV1 ICP6 (Huang et al. 2015) or other cellular proteins like DAI (Upton et al. 2012) to inhibit, interfere or induce programmed necrosis. Interestingly, using an antibody that detects several viral core and capsid proteins showed the association of three viral proteins with RIPK3 during viral infection. This suggests that adenoviruses might also encode proteins that can manipulate the necrotic machinery. Further, previous data showing that RIPK1 and MLKL are dispensable for *dl*922-947 induced cell death might be due to *dl*922-947 encoding proteins interfering with necrotic machinery. Also, data produced using TOV21G showed interesting, albeit partially contradictory results, about the involvement of RIPK3 in adenovirus-induced death leaving room for the involvement of viral proteins that encode inhibitors of necrosis.

Next, RIPK3's effects on viral infectivity, replication and expression of proteins were further assessed. Interestingly RIPK3 expression did not interfere with viral infectivity, but western blot analysis of viral E1A showed that E1A was up-regulated in RIPK3 expressing HeLa cells at 24 hours post-infection. Proteins that are encoded by E1A are involved in the activation of viral transcription and in re-programming cellular gene expression to aid viral replication, therefore up-regulation of E1A in RIPK3 expressing cells might be a result of differences in those cellular events. Considering that it has been shown that the overexpression of RIPK3 alone can trigger cells to undergo programmed necrosis, cells expressing RIPK3 might change the expression of those proteins to avoid the induction of cell death. Interestingly, it has been shown that the over-expression of E1A is able to induce apoptosis (Mymryk, Shire and Bayley 1994, Rao et al. 1992). If RIPK3 expression was to alter the expression of proteins involved in cell death, the up-regulation of E1A would not induce apoptosis in

those cells and rather benefit viral replication and analysis of viral replication showed that at 24 hours post-infection the same or a higher viral titre could be produced in RIPK3 expressing cells compared to non-RIPK3 expressing HeLa Lzrs. This observation was in line with research showing that E1A expression levels affect viral replication. Zheng, et al. observed that high levels of E1A could increase virus replication that resulted in higher viral titres (Zheng et al. 2005). Interestingly, Hela RIPK3 clone D2 was not able to reach similar titres to clone E4 or HeLa Lzrs and produced lower titres from 48 hours post-infection; this might be due to an early induction of cell death through necrosis.

To further assess the therapeutic value of RIPK3 expression, a human xenograft model was used to evaluate whether RIPK3 expression would increase adenovirus efficacy *in vivo*. First, tumour growth of subcutaneous injected HeLa Lzrs and HeLa RIPK3 cells was assessed. Results suggested that expression of RIPK3 slowed subcutaneous growth, as has been observed in previous research using a xenograft model with RIPK3 overexpressing KYSE410 cells (Xu et al. 2014), where they showed that differences in tumour growth were due to RIPK3-mediated necrosis. Once tumours reached between 50-200mm^3, tumours were injected with PBS or 1x10^9 particles of *dl*922-947. IHC showed that there was no difference in E1A and adenoviral core and capsid protein expression between HeLa Lzrs and HeLa RIPK3 expressing tumours. Interestingly, while there was no difference in viral protein expression in tumours, tumours expressing RIPK3 showed significantly higher amounts of virus-induced necrosis. Most importantly, my results indicated that RIPK3 expression significantly improved *dl*922-947 efficacy in this subcutaneous HeLa xenograft model.

Next I aimed to assess the effects of RIPK3 expression and *dl*922-947 infection on innate immune cell migration in human tumour xenografts. Infection with *dl*922-947 appeared to decrease macrophage infiltration, albeit non-significantly. Research published by others also showed that infection with Ad5 showed a decrease in macrophage infiltration in a model of ovarian cancer (Thoma et al. 2013) and work performed by others has further showed that Intravenous Ad5 is absorbed by liver Kupffer cells (Lieber et al. 1997) and IHC on livers of mice that have been injected intravenous with Ad5 showed a reduction in F4/80-positive staining (Khare et al. 2013). Also work published by Passaro, *et al*. showed that

*dl*922-947 infection impaired macrophage infiltration in an anaplastic thyroid carcinoma model (Passaro et al. 2016). Interestingly, *dl*922-947 infection lead to a significant increase in neutrophil infiltration compared to PBS treated tumours. For a long time it has been thought that necrosis is more pro-inflammatory than apoptosis, but recent research has shown the opposite. Kearney, *et al*. have shown that TNF-induced necrosis suppresses the production of TNF-induced pro-inflammatory cytokines and chemokines through excessive cell death, thereby. Therefore showing that necroptosis can actually suppresses inflammation. When female mice were injected with LPS and LPS/Z.VAD.fmk, LPS treatment alone lead to an increase in splenic neutrophils, F4/80+ macrophages, eosinophils and B- and T-lymphocytes in mice while this effect was diminished in LPS/Z.VAD.fmk treated mice (Kearney et al. 2015).

Concluding this chapter, I have been able to devise a RIPK3 overexpression model in HeLa cells for *in vivo* studies. I have shown that HeLa RIPK3 expressing cells undergo programmed necrosis, which can be rescued by common necrosis inhibitors. Further I have been able to show that RIPK3 expression increases viral cytotoxicity due to an increase in necrosis *in vivo* and that adenovirus infection stimulates the formation of a RIPK3 and MLKL death complex. Western blot analysis of this death complex showed the association of adenoviral proteins, which have not been characterised yet.

Chapter 6

Final Discussion

6 Final Discussion

In 2005, H101 became the first approved oncolytic therapy in combination with chemotherapy for squamous cell cancer of head and neck or oesophagus in China (Garber 2006). Though it showed promising results in clinical and pre-clinical settings, it didn't take long to discover its limitations, which lead to the exploration of other alternative viral vectors for oncolytic therapies. However, for successful use in clinical settings, oncolytic viruses have to fulfil certain criteria to allow for their safe use. They have to replicate selectively in a wide range of tumour cells while not affecting healthy tissues. Further they should be able to induce immunogenic cell death, a form of cell death that can stimulate anti-tumour immunity.

Several adenoviruses have been used in clinical setting (Including ONYX-015, H101 and EnAd), all of which demonstrated their safety for use in patients. Many of those oncolytic adenoviruses have been genetically modified to ensure that they selectively replicate in cancerous cells. One of the most commonly Ad5-based oncolytic adenoviruses carries a 24bp mutation in the E1A gene (E1AΔ24), which is involved in releasing E2F from the Rb/E2F complex to promote cell entry into S-phase for viral replication and due to this mutation E2F cannot be released from the RB/E2F complex, therefore oncolytic viruses carrying this mutation take advantage of cells that have high levels of free E2F for their replication leading to an increase in cancer cell specific lysis and in their safety.

Besides the use of deletion mutants, adenoviruses with transgenes and other modifications are being developed to increase their efficacy or their ability to stimulate an immune-mediated anti-tumour response. Adenoviruses of the serotype 5 (Ad5) are commonly used for Ad-based vectors, but it has been shown that one of the big hurdles in using adenovirus serotype 5 (Ad5)-based vectors is that their primary entry receptor CAR is commonly down-regulated in several human tumours (Hulin-Curtis et al. 2016), although new research from the host lab has shown that in ovarian cancers, CAR expression is up-regulated in paclitaxel-resistant cells. This observation could have positive implications in future clinical use if it can be further validated and offer help to women that are resistant to paclitaxel (Ingemarsdotter et al. 2015). To further increase the transduction of Ad5-based vectors, the viral fiber can be modified by inserting

an RGD-motif. This modification can increase the interaction with integrins, which are highly expressed on some cancers and it also has been shown that the fiber itself can be replaced with other serotype fibers to use different receptors like CD46, which is used by adenoviruses of the serotype 35. Though CD46 is highly expressed on many cancers, this has to be taken with a grain of salt since Ad5 vectors bearing the Ad35 fiber knob proteins also down-regulate CD46.

Though cancer cell specific lysis has been shown to be effective *in vitro*, xenograft models and certainly human solid tumours are considerably more complex systems, since they are heterogeneous structures that contain not only malignant cells but also cells such as fibroblasts, endothelial cells and immune cells, which make up the tumour microenvironment that helps promote tumour growth. Dense extracellular matrix (ECM), abnormal vasculature, cancer-associated fibroblasts, increased fluid pressure and hypoxic areas within the tumour can hinder viral spread, therefore oncolytic adenoviruses that can target the extracellular matrix and angiogenesis are needed to increase anti-tumour efficacy. Over the past years oncolytic adenoviruses expressing molecules that disrupt the ECM (Lee et al. 2013, Vera et al. 2016), target abnormal vasculature (Thaci et al. 2013, Choi et al. 2015), target hypoxic environments (Cuevas et al. 2003, Post et al. 2004), that modulate the immune status of the tumour to aid immune cell infiltration (Koski et al. 2010, Ranki et al. 2016, Vassilev et al. 2015) or express cytokines (Hirvinen et al. 2015) to induce cell death or activate and stimulate immune cells (Manetti et al. 1993, Freytag, Barton and Zhang 2013, Pesonen et al. 2012) have be generated and shown to increase viral spread in tumour models and reduce tumour formation and progression. But as research by others has shown, extensive research has to be put into those modified viruses since the insertion of target peptides can also change or alter viral tropisms (Lucas et al. 2015).

Besides improving oncolytic viruses by using modifications, better understanding of viral infection, replication, spread and virus-induced killing can further help to improve their efficacy. In this thesis, I aimed to investigate how the Ad5 deletion mutant *dl*922-947 induces cell death in ovarian cancer cells. A special emphasis was put on the involvement of programmed necrosis in *dl*922-947-induced death in ovarian cancer, since research published by the host lab and

others showed that *dl*922-947 does not induce apoptosis and death rather resembled necrosis (Baird et al. 2008).

I have been able to show that during infection cells undergo morphological changes that strongly resemble necrosis rather than what for a long time has been thought to be a death of an apoptotic nature. Interestingly, upon further characterisation it was observed that cell death induced by *dl*922-947 was independent of TNF-α, RIPK1 and MLKL, which form part of the major components of the classical programmed necrosis pathway. Also necrosis induced by the ripoptosome could be excluded since RIPK1 is a critical component of this pathway, but showed to be redundant in *dl*922-947-induced death. Further, using a RIPK3 overexpression model, I was able to show that RIPK3 expression significantly increases viral efficacy due to an increase in necrosis *in vivo* and further stimulates the formation of an RIPK3/MLKL containing complex that associates with unknown viral proteins. These results lead to my conclusion that cell death-induced by *dl*922-947 heavily depends on the cellular context and that upon viral infection several different cell death mechanisms can be induced. In the context of endogenous RIPK3 expression *dl*922-947 does not induce apoptosis as shown by the host lab (Baird et al. 2008) and by research showing that adenoviruses efficiently block apoptosis. Interestingly, during *dl*922-947 infection cells undergo morphological changes that resemble programmed necrosis even though death is RIPK1, MLKL and TNF-α-independent and only partly RIPK3-dependent. The use of multiple parallel death pathway modalities by a cell could explain this and in the case of Influenza A virus, Nogusa et al, have shown that RIPK3 can activate parallel pathways of MLKL-driven necroptosis and FADD-mediated apoptosis (Nogusa et al. 2016). Another indicator is that adenoviruses do not encode any direct inhibitors of caspases or in the case of programmed necrosis; they do not encode a direct inhibitor of caspase-8, which is needed for successful induction of RIPK3, but upon inhibition of caspase-8, cells can efficiently induce programmed necrosis. Interestingly, cells do not undergo apoptosis even when they do not express RIPK3, which could be an indicator for the involvement of another cell death mechanisms other than apoptosis or classic programmed necrosis, but with necrotic morphology. In the case of RIPK3 overexpression, cells undergo RIPK3-dependent cell death that involves the formation of a RIPK3/MLKL containing

death complex that associates with viral proteins and efficiently leads to necrosis. Figure 6-1 summarises the scenarios of death-induced by *dl*922-947 depending on RIPK3 status in ovarian cancer cells.

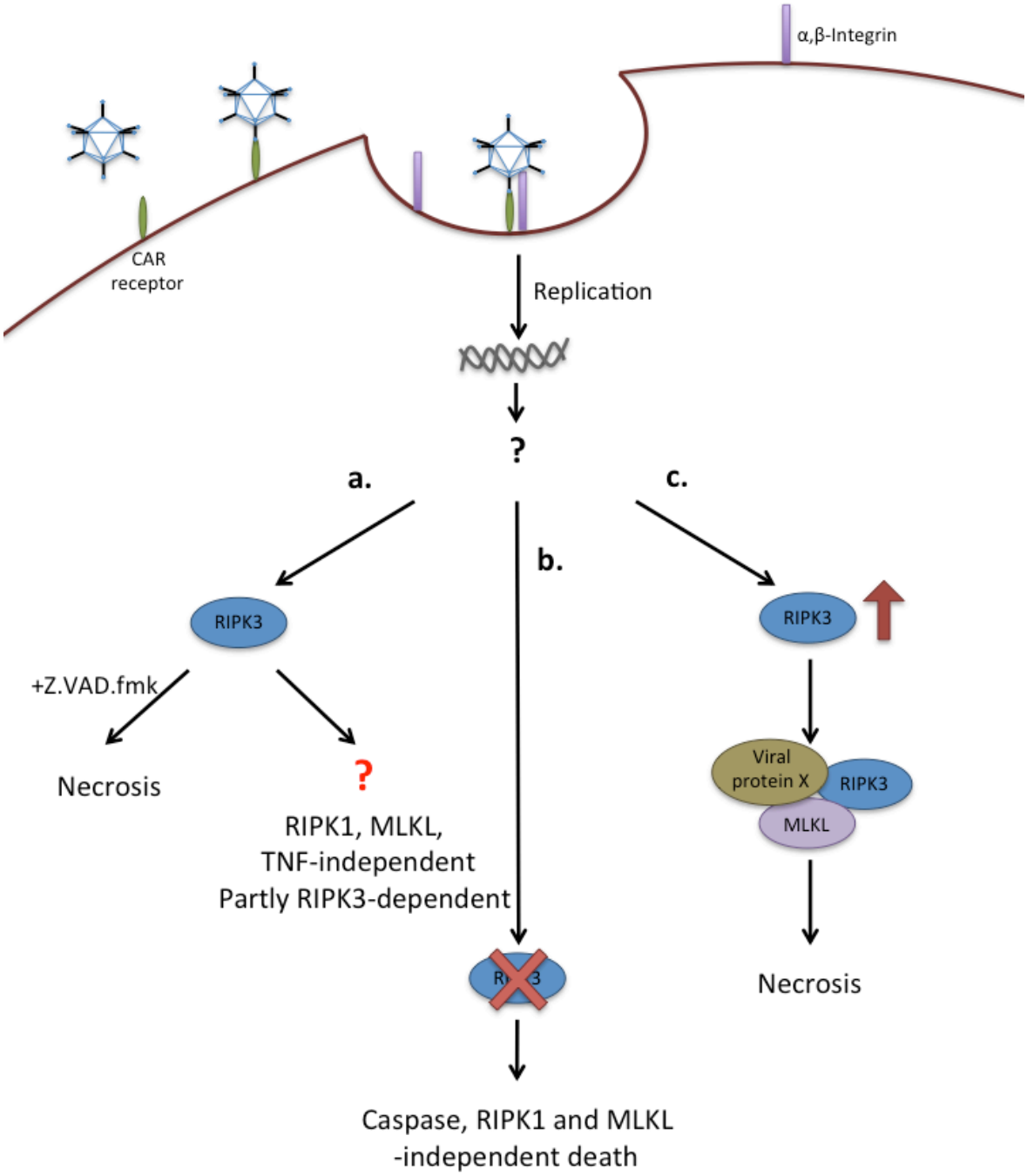

Figure 6-1: Cell death modalities induced by *dl*922-947 depending on RIPK3 status in ovarian cancer cells *in vitro*

A) In the presence of endogenous RIPK3 levels cells undergo RIPK1, MLKL and TNF-α-independent cell death that is partially RIPK3-dependent.

B) When RIPK3 is not expressed cell undergo cell death that resembles necrosis, but is RIPK1, RIPK3 and MLKL-independent but not apoptotic.

C) When RIPK3 is overexpressed cells form a RIPK3/MLKL containing complex with unknown viral proteins that efficiently induces RIPK3-dependent necrosis *in vitro*.

In addition to necrosis induced through TNF/TNFR and the ripoptosome, other pathways of programmed necrosis have been described in the recent years. One of those includes the induction of regulated necrosis through TLR3 and TLR4. Interestingly, it has been shown that necrosis induced by those TLR's can be independent of RIPK1 and especially in the context of adenovirus infection, where TLR's will be activated might be worth of further investigation. Of special interest here is necrosis-induced by TLR3. TLR3 is located at the endosome, where it detects PAMPs like dsRNA, which are produced as part of the viral replication cycle, while those RNA transcripts are common to RNA viruses, it has been suggested that DNA viruses might produce RNA transcripts that can engage TLR3 (Hoebe et al. 2003) as well. Therefore *dl*922-947 could also use an alternative form of programmed necrosis that has not been covered in this thesis.

One of the main questions that remains, however, is if inducing necrosis in cancer cells is of therapeutic value. For a long time, it was thought that apoptosis does not induce inflammation. The reason behind this was that upon apoptosis cells undergo organised morphological changes that include cell shrinkage and the initial maintenance of their plasma integrity before they are being ingested by phagocytes. Necrotic cell death on the other hand has been associated with stimulating a strong host inflammatory response due to cell swelling and the rapid loss of membrane integrity, which leads to the release of damage-associated molecular patterns (DAMPS) and the attraction and infiltration of immune cells leading to immunogenic cell death. However, research has shown that things are more complicated than that and that apoptosis can be indeed of immunogenic nature while cells dying from necrosis can be less immunogenic. Kearney, *et al*. have shown that TNF-induced necrosis suppresses the production of TNF-induced pro-inflammatory cytokines and chemokines through excessive cell death, and showed that necroptosis can actually suppress inflammation. Further, the early and excessive induction of death can hinder viral replication and therefore reduce further infection of tumour cells. Therefore, though necrosis was thought to be favourable due to its fast acting dynamics and its association with the release of DAMP's, the real benefits of inducing necrosis need to be further evaluated. Especially in a viral context this includes the characterisation and identification of DAMP's that are

being released, how necrosis affects the production of inflammatory cytokines and chemokines, the production of viral titres and viral intra-tumoural spread and its importance towards inducing immunogenic cell death.

In the past few years, oncolytic virotherapy has advanced considerably with the development of highly selective strains and the generation of strains that express therapeutic gene products that showed effective anti-tumour properties in pre-clinical models. One of those oncolytic adenoviruses is EnAd, which is currently undergoing several early phase clinical trials, one of which evaluates its use as a treatment for women with platinum-resistant ovarian cancer, making adenovirus-based oncolytic therapy an interesting and promising therapeutic approach for cancer.

References

Abou El Hassan, M. A., I. van der Meulen-Muileman, S. Abbas & F. A. Kruyt (2004) Conditionally replicating adenoviruses kill tumor cells via a basic apoptotic machinery-independent mechanism that resembles necrosis-like programmed cell death. *J Virol,* 78**,** 12243-51.

Ahmed, A. A., D. Etemadmoghadam, J. Temple, A. G. Lynch, M. Riad, R. Sharma, C. Stewart, S. Fereday, C. Caldas, A. Defazio, D. Bowtell & J. D. Brenton (2010) Driver mutations in TP53 are ubiquitous in high grade serous carcinoma of the ovary. *J Pathol,* 221**,** 49-56.

Alonso, M. M., M. Cascallo, C. Gomez-Manzano, H. Jiang, B. N. Bekele, A. Perez-Gimenez, F. F. Lang, Y. Piao, R. Alemany & J. Fueyo (2007) ICOVIR-5 shows E2F1 addiction and potent antiglioma effect in vivo. *Cancer Res,* 67**,** 8255-63.

Alonso, M. M., H. Jiang, T. Yokoyama, J. Xu, N. B. Bekele, F. F. Lang, S. Kondo, C. Gomez-Manzano & J. Fueyo (2008) Delta-24-RGD in combination with RAD001 induces enhanced anti-glioma effect via autophagic cell death. *Mol Ther,* 16**,** 487-93.

Anders, M., C. Christian, M. McMahon, F. McCormick & W. M. Korn (2003) Inhibition of the Raf/MEK/ERK pathway up-regulates expression of the coxsackievirus and adenovirus receptor in cancer cells. *Cancer Res.,* 63**,** 2088-2095.

Anderson, B. D., T. Nakamura, S. J. Russell & K. W. Peng (2004) High CD46 receptor density determines preferential killing of tumor cells by oncolytic measles virus. *Cancer Res,* 64**,** 4919-26.

Andtbacka, R. H., H. L. Kaufman, F. Collichio, T. Amatruda, N. Senzer, J. Chesney, K. A. Delman, L. E. Spitler, I. Puzanov, S. S. Agarwala, M. Milhem, L. Cranmer, B. Curti, K. Lewis, M. Ross, T. Guthrie, G. P. Linette, G. A. Daniels, K. Harrington, M. R. Middleton, W. H. Miller, Jr., J. S. Zager, Y. Ye, B. Yao, A. Li, S. Doleman, A. VanderWalde, J. Gansert & R. S. Coffin (2015) Talimogene Laherparepvec Improves Durable Response Rate in Patients With Advanced Melanoma. *J Clin Oncol,* 33**,** 2780-8.

Anglesio, M. S., S. Kommoss, M. C. Tolcher, B. Clarke, L. Galletta, H. Porter, S. Damaraju, S. Fereday, B. J. Winterhoff, S. E. Kalloger, J. Senz, W. Yang, H. Steed, G. Allo, S. Ferguson, P. Shaw, A. Teoman, J. J. Garcia, J. K. Schoolmeester, J. Bakkum-Gamez, A. V. Tinker, D. D. Bowtell, D. G. Huntsman, C. B. Gilks & J. N. McAlpine (2013) Molecular characterization of mucinous ovarian tumours supports a stratified treatment approach with HER2 targeting in 19% of carcinomas. *J Pathol,* 229**,** 111-20.

Attrill, H. L., S. A. Cumming, J. B. Clements & S. V. Graham (2002) The herpes simplex virus type 1 US11 protein binds the coterminal UL12, UL13, and UL14 RNAs and regulates UL13 expression in vivo. *J Virol,* 76**,** 8090-100.

Avci, N. G., Y. Fan, A. Dragomir, Y. M. Akay, C. Gomez-Manzano, J. Fueyo-Margareto & M. Akay (2015) Delta-24-RGD Induces Cytotoxicity of Glioblastoma Spheroids in Three Dimensional PEG Microwells. *IEEE Trans Nanobioscience,* 14**,** 946-51.

Baehrecke, E. H. (2003) Autophagic programmed cell death in Drosophila. *Cell Death Differ,* 10**,** 940-5.

Baird, S. K., J. L. Aerts, A. Eddaoudi, M. Lockley, N. R. Lemoine & I. A. McNeish (2008) Oncolytic adenoviral mutants induce a novel mode of programmed cell death in ovarian cancer. *Oncogene,* 27**,** 3081-3090.

Banerjee, A. (2013) Bernard Lown: the nonagenarian blogger with a lifelong thirst for combining clinical practice and social responsibility. *Eur Heart J,* 34**,** 1316-7.

Banerjee, S. & S. B. Kaye (2013) New strategies in the treatment of ovarian cancer: current clinical perspectives and future potential. *Clin Cancer Res,* 19**,** 961-8.

Bauerschmitz, G. J., A. Kanerva, M. Wang, I. Herrmann, D. R. Shaw, T. V. Strong, R. Desmond, D. T. Rein, P. Dall, D. T. Curiel & A. Hemminki (2004) Evaluation of a selectively oncolytic adenovirus for local and systemic treatment of cervical cancer. *Int J Cancer,* 111**,** 303-9.

Bauzon, M., F. Jin, P. Kretschmer & T. Hermiston (2009) In vitro analysis of cidofovir and genetically engineered TK expression as potential approaches for the intervention of ColoAd1-based treatment of cancer. *Gene Ther,* 16**,** 1169-74.

Bazan-Peregrino, M., R. C. Carlisle, R. Hernandez-Alcoceba, R. Iggo, K. Homicsko, K. D. Fisher, G. Hallden, V. Mautner, Y. Shen & L. W. Seymour (2008) Comparison of molecular strategies for breast cancer virotherapy using oncolytic adenovirus. *Hum Gene Ther,* 19**,** 873-86.

Bazan-Peregrino, M., R. C. Sainson, R. C. Carlisle, C. Thoma, R. A. Waters, C. Arvanitis, A. L. Harris, R. Hernandez-Alcoceba & L. W. Seymour (2013) Combining virotherapy and angiotherapy for the treatment of breast cancer. *Cancer Gene Ther,* 20**,** 461-8.

Beltrami, E., J. Plescia, J. C. Wilkinson, C. S. Duckett & D. C. Altieri (2004) Acute ablation of survivin uncovers p53-dependent mitotic checkpoint functions and control of mitochondrial apoptosis. *J. Biol. Chem.,* 279**,** 2077-2084.

Benedict, C. A., P. S. Norris, T. I. Prigozy, J. L. Bodmer, J. A. Mahr, C. T. Garnett, F. Martinon, J. Tschopp, L. R. Gooding & C. F. Ware (2001) Three adenovirus E3 proteins cooperate to evade apoptosis by tumor necrosis factor-related apoptosis-inducing ligand receptor-1 and -2. *J. Biol. Chem.,* 276**,** 3270-3278.

BenJilani, K. E., J. P. Gaillard, F. Petit, D. Arnoult, A. S. Roumier, M. Labalette, J. C. Ameisen & J. Estaquier (2002) A suppressive effect of the adenovirus 5 protein E1B 55K on apoptosis induced by IL-3 deprivation and gamma-irradiation. *Biol Cell,* 94**,** 77-89.

Bergelson, J., J. Cunningham, G. Droguett, E. Kurt-Jones, A. Frithivas, J. Hong, M. Horwitz, R. Crowell & R. Finberg (1997) Isolation of a common receptor for coxsackie B and adenoviruses 2 and 5. *Science,* 275**,** 1320-1323.

Berger, S. B., J. Bertin & P. J. Gough (2015a) Drilling into RIP1 biology: what compounds are in your toolkit? *Cell Death Dis,* 6**,** e1889.

Berger, S. B., P. Harris, R. Nagilla, V. Kasparcova, S. Hoffman, B. Swift, L. Dare, M. Schaeffer, C. Capriotti, M. Ouellette, B. W. King, D. Wisnoski, J. Cox, M. Reilly, R. W. Marquis, J. Bertin & P. J. Gough (2015b) Characterization of GSK'963: a structurally distinct, potent and selective inhibitor of RIP1 kinase. *Cell Death Discov,* 1**,** 15009.

Bertrand, M. J. & P. Vandenabeele (2011) The Ripoptosome: death decision in the cytosol. *Mol Cell,* 43**,** 323-5.

Bertrand, R., E. Solary, P. O'Connor, K. W. Kohn & Y. Pommier (1994) Induction of a common pathway of apoptosis by staurosporine. *Exp Cell Res,* 211**,** 314-21.

Bett, A. J., V. Krougliak & F. L. Graham (1995) DNA sequence of the deletion/insertion in early region 3 of Ad5 dl309. *Virus Res,* 39**,** 75-82.

Bhattacharyya, M., J. Francis, A. Eddouadi, N. R. Lemoine & G. Hallden (2011) An oncolytic adenovirus defective in pRb-binding (dl922-947) can efficiently eliminate pancreatic cancer cells and tumors in vivo in combination with 5-FU or gemcitabine. *Cancer Gene Ther,* 18**,** 734-43.

Blander, J. M. (2014) A long-awaited merger of the pathways mediating host defence and programmed cell death. *Nat Rev Immunol,* 14**,** 601-18.

Botta, G., C. Passaro, S. Libertini, A. Abagnale, S. Barbato, A. S. Maione, G. Hallden, F. Beguinot, P. Formisano & G. Portella (2012) Inhibition of autophagy enhances the effects of E1A-defective oncolytic adenovirus dl922-947 against glioma cells in vitro and in vivo. *Hum Gene Ther,* 23**,** 623-34.

Boyer, J., K. Rohleder & G. Ketner (1999) Adenovirus E4 34k and E4 11k inhibit double strand break repair and are physically associated with the cellular DNA-dependent protein kinase. *Virology,* 263**,** 307-12.

Brestovitsky, A., K. Nebenzahl-Sharon, P. Kechker, R. Sharf & T. Kleinberger (2016) The Adenovirus E4orf4 Protein Provides a Novel Mechanism for Inhibition of the DNA Damage Response. *PLoS Pathog,* 12**,** e1005420.

Burger, R. A., M. F. Brady, M. A. Bookman, G. F. Fleming, B. J. Monk, H. Huang, R. S. Mannel, H. D. Homesley, J. Fowler, B. E. Greer, M. Boente, M. J. Birrer, S. X. Liang & G. Gynecologic Oncology (2011) Incorporation of bevacizumab in the primary treatment of ovarian cancer. *N Engl J Med,* 365**,** 2473-2483.

Burke, J. M., D. L. Lamm, M. V. Meng, J. J. Nemunaitis, J. J. Stephenson, J. C. Arseneau, J. Aimi, S. Lerner, A. W. Yeung, T. Kazarian, D. J. Maslyar & J. M. McKiernan (2012) A first in human phase 1 study of CG0070, a GM-CSF expressing oncolytic adenovirus, for the treatment of nonmuscle invasive bladder cancer. *J Urol,* 188**,** 2391-7.

Buys, S. S., E. Partridge, A. Black, C. C. Johnson, L. Lamerato, C. Isaacs, D. J. Reding, R. T. Greenlee, L. A. Yokochi, B. Kessel, E. D. Crawford, T. R. Church, G. L. Andriole, J. L. Weissfeld, M. N. Fouad, D. Chia, B. O'Brien, L. R. Ragard, J. D. Clapp, J. M. Rathmell, T. L. Riley, P. Hartge, P. F. Pinsky, C. S. Zhu, G. Izmirlian, B. S. Kramer, A. B. Miller, J. L. Xu, P. C. Prorok, J. K. Gohagan, C. D. Berg & P. P. Team (2011) Effect of screening on ovarian cancer mortality: the Prostate, Lung, Colorectal and Ovarian (PLCO) Cancer Screening Randomized Controlled Trial. *JAMA,* 305**,** 2295-303.

Cai, Z., S. Jitkaew, J. Zhao, H. C. Chiang, S. Choksi, J. Liu, Y. Ward, L. G. Wu & Z. G. Liu (2014) Plasma membrane translocation of trimerized MLKL protein is required for TNF-induced necroptosis. *Nat Cell Biol,* 16**,** 55-65.

Cancer Genome Atlas Research, N. (2011) Integrated genomic analyses of ovarian carcinoma. *Nature,* 474**,** 609-15.

Carlin, C. R., A. E. Tollefson, H. A. Brady, B. L. Hoffman & W. S. Wold (1989) Epidermal growth factor receptor is down-regulated by a 10,400 MW protein encoded by the E3 region of adenovirus. *Cell,* 57**,** 135-44.

Cascallo, M., M. M. Alonso, J. J. Rojas, A. Perez-Gimenez, J. Fueyo & R. Alemany (2007) Systemic toxicity-efficacy profile of ICOVIR-5, a potent and selective oncolytic adenovirus based on the pRB pathway. *Mol Ther,* 15**,** 1607-15.

Cerullo, V., I. Diaconu, V. Romano, M. Hirvinen, M. Ugolini, S. Escutenaire, S. L. Holm, A. Kipar, A. Kanerva & A. Hemminki (2012) An Oncolytic Adenovirus Enhanced for Toll-like Receptor 9 Stimulation Increases Antitumor Immune Responses and Tumor Clearance. *Mol Ther,* 20**,** 2076-86.

Ch'en, I. L., D. R. Beisner, A. Degterev, C. Lynch, J. Yuan, A. Hoffmann & S. M. Hedrick (2008) Antigen-mediated T cell expansion regulated by parallel pathways of death. *Proc Natl Acad Sci U S A,* 105**,** 17463-8.

Chan, F. K., J. Shisler, J. G. Bixby, M. Felices, L. Zheng, M. Appel, J. Orenstein, B. Moss & M. J. Lenardo (2003) A role for tumor necrosis factor receptor-2 and receptor-interacting protein in programmed necrosis and antiviral responses. *J Biol Chem,* 278**,** 51613-21.

Chen, V. W., B. Ruiz, J. L. Killeen, T. R. Cote, X. C. Wu & C. N. Correa (2003) Pathology and classification of ovarian tumors. *Cancer,* 97**,** 2631-42.

Chen, X., W. Li, J. Ren, D. Huang, W. T. He, Y. Song, C. Yang, W. Li, X. Zheng, P. Chen & J. Han (2014) Translocation of mixed lineage kinase domain-like protein to plasma membrane leads to necrotic cell death. *Cell Res,* 24**,** 105-21.

Cherubini, G., C. Kallin, A. Mozetic, K. Hammaren-Busch, H. Muller, N. R. Lemoine & G. Hallden (2011) The oncolytic adenovirus AdDeltaDelta enhances selective cancer cell killing in combination with DNA-damaging drugs in pancreatic cancer models. *Gene Ther,* 18**,** 1157-65.

Chi, C., H. Zhu, M. Han, Y. Zhuang, X. Wu & T. Xu (2010) Disruption of lysosome function promotes tumor growth and metastasis in Drosophila. *J Biol Chem,* 285**,** 21817-23.

Chin, Y. R. & M. S. Horwitz (2005) Mechanism for removal of tumor necrosis factor receptor 1 from the cell surface by the adenovirus RIDalpha/beta complex. *J Virol,* 79**,** 13606-17.

--- (2006) Adenovirus RID complex enhances degradation of internalized tumour necrosis factor receptor 1 without affecting its rate of endocytosis. *J Gen Virol,* 87**,** 3161-7.

Chiocca, E. A. & S. D. Rabkin (2014) Oncolytic viruses and their application to cancer immunotherapy. *Cancer Immunol Res,* 2**,** 295-300.

Cho, Y. S., S. Challa, D. Moquin, R. Genga, T. D. Ray, M. Guildford & F. K. Chan (2009) Phosphorylation-driven assembly of the RIP1-RIP3 complex regulates programmed necrosis and virus-induced inflammation. *Cell,* 137**,** 1112-1123.

Choi, I. K., H. Shin, E. Oh, J. Y. Yoo, J. K. Hwang, K. Shin, D. C. Yu & C. O. Yun (2015) Potent and long-term antiangiogenic efficacy mediated by FP3-expressing oncolytic adenovirus. *Int J Cancer,* 137**,** 2253-69.

Clem, R. J., M. Fechheimer & L. K. Miller (1991) Prevention of apoptosis by a baculovirus gene during infection of insect cells. *Science,* 254**,** 1388-90.

Coffin, J. 1996. *Retroviridae*: The viruses and their replication. In *Fields' Virology,* eds. B. Fields, D. Knipe, P. Howley, R. Chanock, J. Melnick, T. Monatu, B. Roizman & S. Straus, 1767-1836. Philadelphia: Lippincott-Raven.

Coleman, M. P., D. Forman, H. Bryant, J. Butler, B. Rachet, C. Maringe, U. Nur, E. Tracey, M. Coory, J. Hatcher, C. E. McGahan, D. Turner, L. Marrett, M. L. Gjerstorff, T. B. Johannesen, J. Adolfsson, M. Lambe, G. Lawrence, D. Meechan, E. J. Morris, R. Middleton, J. Steward, M. A. Richards & I. M. W. Group (2011) Cancer survival in Australia, Canada, Denmark, Norway, Sweden, and the UK, 1995-2007 (the International Cancer Benchmarking Partnership): an analysis of population-based cancer registry data. *Lancet,* 377**,** 127-138.

Connell, C. M., A. Shibata, L. A. Tookman, K. M. Archibald, M. B. Flak, K. J. Pirlo, M. Lockley, S. P. Wheatley & I. A. McNeish (2011) Genomic DNA damage and ATR-Chk1 signaling determine oncolytic adenoviral efficacy in human ovarian cancer cells. *J. Clin. Invest.,* 121**,** 1283-1297.

Cripe, T. P., M. C. Ngo, J. I. Geller, C. U. Louis, M. A. Currier, J. M. Racadio, A. J. Towbin, C. M. Rooney, A. Pelusio, A. Moon, T. H. Hwang, J. M. Burke, J. C. Bell, D. H. Kirn & C. J. Breitbach (2015) Phase 1 study of intratumoral Pexa-Vec (JX-594), an oncolytic and immunotherapeutic vaccinia virus, in pediatric cancer patients. *Mol Ther,* 23**,** 602-8.

Cuconati, A., K. Degenhardt, R. Sundararajan, A. Anschel & E. White (2002) Bak and Bax function to limit adenovirus replication through apoptosis induction. *J. Virol.,* 76**,** 4547-4558.

Cuesta, R., Q. Xi & R. J. Schneider (2004) Structural basis for competitive inhibition of eIF4G-Mnk1 interaction by the adenovirus 100-kilodalton protein. *J. Virol.,* 78**,** 7707-7716.

Cuevas, Y., R. Hernandez-Alcoceba, J. Aragones, S. Naranjo-Suarez, M. C. Castellanos, M. A. Esteban, S. Martin-Puig, M. O. Landazuri & L. del Peso (2003) Specific oncolytic effect of a new hypoxia-inducible factor-dependent replicative adenovirus on von Hippel-Lindau-defective renal cell carcinomas. *Cancer Res,* 63**,** 6877-84.

Davison, E., I. Kirby, J. Whitehouse, I. Hart, J. F. Marshall & G. Santis (2001) Adenovirus type 5 uptake by lung adenocarcinoma cells in culture correlates with Ad5 fibre binding is mediated by alpha(v)beta1 integrin and can be modulated by changes in beta1 integrin function. *J Gene Med,* 3**,** 550-9.

de Haro, C., R. Mendez & J. Santoyo (1996) The eIF-2alpha kinases and the control of protein synthesis. *FASEB J,* 10**,** 1378-87.

Debbas, M. & E. White (1993) Wild-type p53 mediates apoptosis by E1A, which is inhibited by E1B. *Genes Dev,* 7**,** 546-54.

Degenhardt, K., R. Mathew, B. Beaudoin, K. Bray, D. Anderson, G. Chen, C. Mukherjee, Y. Shi, C. Gelinas, Y. Fan, D. A. Nelson, S. Jin & E. White (2006) Autophagy promotes tumor cell survival and restricts necrosis, inflammation, and tumorigenesis. *Cancer Cell,* 10**,** 51-64.

Degterev, A., J. Hitomi, M. Germscheid, I. L. Ch'en, O. Korkina, X. Teng, D. Abbott, G. D. Cuny, C. Yuan, G. Wagner, S. M. Hedrick, S. A. Gerber, A. Lugovskoy & J. Yuan (2008) Identification of RIP1 kinase as a specific cellular target of necrostatins. *Nat. Chem. Biol.,* 4**,** 313-321.

Degterev, A., J. L. Maki & J. Yuan (2013) Activity and specificity of necrostatin-1, small-molecule inhibitor of RIP1 kinase. *Cell Death Differ,* 20**,** 366.

Dembinski, J. L., E. L. Spaeth, J. Fueyo, C. Gomez-Manzano, M. Studeny, M. Andreeff & F. C. Marini (2010) Reduction of nontarget infection and systemic toxicity by targeted delivery of conditionally replicating viruses transported in mesenchymal stem cells. *Cancer Gene Ther,* 17**,** 289-97.

Dock, G. (1904) The influence of complicating diseases upon leukemia. *The American Journal of the Medical Sciences***,** 563-592.

Doerfler, W. 1996. Adenoviruses. In *Medical Microbiology,* ed. S. Baron. Galveston (TX).

Dondelinger, Y., W. Declercq, S. Montessuit, R. Roelandt, A. Goncalves, I. Bruggeman, P. Hulpiau, K. Weber, C. A. Sehon, R. W. Marquis, J. Bertin, P. J. Gough, S. Savvides, J. C. Martinou, M. J. Bertrand & P. Vandenabeele (2014) MLKL compromises plasma membrane integrity by binding to phosphatidylinositol phosphates. *Cell Rep,* 7**,** 971-81.

Dondelinger, Y., P. Hulpiau, Y. Saeys, M. J. Bertrand & P. Vandenabeele (2016) An evolutionary perspective on the necroptotic pathway. *Trends Cell Biol,* 26**,** 721-32.

Dorig, R. E., A. Marcil, A. Chopra & C. D. Richardson (1993) The human CD46 molecule is a receptor for measles virus (Edmonston strain). *Cell,* 75**,** 295-305.

Dranoff, G., E. Jaffee, A. Lazenby, P. Golumbek, H. Levitsky, K. Brose, V. Jackson, H. Hamada, D. Pardoll & R. C. Mulligan (1993) Vaccination with irradiated tumor cells engineered to secrete murine granulocyte-macrophage colony-stimulating factor stimulates potent, specific, and long-lasting anti-tumor immunity. *Proc Natl Acad Sci U S A,* 90**,** 3539-43.

Ekert, P. G., J. Silke & D. L. Vaux (1999) Caspase inhibitors. *Cell Death Differ,* 6**,** 1081-6.

Elsing, A. & H. G. Burgert (1998) The adenovirus E3/10.4K-14.5K proteins down-modulate the apoptosis receptor Fas/Apo-1 by inducing its internalization. *Proc Natl Acad Sci U S A,* 95**,** 10072-7.

Falcieri, E., A. M. Martelli, R. Bareggi, A. Cataldi & L. Cocco (1993) The protein kinase inhibitor staurosporine induces morphological changes typical of apoptosis in MOLT-4 cells without concomitant DNA fragmentation. *Biochem Biophys Res Commun,* 193**,** 19-25.

Fan, T. J., L. H. Han, R. S. Cong & J. Liang (2005) Caspase family proteases and apoptosis. *Acta Biochim Biophys Sin (Shanghai),* 37**,** 719-27.

Feoktistova, M., P. Geserick, B. Kellert, D. P. Dimitrova, C. Langlais, M. Hupe, K. Cain, M. Macfarlane, G. Hacker & M. Leverkus (2011) cIAPs Block Ripoptosome Formation, a RIP1/Caspase-8 Containing Intracellular Cell Death Complex Differentially Regulated by cFLIP Isoforms. *Mol Cell,* 43**,** 449-463.

Fessler, S. P., Y. R. Chin & M. S. Horwitz (2004) Inhibition of tumor necrosis factor (TNF) signal transduction by the adenovirus group C RID complex involves downregulation of surface levels of TNF receptor 1. *J Virol,* 78**,** 13113-21.

Flak, M. B., C. M. Connell, C. Chelala, K. Archibald, M. A. Salako, K. J. Pirlo, M. Lockley, S. P. Wheatley, F. R. Balkwill & I. A. McNeish (2010) p21 promotes oncolytic adenoviral activity in ovarian cancer and is a potential biomarker. *Mol. Cancer,* 9**,** 175.

Fong, P. C., D. S. Boss, T. A. Yap, A. Tutt, P. Wu, M. Mergui-Roelvink, P. Mortimer, H. Swaisland, A. Lau, M. J. O'Connor, A. Ashworth, J. Carmichael, S. B. Kaye, J. H. Schellens & J. S. de Bono (2009) Inhibition of poly(ADP-ribose) polymerase in tumors from BRCA mutation carriers. *N Engl J Med,* 361**,** 123-34.

Freytag, S. O., K. N. Barton & Y. Zhang (2013) Efficacy of oncolytic adenovirus expressing suicide genes and interleukin-12 in preclinical model of prostate cancer. *Gene Ther,* 20**,** 1131-9.

Fuchs, Y. & H. Steller (2015) Live to die another way: modes of programmed cell death and the signals emanating from dying cells. *Nat Rev Mol Cell Biol,* 16**,** 329-44.

Fueyo, J., R. Alemany, C. Gomez-Manzano, G. N. Fuller, A. Khan, C. A. Conrad, T.-J. Liu, H. Jiang, M. G. Lemoine, K. Suzuki, R. Sawaya, D. T. Curiel, W. K. A. Yung & F. F. Lang (2003) Preclinical characterization of the antiglioma activity of a tropism-enhanced adenovirus targeted to the retinoblastoma pathway. *J. Natl. Cancer Inst.,* 95**,** 652-660.

Gagliardini, V., P. A. Fernandez, R. K. Lee, H. C. Drexler, R. J. Rotello, M. C. Fishman & J. Yuan (1994) Prevention of vertebrate neuronal death by the crmA gene. *Science,* 263**,** 826-8.

Galanis, E., S. N. Markovic, V. J. Suman, G. J. Nuovo, R. G. Vile, T. J. Kottke, W. K. Nevala, M. A. Thompson, J. E. Lewis, K. M. Rumilla, V. Roulstone, K. Harrington, G. P. Linette, W. J. Maples, M. Coffey, J. Zwiebel & K. Kendra (2012) Phase II trial of intravenous administration of Reolysin((R)) (Reovirus Serotype-3-dearing Strain) in patients with metastatic melanoma. *Mol Ther,* 20**,** 1998-2003.

Galanis, E., S. H. Okuno, A. G. Nascimento, B. D. Lewis, R. A. Lee, A. M. Oliveira, J. A. Sloan, P. Atherton, J. H. Edmonson, C. Erlichman, B. Randlev, Q. Wang, S. Freeman & J. Rubin (2005) Phase I-II trial of ONYX-015 in combination with MAP chemotherapy in patients with advanced sarcomas. *Gene Ther,* 12**,** 437-45.

Ganly, I., D. Kirn, S. G. Eckhardt, G. I. Rodriguez, D. S. Soutar, R. Otto, A. G. Robertson, O. Park, M. L. Gulley, C. Heise, D. D. VonHoff & S. B. Kaye (2001) A phase I study of Onyx-015, an ELB-attenuated adenovirus, administered intratumorally to patients with recurrent head and neck cancer (vol 6, pg 798, 2000). *Clinical Cancer Research,* 7**,** 754-754.

Garber, K. (2006) China approves world's first oncolytic virus therapy for cancer treatment. *J. Natl. Cancer Inst.,* 98**,** 298-300.

Garcia-Calvo, M., E. Peterson, B. Leiting, R. Ruel, D. Nicholson & N. Thornberry (1998) Inhibition of human caspases by peptide-based and macromolecular inhibitors. *J. Biol Chem.,* 273**,** 32608-32613.

Garcia-Castro, J., R. Alemany, M. Cascallo, J. Martinez-Quintanilla, M. Arriero Mdel, A. Lassaletta, L. Madero & M. Ramirez (2010) Treatment of metastatic neuroblastoma with systemic oncolytic virotherapy delivered by autologous mesenchymal stem cells: an exploratory study. *Cancer Gene Ther,* 17**,** 476-83.

Goldsmith, K., W. Chen, D. C. Johnson & R. L. Hendricks (1998) Infected cell protein (ICP)47 enhances herpes simplex virus neurovirulence by blocking the CD8+ T cell response. *J Exp Med,* 187**,** 341-8.

Gollamudi, R., M. H. Ghalib, K. K. Desai, I. Chaudhary, B. Wong, M. Einstein, M. Coffey, G. M. Gill, K. Mettinger, J. M. Mariadason, S. Mani & S. Goel (2010) Intravenous administration of Reolysin, a live replication competent RNA virus is safe in patients with advanced solid tumors. *Invest New Drugs,* 28**,** 641-9.

Green, N. K., A. Hale, R. Cawood, S. Illingworth, C. Herbert, T. Hermiston, V. Subr, K. Ulbrich, N. van Rooijen, L. W. Seymour & K. D. Fisher (2012) Tropism ablation and stealthing of oncolytic adenovirus enhances systemic delivery to tumors and improves virotherapy of cancer. *Nanomedicine (Lond),* 7**,** 1683-95.

Greig, S. L. (2016) Talimogene Laherparepvec: First Global Approval. *Drugs,* 76**,** 147-54.

Gunther, C., E. Martini, N. Wittkopf, K. Amann, B. Weigmann, H. Neumann, M. J. Waldner, S. M. Hedrick, S. Tenzer, M. F. Neurath & C. Becker (2011) Caspase-8 regulates TNF-alpha-induced epithelial necroptosis and terminal ileitis. *Nature,* 477**,** 335-9.

Guo, H., S. Omoto, P. A. Harris, J. N. Finger, J. Bertin, P. J. Gough, W. J. Kaiser & E. S. Mocarski (2015) Herpes simplex virus suppresses necroptosis in human cells. *Cell Host Microbe,* 17**,** 243-51.

Hamid, O., M. L. Varterasian, S. Wadler, J. R. Hecht, A. Benson, III, E. Galanis, M. Uprichard, C. Omer, P. Bycott, R. C. Hackman & A. F. Shields (2003) Phase II trial of intravenous CI-1042 in patients with metastatic colorectal cancer. *J. Clin. Oncol.,* 21**,** 1498-1504.

Hamm, C. A., J. W. Stevens, H. Xie, E. F. Vanin, J. A. Morcuende, H. Abdulkawy, E. A. Seftor, S. T. Sredni, J. M. Bischof, D. Wang, S. Malchenko, F. Bonaldo Mde, T. L. Casavant, M. J. Hendrix & M. B. Soares (2010) Microenvironment alters epigenetic and gene expression profiles in Swarm rat chondrosarcoma tumors. *BMC Cancer,* 10**,** 471.

Han, J., P. Sabbatini, D. Perez, L. Rao, D. Modha & E. White (1996a) The E1B 19K protein blocks apoptosis by interacting with and inhibiting the p53-inducible and death-promoting Bax protein. *Genes Dev,* 10**,** 461-77.

Han, J., P. Sabbatini & E. White (1996b) Induction of apoptosis by human Nbk/Bik, a BH3-containing protein that interacts with E1B 19K. *Mol Cell Biol,* 16**,** 5857-64.

Han, J., C. Q. Zhong & D. W. Zhang (2011a) Programmed necrosis: backup to and competitor with apoptosis in the immune system. *Nat Immunol,* 12**,** 1143-9.

Han, Q., S. Duan, G. Zhang, Z. Li, N. Li, Q. Zhu, Y. Lv, J. Chen & Z. Liu (2011b) Associations between cytotoxic T lymphocyte-associated antigen-4 polymorphisms and serum tumor necrosis factor-alpha and interferon-gamma levels in patients with chronic hepatitis B virus infection. *Inflamm Res,* 60**,** 1071-8.

Han, W., L. Li, S. Qiu, Q. Lu, Q. Pan, Y. Gu, J. Luo & X. Hu (2007) Shikonin circumvents cancer drug resistance by induction of a necroptotic death. *Mol Cancer Ther,* 6**,** 1641-9.

Hanahan, D. & R. A. Weinberg (2000) The hallmarks of cancer. *Cell,* 100**,** 57-70.

--- (2011) Hallmarks of cancer: the next generation. *Cell,* 144**,** 646-674.

He, S., Y. Liang, F. Shao & X. Wang (2011) Toll-like receptors activate programmed necrosis in macrophages through a receptor-interacting kinase-3-mediated pathway. *Proc Natl Acad Sci U S A,* 108**,** 20054-9.

He, S., L. Wang, L. Miao, T. Wang, F. Du, L. Zhao & X. Wang (2009) Receptor interacting protein kinase-3 determines cellular necrotic response to TNF-alpha. *Cell,* 137**,** 1100-11.

Heise, C., T. Hermiston, L. Johnson, G. Brooks, A. Sampson-Johannes, A. Williams, L. Hawkins & D. Kirn (2000) An adenovirus E1A mutant that demonstrates potent and selective systemic anti-tumoral efficacy. *Nature Med.,* 6**,** 1134-1139.

Hemminki, O., S. Parviainen, J. Juhila, R. Turkki, N. Linder, J. Lundin, M. Kankainen, A. Ristimaki, A. Koski, I. Liikanen, M. Oksanen, D. M. Nettelbeck, K. Kairemo, K. Partanen, T. Joensuu, A. Kanerva & A. Hemminki (2015) Immunological data from cancer patients treated with Ad5/3-E2F-Delta24-GMCSF suggests utility for tumor immunotherapy. *Oncotarget,* 6**,** 4467-81.

Hildebrand, J. M., M. C. Tanzer, I. S. Lucet, S. N. Young, S. K. Spall, P. Sharma, C. Pierotti, J. M. Garnier, R. C. Dobson, A. I. Webb, A. Tripaydonis, J. J. Babon, M. D. Mulcair, M. J. Scanlon, W. S. Alexander, A. F. Wilks, P. E. Czabotar, G. Lessene, J. M. Murphy & J. Silke (2014) Activation of the pseudokinase MLKL unleashes the four-helix bundle domain to induce membrane localization and necroptotic cell death. *Proc Natl Acad Sci U S A,* 111**,** 15072-7.

Hirvinen, M., M. Rajecki, M. Kapanen, S. Parviainen, N. Rouvinen-Lagerstrom, I. Diaconu, P. Nokisalmi, M. Tenhunen, A. Hemminki & V. Cerullo (2015) Immunological effects of a tumor necrosis factor alpha-armed oncolytic adenovirus. *Hum Gene Ther,* 26**,** 134-44.

Hoebe, K., X. Du, P. Georgel, E. Janssen, K. Tabeta, S. O. Kim, J. Goode, P. Lin, N. Mann, S. Mudd, K. Crozat, S. Sovath, J. Han & B. Beutler (2003) Identification of Lps2 as a key transducer of MyD88-independent TIR signalling. *Nature,* 424**,** 743-8.

Holler, N., T. Kataoka, J. L. Bodmer, P. Romero, J. Romero, D. Deperthes, J. Engel, J. Tschopp & P. Schneider (2000a) Development of improved soluble inhibitors of FasL and CD40L based on oligomerized receptors. *J Immunol Methods,* 237**,** 159-73.

Holler, N., R. Zaru, O. Micheau, M. Thome, A. Attinger, S. Valitutti, J. L. Bodmer, P. Schneider, B. Seed & J. Tschopp (2000b) Fas triggers an alternative, caspase-8-independent cell death pathway using the kinase RIP as effector molecule. *Nat Immunol,* 1**,** 489-95.

Horwitz, M. 1996. Adenoviruses. In *Fields' Virology,* eds. B. Fields, D. Knipe, P. Howley, R. Chanock, J. Melnick, T. Monatu, B. Roizman & S. Straus, 2149-2171. Philadelphia: Lippincott-Raven.

Huang, C., Y. Luo, J. Zhao, F. Yang, H. Zhao, W. Fan & P. Ge (2013) Shikonin kills glioma cells through necroptosis mediated by RIP-1. *PLoS One,* 8**,** e66326.

Huang, Z., S. Q. Wu, Y. Liang, X. Zhou, W. Chen, L. Li, J. Wu, Q. Zhuang, C. Chen, J. Li, C. Q. Zhong, W. Xia, R. Zhou, C. Zheng & J. Han (2015) RIP1/RIP3 binding to HSV-1 ICP6 initiates necroptosis to restrict virus propagation in mice. *Cell Host Microbe,* 17**,** 229-42.

Hulin-Curtis, S. L., H. Uusi-Kerttula, R. Jones, L. Hanna, J. D. Chester & A. L. Parker (2016) Evaluation of CD46 re-targeted adenoviral vectors for clinical ovarian cancer intraperitoneal therapy. *Cancer Gene Ther,* 23**,** 229-34.

Igaki, T., H. Kanda, Y. Yamamoto-Goto, H. Kanuka, E. Kuranaga, T. Aigaki & M. Miura (2002) Eiger, a TNF superfamily ligand that triggers the Drosophila JNK pathway. *EMBO J,* 21**,** 3009-18.

Ingemarsdotter, C. K., L. A. Tookman, A. Browne, K. Pirlo, R. Cutts, C. Chelela, K. F. Khurrum, E. Y. Leung, S. Dowson, L. Webber, I. Khan, D. Ennis, N. Syed, T. R. Crook, J. D. Brenton, M. Lockley & I. A. McNeish (2015) Paclitaxel resistance increases oncolytic adenovirus efficacy via upregulated CAR expression and dysfunctional cell cycle control. *Mol Oncol,* 9**,** 791-805.

Ito, H., H. Aoki, F. Kuhnel, Y. Kondo, S. Kubicka, T. Wirth, E. Iwado, A. Iwamaru, K. Fujiwara, K. R. Hess, F. F. Lang, R. Sawaya & S. Kondo (2006) Autophagic cell death of malignant glioma cells induced by a conditionally replicating adenovirus. *J. Natl. Cancer Inst.,* 98**,** 625-636.

Jacobs, I. J., U. Menon, A. Ryan, A. Gentry-Maharaj, M. Burnell, J. K. Kalsi, N. N. Amso, S. Apostolidou, E. Benjamin, D. Cruickshank, D. N. Crump, S. K. Davies, A. Dawnay, S. Dobbs, G. Fletcher, J. Ford, K. Godfrey, R. Gunu, M. Habib, R. Hallett, J. Herod, H. Jenkins, C. Karpinskyj, S. Leeson, S. J. Lewis, W. R. Liston, A. Lopes, T. Mould, J. Murdoch, D. Oram, D. J. Rabideau, K. Reynolds, I. Scott, M. W. Seif, A. Sharma, N. Singh, J. Taylor, F. Warburton, M. Widschwendter, K. Williamson, R. Woolas, L. Fallowfield, A. J. McGuire, S. Campbell, M. Parmar & S. J. Skates (2016) Ovarian cancer screening and mortality in the UK Collaborative Trial of Ovarian Cancer Screening (UKCTOCS): a randomised controlled trial. *Lancet,* 387**,** 945-56.

Jayson, G. C., E. C. Kohn, H. C. Kitchener & J. A. Ledermann (2014) Ovarian cancer. *Lancet,* 384**,** 1376-88.

Jiang, H., K. Clise-Dwyer, K. E. Ruisaard, X. Fan, W. Tian, J. Gumin, M. L. Lamfers, A. Kleijn, F. F. Lang, W. K. Yung, L. M. Vence, C. Gomez-Manzano & J. Fueyo (2014) Delta-24-RGD oncolytic adenovirus elicits anti-glioma immunity in an immunocompetent mouse model. *PLoS One,* 9**,** e97407.

Jiang, H., C. Gomez-Manzano, H. Aoki, M. M. Alonso, S. Kondo, F. McCormick, J. Xu, Y. Kondo, B. N. Bekele, H. Colman, F. F. Lang & J. Fueyo (2007) Examination of the therapeutic potential of Delta-24-RGD in brain tumor stem cells: role of autophagic cell death. *J. Natl. Cancer Inst.,* 99**,** 1410-1414.

Kaiser, W. J., H. Sridharan, C. Huang, P. Mandal, J. W. Upton, P. J. Gough, C. A. Sehon, R. W. Marquis, J. Bertin & E. S. Mocarski (2013a) Toll-like receptor 3-mediated necrosis via TRIF, RIP3, and MLKL. *J Biol Chem,* 288**,** 31268-79.

Kaiser, W. J., J. W. Upton & E. S. Mocarski (2013b) Viral modulation of programmed necrosis. *Curr Opin Virol,* 3**,** 296-306.

Kalai, M., G. Van Loo, T. Vanden Berghe, A. Meeus, W. Burm, X. Saelens & P. Vandenabeele (2002) Tipping the balance between necrosis and apoptosis in human and murine cells treated with interferon and dsRNA. *Cell Death Differ,* 9**,** 981-94.

Kaliberov, S. A., L. N. Kaliberova, H. Yan, V. Kapoor & D. E. Hallahan (2016) Retargeted adenoviruses for radiation-guided gene delivery. *Cancer Gene Ther*.

Kang, T. B., S. H. Yang, B. Toth, A. Kovalenko & D. Wallach (2013) Caspase-8 blocks kinase RIPK3-mediated activation of the NLRP3 inflammasome. *Immunity,* 38**,** 27-40.

Katze, M. G. (1995) Regulation of the interferon-induced PKR: can viruses cope? *Trends Microbiol,* 3**,** 75-8.

Kaye, S. B., J. Lubinski, U. Matulonis, J. E. Ang, C. Gourley, B. Y. Karlan, A. Amnon, K. M. Bell-McGuinn, L. M. Chen, M. Friedlander, T. Safra, I. Vergote, M. Wickens, E. S. Lowe, J. Carmichael & B. Kaufman (2012) Phase II, open-label, randomized, multicenter study comparing the efficacy and safety of olaparib, a poly (ADP-ribose) polymerase inhibitor, and pegylated liposomal doxorubicin in patients with BRCA1 or BRCA2 mutations and recurrent ovarian cancer. *J Clin Oncol,* 30**,** 372-9.

Kearney, C. J., S. P. Cullen, G. A. Tynan, C. M. Henry, D. Clancy, E. C. Lavelle & S. J. Martin (2015) Necroptosis suppresses inflammation via termination of TNF- or LPS-induced cytokine and chemokine production. *Cell Death Differ,* 22**,** 1313-27.

Khare, R., M. L. Hillestad, Z. Xu, A. P. Byrnes & M. A. Barry (2013) Circulating antibodies and macrophages as modulators of adenovirus pharmacology. *J Virol,* 87**,** 3678-86.

Khuri, F., J. Nemunatis, I. Ganly, J. Arseneau, I. Tannock, L. Romerl, M. Gore, J. Ironside, R. MacDougall, C. Heise, B. Randlev, A. Gillenwater, P. Bruso, S. Kaye, W. Hong & D. Kirn (2000) A controlled trial of intratumoral ONYX-015, a selectively-replicating adenovirus, in combination with cisplatin and 5-fluorouracil in patients with recurrent head and neck cancer. *Nature Med.,* 6**,** 879-885.

Kicielinski, K. P., E. A. Chiocca, J. S. Yu, G. M. Gill, M. Coffey & J. M. Markert (2014) Phase 1 clinical trial of intratumoral reovirus infusion for the treatment of recurrent malignant gliomas in adults. *Mol Ther,* 22**,** 1056-62.

Koebel, C. M., W. Vermi, J. B. Swann, N. Zerafa, S. J. Rodig, L. J. Old, M. J. Smyth & R. D. Schreiber (2007) Adaptive immunity maintains occult cancer in an equilibrium state. *Nature,* 450**,** 903-7.

Koh, J. Y., M. B. Wie, B. J. Gwag, S. L. Sensi, L. M. Canzoniero, J. Demaro, C. Csernansky & D. W. Choi (1995) Staurosporine-induced neuronal apoptosis. *Exp Neurol,* 135**,** 153-9.

Kolb, E. A., V. Sampson, D. Stabley, A. Walter, K. Sol-Church, T. Cripe, P. Hingorani, C. H. Ahern, B. J. Weigel, J. Zwiebel & S. M. Blaney (2015) A phase I trial and viral clearance study of reovirus (Reolysin) in children with relapsed or refractory extra-cranial solid tumors: a Children's Oncology Group Phase I Consortium report. *Pediatr Blood Cancer,* 62**,** 751-8.

Koo, G. B., M. J. Morgan, D. G. Lee, W. J. Kim, J. H. Yoon, J. S. Koo, S. I. Kim, S. J. Kim, M. K. Son, S. S. Hong, J. M. Levy, D. A. Pollyea, C. T. Jordan, P. Yan, D. Frankhouser, D. Nicolet, K. Maharry, G. Marcucci, K. S. Choi, H. Cho, A. Thorburn & Y. S. Kim (2015) Methylation-dependent loss of RIP3 expression in cancer represses programmed necrosis in response to chemotherapeutics. *Cell Res,* 25**,** 707-25.

Koski, A., L. Kangasniemi, S. Escutenaire, S. Pesonen, V. Cerullo, I. Diaconu, P. Nokisalmi, M. Raki, M. Rajecki, K. Guse, T. Ranki, M. Oksanen, S. L. Holm, E. Haavisto, A. Karioja-Kallio, L. Laasonen, K. Partanen, M. Ugolini, A. Helminen, E. Karli, P. Hannuksela, T. Joensuu, A. Kanerva & A. Hemminki (2010) Treatment of cancer patients with a serotype 5/3 chimeric oncolytic adenovirus expressing GMCSF. *Mol. Ther.,* 18**,** 1874-1884.

Kovalenko, A., J. C. Kim, T. B. Kang, A. Rajput, K. Bogdanov, O. Dittrich-Breiholz, M. Kracht, O. Brenner & D. Wallach (2009) Caspase-8 deficiency in epidermal keratinocytes triggers an inflammatory skin disease. *J Exp Med,* 206**,** 2161-77.

Kroemer, G., L. Galluzzi, P. Vandenabeele, J. Abrams, E. S. Alnemri, E. H. Baehrecke, M. V. Blagosklonny, W. S. El-Deiry, P. Golstein, D. R. Green, M. Hengartner, R. A. Knight, S. Kumar, S. A. Lipton, W. Malorni, G. Nunez, M. E. Peter, J. Tschopp, J. Yuan, M. Piacentini, B. Zhivotovsky & G. Melino (2009) Classification of cell death: recommendations of the Nomenclature Committee on Cell Death 2009. *Cell Death Differ,* 16**,** 3-11.

Kroemer, G. & M. Jaattela (2005) Lysosomes and autophagy in cell death control. *Nat Rev Cancer,* 5**,** 886-97.

Kuhn, I., P. Harden, M. Bauzon, C. Chartier, J. Nye, S. Thorne, T. Reid, S. Ni, A. Lieber, K. Fisher, L. Seymour, G. M. Rubanyi, R. N. Harkins & T. W. Hermiston (2008) Directed evolution generates a novel oncolytic virus for the treatment of colon cancer. *PLoS ONE,* 3**,** e2409.

Laster, S., J. Wood & L. Gooding (1988) Tumor necrosis factor can induce both apoptotic and necrotic forms of cell lysis. *J. Immunol.,* 141**,** 2629-2635.

Laurie, S. A., J. C. Bell, H. L. Atkins, J. Roach, M. K. Bamat, J. D. O'Neil, M. S. Roberts, W. S. Groene & R. M. Lorence (2006) A phase 1 clinical study of intravenous administration of PV701, an oncolytic virus, using two-step desensitization. *Clin Cancer Res,* 12**,** 2555-62.

Lawlor, K. E., N. Khan, A. Mildenhall, M. Gerlic, B. A. Croker, A. A. D'Cruz, C. Hall, S. Kaur Spall, H. Anderton, S. L. Masters, M. Rashidi, I. P. Wicks, W. S. Alexander, Y. Mitsuuchi, C. A. Benetatos, S. M. Condon, W. W. Wong, J. Silke, D. L. Vaux & J. E. Vince (2015) RIPK3 promotes cell death and NLRP3 inflammasome activation in the absence of MLKL. *Nat Commun,* 6**,** 6282.

Lee, S. Y., H. R. Park, J. Rhee, Y. M. Park & S. H. Kim (2013) Therapeutic effect of oncolytic adenovirus expressing relaxin in radioresistant oral squamous cell carcinoma. *Oncol Res,* 20**,** 419-25.

Li, J., T. McQuade, A. B. Siemer, J. Napetschnig, K. Moriwaki, Y. S. Hsiao, E. Damko, D. Moquin, T. Walz, A. McDermott, F. K. Chan & H. Wu (2012) The RIP1/RIP3 Necrosome Forms a Functional Amyloid Signaling Complex Required for Programmed Necrosis. *Cell,* 150**,** 339-50.

Lichtenstein, D. L., K. Doronin, K. Toth, M. Kuppuswamy, W. S. Wold & A. E. Tollefson (2004) Adenovirus E3-6.7K protein is required in conjunction with the E3-RID protein complex for the internalization and degradation of TRAIL receptor 2. *J Virol,* 78**,** 12297-307.

Lichtenstein, D. L., P. Krajcsi, D. J. Esteban, A. E. Tollefson & W. S. Wold (2002) Adenovirus RIDbeta subunit contains a tyrosine residue that is critical for RID-mediated receptor internalization and inhibition of Fas- and TRAIL-induced apoptosis. *J Virol,* 76**,** 11329-42.

Lieber, A., C. Y. He, L. Meuse, D. Schowalter, I. Kirillova, B. Winther & M. A. Kay (1997) The role of Kupffer cell activation and viral gene expression in early liver toxicity after infusion of recombinant adenovirus vectors. *J. Virol.,* 71**,** 8798-8807.

Lisby, M., J. H. Barlow, R. C. Burgess & R. Rothstein (2004) Choreography of the DNA damage response: spatiotemporal relationships among checkpoint and repair proteins. *Cell,* 118**,** 699-713.

Liu, B. L., M. Robinson, Z. Q. Han, R. H. Branston, C. English, P. Reay, Y. McGrath, S. K. Thomas, M. Thornton, P. Bullock, C. A. Love & R. S. Coffin (2003) ICP34.5 deleted herpes simplex virus with enhanced oncolytic, immune stimulating, and anti-tumour properties. *Gene Ther.,* 10**,** 292-303.

Lockley, M., M. Fernandez, Y. Wang, N. F. Li, S. E. Conroy, N. R. Lemoine & I. A. McNeish (2006) Activity of the adenoviral E1A deletion mutant dl922-947 in ovarian cancer: comparison with adenovirus wild-type, bioluminescence monitoring and intraperitoneal delivery in icodextrin. *Cancer Res.,* 66**,** 989-998.

Lomonosova, E., T. Subramanian & G. Chinnadurai (2002) Requirement of BAX for efficient adenovirus-induced apoptosis. *J. Virol.,* 76**,** 11283-11290.

Lomonosova, E., T. Subramanian & G. Chinnadurai (2005) Mitochondrial localization of p53 during adenovirus infection and regulation of its activity by E1B-19K. *Oncogene,* 24**,** 6796-808.

Lowe, S. W. & H. E. Ruley (1993) Stabilization of the p53 tumor suppressor is induced by adenovirus 5 E1A and accompanies apoptosis. *Genes Dev,* 7**,** 535-45.

Lucas, T., K. Benihoud, F. Vigant, C. Q. Schmidt, A. Wortmann, M. G. Bachem, T. Simmet & S. Kochanek (2015) Hexon modification to improve the activity of oncolytic adenovirus vectors against neoplastic and stromal cells in pancreatic cancer. *PLoS One,* 10**,** e0117254.

Luo, K., E. Ehrlich, Z. Xiao, W. Zhang, G. Ketner & X. F. Yu (2007) Adenovirus E4orf6 assembles with Cullin5-ElonginB-ElonginC E3 ubiquitin ligase through an HIV/SIV Vif-like BC-box to regulate p53. *FASEB J,* 21**,** 1742-50.

Mach, N., S. Gillessen, S. B. Wilson, C. Sheehan, M. Mihm & G. Dranoff (2000) Differences in dendritic cells stimulated in vivo by tumors engineered to secrete granulocyte-macrophage colony-stimulating factor or Flt3-ligand. *Cancer Res,* 60**,** 3239-46.

Maheswaran, S., C. Englert, S. B. Lee, R. M. Ezzel, J. Settleman & D. A. Haber (1998) E1B 55K sequesters WT1 along with p53 within a cytoplasmic body in adenovirus-transformed kidney cells. *Oncogene,* 16**,** 2041-50.

Makower, D., A. Rozenblit, H. Kaufman, M. Edelman, M. E. Lane, J. Zwiebel, H. Haynes & S. Wadler (2003) Phase II clinical trial of intralesional administration of the oncolytic adenovirus ONYX-015 in patients with hepatobiliary tumors with correlative p53 studies. *Clin Cancer Res,* 9**,** 693-702.

Manetti, R., P. Parronchi, M. G. Giudizi, M. P. Piccinni, E. Maggi, G. Trinchieri & S. Romagnani (1993) Natural killer cell stimulatory factor (interleukin 12 [IL-12]) induces T helper type 1 (Th1)-specific immune responses and inhibits the development of IL-4-producing Th cells. *J Exp Med,* 177**,** 1199-204.

Marcellus, R. C., J. G. Teodoro, T. Wu, D. E. Brough, G. Ketner, G. C. Shore & P. E. Branton (1996) Adenovirus type 5 early region 4 is responsible for E1A-induced p53-independent apoptosis. *J Virol,* 70**,** 6207-15.

Medzhitov, R. (2009) Approaching the asymptote: 20 years later. *Immunity,* 30**,** 766-75.

Mittereder, N., K. March & B. Trapnell (1996) Evaluation of the concentration and bioactivity of adenovirus vectors for gene therapy. *J. Virol.,* 70**,** 7498-7509.

Morgan, M. J. & Y. S. Kim (2015) The serine threonine kinase RIP3: lost and found. *BMB Rep,* 48**,** 303-12.

Morris, D. G., X. Feng, L. M. DiFrancesco, K. Fonseca, P. A. Forsyth, A. H. Paterson, M. C. Coffey & B. Thompson (2013) REO-001: A phase I trial of percutaneous intralesional administration of reovirus type 3 dearing (Reolysin(R)) in patients with advanced solid tumors. *Invest New Drugs,* 31**,** 696-706.

Mosmann, T. (1983) Rapid colorimetric assay for cellular growth and survival: application to proliferation and cytotoxicity assays. *J Immunol Methods,* 65**,** 55-63.

Murphy, J. M., P. E. Czabotar, J. M. Hildebrand, I. S. Lucet, J. G. Zhang, S. Alvarez-Diaz, R. Lewis, N. Lalaoui, D. Metcalf, A. I. Webb, S. N. Young, L. N. Varghese, G. M. Tannahill, E. C. Hatchell, I. J. Majewski, T. Okamoto, R. C. Dobson, D. J. Hilton, J. J. Babon, N. A. Nicola, A. Strasser, J. Silke & W. S. Alexander (2013) The pseudokinase MLKL mediates necroptosis via a molecular switch mechanism. *Immunity,* 39**,** 443-53.

Mymryk, J. S., K. Shire & S. T. Bayley (1994) Induction of apoptosis by adenovirus type 5 E1A in rat cells requires a proliferation block. *Oncogene,* 9**,** 1187-93.

Nemunaitis, J., I. Ganly, F. Khuri, J. Arseneau, J. Kuhn, T. McCarty, S. Landers, P. Maples, L. Romel, B. Randlev, T. Reid, S. Kaye & D. Kirn (2000) Selective replication and oncolysis in p53 mutant tumors with ONYX-015, an E1B-55kD gene-deleted adenovirus, in patients with advanced head and neck cancer: a phase II trial. *Cancer Res,* 60**,** 6359-6366.

Nemunaitis, J., F. Khuri, I. Ganly, J. Arseneau, M. Posner, E. Vokes, J. Kuhn, T. McCarty, S. Landers, A. Blackburn, L. Romel, B. Randlev, S. Kaye & D. Kirn (2001) Phase II trial of intratumoral administration of ONYX-015, a replication-selective adenovirus, in patients with refractory head and neck cancer. *Journal of Clinical Oncology,* 19**,** 289-298.

Nogusa, S., R. J. Thapa, C. P. Dillon, S. Liedmann, T. H. Oguin, 3rd, J. P. Ingram, D. A. Rodriguez, R. Kosoff, S. Sharma, O. Sturm, K. Verbist, P. J. Gough, J. Bertin, B. M. Hartmann, S. C. Sealfon, W. J. Kaiser, E. S. Mocarski, C. B. Lopez, P. G. Thomas, A. Oberst, D. R. Green & S. Balachandran (2016) RIPK3 Activates Parallel Pathways of MLKL-Driven Necroptosis and FADD-Mediated Apoptosis to Protect against Influenza A Virus. *Cell Host Microbe,* 20**,** 13-24.

Nokisalmi, P., S. Pesonen, S. Escutenaire, M. Sarkioja, M. Raki, V. Cerullo, L. Laasonen, R. Alemany, J. Rojas, M. Cascallo, K. Guse, M. Rajecki, L. Kangasniemi, E. Haavisto, A. Karioja-Kallio, P. Hannuksela, M. Oksanen, A. Kanerva, T. Joensuu, L. Ahtiainen & A. Hemminki (2010) Oncolytic adenovirus ICOVIR-7 in patients with advanced and refractory solid tumors. *Clin Cancer Res,* 16**,** 3035-43.

Norman, K. L., K. Hirasawa, A. D. Yang, M. A. Shields & P. W. Lee (2004) Reovirus oncolysis: the Ras/RalGEF/p38 pathway dictates host cell permissiveness to reovirus infection. *Proc Natl Acad Sci U S A,* 101**,** 11099-104.

O'Shea, C., L. Johnson, B. Bagus, S. Choi, C. Nicholas, A. Shen, L. Boyle, K. Pandey, C. Soria, J. Kunich, Y. Shen, G. Habets, D. Ginzinger & F. McCormick (2004) Late viral RNA export, rather than p53 inactivation, determines ONYX-015 tumor selectivity. *Cancer Cell,* 6**,** 611-623.

Okegawa, T., Y. Li, R. C. Pong, J. M. Bergelson, J. Zhou & J. T. Hsieh (2000) The dual impact of coxsackie and adenovirus receptor expression on human prostate cancer gene therapy. *Cancer Res,* 60**,** 5031-6.

Olson, T. A., D. Mohanraj, L. F. Carson & S. Ramakrishnan (1994) Vascular permeability factor gene expression in normal and neoplastic human ovaries. *Cancer Res,* 54**,** 276-80.

Pack, G. T. (1950) Note on the experimental use of rabies vaccine for melanomatosis. *AMA Arch Derm Syphilol,* 62**,** 694-5.

Parato, K. A., C. J. Breitbach, F. Le Boeuf, J. Wang, C. Storbeck, C. Ilkow, J. S. Diallo, T. Falls, J. Burns, V. Garcia, F. Kanji, L. Evgin, K. Hu, F. Paradis, S. Knowles, T. H. Hwang, B. C. Vanderhyden, R. Auer, D. H. Kirn & J. C. Bell (2012) The oncolytic poxvirus JX-594 selectively replicates in and destroys cancer cells driven by genetic pathways commonly activated in cancers. *Mol Ther,* 20**,** 749-58.

Passaro, C., F. Borriello, V. Vastolo, S. Di Somma, E. Scamardella, V. Gigantino, R. Franco, G. Marone & G. Portella (2016) The oncolytic virus dl922-947 reduces IL-8/CXCL8 and MCP-1/CCL2 expression and impairs angiogenesis and macrophage infiltration in anaplastic thyroid carcinoma. *Oncotarget,* 7**,** 1500-15.

Pelner, L., G. A. Fowler & H. C. Nauts (1958) Effects of concurrent infections and their toxins on the course of leukemia. *Acta Med Scand Suppl,* 338**,** 1-47.

Perez, D. & E. White (1998) E1B 19K inhibits Fas-mediated apoptosis through FADD-dependent sequestration of FLICE. *J Cell Biol,* 141**,** 1255-66.

--- (2000) TNF-alpha signals apoptosis through a bid-dependent conformational change in Bax that is inhibited by E1B 19K. *Mol Cell,* 6**,** 53-63.

Perren, T. J., A. M. Swart, J. Pfisterer, J. A. Ledermann, E. Pujade-Lauraine, G. Kristensen, M. S. Carey, P. Beale, A. Cervantes, C. Kurzeder, A. du Bois, J. Sehouli, R. Kimmig, A. Stahle, F. Collinson, S. Essapen, C. Gourley, A. Lortholary, F. Selle, M. R. Mirza, A. Leminen, M. Plante, D. Stark, W. Qian, M. K. Parmar, A. M. Oza & I. Investigators (2011) A phase 3 trial of bevacizumab in ovarian cancer. *N Engl J Med,* 365**,** 2484-2496.

Pesonen, S., I. Diaconu, L. Kangasniemi, T. Ranki, A. Kanerva, S. K. Pesonen, U. Gerdemann, A. M. Leen, K. Kairemo, M. Oksanen, E. Haavisto, S. L. Holm, A. Karioja-Kallio, S. Kauppinen, K. P. Partanen, L. Laasonen, T. Joensuu, T. Alanko, V. Cerullo & A. Hemminki (2012) Oncolytic immunotherapy of advanced solid tumors with a CD40L-expressing replicating adenovirus: assessment of safety and immunologic responses in patients. *Cancer Res,* 72**,** 1621-31.

Post, D. E., N. S. Devi, Z. Li, D. J. Brat, B. Kaur, A. Nicholson, J. J. Olson, Z. Zhang & E. G. Van Meir (2004) Cancer therapy with a replicating oncolytic adenovirus targeting the hypoxic microenvironment of tumors. *Clin Cancer Res,* 10**,** 8603-12.

Premalata, C. S., K. Umadevi, K. Shobha, M. Anurekha & L. Krishnamoorthy (2016) Expression of VEGF-A in Epithelial Ovarian Cancer: Correlation with Morphologic Types, Grade and Clinical Stage. *Gulf J Oncolog,* 1**,** 49-54.

Prestwich, R. J., E. J. Ilett, F. Errington, R. M. Diaz, L. P. Steele, T. Kottke, J. Thompson, F. Galivo, K. J. Harrington, H. S. Pandha, P. J. Selby, R. G. Vile & A. A. Melcher (2009) Immune-mediated antitumor activity of reovirus is required for therapy and is independent of direct viral oncolysis and replication. *Clin Cancer Res,* 15**,** 4374-81.

Qiao, J., M. Dey, A. L. Chang, J. W. Kim, J. Miska, A. Ling, M. N. D, Y. Han, L. Zhang & M. S. Lesniak (2015) Intratumoral oncolytic adenoviral treatment modulates the glioma microenvironment and facilitates systemic tumor-antigen-specific T cell therapy. *Oncoimmunology,* 4**,** e1022302.

Quarato, G., C. S. Guy, C. R. Grace, F. Llambi, A. Nourse, D. A. Rodriguez, R. Wakefield, S. Frase, T. Moldoveanu & D. R. Green (2016) Sequential Engagement of Distinct MLKL Phosphatidylinositol-Binding Sites Executes Necroptosis. *Mol Cell,* 61**,** 589-601.

Ramirez, M., J. Garcia-Castro & R. Alemany (2010) Oncolytic virotherapy for neuroblastoma. *Discov Med,* 10**,** 387-93.

Ranheim, T. S., J. Shisler, T. M. Horton, L. J. Wold, L. R. Gooding & W. S. Wold (1993) Characterization of mutants within the gene for the adenovirus E3 14.7-kilodalton protein which prevents cytolysis by tumor necrosis factor. *J Virol,* 67**,** 2159-67.

Ranki, T., S. Pesonen, A. Hemminki, K. Partanen, K. Kairemo, T. Alanko, J. Lundin, N. Linder, R. Turkki, A. Ristimaki, E. Jager, J. Karbach, C. Wahle, M. Kankainen, C. Backman, M. von Euler, E. Haavisto, T. Hakonen, R. Heiskanen, M. Jaderberg, J. Juhila, P. Priha, L. Suoranta, L. Vassilev, A. Vuolanto & T. Joensuu (2016) Phase I study with ONCOS-102 for the treatment of solid tumors - an evaluation of clinical response and exploratory analyses of immune markers. *J Immunother Cancer,* 4**,** 17.

Rao, L., M. Debbas, P. Sabbatini, D. Hockenbery, S. Korsmeyer & E. White (1992) The adenovirus E1A proteins induce apoptosis, which is inhibited by the E1B 19-kDa and Bcl-2 proteins. *Proc. Natl. Acad. Sci. USA,* 89**,** 7742-7746.

Raper, S. E., N. Chirmule, F. S. Lee, N. A. Wivel, A. Bagg, G. P. Gao, J. M. Wilson & M. L. Batshaw (2003) Fatal systemic inflammatory response syndrome in a ornithine transcarbamylase deficient patient following adenoviral gene transfer. *Mol. Genet. Metab.,* 80**,** 148-158.

Reid, T., E. Galanis, J. Abbruzzese, D. Sze, J. Andrews, L. Romel, M. Hatfield, J. Rubin & D. Kirn (2001) Intra-arterial administration of a replication-selective adenovirus (dl1520) in patients with colorectal carcinoma metastatic to the liver: a phase I trial. *Gene Ther.,* 8**,** 1618-1626.

Reid, T., E. Galanis, J. Abbruzzese, D. Sze, L. M. Wein, J. Andrews, B. Randlev, C. Heise, M. Uprichard, M. Hatfield, L. Rome, J. Rubin & D. Kirn (2002) Hepatic arterial infusion of a replication-selective oncolytic adenovirus (dl1520): Phase II viral, immunologic, and clinical endpoints. *Cancer Res.,* 62**,** 6070-6079.

Reynolds, J. E., J. Li, R. W. Craig & A. Eastman (1996) BCL-2 and MCL-1 expression in Chinese hamster ovary cells inhibits intracellular acidification and apoptosis induced by staurosporine. *Exp Cell Res,* 225**,** 430-6.

Rodriguez, D. A., R. Weinlich, S. Brown, C. Guy, P. Fitzgerald, C. P. Dillon, A. Oberst, G. Quarato, J. Low, J. G. Cripps, T. Chen & D. R. Green (2016) Characterization of RIPK3-mediated phosphorylation of the activation loop of MLKL during necroptosis. *Cell Death Differ,* 23**,** 76-88.

Rowe, W. P., R. J. Huebner, L. K. Gilmore, R. H. Parrott & T. G. Ward (1953) Isolation of a cytopathogenic agent from human adenoids undergoing spontaneous degeneration in tissue culture. *Proc Soc Exp Biol Med,* 84**,** 570-3.

Sade-Feldman, M., J. Kanterman, E. Ish-Shalom, M. Elnekave, E. Horwitz & M. Baniyash (2013) Tumor necrosis factor-alpha blocks differentiation and enhances suppressive activity of immature myeloid cells during chronic inflammation. *Immunity,* 38**,** 541-54.

Sakurai, F., K. Akitomo, K. Kawabata, T. Hayakawa & H. Mizuguchi (2007) Downregulation of human CD46 by adenovirus serotype 35 vectors. *Gene Ther,* 14**,** 912-9.

Salako, M. A., H. Kulbe, C. K. Ingemarsdotter, K. J. Pirlo, S. L. Williams, M. Lockley, F. R. Balkwill & I. A. McNeish (2011) Inhibition of the Inflammatory Cytokine TNF-alpha Increases Adenovirus Activity in Ovarian Cancer via Modulation of cIAP1/2 Expression. *Mol. Ther.,* 19**,** 490-499.

Satoh, M., H. Wang, S. Ishidoya, H. Abe, T. Moriya, H. Hamada & Y. Arai (2007) Oncolytic virotherapy for prostate cancer by E1A, E1B mutant adenovirus. *Urology,* 70**,** 1243-8.

Sborov, D. W., G. J. Nuovo, A. Stiff, T. Mace, G. B. Lesinski, D. M. Benson, Jr., Y. A. Efebera, A. E. Rosko, F. Pichiorri, M. R. Grever & C. C. Hofmeister (2014) A phase I trial of single-agent reolysin in patients with relapsed multiple myeloma. *Clin Cancer Res,* 20**,** 5946-55.

Scaffidi, P., T. Misteli & M. E. Bianchi (2002) Release of chromatin protein HMGB1 by necrotic cells triggers inflammation. *Nature,* 418**,** 191-195.

Schneider-Brachert, W., V. Tchikov, O. Merkel, M. Jakob, C. Hallas, M. L. Kruse, P. Groitl, A. Lehn, E. Hildt, J. Held-Feindt, T. Dobner, D. Kabelitz, M. Kronke & S. Schutze (2006) Inhibition of TNF receptor 1 internalization by adenovirus 14.7K as a novel immune escape mechanism. *J. Clin. Invest.,* 116**,** 2901-2913.

Schreiner, S., P. Wimmer, H. Sirma, R. D. Everett, P. Blanchette, P. Groitl & T. Dobner (2010) Proteasome-dependent degradation of Daxx by the viral E1B-55K protein in human adenovirus-infected cells. *J Virol,* 84**,** 7029-38.

Schwartz, R. A., S. S. Lakdawala, H. D. Eshleman, M. R. Russell, C. T. Carson & M. D. Weitzman (2008) Distinct requirements of adenovirus E1b55K protein for degradation of cellular substrates. *J Virol,* 82**,** 9043-55.

Shah, G. A. & C. C. O'Shea (2015) Viral and Cellular Genomes Activate Distinct DNA Damage Responses. *Cell,* 162**,** 987-1002.

Shashkova, E. V., S. M. May & M. A. Barry (2009) Characterization of human adenovirus serotypes 5, 6, 11, and 35 as anticancer agents. *Virology,* 394**,** 311-20.

Shenk, T. 2001. Adenoviridae: the viruses and their replication. In *Fields Virology,* eds. D. M. Knipe & P. M. Howley, 2265-2300. Philadelphia: Lippincott, Williams and Wilkins.

Sherr, C. J. & F. McCormick (2002) The RB and p53 pathways in cancer. *Cancer Cell,* 2**,** 103-112.

Shimizu, S., T. Kanaseki, N. Mizushima, T. Mizuta, S. Arakawa-Kobayashi, C. B. Thompson & Y. Tsujimoto (2004) Role of Bcl-2 family proteins in a non-apoptotic programmed cell death dependent on autophagy genes. *Nat Cell Biol,* 6**,** 1221-8.

Shisler, J., C. Yang, B. Walter, C. F. Ware & L. R. Gooding (1997) The adenovirus E3-10.4K/14.5K complex mediates loss of cell surface Fas (CD95) and resistance to Fas-induced apoptosis. *J Virol,* 71**,** 8299-306.

Shmulevitz, M., P. Marcato & P. W. Lee (2005) Unshackling the links between reovirus oncolysis, Ras signaling, translational control and cancer. *Oncogene,* 24**,** 7720-8.

Sibbald, B. (2001) Death but one unintended consequence of gene-therapy trial. *CMAJ,* 164**,** 1612.

Silke, J., J. A. Rickard & M. Gerlic (2015) The diverse role of RIP kinases in necroptosis and inflammation. *Nat Immunol,* 16**,** 689-97.

Singer, G., R. Oldt, 3rd, Y. Cohen, B. G. Wang, D. Sidransky, R. J. Kurman & M. Shih Ie (2003) Mutations in BRAF and KRAS characterize the development of low-grade ovarian serous carcinoma. *J Natl Cancer Inst,* 95**,** 484-6.

Stark, G. R., I. M. Kerr, B. R. Williams, R. H. Silverman & R. D. Schreiber (1998) How cells respond to interferons. *Annu Rev Biochem,* 67**,** 227-64.

Steller, H. (2008) Regulation of apoptosis in Drosophila. *Cell Death Differ,* 15**,** 1132-8.

Stolarek, R., C. Gomez-Manzano, H. Jiang, G. Suttle, M. G. Lemoine & J. Fueyo (2004) Robust infectivity and replication of Delta-24 adenovirus induce cell death in human medulloblastoma. *Cancer Gene Ther,* 11**,** 713-20.

Stone, D., A. Furthmann, V. Sandig & A. Lieber (2003) The complete nucleotide sequence, genome organization, and origin of human adenovirus type 11. *Virology,* 309**,** 152-65.

Strong, J. E., M. C. Coffey, D. Tang, P. Sabinin & P. W. Lee (1998) The molecular basis of viral oncolysis: usurpation of the Ras signaling pathway by reovirus. *EMBO J,* 17**,** 3351-62.

Subramanian, T., S. Vijayalingam, M. Kuppuswamy & G. Chinnadurai (2015) Interaction of cellular proteins with BCL-xL targeted to cytoplasmic inclusion bodies in adenovirus infected cells. *Virology,* 483**,** 21-31.

Sun, L., H. Wang, Z. Wang, S. He, S. Chen, D. Liao, L. Wang, J. Yan, W. Liu, X. Lei & X. Wang (2012) Mixed lineage kinase domain-like protein mediates necrosis signaling downstream of RIP3 kinase. *Cell,* 148**,** 213-227.

Sun, X., J. Yin, M. A. Starovasnik, W. J. Fairbrother & V. M. Dixit (2002) Identification of a novel homotypic interaction motif required for the phosphorylation of receptor-interacting protein (RIP) by RIP3. *J Biol Chem,* 277**,** 9505-11.

Sundararajan, R., A. Cuconati, D. Nelson & E. White (2001) Tumor Necrosis Factor-alpha induces Bax-Bak interaction and apoptosis, which is inhibited by adenovirus E1B 19K. *J. Biol. Chem.,* 276**,** 45120-45127.

Sundararajan, R. & E. White (2001) E1B 19K blocks Bax oligomerization and tumor necrosis factor alpha-mediated apoptosis. *J Virol,* 75**,** 7506-16.

Taipale, K., I. Liikanen, J. Juhila, R. Turkki, S. Tahtinen, M. Kankainen, L. Vassilev, A. Ristimaki, A. Koski, A. Kanerva, I. Diaconu, V. Cerullo, M. Vaha-Koskela, M. Oksanen, N. Linder, T. Joensuu, J. Lundin & A. Hemminki (2016) Chronic Activation of Innate Immunity Correlates With Poor Prognosis in Cancer Patients Treated With Oncolytic Adenovirus. *Mol Ther,* 24**,** 175-83.

Tait, S. W. & D. R. Green (2010) Mitochondria and cell death: outer membrane permeabilization and beyond. *Nat Rev Mol Cell Biol,* 11**,** 621-32.

Takahashi, N., L. Duprez, S. Grootjans, A. Cauwels, W. Nerinckx, J. B. DuHadaway, V. Goossens, R. Roelandt, F. Van Hauwermeiren, C. Libert, W. Declercq, N. Callewaert, G. C. Prendergast, A. Degterev, J. Yuan & P. Vandenabeele (2012) Necrostatin-1 analogues: critical issues on the specificity, activity and in vivo use in experimental disease models. *Cell Death Dis,* 3**,** e437.

Takeda, M., M. Kobayashi, T. Osaki, I. Shirato & H. Endou (1997) Staurosporine-induced apoptosis of immortalized mouse proximal tubule cells is modulated by bcl-2 expression level. *Biochem Mol Biol Int,* 42**,** 649-56.

Tarakanova, V. L. & W. S. Wold (2010) Adenovirus E1A and E1B-19K proteins protect human hepatoma cells from transforming growth factor beta1-induced apoptosis. *Virus Res,* 147**,** 67-76.

TCGA (2011) Integrated genomic analyses of ovarian carcinoma. *Nature,* 474**,** 609-615.

Tenev, T., K. Bianchi, M. Darding, M. Broemer, C. Langlais, F. Wallberg, A. Zachariou, J. Lopez, M. Macfarlane, K. Cain & P. Meier (2011) The Ripoptosome, a Signaling Platform that Assembles in Response to Genotoxic Stress and Loss of IAPs. *Mol Cell,* 43**,** 432-448.

Thaci, B., I. V. Ulasov, A. U. Ahmed, S. D. Ferguson, Y. Han & M. S. Lesniak (2013) Anti-angiogenic therapy increases intratumoral adenovirus distribution by inducing collagen degradation. *Gene Ther,* 20**,** 318-27.

Thapa, R. J., S. Nogusa, P. Chen, J. L. Maki, A. Lerro, M. Andrake, G. F. Rall, A. Degterev & S. Balachandran (2013) Interferon-induced RIP1/RIP3-mediated necrosis requires PKR and is licensed by FADD and caspases. *Proc Natl Acad Sci U S A,* 110**,** E3109-18.

Thoma, C., V. Bachy, P. Seaton, N. K. Green, D. R. Greaves, L. Klavinskis, L. W. Seymour & J. Morrison (2013) Adenovirus serotype 11 causes less long-term intraperitoneal inflammation than serotype 5: implications for ovarian cancer therapy. *Virology,* 447**,** 74-83.

Thorsteinsson, L., G. M. O'Dowd, P. M. Harrington & P. M. Johnson (1998) The complement regulatory proteins CD46 and CD59, but not CD55, are highly expressed by glandular epithelium of human breast and colorectal tumour tissues. *APMIS,* 106**,** 869-78.

Toda, M., R. L. Martuza & S. D. Rabkin (2000) Tumor growth inhibition by intratumoral inoculation of defective herpes simplex virus vectors expressing granulocyte-macrophage colony-stimulating factor. *Mol Ther,* 2**,** 324-9.

Tollefson, A. E., T. W. Hermiston, D. L. Lichtenstein, C. F. Colle, R. A. Tripp, T. Dimitrov, K. Toth, C. E. Wells, P. C. Doherty & W. S. Wold (1998) Forced degradation of Fas inhibits apoptosis in adenovirus-infected cells. *Nature,* 392**,** 726-30.

Tollefson, A. E., A. Scaria, T. W. Hermiston, J. S. Ryerse, L. J. Wold & W. S. Wold (1996) The adenovirus death protein (E3-11.6K) is required at very late stages of infection for efficient cell lysis and release of adenovirus from infected cells. *J. Virol.,* 70**,** 2296-2306.

Tollefson, A. E., A. R. Stewart, S. P. Yei, S. K. Saha & W. S. Wold (1991) The 10,400- and 14,500-dalton proteins encoded by region E3 of adenovirus form a complex and function together to down-regulate the epidermal growth factor receptor. *J Virol,* 65**,** 3095-105.

Tollefson, A. E., K. Toth, K. Doronin, M. Kuppuswamy, O. A. Doronina, D. L. Lichtenstein, T. W. Hermiston, C. A. Smith & W. S. Wold (2001) Inhibition of TRAIL-induced apoptosis and forced internalization of TRAIL receptor 1 by adenovirus proteins. *J Virol,* 75**,** 8875-87.

Tomasella, A., A. Blangy & C. Brancolini (2014) A receptor-interacting protein 1 (RIP1)-independent necrotic death under the control of protein phosphatase PP2A that involves the reorganization of actin cytoskeleton and the action of cofilin-1. *J Biol Chem,* 289**,** 25699-710.

Tong, A. W., N. Senzer, V. Cerullo, N. S. Templeton, A. Hemminki & J. Nemunaitis (2012) Oncolytic viruses for induction of anti-tumor immunity. *Curr Pharm Biotechnol,* 13**,** 1750-60.

Tookman, L. A., A. K. Browne, C. M. Connell, G. Bridge, C. K. Ingemarsdotter, S. Dowson, A. Shibata, M. Lockley, S. A. Martin & I. A. McNeish (2016) RAD51 and BRCA2 Enhance Oncolytic Adenovirus Type 5 Activity in Ovarian Cancer. *Mol Cancer Res,* 14**,** 44-55.

Tuve, S., H. Wang, C. Ware, Y. Liu, A. Gaggar, K. Bernt, D. Shayakhmetov, Z. Li, R. Strauss, D. Stone & A. Lieber (2006) A new group B adenovirus receptor is expressed at high levels on human stem and tumor cells. *J Virol,* 80**,** 12109-20.

Upton, J. W., W. J. Kaiser & E. S. Mocarski (2010) Virus inhibition of RIP3-dependent necrosis. *Cell Host Microbe,* 7**,** 302-13.

--- (2012) DAI/ZBP1/DLM-1 complexes with RIP3 to mediate virus-induced programmed necrosis that is targeted by murine cytomegalovirus vIRA. *Cell Host Microbe,* 11**,** 290-297.

Vandenabeele, P., W. Declercq, F. Van Herreweghe & T. Vanden Berghe (2010a) The role of the kinases RIP1 and RIP3 in TNF-induced necrosis. *Sci Signal,* 3**,** re4.

Vandenabeele, P., L. Galluzzi, T. Vanden Berghe & G. Kroemer (2010b) Molecular mechanisms of necroptosis: an ordered cellular explosion. *Nat Rev Mol Cell Biol,* 11**,** 700-714.

Vandenabeele, P., S. Grootjans, N. Callewaert & N. Takahashi (2013) Necrostatin-1 blocks both RIPK1 and IDO: consequences for the study of cell death in experimental disease models. *Cell Death Differ,* 20**,** 185-7.

Vanlangenakker, N., T. Vanden Berghe & P. Vandenabeele (2012) Many stimuli pull the necrotic trigger, an overview. *Cell Death Differ,* 19**,** 75-86.

Varga A, P.-P. S., Ott PA, Mehnert JM, Berton-Rigaud D, Johnson EA (2015) Antitumour activity and safety of pembrolizumab in patients (pts) with PD-L1 positive advanced ovarian cancer: Interim results from a phase Ib study. *AscoMeetAbstr,* 33**,** (Suppl 15):5510.

Vasey, P. A., G. C. Jayson, A. Gordon, H. Gabra, R. Coleman, R. Atkinson, D. Parkin, J. Paul, A. Hay, S. B. Kaye & On behalf of the Scottish Gynaecological Cancer Trials Group (2004) Phase III randomized trial of docetaxel-carboplatin versus paclitaxel-carboplatin as first-line chemotherapy for ovarian carcinoma. *J. Natl. Cancer Inst.,* 96**,** 1682-1691.

Vassilev, L., T. Ranki, T. Joensuu, E. Jager, J. Karbach, C. Wahle, K. Partanen, K. Kairemo, T. Alanko, R. Turkki, N. Linder, J. Lundin, A. Ristimaki, M. Kankainen, A. Hemminki, C. Backman, K. Dienel, M. von Euler, E. Haavisto, T. Hakonen, J. Juhila, M. Jaderberg, P. Priha, A. Vuolanto & S. Pesonen (2015) Repeated intratumoral administration of ONCOS-102 leads to systemic antitumor CD8+ T-cell response and robust cellular and transcriptional immune activation at tumor site in a patient with ovarian cancer. *Oncoimmunology,* 4**,** e1017702.

Vaughan, S., J. I. Coward, R. C. Bast, Jr., A. Berchuck, J. S. Berek, J. D. Brenton, G. Coukos, C. C. Crum, R. Drapkin, D. Etemadmoghadam, M. Friedlander, H. Gabra, S. B. Kaye, C. J. Lord, E. Lengyel, D. A. Levine, I. A. McNeish, U. Menon, G. B. Mills, K. P. Nephew, A. M. Oza, A. K. Sood, E. A. Stronach, H. Walczak, D. D. Bowtell & F. R. Balkwill (2011) Rethinking ovarian cancer: recommendations for improving outcomes. *Nat. Rev. Cancer,* 11**,** 719-725.

Vera, B., N. Martinez-Velez, E. Xipell, A. Acanda de la Rocha, A. Patino-Garcia, J. Saez-Castresana, M. Gonzalez-Huarriz, M. Cascallo, R. Alemany & M. M. Alonso (2016) Characterization of the Antiglioma Effect of the Oncolytic Adenovirus VCN-01. *PLoS One,* 11**,** e0147211.

Vercammen, D., R. Beyaert, G. Denecker, V. Goossens, G. Van Loo, W. Declercq, J. Grooten, W. Fiers & P. Vandenabeele (1998) Inhibition of caspases increases the sensitivity of L929 cells to necrosis mediated by tumor necrosis factor. *J Exp Med,* 187**,** 1477-85.

Wallach, D., T. B. Kang, S. H. Yang & A. Kovalenko (2014) The in vivo significance of necroptosis: lessons from exploration of caspase-8 function. *Cytokine Growth Factor Rev,* 25**,** 157-65.

Walsh, D. (2010) Manipulation of the host translation initiation complex eIF4F by DNA viruses. *Biochem Soc Trans,* 38**,** 1511-6.

Wang, H., M. Satoh, H. Abe, M. Sunamura, T. Moriya, S. Ishidoya, S. Saito, H. Hamada & Y. Arai (2006) Oncolytic viral therapy by bladder instillation using an E1A, E1B double-restricted adenovirus in an orthotopic bladder cancer model. *Urology,* 68**,** 674-81.

Wang, H., L. Sun, L. Su, J. Rizo, L. Liu, L. F. Wang, F. S. Wang & X. Wang (2014a) Mixed lineage kinase domain-like protein MLKL causes necrotic membrane disruption upon phosphorylation by RIP3. *Mol Cell,* 54**,** 133-46.

Wang, X., Y. Li, S. Liu, X. Yu, L. Li, C. Shi, W. He, J. Li, L. Xu, Z. Hu, L. Yu, Z. Yang, Q. Chen, L. Ge, Z. Zhang, B. Zhou, X. Jiang, S. Chen & S. He (2014b) Direct activation of RIP3/MLKL-dependent necrosis by herpes simplex virus 1 (HSV-1) protein ICP6 triggers host antiviral defense. *Proc Natl Acad Sci U S A,* 111**,** 15438-43.

Werneburg, N. W., M. E. Guicciardi, S. F. Bronk & G. J. Gores (2002) Tumor necrosis factor-alpha-associated lysosomal permeabilization is cathepsin B dependent. *Am J Physiol Gastrointest Liver Physiol,* 283**,** G947-56.

Whilding, L. M., K. M. Archibald, H. Kulbe, F. R. Balkwill, D. Oberg & I. A. McNeish (2013) Vaccinia virus induces programmed necrosis in ovarian cancer cells. *Mol Ther*.

White, E., P. Sabbatini, M. Debbas, W. S. Wold, D. I. Kusher & L. R. Gooding (1992) The 19-kilodalton adenovirus E1B transforming protein inhibits programmed cell death and prevents cytolysis by tumor necrosis factor alpha. *Mol Cell Biol,* 12**,** 2570-80.

Wickham, T. J., P. Mathias, D. A. Cheresh & G. R. Nemerow (1993) Integrins alpha v beta 3 and alpha v beta 5 promote adenovirus internalization but not virus attachment. *Cell,* 73**,** 309-19.

Wilson, C. A. & J. L. Browning (2002) Death of HT29 adenocarcinoma cells induced by TNF family receptor activation is caspase-independent and displays features of both apoptosis and necrosis. *Cell Death Differ,* 9**,** 1321-33.

Wirth, T., L. Zender, B. Schulte, B. Mundt, R. Plentz, K. L. Rudolph, M. Manns, S. Kubicka & F. Kuhnel (2003) A telomerase-dependent conditionally replicating adenovirus for selective treatment of cancer. *Cancer Res,* 63**,** 3181-8.

Wong, H. H., G. Jiang, R. Gangeswaran, P. Wang, J. Wang, M. Yuan, H. Wang, V. Bhakta, H. Muller, N. R. Lemoine & Y. Wang (2012) Modification of the early gene enhancer-promoter improves the oncolytic potency of adenovirus 11. *Mol Ther,* 20**,** 306-16.

Workman, P., E. O. Aboagye, F. Balkwill, A. Balmain, G. Bruder, D. J. Chaplin, J. A. Double, J. Everitt, D. A. Farningham, M. J. Glennie, L. R. Kelland, V. Robinson, I. J. Stratford, G. M. Tozer, S. Watson, S. R. Wedge, S. A. Eccles & I. Committee of the National Cancer Research (2010) Guidelines for the welfare and use of animals in cancer research. *Br. J. Cancer,* 102**,** 1555-1577.

Wu, X. N., Z. H. Yang, X. K. Wang, Y. Zhang, H. Wan, Y. Song, X. Chen, J. Shao & J. Han (2014) Distinct roles of RIP1-RIP3 hetero- and RIP3-RIP3 homo-interaction in mediating necroptosis. *Cell Death Differ,* 21**,** 1709-20.

Xia, B., S. Fang, X. Chen, H. Hu, P. Chen, H. Wang & Z. Gao (2016) MLKL forms cation channels. *Cell Res,* 26**,** 517-28.

Xia, Z. J., J. H. Chang, L. Zhang, W. Q. Jiang, Z. Z. Guan, J. W. Liu, Y. Zhang, X. H. Hu, G. H. Wu, H. Q. Wang, Z. C. Chen, J. C. Chen, Q. H. Zhou, J. W. Lu, Q. X. Fan, J. J. Huang & X. Zheng (2004) Phase III randomized clinical trial of intratumoral injection of E1B gene-deleted adenovirus (H101) combined with cisplatin-based chemotherapy in treating squamous cell cancer of head and neck or esophagus. *Ai Zheng,* 23**,** 1666-1670.

Xiao, Q., D. Zhou, A. A. Rucki, J. Williams, J. Zhou, G. Mo, A. Murphy, K. Fujiwara, J. Kleponis, B. Salman, C. L. Wolfgang, R. A. Anders, S. Zheng, E. M. Jaffee & L. Zheng (2016) Cancer-Associated Fibroblasts in Pancreatic Cancer Are Reprogrammed by Tumor-Induced Alterations in Genomic DNA Methylation. *Cancer Res,* 76**,** 5395-404.

Xu, Y., Z. Lin, N. Zhao, L. Zhou, F. Liu, Z. Cichacz, L. Zhang, Q. Zhan & X. Zhao (2014) Receptor interactive protein kinase 3 promotes Cisplatin-triggered necrosis in apoptosis-resistant esophageal squamous cell carcinoma cells. *PLoS One,* 9**,** e100127.

Ying, B., A. E. Tollefson & W. S. Wold (2010) Identification of a previously unrecognized promoter that drives expression of the UXP transcription unit in the human adenovirus type 5 genome. *J Virol,* 84**,** 11470-8.

Zanardi, T. A., S. Yei, D. L. Lichtenstein, A. E. Tollefson & W. S. Wold (2003) Distinct domains in the adenovirus E3 RIDalpha protein are required for degradation of Fas and the epidermal growth factor receptor. *J Virol,* 77**,** 11685-96.

Zhao, J., S. Jitkaew, Z. Cai, S. Choksi, Q. Li, J. Luo & Z. G. Liu (2012) Mixed lineage kinase domain-like is a key receptor interacting protein 3 downstream component of TNF-induced necrosis. *Proc Natl Acad Sci U S A,* 109**,** 5322-7.

Zheng, X., X. M. Rao, C. Snodgrass, M. Wang, Y. Dong, K. M. McMasters & H. S. Zhou (2005) Adenoviral E1a expression levels affect virus-selective replication in human cancer cells. *Cancer Biol Ther,* 4**,** 1255-62.

Zong, W. X., D. Ditsworth, D. E. Bauer, Z. Q. Wang & C. B. Thompson (2004) Alkylating DNA damage stimulates a regulated form of necrotic cell death. *Genes Dev,* 18**,** 1272-82.

Zong, W. X. & C. B. Thompson (2006) Necrotic death as a cell fate. *Genes Dev,* 20**,** 1-15.

Zou, J., T. Kawai, T. Tsuchida, T. Kozaki, H. Tanaka, K. S. Shin, H. Kumar & S. Akira (2013) Poly IC triggers a cathepsin D- and IPS-1-dependent pathway to enhance cytokine production and mediate dendritic cell necroptosis. *Immunity,* 38**,** 717-28.

Weblinks

1.) https://www.accessdata.fda.gov/scripts/opdlisting/oopd/listResult.cfm (accessed 12.10.2016 at 11:37)

2.) http://www.cancerresearchuk.org/health-professional/cancer-statistics/statistics-by-cancer-type/ovarian-cancer/incidence#heading-One (accessed 19.10.2016 at 13:11)

3.) http://www.cancerresearchuk.org/health-professional/cancer-statistics/statistics-by-cancer-type/ovarian-cancer/incidence#heading-Three (accessed 19.10.2016 at 13:13)

4.) http://www.cancerresearchuk.org/health-professional/cancer-statistics/statistics-by-cancer-type/ovarian-cancer/survival#heading-Three (accessed 19.10.2016 at 13:15)